DTNSRDC-79/003

DAVID W. TAYLOR NAVAL SHIP RESEARCH AND DEVELOPMENT CENTER

Bethesda, Maryland 20084

LEVEL III

AERODYNAMIC CHARACTERISTICS OF THE CLOSE-COUPLED CANARD AS APPLIED TC LOW-TO-MODERATE SWEPT WINGS VOLUME 3: TRANSONIC-SUPERSONIC SPEED REGIME

by

David W. Lacey

APPROVED FOR PUBLIC RELEASE: DISTRIBUTION UNLIMITED

AVIATION AND SURFACE EFFECTS DEPARTMENT
RESEARCH AND DEVELOPMENT REPORT

December 1979 DTNSRDC-79/003

AERODYNAMIC CHARACTERISTICS OF THE CLOSE-COUPLED CANARD AS APPLIED TO LOW-TO-MODERATE SWEPT WINGS — VOLUME 3: TRANSONIC-SUPERSONIC SPEED REGIME

MAJOR DTNSRDC ORGANIZATIONAL COMPONENTS

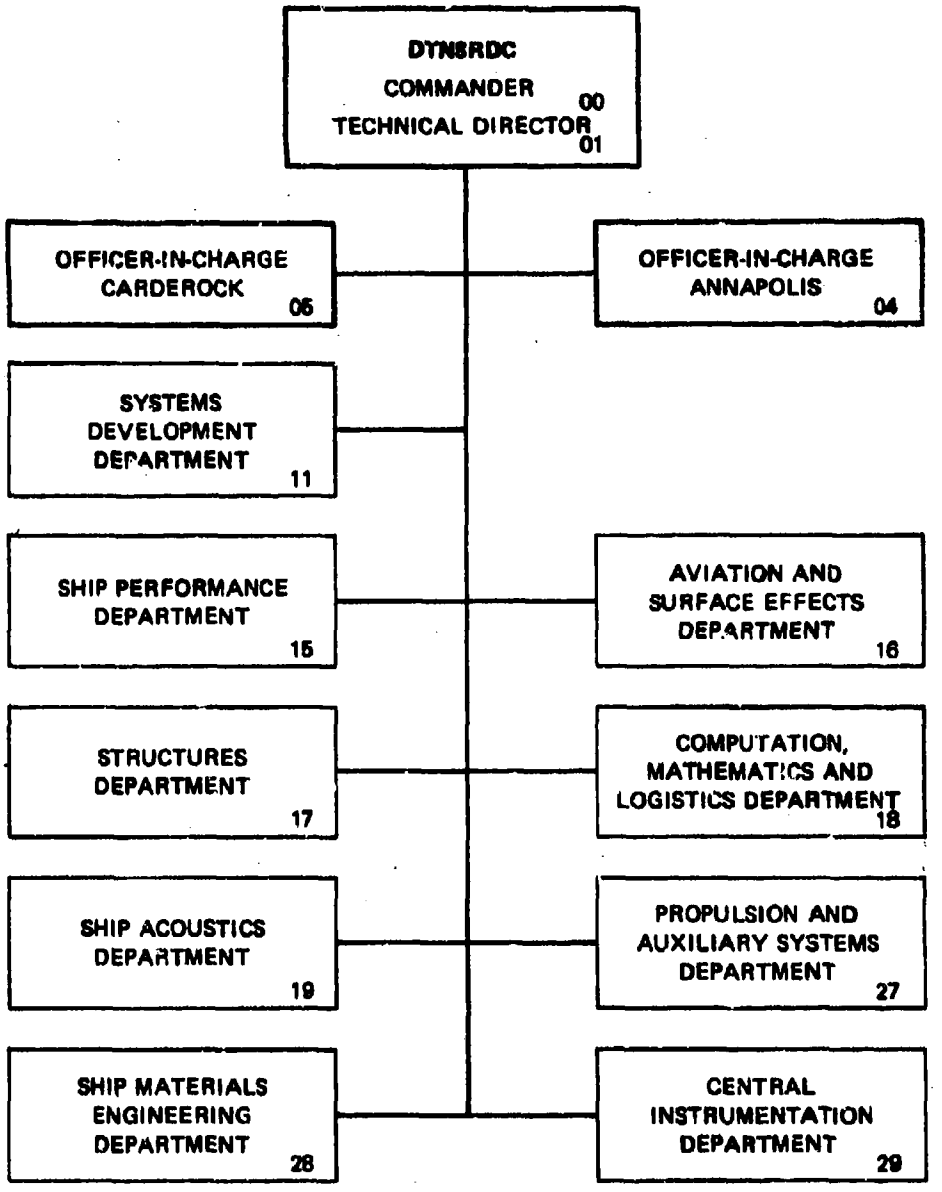

1061122

UNCLASSIFIED

SECURITY CLASSIFICATION OF THIS PAGE (When Data Entered)

REPORT DOCUMENTATION PAGE

READ INSTRUCTIONS BEFORE COMPLETING FORM

14

1. REPORT NUMBER: DTNSRDC-79/003

2. GOVT ACCESSION NO.: AD-A085065

3. RECIPIENT'S CATALOG NUMBER: 9

6

4. TITLE (and Subtitle): AERODYNAMIC CHARACTERISTICS OF THE CLOSE-COUPLED CANARD AS APPLIED TO LOW-TO-MODERATE SWEPT WINGS. VOLUME 3. TRANSONIC-SUPERSONIC SPEED REGIME.

5. TYPE OF REPORT & PERIOD COVERED: Final rept. 1970-1974

6. PERFORMING ORG. REPORT NUMBER

10

7. AUTHOR(s): David W. Lacey

8. CONTRACT OR GRANT NUMBER(s)

9. PERFORMING ORGANIZATION NAME AND ADDRESS: David W. Taylor Naval Ship Research and Development Center, Bethesda, Maryland 20084

10. PROGRAM ELEMENT, PROJECT, TASK AREA & WORK UNIT NUMBERS: Program Element 62241N; Task Area WF 1-41421-09; Work Unit 1600-079

11. CONTROLLING OFFICE NAME AND ADDRESS

12 183

11

12. REPORT DATE: December 1979

13. NUMBER OF PAGES: 184

14. MONITORING AGENCY NAME & ADDRESS (if different from Controlling Office): Naval Air Systems Command, AIR 320, Washington, D.C. 20361

15. SECURITY CLASS. (of this report): UNCLASSIFIED

15a. DECLASSIFICATION/DOWNGRADING SCHEDULE

16. DISTRIBUTION STATEMENT (of this Report)

APPROVED FOR PUBLIC RELEASE: DISTRIBUTION UNLIMITED

DTIC ELECTE JUN 5 1980 C

17. DISTRIBUTION STATEMENT (of the abstract entered in Block 20, if different from Report)

16 F14142

18. SUPPLEMENTARY NOTES

17 WF1414210 9

19. KEY WORDS (Continue on reverse side if necessary and identify by block number)

Canards	Drag
Transonic	Pitching Moment
Supersonic	Buffet
Lift	Research Models

20. ABSTRACT (Continue on reverse side if necessary and identify by block number)

An analysis of the effects of canard shape, position, and deflection on the aerodynamic characteristics of two general research models having leading edge sweep angles of 25 and 50 degrees is presented. The analysis ~~is a summary of the~~ summarizes findings of three experimental transonic wind-tunnel programs and one supersonic wind-tunnel program conducted at ~~the~~ David W. ~~Taylor~~ Naval Ship Research and ~~Development~~ Center between 1970 and 1974. The

(Continued on reverse side)

DD FORM 1 JAN 73 1473 EDITION OF 1 NOV 65 IS OBSOLETE S/N 0102-LF-014-6601

UNCLASSIFIED

SECURITY CLASSIFICATION OF THIS PAGE (When Data Entered)

387682 DW

(Block 20 continued)

analysis is based on four canard geometries varying in planform from a 60-degree delta to a 25-degree swept wing, high aspect ratio canard. The canards were tested at several positions and deflected from -10 to +10 degrees. In addition, configurations consisting of a horizontal tail and a canard with horizontal tails are analyzed.

The results of the analysis indicate that the canard is effective in increasing lift and decreasing drag at Mach numbers from subsonic to high transonic speeds by delaying wing separation. The effectiveness of the canard is, however, decreased with increasing Mach number. At supersonic speeds the canard has little or no favorable effects on lift or drag.

It is further shown that the horizontal tail is a superior trimming device than the close-coupled canard at low-to-moderate angles of attack and that a configuration consisting of canard, wing, and horizontal tail is superior in performance, to either canard or horizontal tail at high angles of attack.

FOREWORD

This report summarizes the findings of close-coupled canard research performed by the Aviation and Surface Effects Department of the David W. Taylor Naval Ship Research and Development Center. The work was performed between 1970 and 1974 and was funded by the Naval Air Systems Command (AIR 320). The purpose of the report is to provide a summary of the aerodynamic findings obtained from a series of wind tunnel evaluations involving three general research models and the F-4 aircraft. The report is presented in four volumes--Volume 1: General Trends; Volume 2: Subsonic Speed Regime; Volume 3: Transonic-Supersonic Speed Regime; and Volume 4: F-4 Phantom II Aircraft.

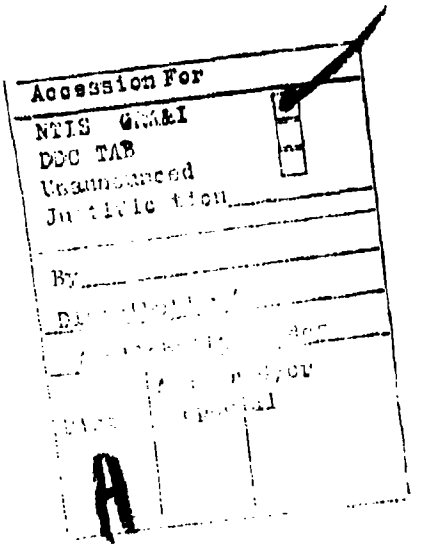

TABLE OF CONTENTS

LIST OF FIGURES

LIST OF TABLES

NOTATION

A	Axial force, pounds
AR	Aspect ratio
C_A	Axial force coefficient A/qS_w
C_D	Drag coefficient, D/qS_w
$C_{D_{min}}$	Minimum drag coefficient
C_{D_δ}	$\partial C_D/\partial\delta$
C_l	Canard
C_L	Lift coefficient, L/qS_w
$C_{L_{B.O.}}$	Buffet onset lift coefficient
$C_{L_{25}}$	Lift coefficient evaluated at α = 25 degrees
C_{L_α}	$\partial C_L/\partial\alpha$
C_{L_δ}	$\partial C_L/\partial\delta$
C_M	Pitching moment coefficient, pitching moment/qS_w
$C_{M_{WB}}$	Pitching moment coefficient of body and wing
C_{M_0}	Zero lift pitching moment
$C_{M_{25}}$	Pitching moment coefficient evaluated at α = 25 degrees
C_{M_α}	$\partial C_M/\partial\alpha$
C_{M_δ}	$\partial C_M/\partial\delta$

C_N	Normal force coefficient N/qS_w
$\bar{c}$	Mean aerodynamic chord, inches
D	Drag, pounds
H_T	Horizontal tail
i	Canard shape
j	Canard position
k_1	Induced drag factor
L	Lift, pounds
L/D	Lift-to-drag ratio
$(L/D)_{max}$	Maximum lift-to-drag ratio
ℓ_c	Distance between center of gravity of wing and/or canard/tail pivot location, inches
M	Mach number
N	Normal force, pounds
P_j	Canard position
q	Dynamic pressure, pounds per square foot
S_W	Wing reference area, square feet
WB	Wing-body
$\bar{x}$	Longitudinal distance, inches
$\bar{z}$	Vertical distance, inches
α	Angle of attack, degrees
$\Delta C_A/\Delta C_L$	Axial force slope
ΔC_D	$C_D - C_{D_{WB}}$

ΔC_L	$C_L - C_{L_{WB}}$
ΔC_M	$C_M - C_{M_{WB}}$
δ_c	Canard deflection angle, degrees
σ	RMS, root mean square bending moment, inch-pounds

ABSTRACT

An analysis of the effects of canard shape, position, and deflection on the aerodynamic characteristics of two general research models having leading edge sweep angles of 25 and 50 degrees is presented. The analysis is a summary of the findings of three experimental transonic wind-tunnel programs and one supersonic wind-tunnel program conducted at the David W. Taylor Naval Ship Research and Development Center between 1970 and 1974. The analysis is based on four canard geometries varying in planform from a 60-degree delta to a 25-degree swept wing, high aspect ratio canard. The canards were tested at several positions and deflected from -10 to +10 degrees. In addition, configurations consisting of a horizontal tail and a canard with horizontal tails are analyzed.

The results of the analysis inidcate that the canard is effective in increasing lift and decreasing drag at Mach numbers from subsonic to high transonic speeds by delaying wing separation. The effectiveness of the canard is, however, decreased with increasing Mach number. At supersonic speeds the canard has little or no favorable effects on lift or drag.

It is further shown that the horizontal tail is a more superior trimming device than the close-coupled canard at low-to-moderate angles of attack and that a configuration consisting of canard, wing, and horizontal tail is superior, in performance, to either canard or horizontal tail at high angles of attack.

ADMINISTRATIVE INFORMATION

This work was undertaken by the Aircraft Division of the Aviation and Surface Effects Department of the David W. Taylor Naval Ship Research and Development Center (DTNSRDC). The program was sponsored by the Naval Air Systems Command (AIR 320) and was funded under WF 41432-09, Work Unit 1600-078.

INTRODUCTION

The previous volumes of this report have dealt almost exclusively with the close-coupled canard at subsonic speeds. This volume includes the work on canards to transonic and supersonic speed regimes. The trends noted in Volumes 1 and 2 are also evident at transonic speeds albeit

modified to some extent. The primary features to be discussed will be the effect of canard position, shape, and deflection at transonic speeds from Mach numbers (M) of 0.6 to 1.1. The two basic models used in Volumes 1 and 2 were also used in the transonic study and are shown in Figure 1. Similarly, the four canard geometries used in the previous volumes are used in the present volume. The canards are shown in Figure 2. Pertinent dimensions of the models and canards are given in Appendix A.

The data[1-3*] on which this volume is based were obtained in the DTNSRDC 7-foot × 10-foot transonic wind tunnel.

Supersonic data were obtained in the DTNSRDC 18-inch supersonic blowdown tunnel. The model used in obtaining this data is a geometrically similar half model of the 50-degree sweep model and is shown in Figure 3. Data at supersonic speeds were obtained at M = 1.88 and 2.48. In the supersonic wind-tunnel program only the truncated 45-degree delta canard, C_0, was used.

The organization of this volume is similar to the organization of Volume 2; the major sections are lift, drag, and pitching moment at transonic speeds, and an additional section on the effect of the canard on buffet onset and buffet intensity.

The supersonic data are presented as a separate section. Subtopics under each major section include the effects of canard position, deflection, and shape. Comparisons are made between canard and horizontal tail and data are presented on configurations consisting of canard, wing, and horizontal tail. This configuration will be referred to as the trisurface configuration. As with Volume 2, data and analysis are presented for both 25- and 50-degree sweep models.

The majority of the data are presented as incremental changes in lift and pitching moment at constant angle of attack as a function of Mach number. Drag is presented as lift-to-drag ratio L/D, induced drag factor, and minimum drag $C_{D_{min}}$ as a function of Mach number at constant lift coefficient. Buffet data are presented in the form of buffet onset lift coefficient and angle of attack, and buffet intensity.

---

*A complete listing of references is given on page 169.

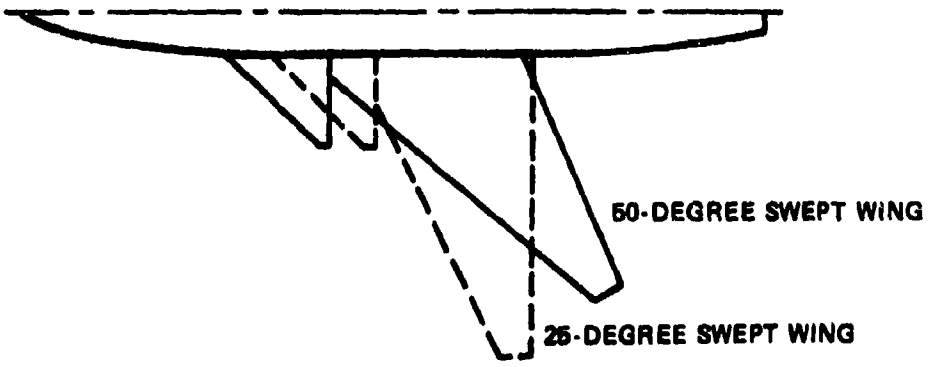

Figure 1 - Sketch of Models

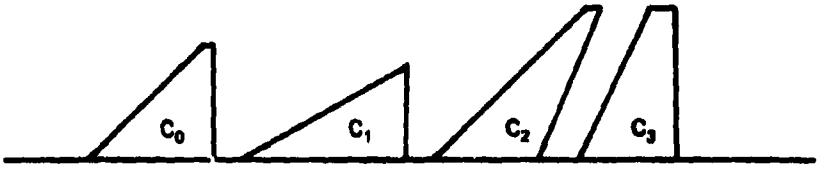

Figure 2 - Canards

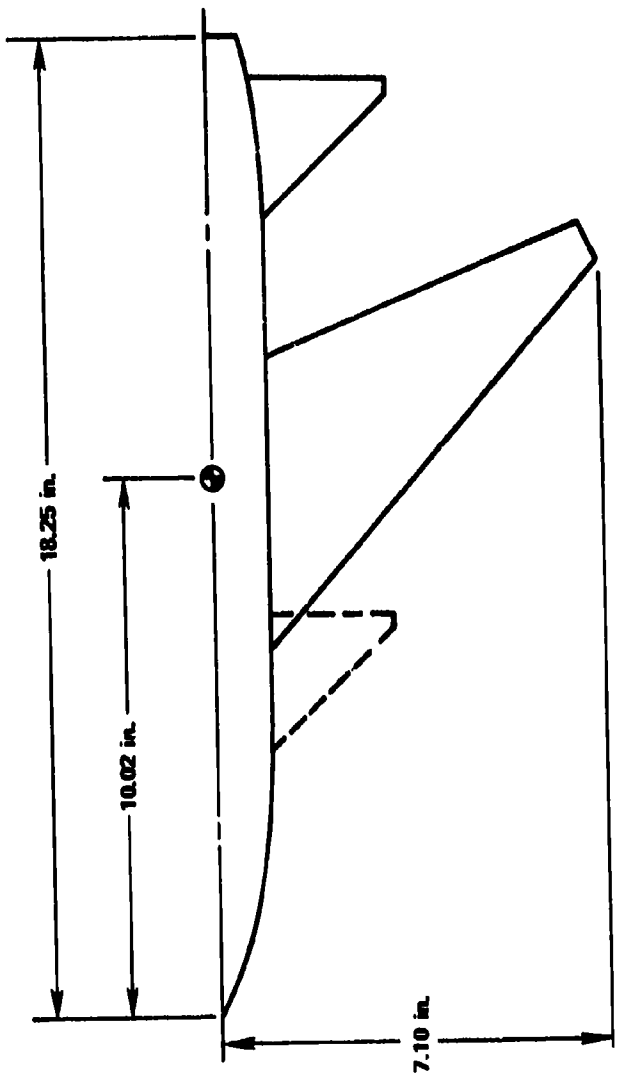

Figure 3 - Supersonic Half-Model

The following analysis will indicate that the favorable results due to the canard at subsonic speeds also occur at transonic speeds and that the canard has only little influence on the lift and drag at supersonic speeds.

LIFT

The variation of lift coefficient with Mach number for both the 25- and 50-degree wing models is shown in Figure 4. The data are for an angle of attack of 25 degrees for both canard on and off. Also included in the figure are the appropriate data points from Volume 2. As shown in three of the four configurations, lift dropped off slightly with increasing Mach number and then increased as true transonic speed is obtained. Where this increase occurs is a function of the wing sweep angle. The point where the increase in lift coefficient with Mach number occurs is at $M = 0.6$ for the 25-degree wing model and approximately $M = 0.7$ for the 50-degree sweep model. What is of primary interest in this figure is the fact that the incremental change between canard on and off is relatively constant with Mach number for both models.

A similar plot for the 50-degree wing at various angles of attack is presented in Figure 5. Mach number range is from 0.6 to 1.1 and shows that the incremental lift is approximately constant with Mach number at constant angle of attack. It should be noted, however, that the influence of Mach number on the lift variation is more pronounced for the basic wing-body than the wing-body canard. This is particularly true at the higher angles of attack. An example of this influence is shown in Figure 6 where the angles of attack required for lift coefficient of 1.0 for the 50-degree wing and 0.9 for the 25-degree wing model are presented. For both models, the angle of attack is relatively constant throughout the Mach number range when the canard is installed. The basic wing-bodies, however, exhibit a pronounced reduction in required angle of attack with increasing Mach number. This behavior is probably due, in part, to the expected increase in lift curve slope C_{L_α} with Mach number, but also is due to a reduction in flow separation over the basic wing with increasing Mach number. This reduction in separation is also expected since a large portion of the wing

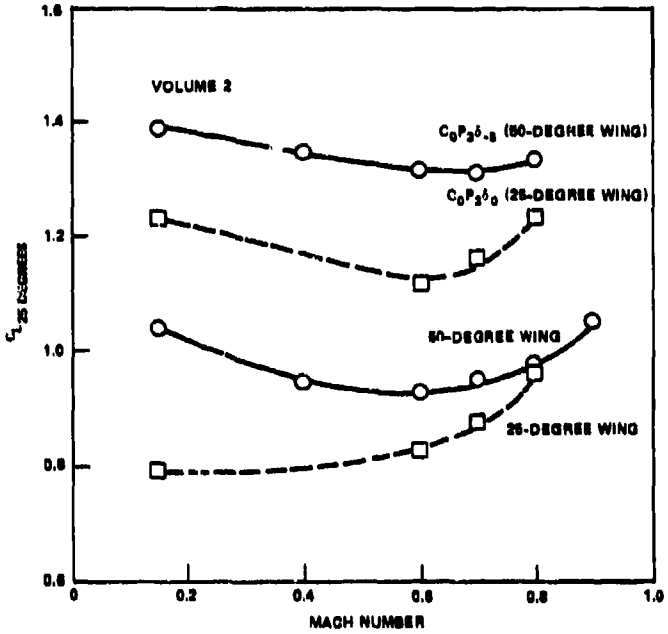

Figure 4 - Lift Variation at 25-Degrees Angle of Attack with Mach Number

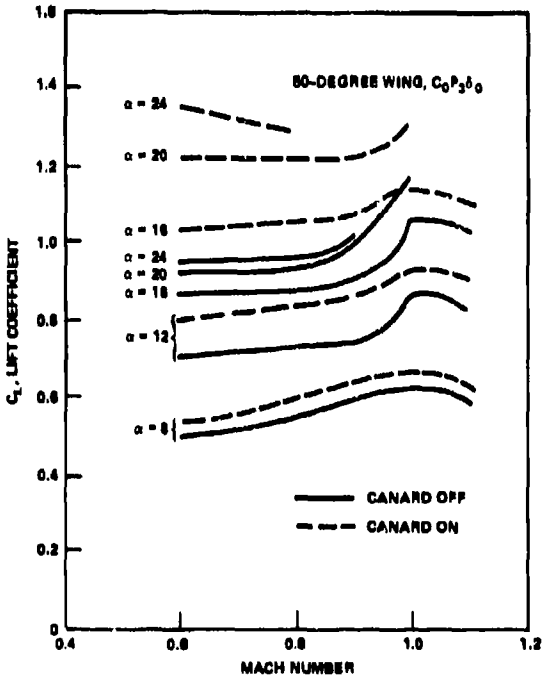

Figure 5 - Lift Coefficient versus Mach Number at Constant Angle of Attack

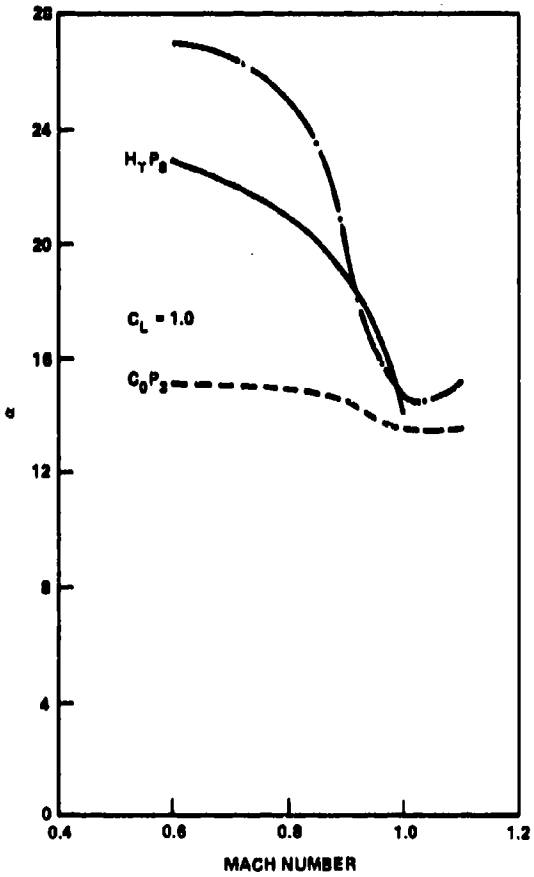

Figure 6a -- Wing at 50 Degrees

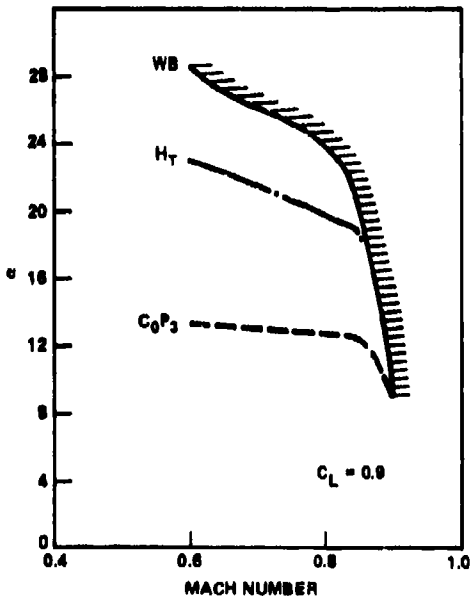

Figure 6b - Wing at 25 Degrees

Figure 6 - Required Angle of Attack

would be in the mixed supersonic-subsonic flow regime. The canard tends to suppress leading edge separation, and with increasing Mach number, less of this separation is in evidence and as expected the canard would have a smaller effect on the total characteristics of the vehicle. This trend will also be noted at supersonic speeds, where the effect of the canard was small. The supersonic effects will be discussed in detail in a later section.

POSITION

It was noted in the previous volumes of this report, that lift was maximum at subsonic speeds at a position where the canard exposed trailing edge was slightly in front of the exposed wing leading edge. Similar results are noted at M = 0.6 as shown in Figure 7. Figure 7 presents data similar to Figure 6, where angle of attack required for C_L = 1.0 and 0.9 is presented. The data indicate that as the canard is moved aft, the required angle of attack is smaller. It is seen that the optimum position P_3 has a relatively flat angle of attack variation with Mach number. The influence of Mach number on the off optimum positions is similar in behavior to the basic wing-body data presented in Figure 6. With increasing Mach number the required angle of attack is rapidly reduced. It can thus be said that at transonic speeds as well as at subsonic speeds, as the flow characteristics of the basic wing are improved the influence of the canard is reduced and the parameters which determine optimum performance of the canard are of lesser importance.

The majority of the data presented in this section is in the form of incremental lift coefficient ΔC_L at constant angle of attack. The first such data are presented in Figure 8, where ΔC_L, for the basic C_0 canard is presented at positions P_1, P_3, and P_7 for the 50-degree wing model. These three positions were the only positions evaluated at Mach numbers greater than 0.9. Data are presented for nominal angles of attack of 12, 16, 20, and 24 degrees. As in the case of subsonic speeds, incremental lift is maximum at position P_3. Position P_3 corresponds to the highest, most aft position. Moving the canard forward or down reduces the incremental lift

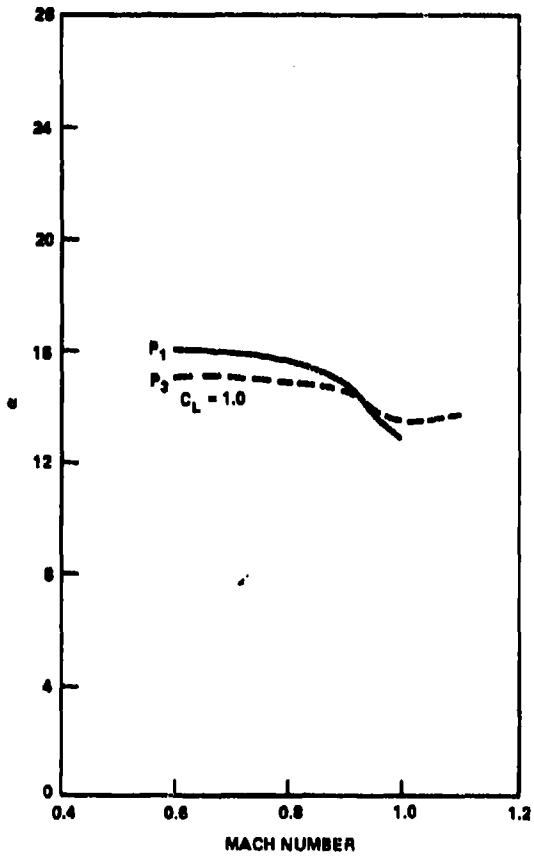

Figure 7a - Longitudinal Position on 50-Degree Wing

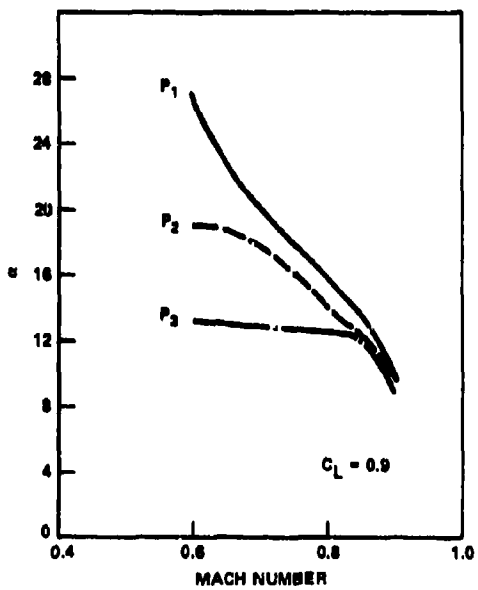

Figure 7b - Longitudinal Position on 25-Degree Wing

Figure 7 - Effect of Canard Longitudinal Position on Required Angle of Attack

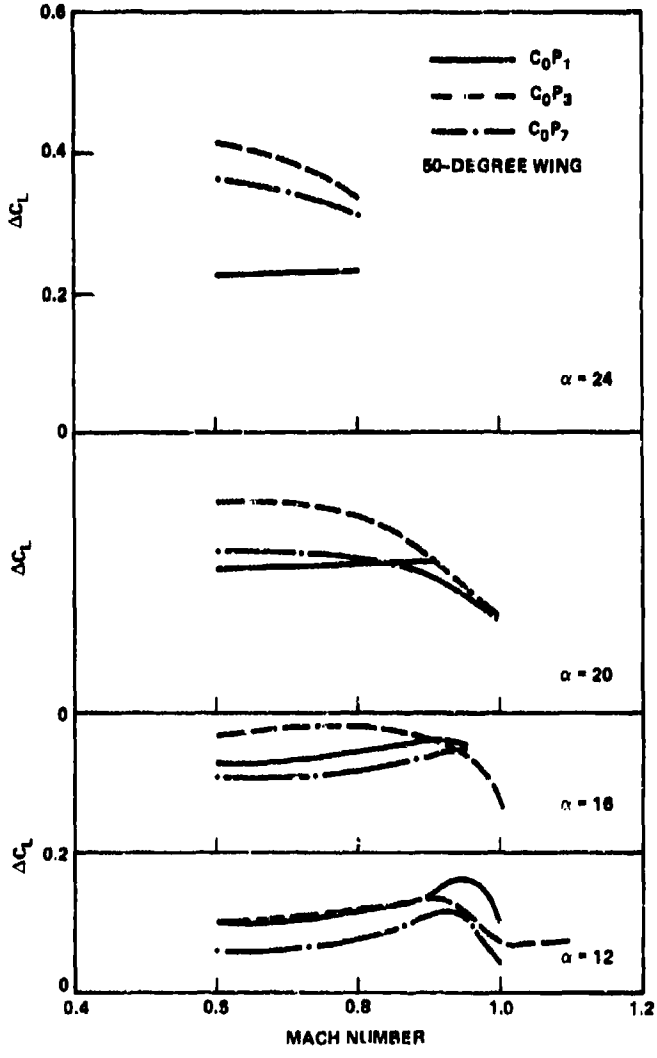

Figure 8 - Effect of Canard Position on Incremental Lift

at Mach numbers below 0.9. As Mach number is increased beyond 0.9, the forward canard had the largest increment at α = 12 degrees. In general at Mach numbers greater than 0.9, little difference is evident in incremental lift due to position.

The effect of longitudinal position for the 25-degree wing is presented in Figure 9. The C_0 canard was evaluated at positions P_1, P_2, and P_3. Similar trends are noted for the 25-degree wing configurations as for the 50-degree wing, i.e., moving the canard aft increased ΔC_L. The data for the 25-degree wing model were limited to a Mach number of 0.85 so the effect of positions at higher Mach numbers are unknown. However, the curves appear to be converging at the higher angles of attack and thus the same behavior of canard position as the 50-degree model is expected.

The effect of longitudinal canard position on the aerodynamic characteristics of the 50-degree model had been well established by the time the transonic wind-tunnel program was run. The majority of the program was concerned with vertical position and only one systematic variation was attempted. These data are shown in Figure 10. The data are for the 60-degree delta C_1, evaluated at positions P_2 and P_3. The subsonic data indicated that the optimum position for this canard was position P_2 and the data at transonic speeds also indicate this to be the case.

The effect of vertical position on incremental lift is presented in Figure 11. The configurations shown are canards C_0, C_1, and C_2 for the 50-degree wing located at positions P_3 and P_6, and canard C_0 located at positions P_2 and P_7, P_3, and P_6 for the 25-degree wing model. In general, lowering the canard reduced the incremental lift. As both Mach number and angle of attack are increased, the differences in incremental lift become smaller and, for canards C_0 and C_1 on the 50-degree wing, crossovers occur and the lower positions become the most effective lift generator. An angle of attack of 25 degrees corresponds closely to the angle of attack for $\Delta C_{L_{max}}$ presented in Volume 2. At subsonic speeds $\Delta C_{L_{max}}$ was higher for the C_0 canard at the low position and was only slightly lower for the C_1 canard. It appears that with increasing Mach number th trends become

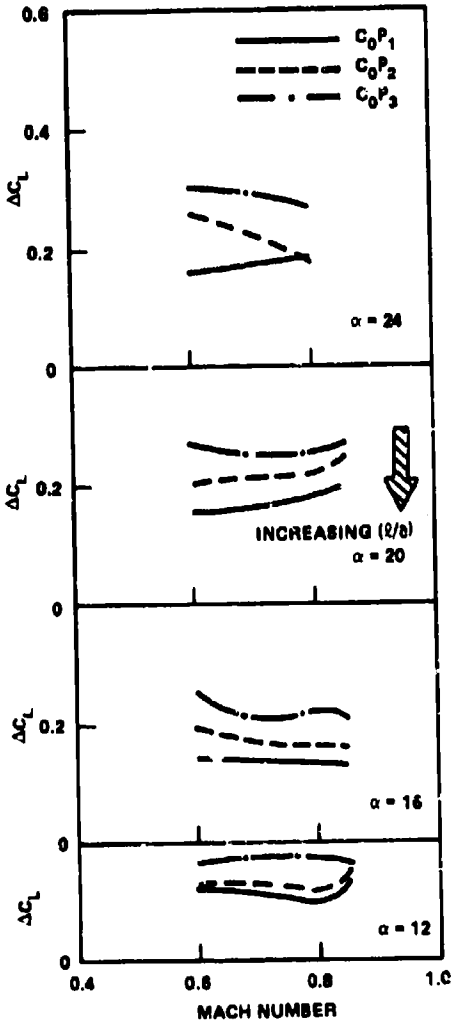

Figure 9 - Effect of Canard Position on Incremental Lift for the 25-Degree Wing

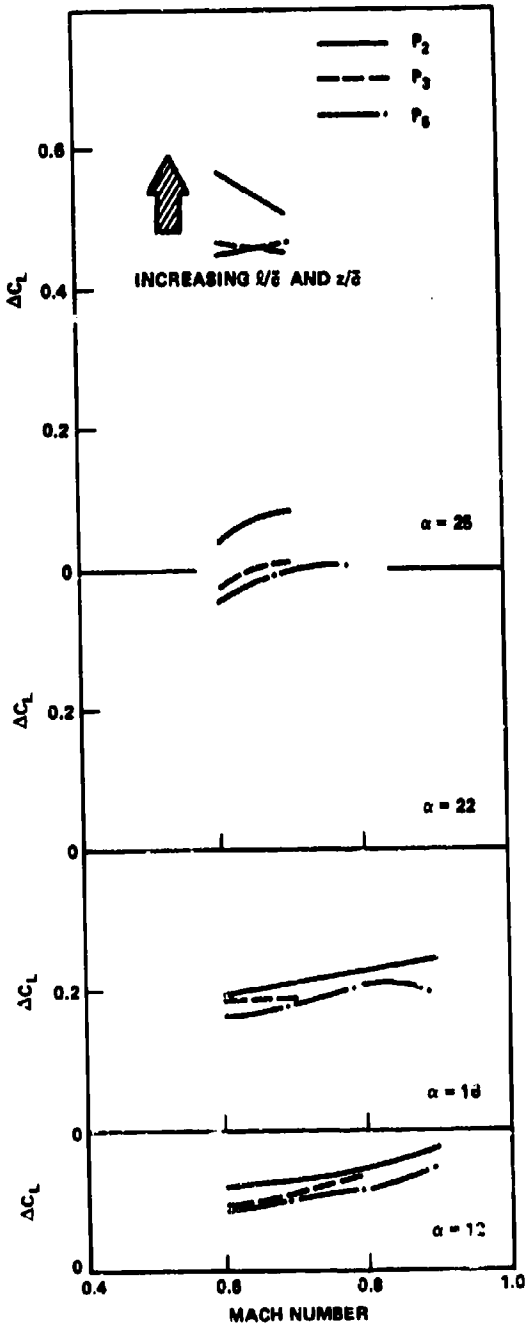

Figure 10 - Effect of Canard C_1, Position on Incremental Lift

Figure 11 - Effect of Canard Vertical Position on Incremental Lift

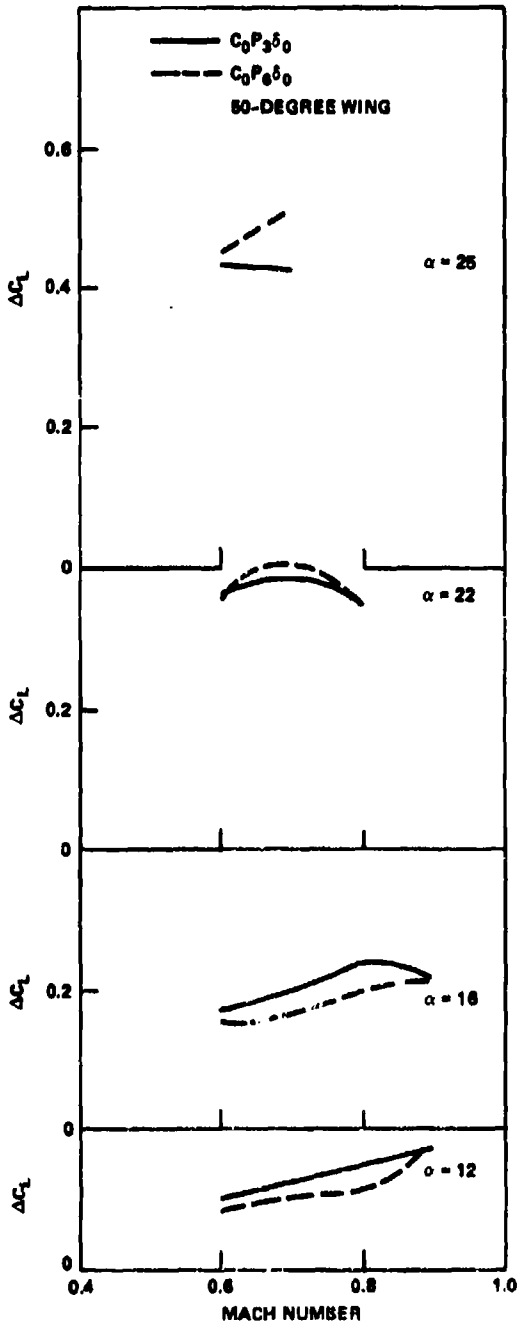

Figure 11a - Canard C_0

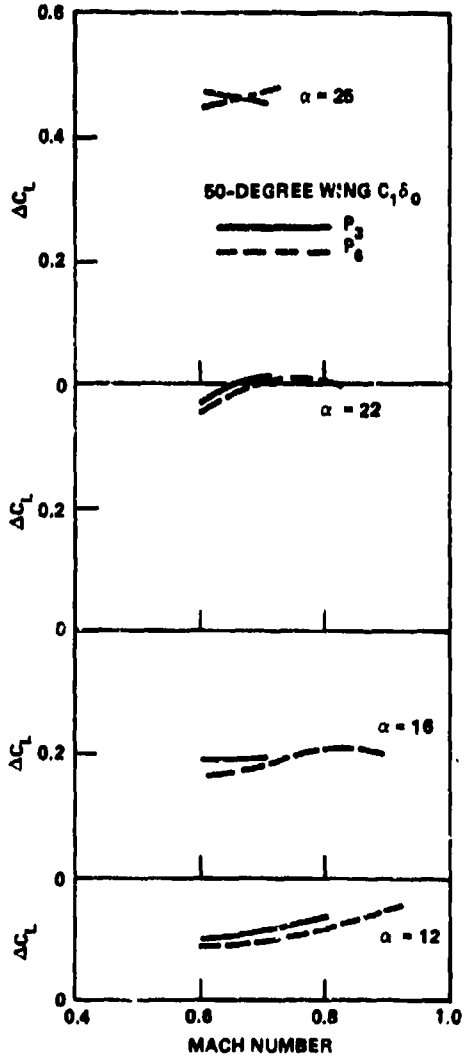

Figure 11b - Canard C_1

Figure 11 (Continued)

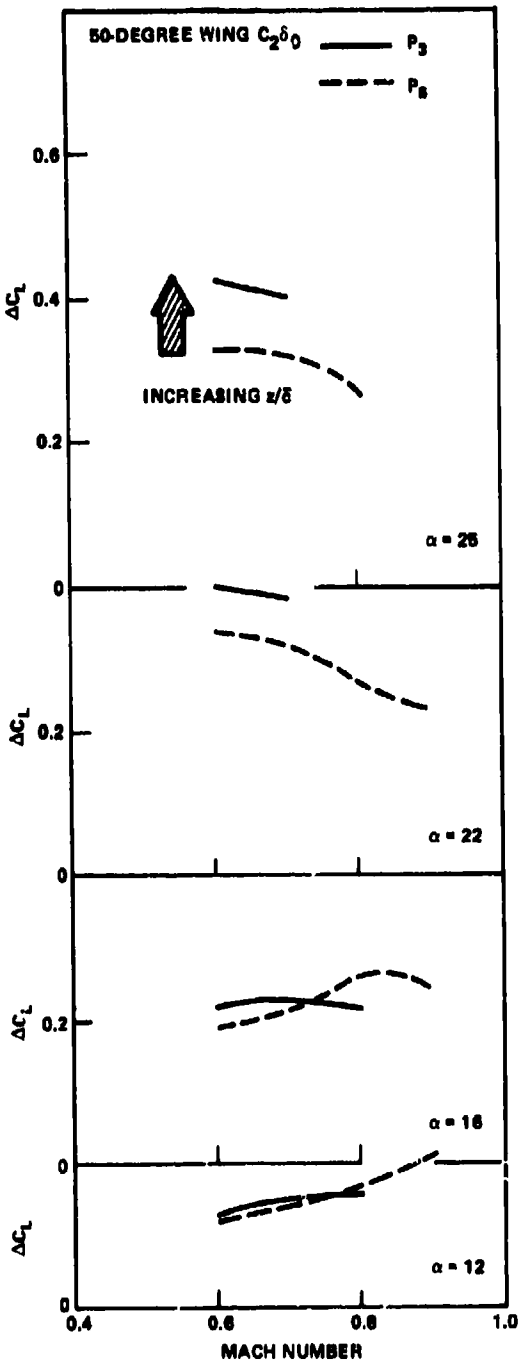

Figure 11c - Canard C_2

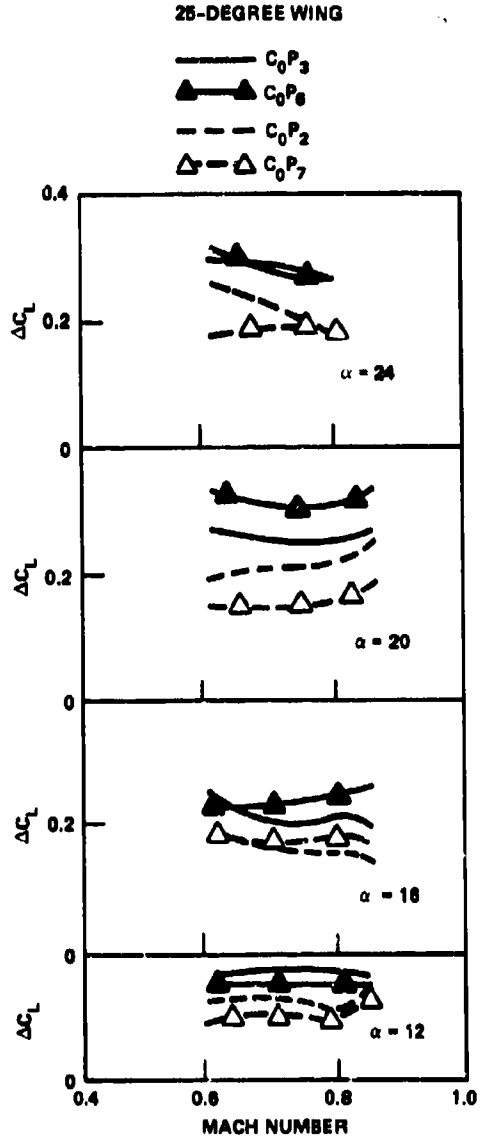

Figure 11d - Canard C_0

more dominant and thus the low position may be advantageous at high transonic Mach numbers. Similar trends are noted for the 25-degree wing model in that crossovers occur at the high angles of attack.

CANARD SHAPE

The effect of canard shape on the 50-degree wing model is presented in Figure 12 for canard shapes C_0, C_1, C_2, and C_3 at position P_3 and shapes C_0, C_1, and C_2 at position P_6. The trends noted are the same as at subsonic speeds. High sweep and low aspect ratio canards generate larger values of incremental lift at high angles of attack. At low angles of attack the reverse is true. The extent of these changes of incremental lift with canard shape is clearly a function of position. At the lower position the differences in incremental lift are clearly larger than those differences at the high position. The trends with increasing Mach number are similar for each position. At low angles of attack (α = 12 and 16) incremental lift increases with increasing Mach number; at the higher angles of attack incremental lift increases and then tends to drop off.

DEFLECTION

It was mentioned in Volume 2 that small negative deflections had a beneficial effect on performance at low angles of attack and only minor unfavorable effects at high angles of attack. For this reason, the majority of the transonic wind-tunnel program was concerned with negative deflections. The effect of such deflections will be discussed in the following section.

As mentioned, the majority of the data were concerned with negative canard deflections, however, certain configurations were evaluated with positive deflections. Those configurations were the C_0 canard at position P_3 for the 50-degree wing and positions P_1 and P_3 for the 25-degree wing. These data are shown in Figure 13. In general, the incremental change in lift due to either positive or negative deflection is relatively constant with Mach number at each angle of attack for all configurations. There are some differences associated with position on the 25-degree wing model.

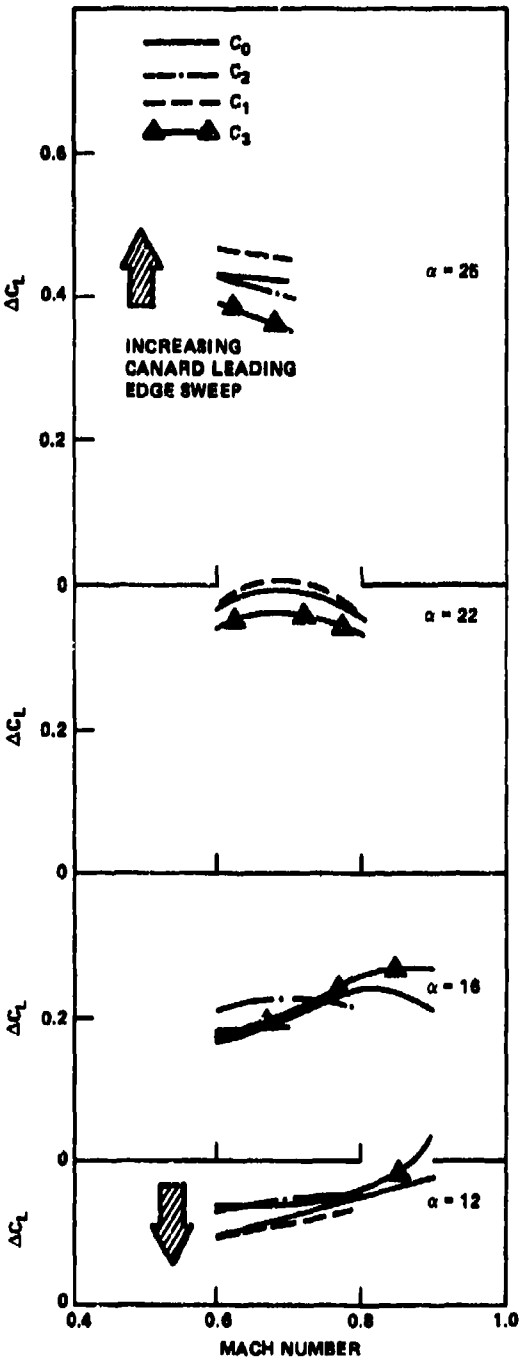

Figure 12a - Position P_3

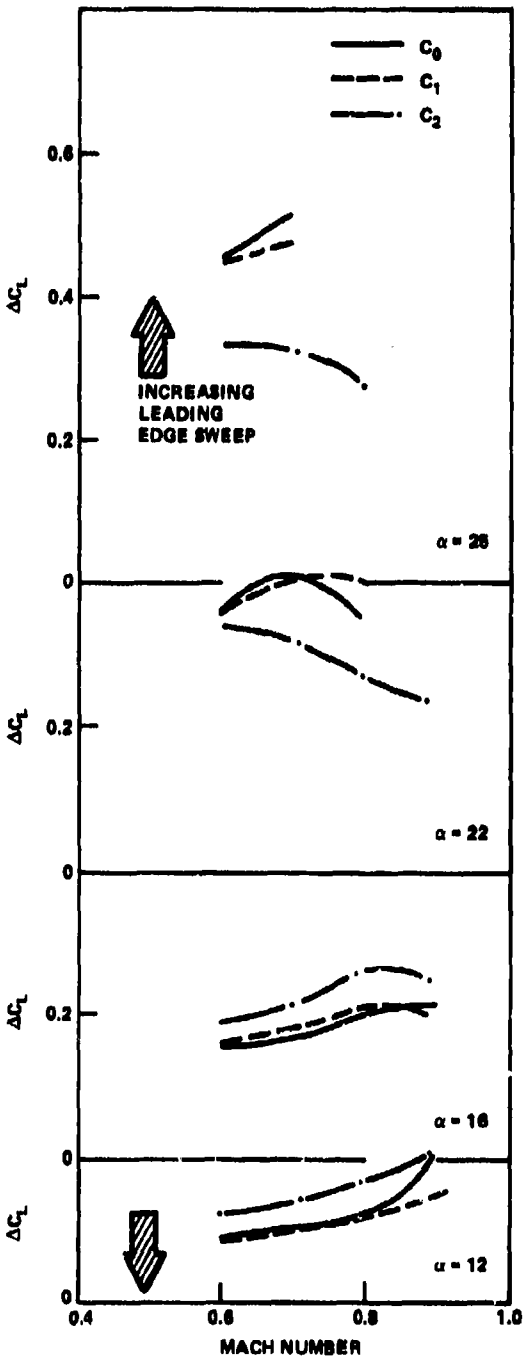

Figure 12b - Position P_6

Figure 12 - Effect of Canard Shape on Incremental Lift

Figure 13 - Effect of Deflection on Incremental Lift at Position P_3

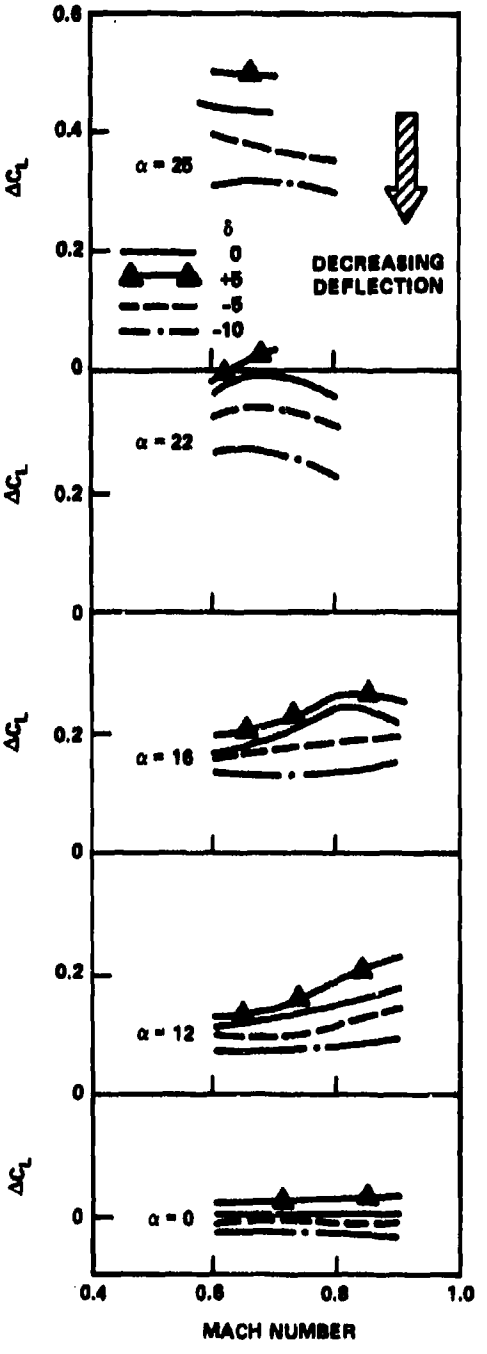

Figure 13a - Position P_3 on 50-Degree Wing

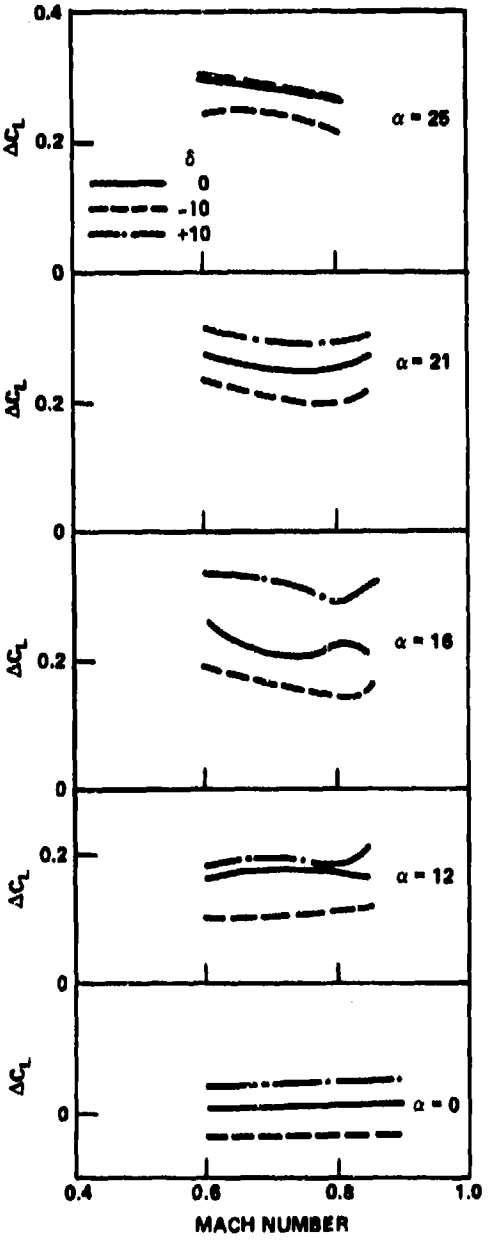

Figure 13b - Position P_3 on 25-Degree Wing

Figure 13 (Continued)

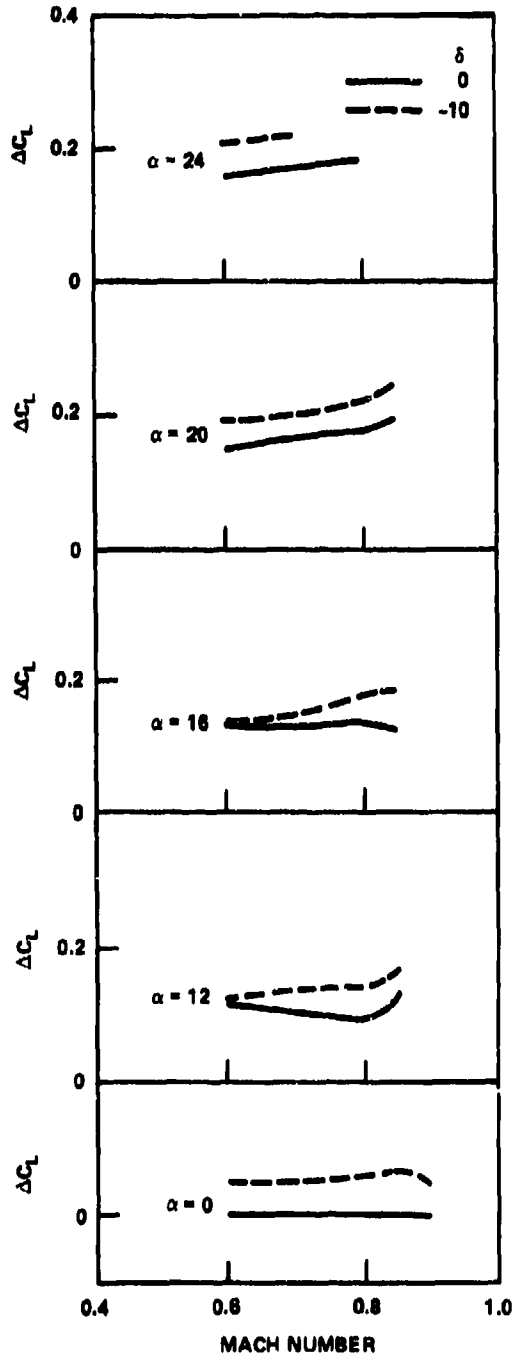

Figure 13c - Position P_1 on 25-Degree Wing

Positive deflection on the most forward position P_1 increased ΔC_L at all angles of attack, however, at the aft position P_3, the effect of positive deflection was small at the highest angle of attack presented.

A comparison between the incremental change due to negative deflection C_{L_δ} for the 25- and 50-degree wings indicates that at low angles of attack C_{L_δ} was greater for the 25-degree wing, however, at high angles of attack C_{L_δ} was greater for the 50-degree wing model. The exact reason for this behavior is unknown, however, it may be due, in part, to the fact that the vertical distance ratio, $Z_t/\sqrt{c}$, is greater for the 25-degree wing model than for the 50-degree model. The canard, when given a negative deflection, increases this gap ratio and thus becomes somewhat less effective in influencing the flow of the wing.

Lowering the canard to position P_6 for both 50- and 25-degree wings indicates similar trends. These data are presented in Figure 14. The incremental lift due to deflection is approximately the same as that of position P_3 for the 50-degree wing at high angles of attack. However, C_{L_δ} is increased for the 25-degree wing indicating that there is a strong effect of vertical trailing edge gap height on incremental lift at high angles of attack when the canard is deflected. A plot of C_{L_δ} at a Mach number of 0.6 is shown in Figure 15. Data are evaluated between canard deflection angles of 0 and -10 degrees. As shown for both wing sweeps, lowering the canard reduced C_{L_δ} at low angles of attack.

The remainder of the deflection data are based on the three other canard shapes C_1, C_2, and C_3. Canard C_1 was evaluated at three positions, P_2, P_3, and P_6 and canards C_2 and C_3 were evaluated at P_3 and P_6. Deflection angle was limited to -5 degrees.

Canard C_1 exhibited maximum incremental lift at position P_2 at 0-degree canard deflection. This is not the case when the canard is deflected. When the canard was deflected to -5 degrees, maximum lift occurred at position P_6. Incremental lift is presented in Figure 16 for the three positions; C_{L_δ} is presented in Figure 17. As shown in Figure 16,

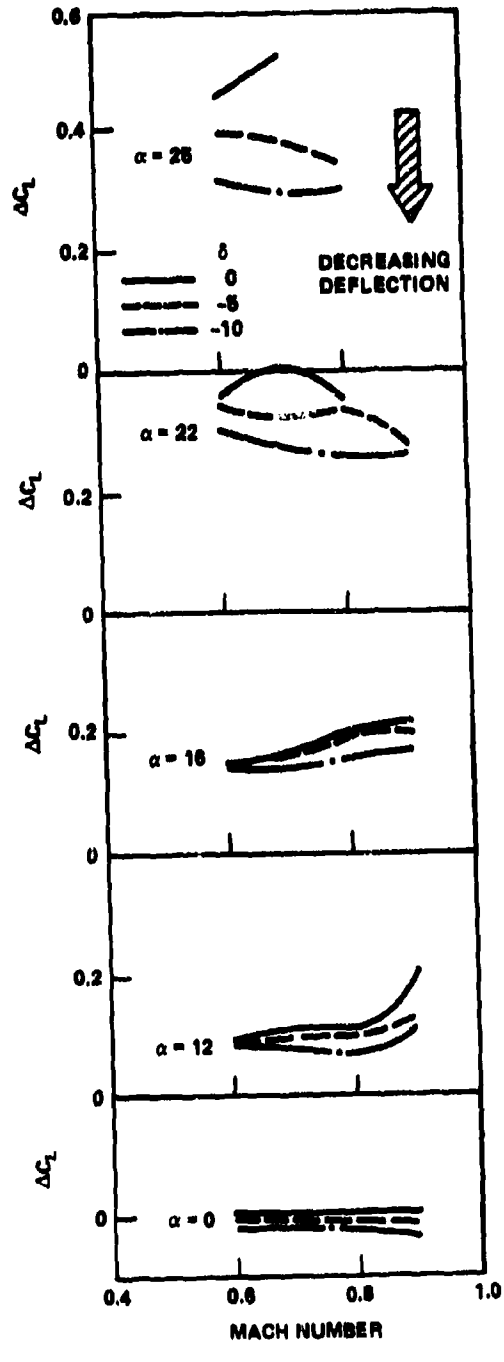

Figure 14a - Deflection on 50-Degree Wing

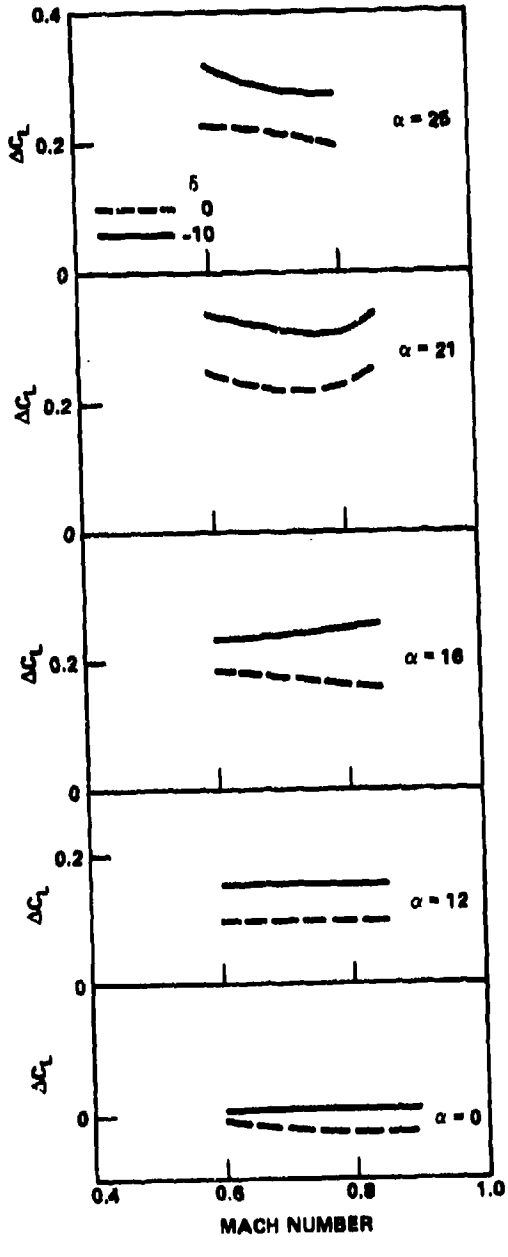

Figure 14b - Deflection on 25-Degree Wing

Figure 14 - Effect of Deflection on Incremental Lift at Position P_6

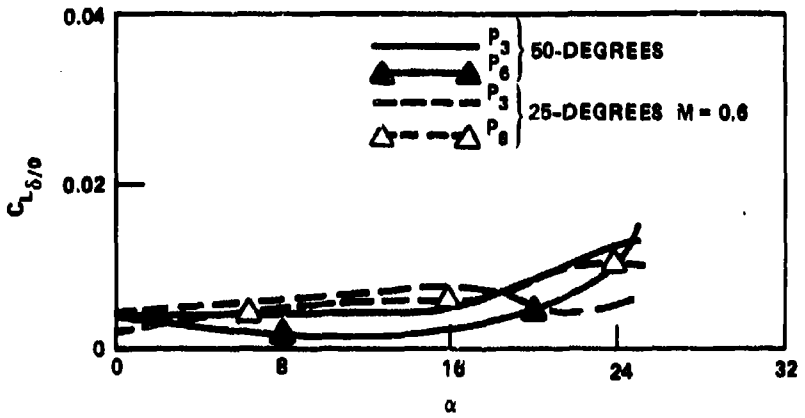

Figure 15 - Comparison of Control Surface Effectiveness for 25- and 50-Degree Wings

Figure 16 - Effect of Deflection on Canard C_l Incremental Lift

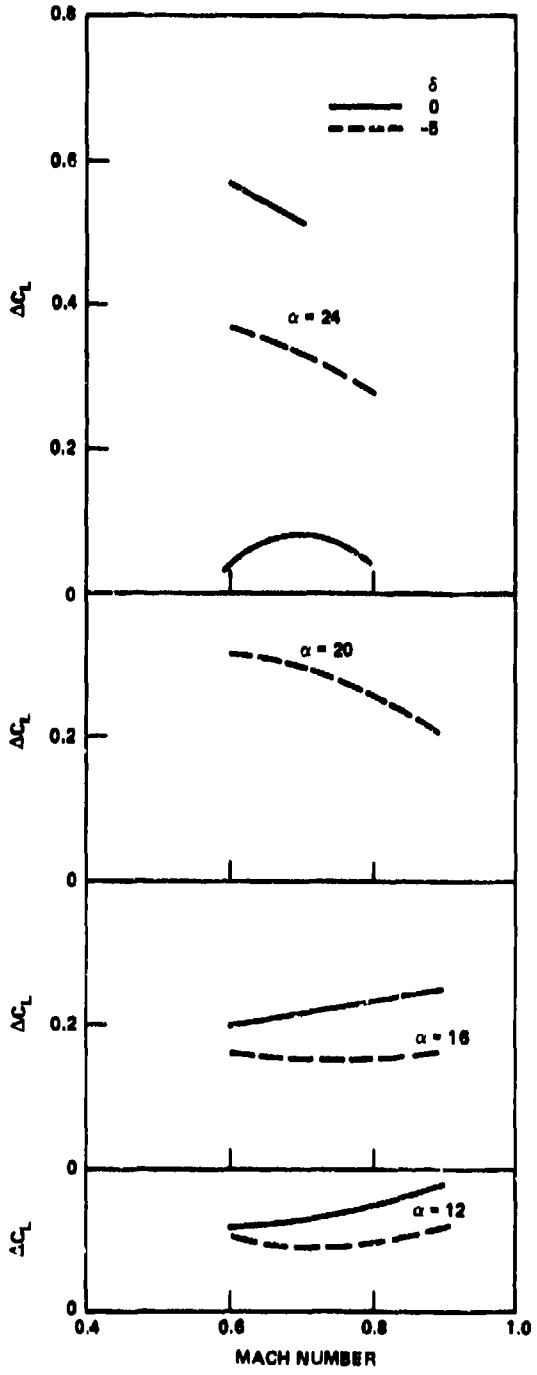

Figure 16a - Position P_2

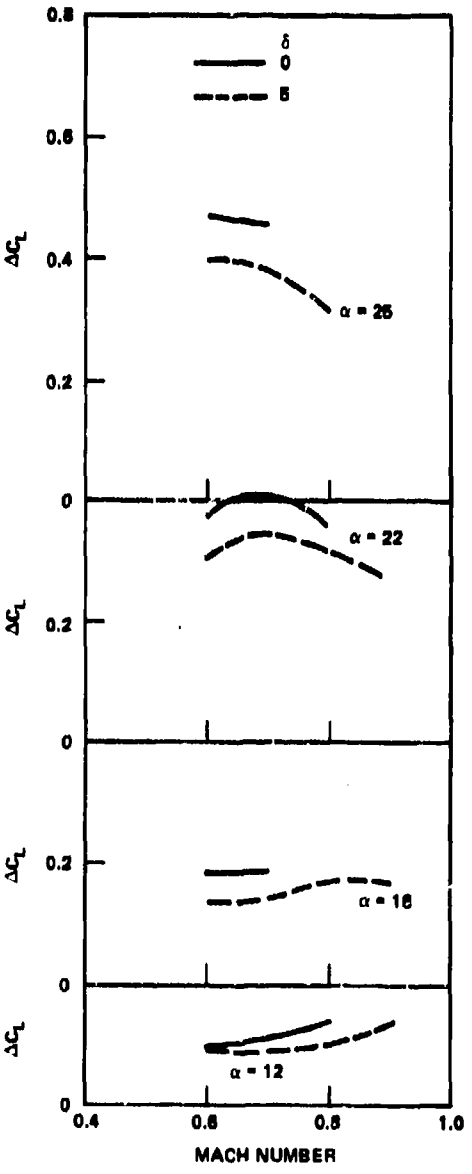

Figure 16b - Position P_3

Figure 16 (Continued)

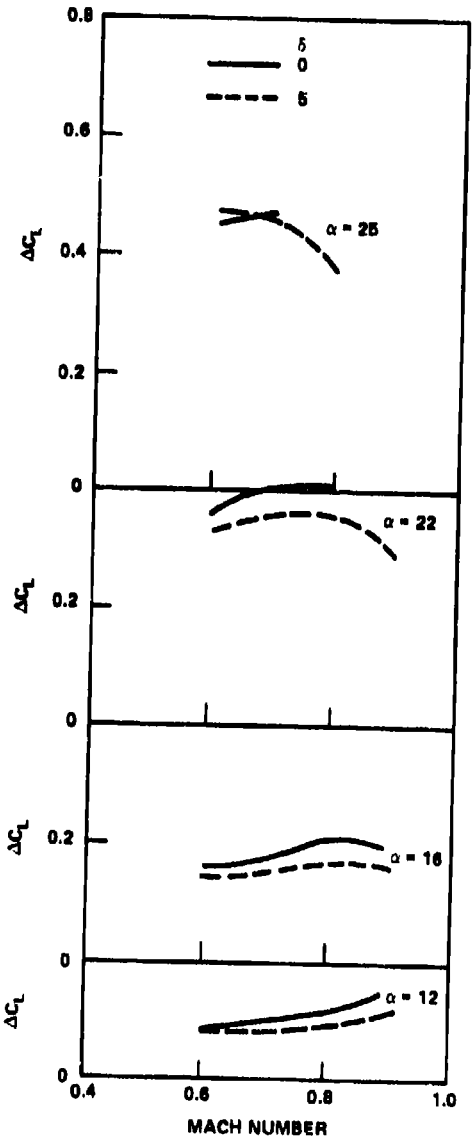

Figure 16c - Position P_6

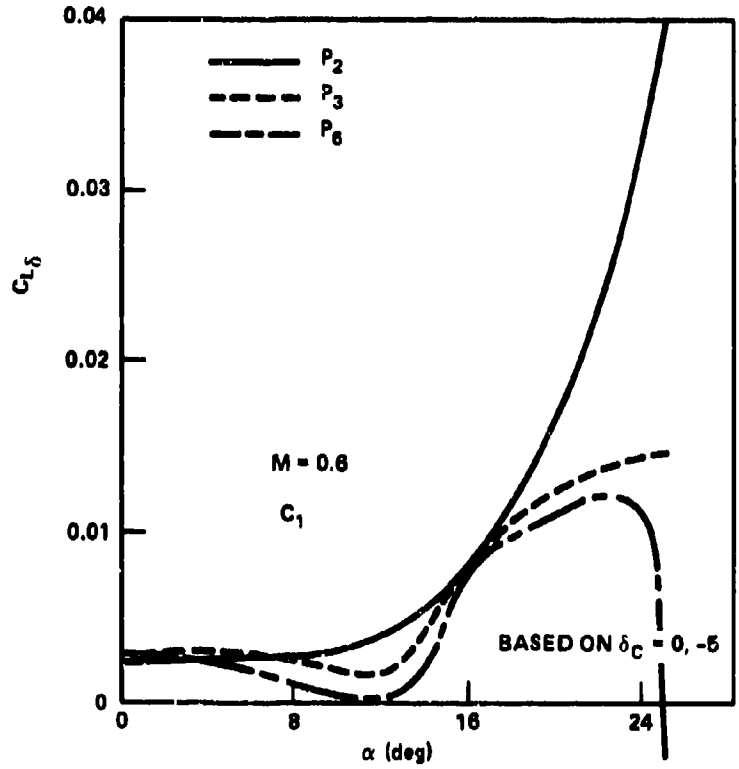

Figure 17 - Control Surface Effectiveness for Canard C_1

large lift losses occurred at position P_2 whereas little lift was lost at position P_6. The large loss in lift ($\Delta C_L = 0.20$) at $\alpha = 25$ degrees for position P_2 is not due to the canard deflection primarily but is due to the gap between wing and canard opening beyond a critical length. The vertical gap at position P_3 is the same as that at position P_2, however, the total gap distance is greater for position P_2 than for position P_3. Insufficient data are available to analyze this trend further but it appears that there is not only a lower gap boundary as discussed in Volume 2 but an upper gap boundary as well.

Similar trends are noted for canard C_2 as shown in Figure 18. Incremental C_L due to deflection was greater at the high position than at the low position. Data were available only at position P_3 for the high aspect ratio canard C_3 and are presented in Figure 19. As shown, C_{L_δ} is approximately constant over most of the Mach number angle of attack range.

TRISURFACE CONFIGURATIONS

The canard, if in proper position for favorable interference, is not as efficient a trimming device for a stable configuration. This is due in part to the short moment arm as well as to the large drag increase caused by positive canard deflections. This increase in drag is particularly severe at low angles of attack. Due to the above reasons, configurations consisting of canards, wing, and horizontal tail were evaluated. A sketch of this configuration is shown in Figure 20. The rationale behind the configuration is to use the horizontal tail for trim at low-to-moderate angles of attack and to supplement the tail trim power with the canard at higher angles of attack when the negative deflection of the tail causes large lift losses.

The incremental lift characteristics for such configurations are shown in Figure 21. Data are shown for both 50- and 25-degree wing configurations. The canard is the basic truncated delta C_0 located at position P_3 for both wing sweeps. As shown in the figures, the trend of the complete configuration with Mach number is very similar to the canard

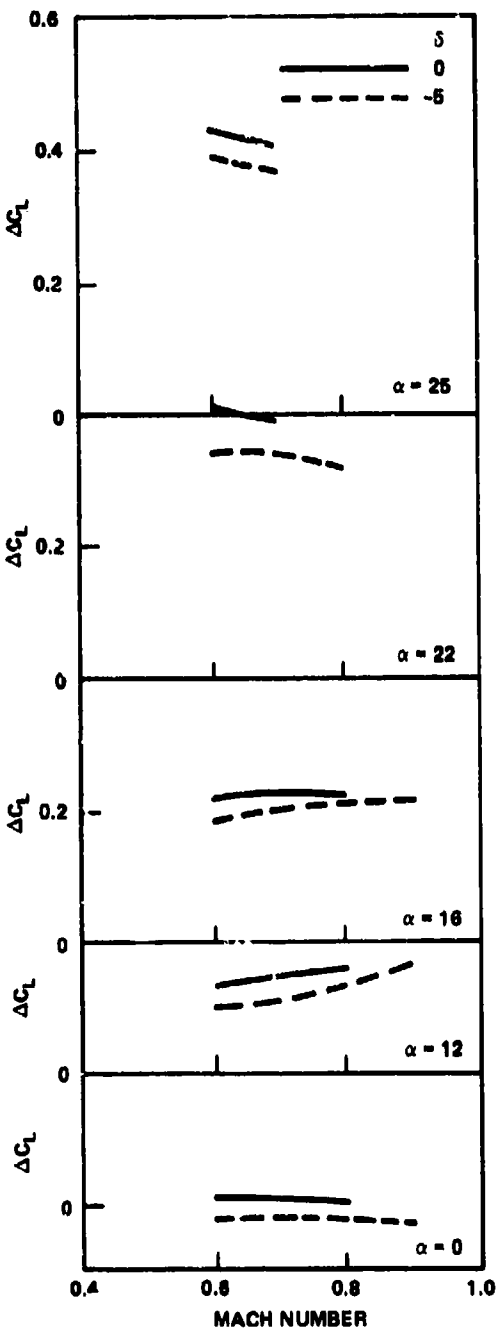

Figure 18a - Position P_3

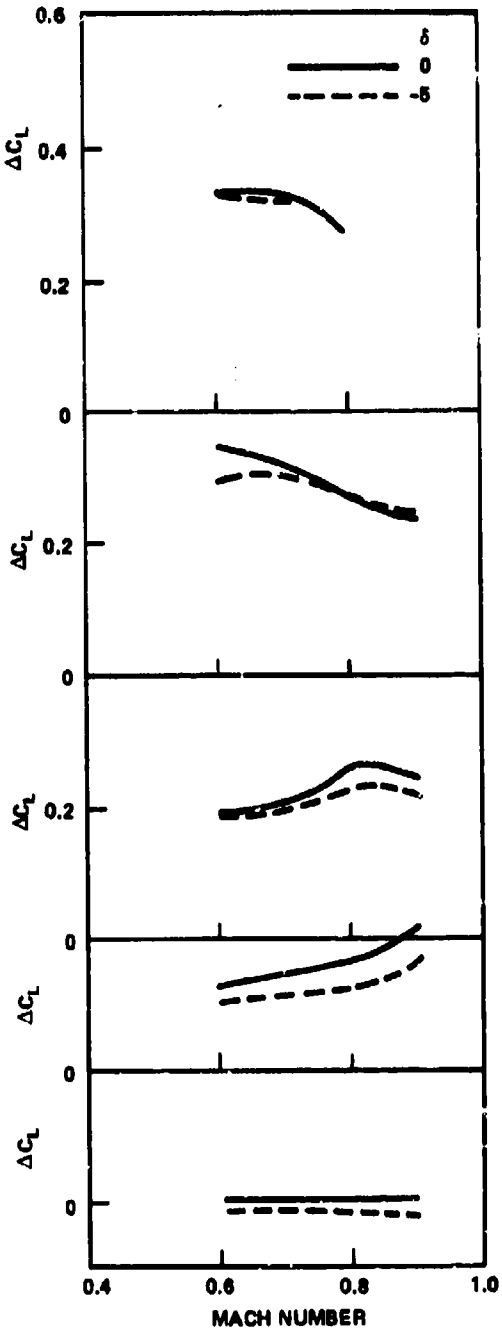

Figure 18b - Position P_6

Figure 18 - Effect of Deflection on Canard C_2 Incremental Lift

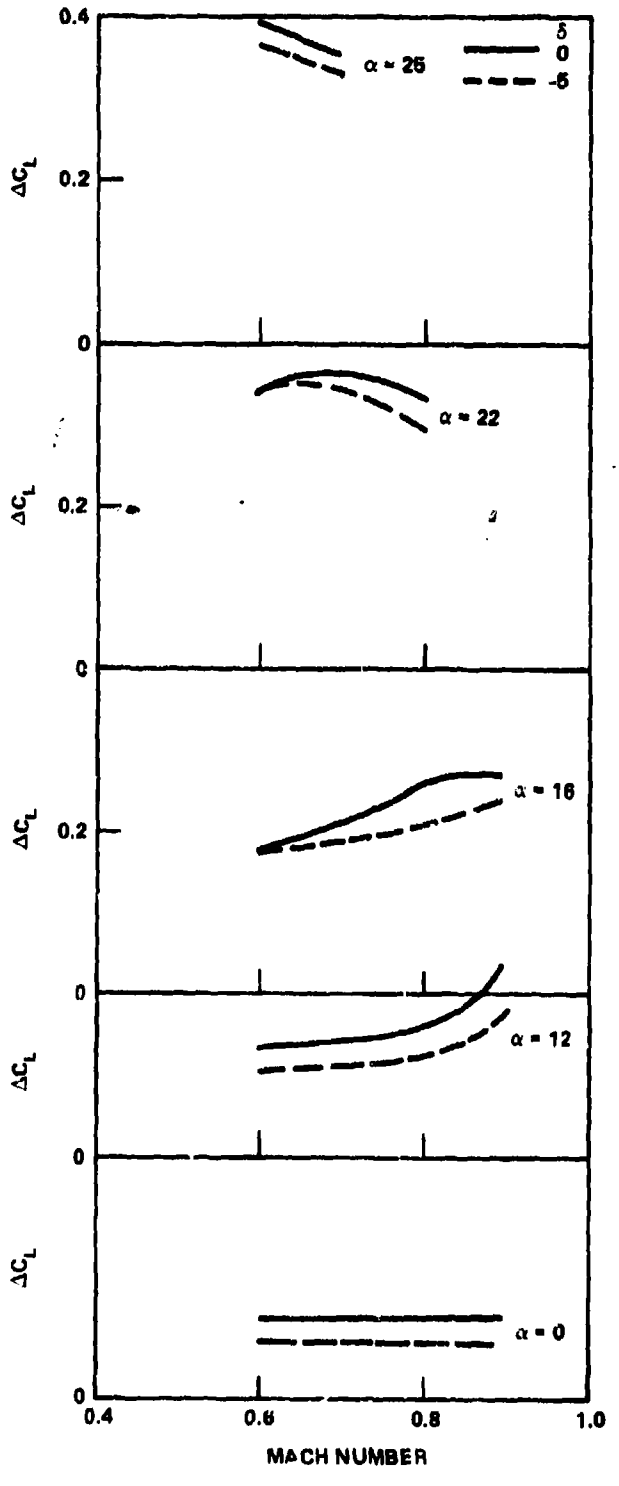

Figure 19 - Effect of Deflection on Canard C_3 Incremental Lift

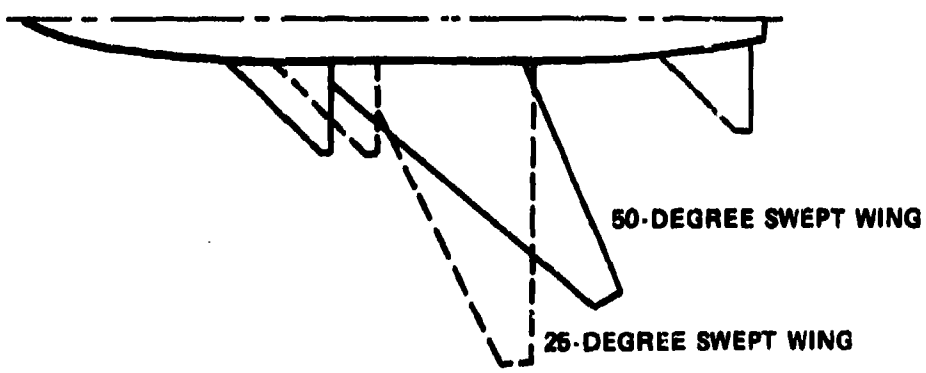

Figure 20 - Trisurface Configuration

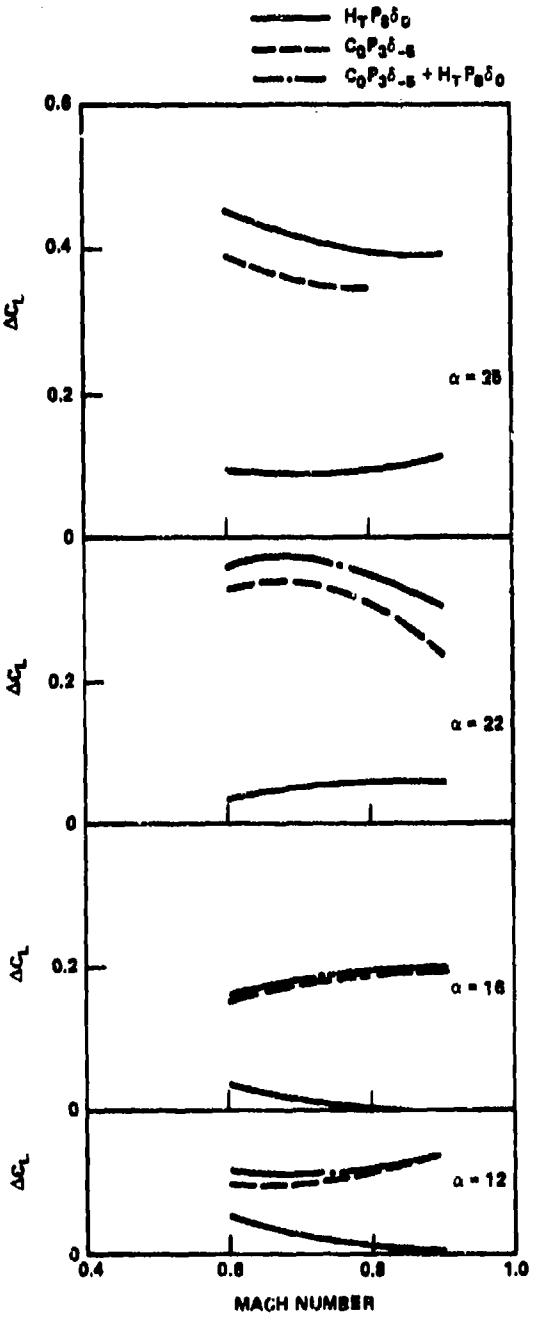

Figure 21a - Incremental Lift on 50-Degree Wing

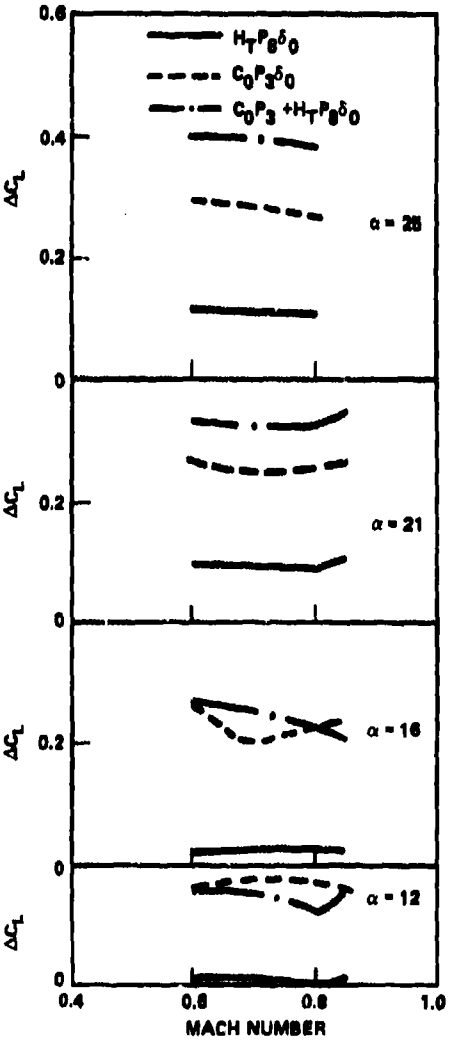

Figure 21b - Incremental Lift on 25-Degree Wing

Figure 21 - Incremental Lift Characteristics of Tail, Canard, and Trisurface Configurations

alone configuration. Figure 22 presents a comparison between the measured incremental lift and the sum of the individual increments of the canard and horizontal tail. In general, the measured data are less than the summed data. This is due to a changing of the downwash of the wing due to the canard, thus reducing the loading of the horizontal tail. The trends with Mach number are very similar, thus indicating that superposition of the increments is reasonable for a first approximation for preliminary design purposes.

PITCHING MOMENT

The variation of pitching moment coefficient with Mach number at an angle of attack of 25 degrees is shown in Figure 23. The configurations are the same as those shown in Figure 4. The canard is the truncated 45-degree delta C_0 located at position P_3. As expected, the pitching moment for both canard off and canard on configurations decreases with increasing Mach number. The canard causes a noseup moment, however, the incremental change between canard off and on is approximately constant with Mach number.

Figure 24 presents pitching moment for the 50-degree wing model at lift coefficients of 0.5 and 1.0. Data are presented for both canard on and off. The Mach number range is from 0.6 to 1.10.

The incremental change between the two configurations is constant at both lift coefficients throughout the Mach number range and the rate of decrease is also constant thereby indicating that the rate of change of neutral point with Mach number is the same for both canard on and off configurations.

POSITION

The effect of canard longitudinal position on the incremental pitching moment is shown in Figure 25. Data are for Mach numbers from 0.6 to 1.10 and the canard positions are P_1 and P_3. As expected, moving the canard forward increases the incremental pitching moment. The aft location had relatively constant values of ΔC_M with Mach number at constant angle of

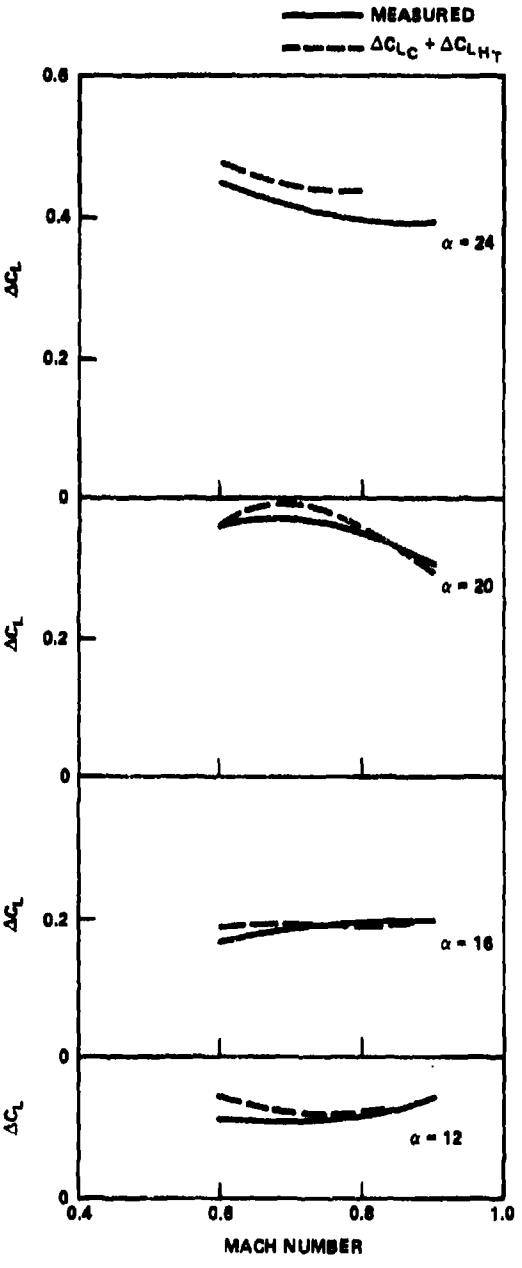

Figure 22a - Incremental Lift on 50-Degree Wing

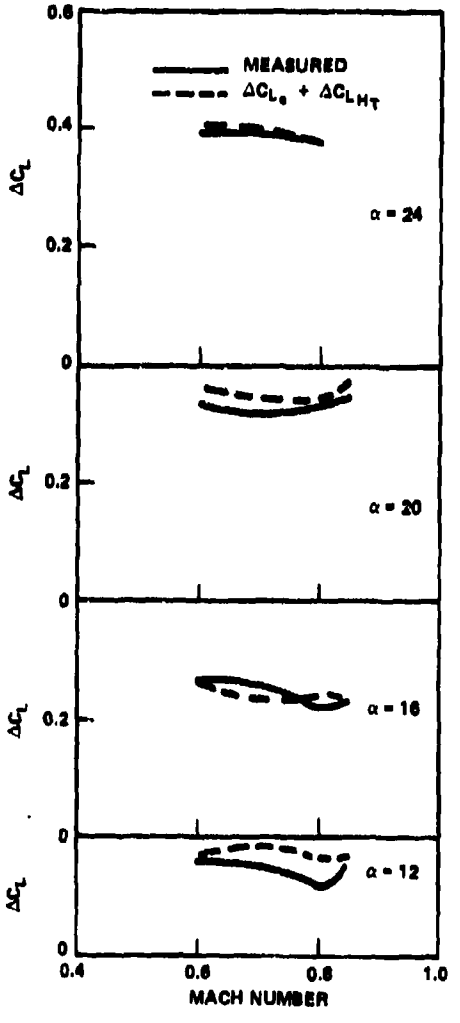

Figure 22b - Incremental Lift on 25-Degree Wing

Figure 22 - Comparison of Measured and Summed Trisurface Incremental Lift

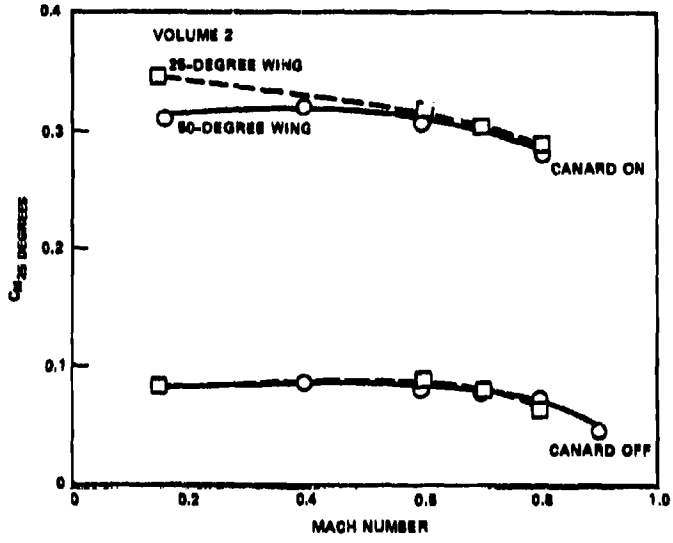

Figure 23 - Pitching Moment at 25-Degrees Angle of Attack

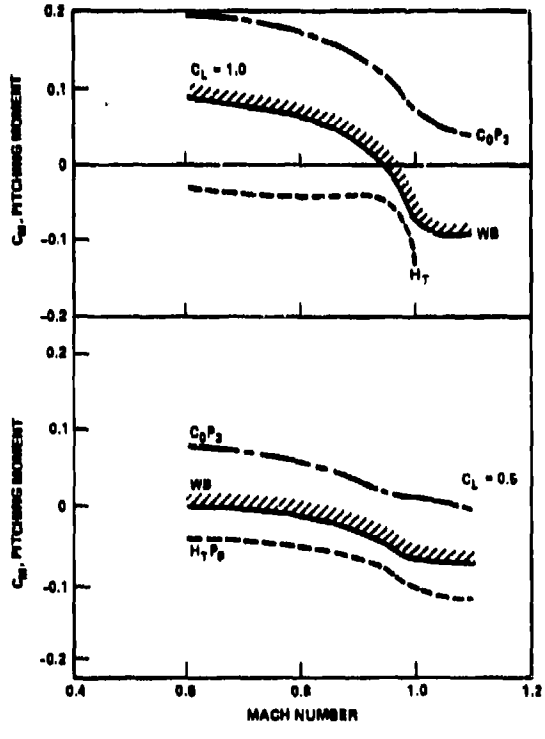

Figure 24 - Comparison of Pitching Moment for Tail, Canard, and Basic Wing-Body at Lift Coefficients of 0.5 and 1.0 for the 50-Degree Sweep Model

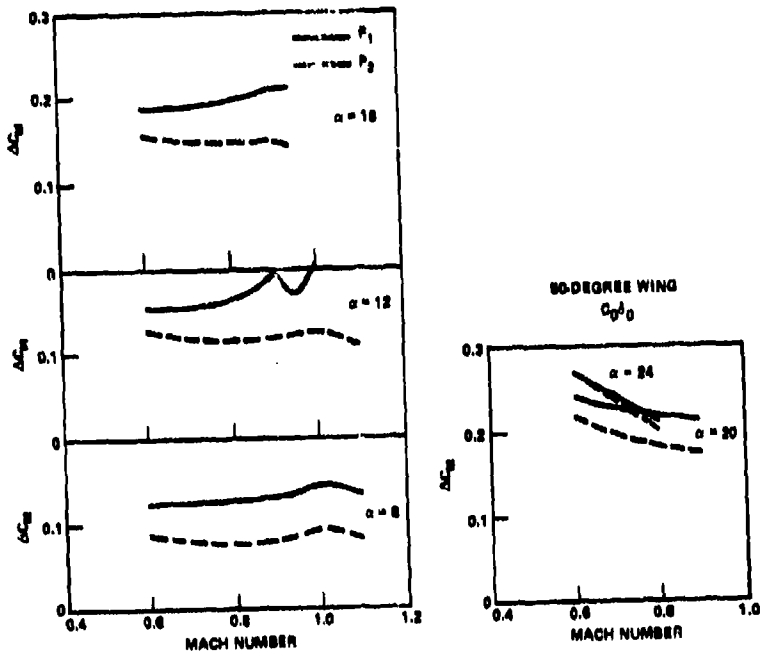

Figure 25 - Effect of Position on Incremental Pitching Moment

attack. This is not the case for the forward position P_1 particularly at α = 12 and 16 degrees. At these angles, the incremental moment increases with increasing Mach number. This behavior in pitching moment is somewhat at odds with the incremental lift data presented in Figure 8. The incremental lift tended to increase at the same rate for both positions. At the higher angles of attack the incremental moment dropped off with increasing Mach number which is keeping with the trends on incremental lift. At low Mach numbers the incremental moment continually increased with increasing angle of attack up to the highest angle of attack presented ($\alpha \approx$ 24 degrees). As Mach number is increased, there is evidence of a distinct stall of the canard for the forward position in that ΔC_M is lower at 24 degrees than at 20 degrees. Similarly, it appears that this stall may also occur for the aft canard P_3 albeit at a higher Mach number. This behavior is at variance with the results observed at subsonic speeds, where no loss in incremental moment was observed for the P_3 position up to angle of attack of 32 degrees and no reduction occurred for the P_1 position up to 28 degrees angle of attack. Thus, it appears that this reduction in moment is purely a Mach number effect.

Similar trends are noted in Figure 26 where the 60-degree delta canard is shown at positions P_2, P_3, and P_6. The change of incremental pitching moment with Mach number is far more severe for the forward position P_2 than for either aft positions.

These trends did not occur for the 25-degree wing model, however. Figure 27 presents data for the C_0 canard at positions P_1, P_2, and P_3. The effectiveness of the forward canard is dropping off with increasing angle of attack. This reduction in effectiveness with forward canard location has been observed, however, from the subsonic data.

The difference in incremental moment behavior between the two wing sweeps may be due, in part, to the canard delaying separation on the swept back wing tips of the 50-degree wing. This shifts the center of pressure of the wing aft thereby reducing the noseup moment of the canard. The 25-degree wing, having little sweep, would not experience this effect on moment.

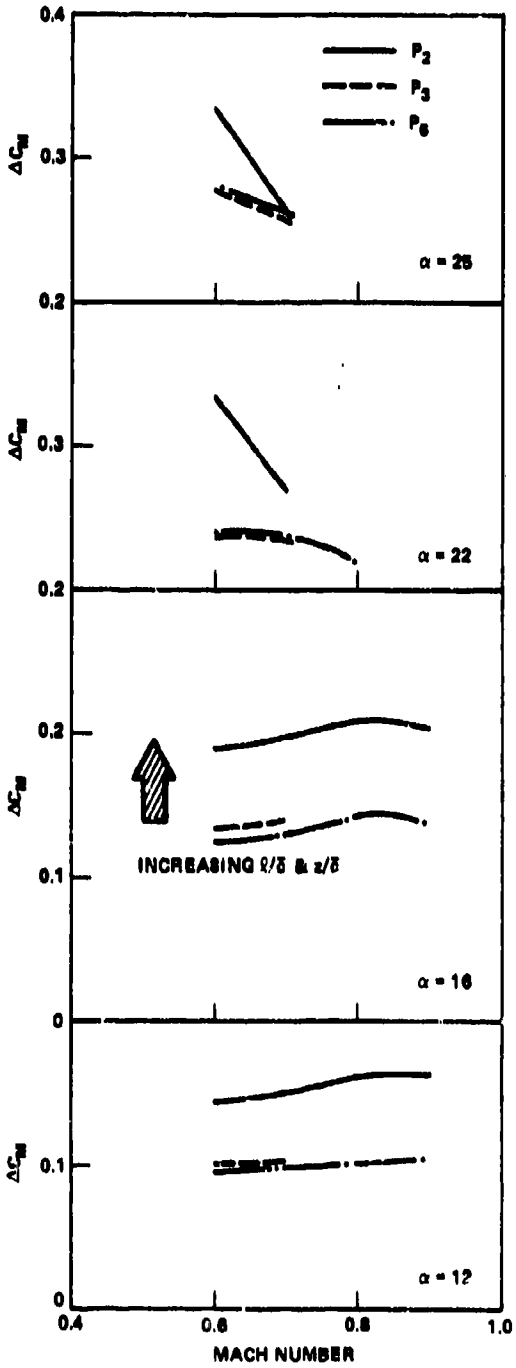

Figure 26 - Effect of Position on Incremental Moment for Canard C_1

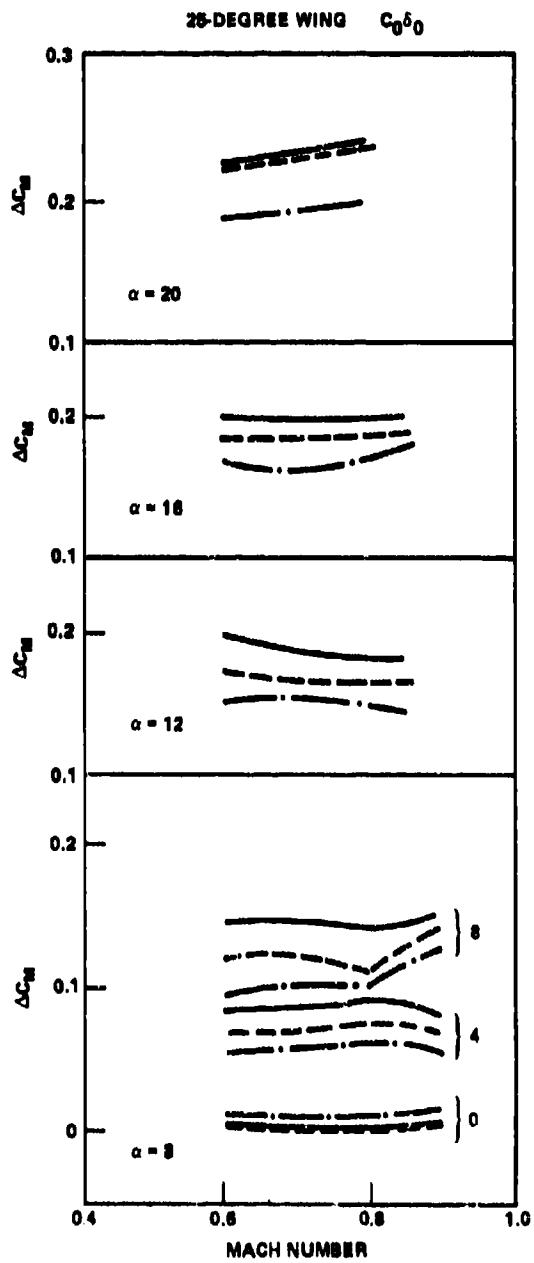

Figure 27 - Effect of Canard Position for 25-Degree Wing Model

When the angle of attack is allowed to vary and pitching moment is plotted against Mach number at constant C_L as in Figure 28, we see the rate of change of moment with Mach number is approximately the same for both canard on and off. Figure 28 presents data for the C_0 canard at positions P_1, P_3, and P_7. Positions P_1 and P_3 exhibit the same trend as the basic wing-body. Position P_7, which is the canard nearly in the wing chord plane, exhibits a dropoff in moment at $C_L = 1.0$ and is approximately the same as position P_3 at $C_L = 0.5$. This dropoff and having the same value as position P_3 indicate that this is a poor canard location. Because position P_7 is located forward of position P_3, the moment should be increased at $C_L = 0.5$ merely based on canard volume coefficient considerations.

The effect of canard position on neutral point shift with Mach number is indicated in Figure 29. Figure 30 presents the identical data, however, the appropriate neutral point variation at M = 0.6 has been subtracted from the data for each configuration. As can be seen in the figures, the neutral point shift with Mach number is approximately the same for the most aft position P_3 as for the basic wing-body. For the other two positions, the stability is increasing at a faster rate than the basic wing-body. This is especially the case for the canard located in the forward position P_1.

The effect of canard vertical position on the incremental pitching moment is presented in Figure 31. In general, the trends with incremental pitching moment with vertical position follow those trends exhibited by the incremental lift characteristics presented in Figure 11. Therefore, the position had the greater lift value also had the largest moment value.

The magnitude of the pitching moment change was usually less than the corresponding lift change indicating that the majority of the lift change is on the wing rather than on the canard. The largest change in pitching moment due to canard vertical position was at positions P_2 and P_7 on the 25-degree wing. Position P_7 is very close to the wing and ΔC_M was reduced approximately 0.1 by lowering the canard.

In general, lowering the canard reduced the incremental pitching moment at low angles of attack and low Mach numbers for the 50-degree wing

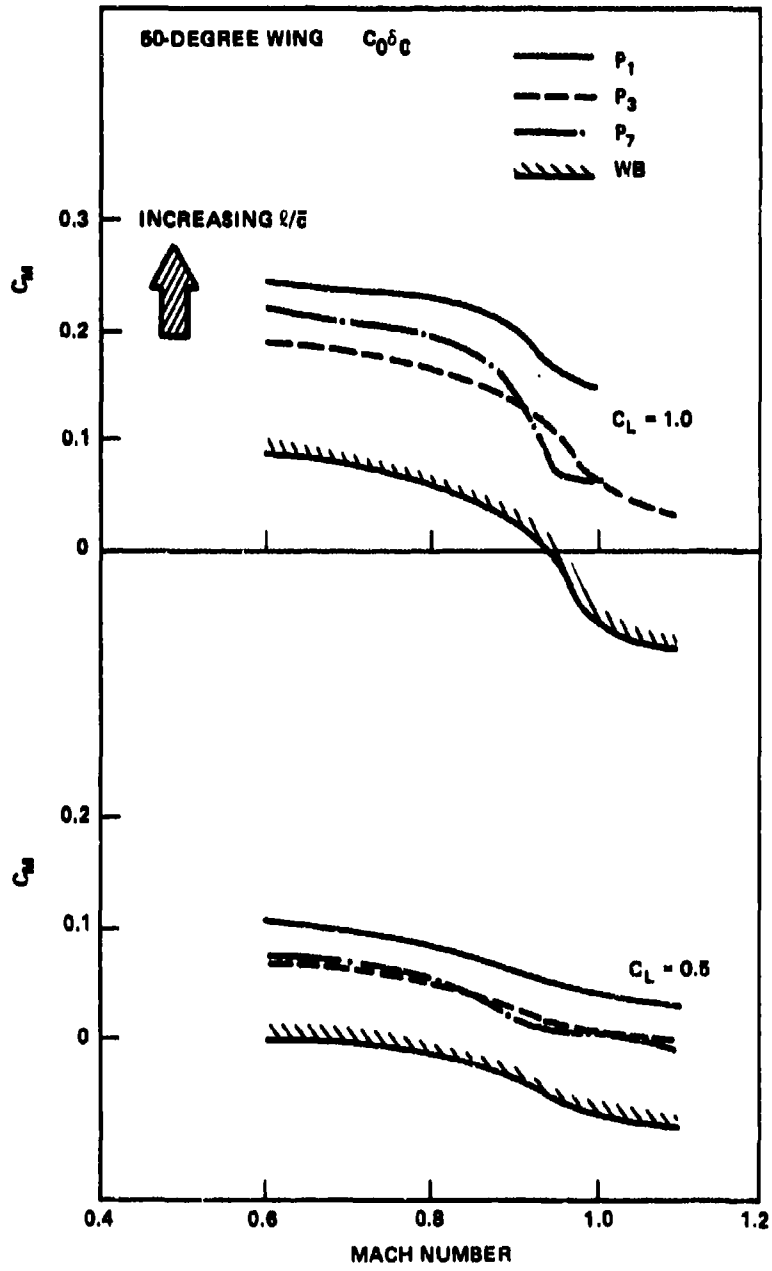

Figure 28 - Pitching Moment Variation with Mach Number at Constant Lift Coefficient

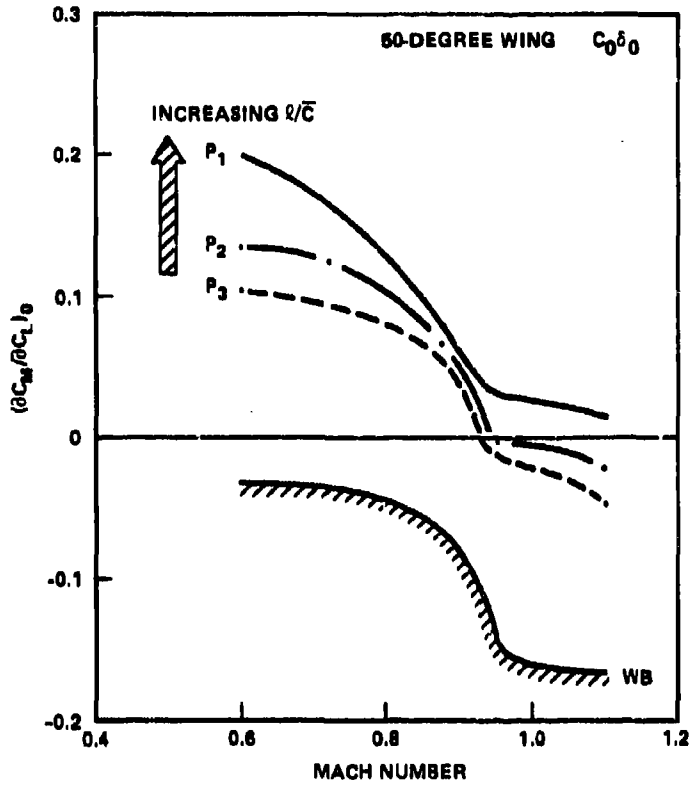

Figure 29 - Neutral Point Variation with Mach Number

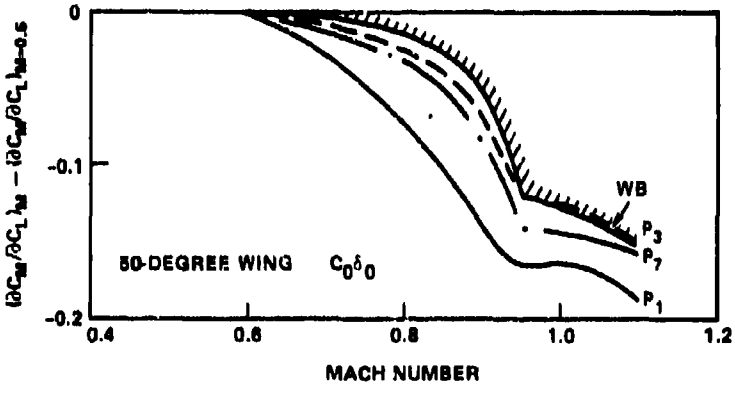

Figure 30 - Incremental Neutral Point Behavior with Mach Number

Figure 31 - Effect of Canard Vertical Position
on Incremental Moment

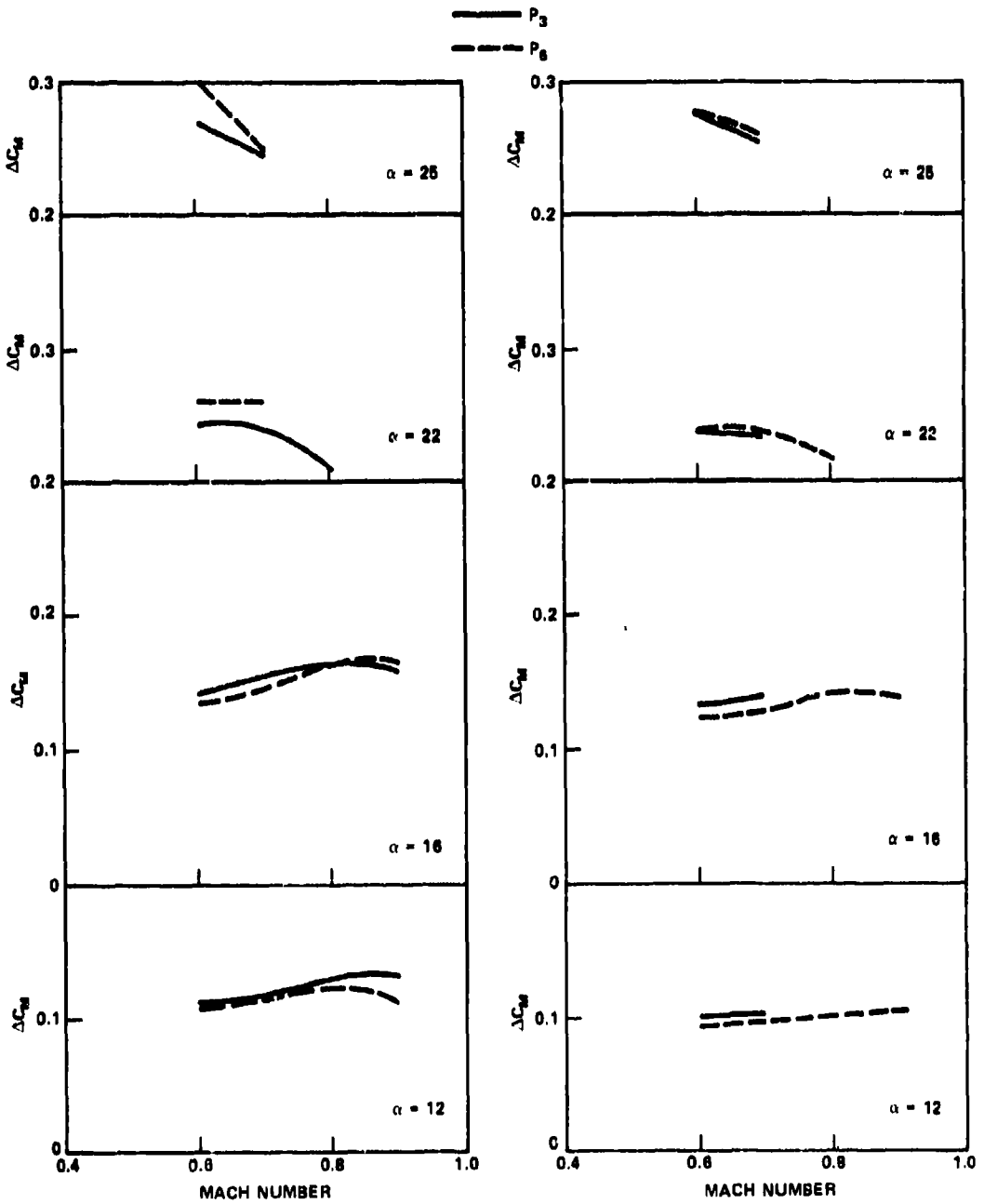

Figure 31a - Canard C_0 on
50-Degree Wing

Figure 31b - Canard C_1 on
50-Degree Wing

Figure 31 (Continued)

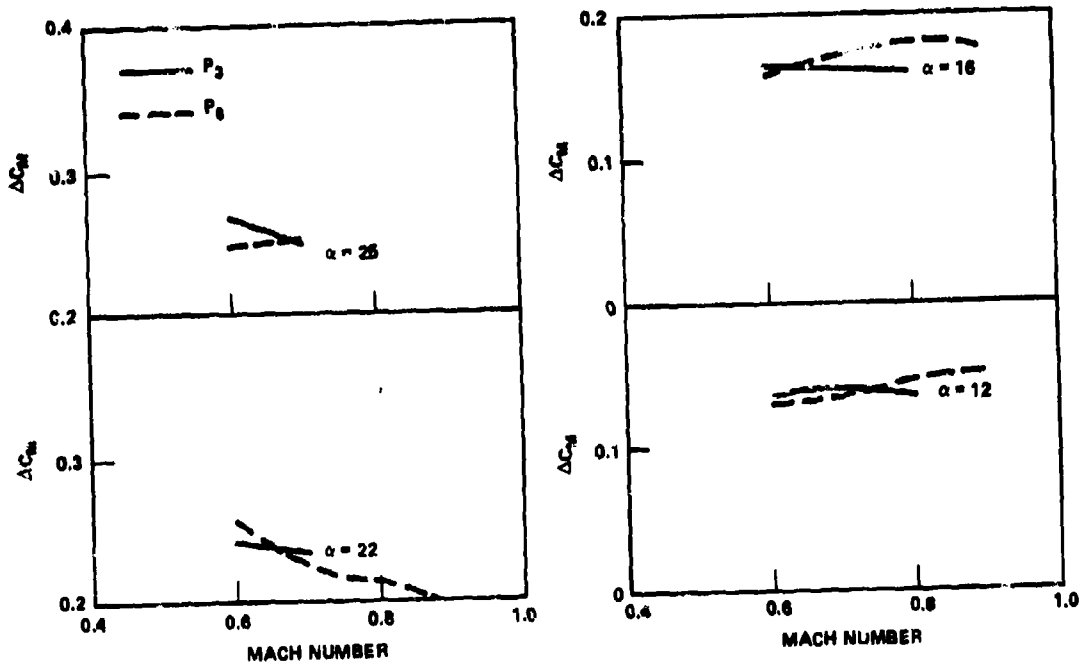

Figure 31c - Canard C_2 on 50-Degree Wing

Figure 31 (Continued)

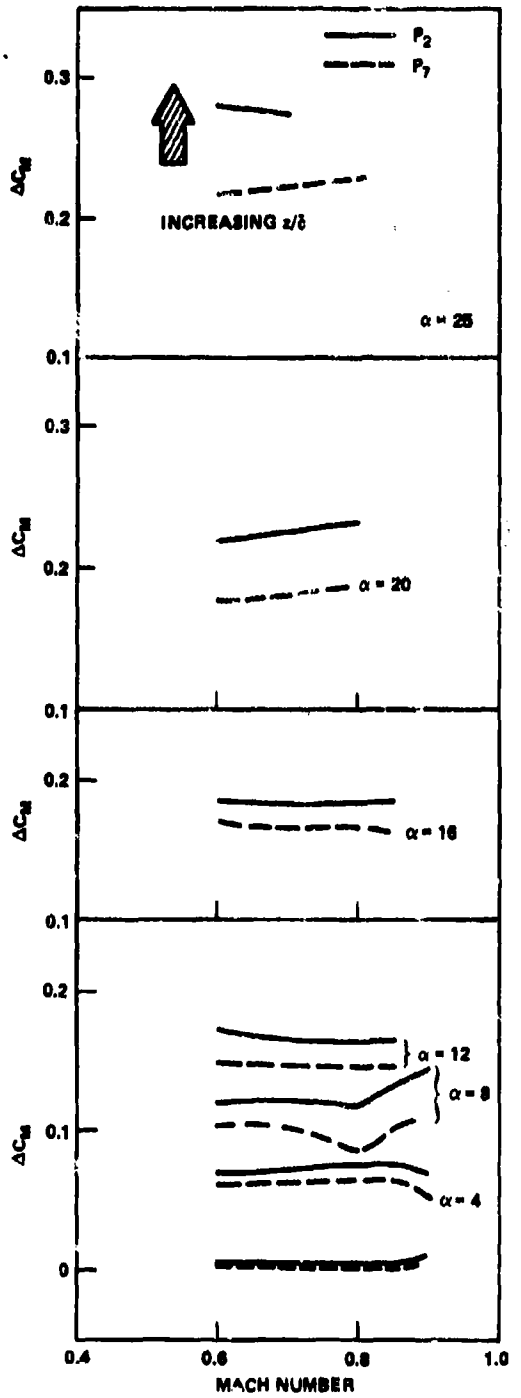

Figure 31d - Canard C_0 on 25-Degree Wing

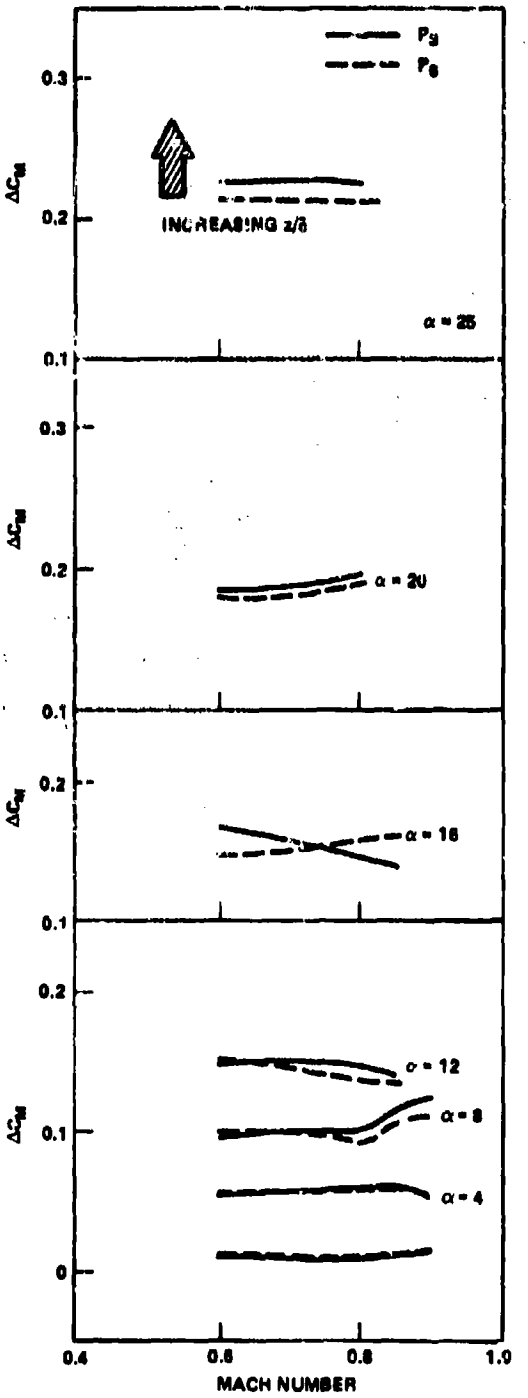

Figure 31e - Canard C_0 on 25-Degree Wing

model. At high Mach numbers the difference in ΔC_M between positions was small. In the case of the 45-degree truncated delta canard C_0, the lower position had a larger incremental moment than the upper position at angles of attack greater than 20 degrees. This behavior was the same for the 60-degree delta canard C_1.

The effect of canard vertical position on the 25-degree wing was somewhat different than that of the 50-degree wing model. Lowering the canard on the 25-degree wing model caused a reduction in incremental pitching moment at both longitudinal stations evaluated.

CANARD SHAPE

The effect of canard shape on the incremental moment characteristics is shown in Figure 32. In Figure 12, it was shown that increasing canard leading edge sweep increased incremental lift at high angles of attack. This, however, is not the case with incremental moment. Canard C_3, the 25-degree high aspect ratio canard had the largest incremental moment at $\alpha = 25$ degrees, but had the lowest incremental lift. This was also the case at $\alpha = 22$ degrees. Since the lift was lower for this canard and the moment greater, the canard had less of an effect on the wing than the higher sweep canards.

At low angles of attack the incremental moment decreases with increasing canard sweep angle. This is to be expected since, as was shown at subsonic speeds in Volume 2, the moment contribution due to the canard is proportional to the individual lift curve slope C_{L_α} of each canard; the low sweep canards have a higher C_{L_α}.

DEFLECTION

The effect of both positive and negative canard deflections on the incremental moment characteristics are presented in Figure 33. Data are presented for position P_3 on the 50-degree wing model, and positions P_1 and P_3 for the 25-degree wing model. The canard is C_0 for both models. As indicated in the figure, at low angles of attack the increment due to deflection is approximately the same for either positive or negative

Figure 32 - Effect of Canard Shape on Incremental Moment for the 50-Degree Wing

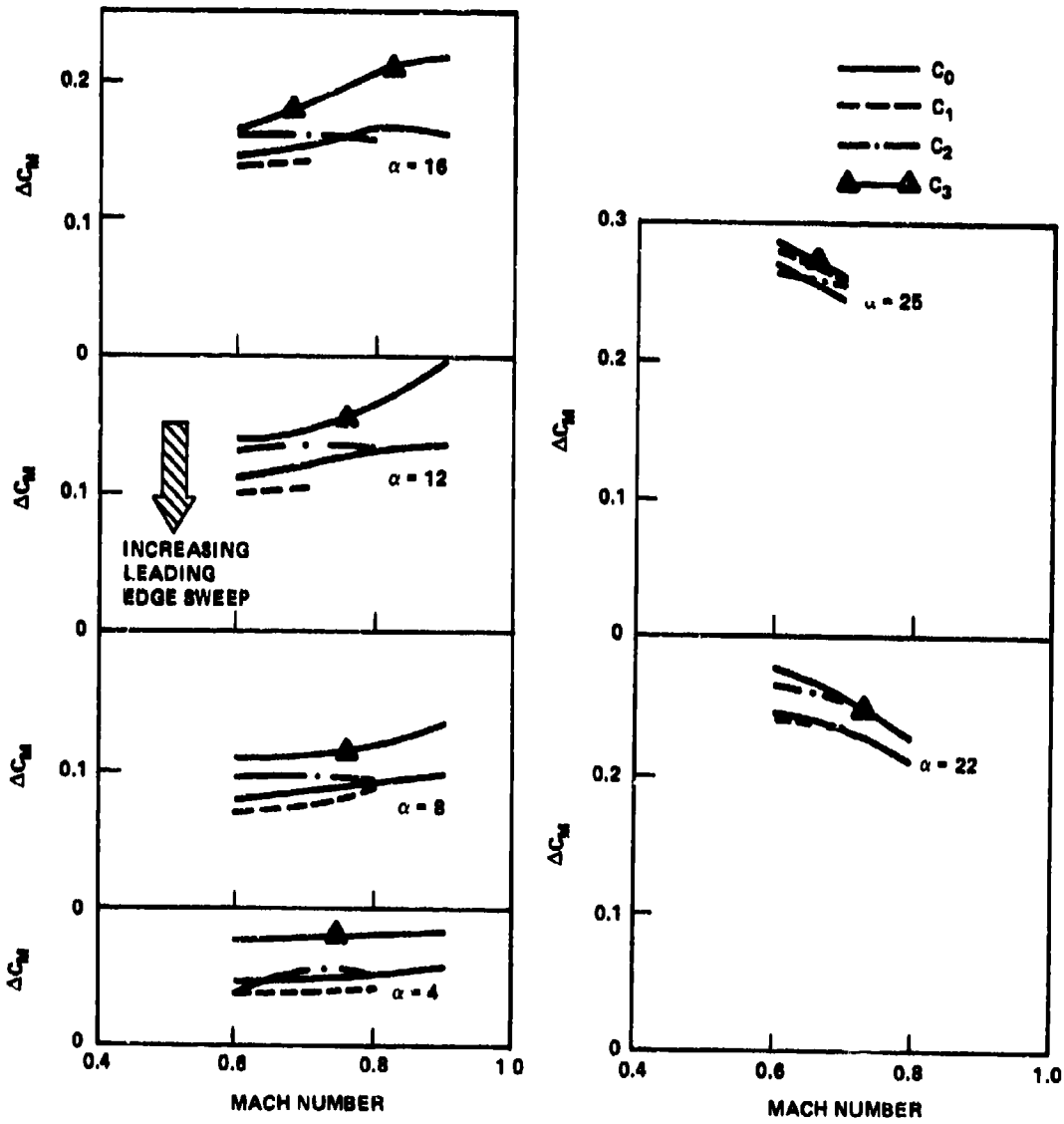

Figure 32a - Position P_3

Figure 32 - (Continued)

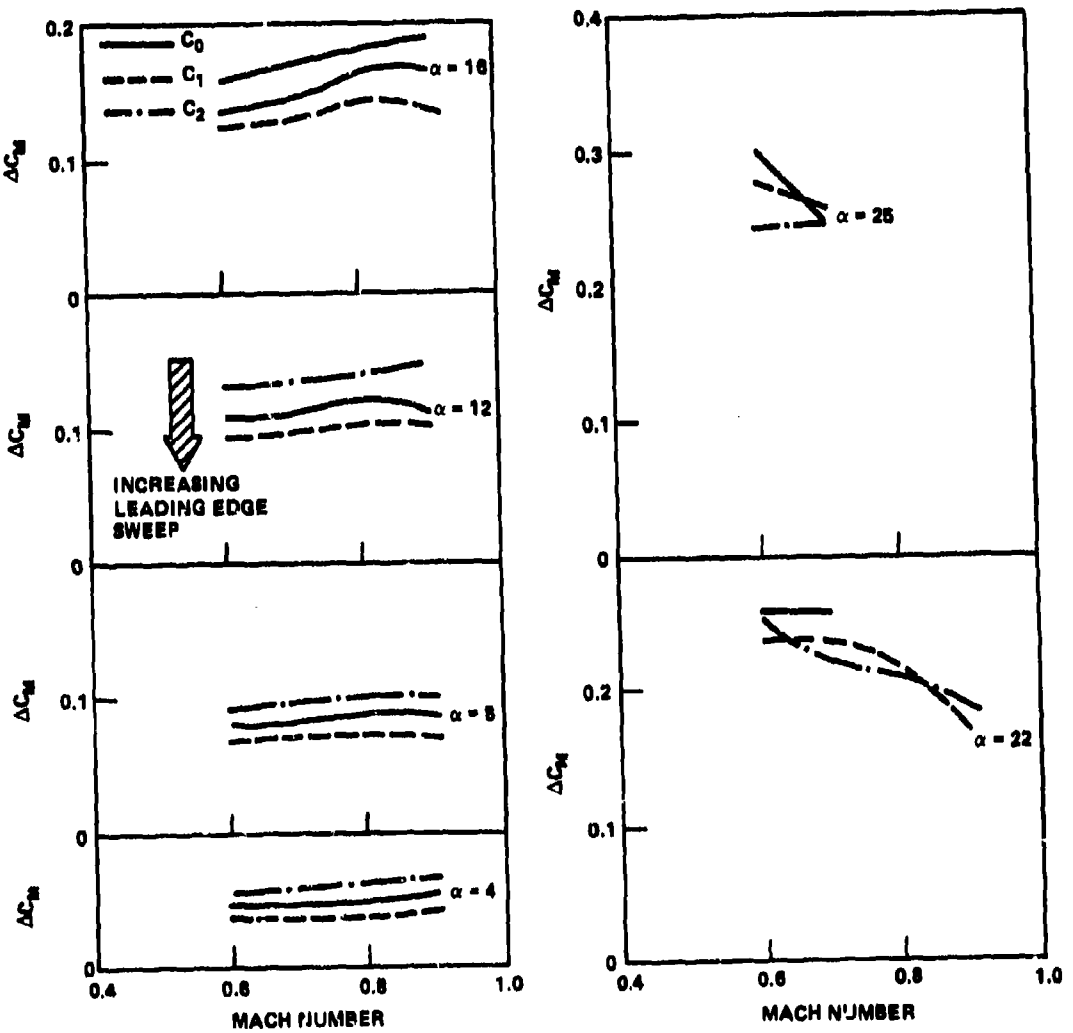

Figure 32b - Postion P_6

Figure 33 - Effect of Canard Deflection on Incremental Moment

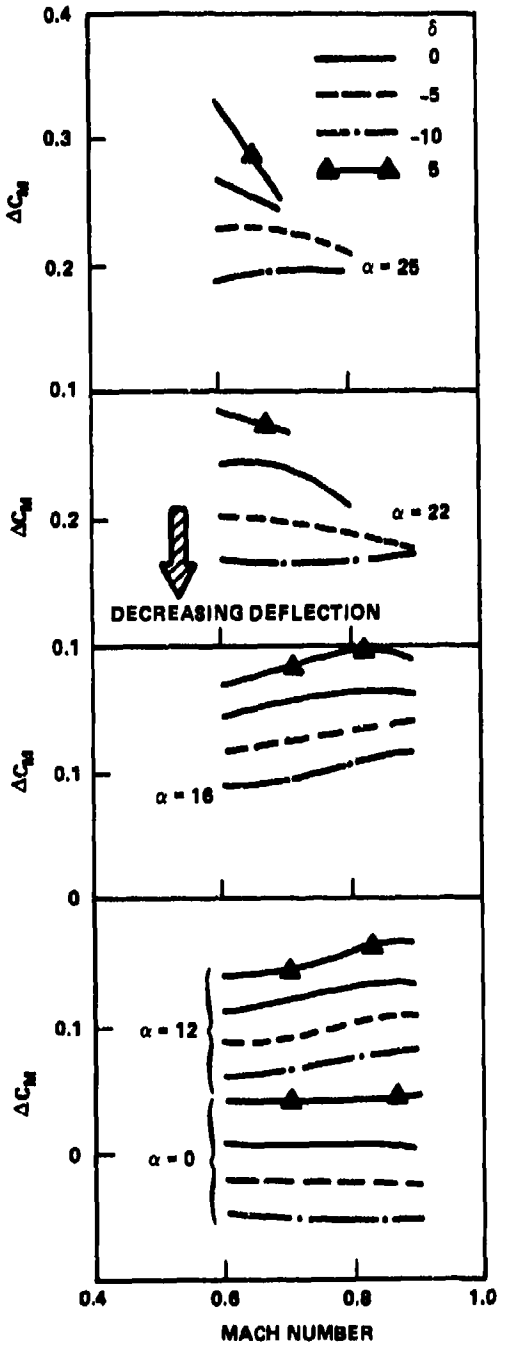

Figure 33a - Position P_3 on 25-Degree Wing

Figure 33 (Continued)

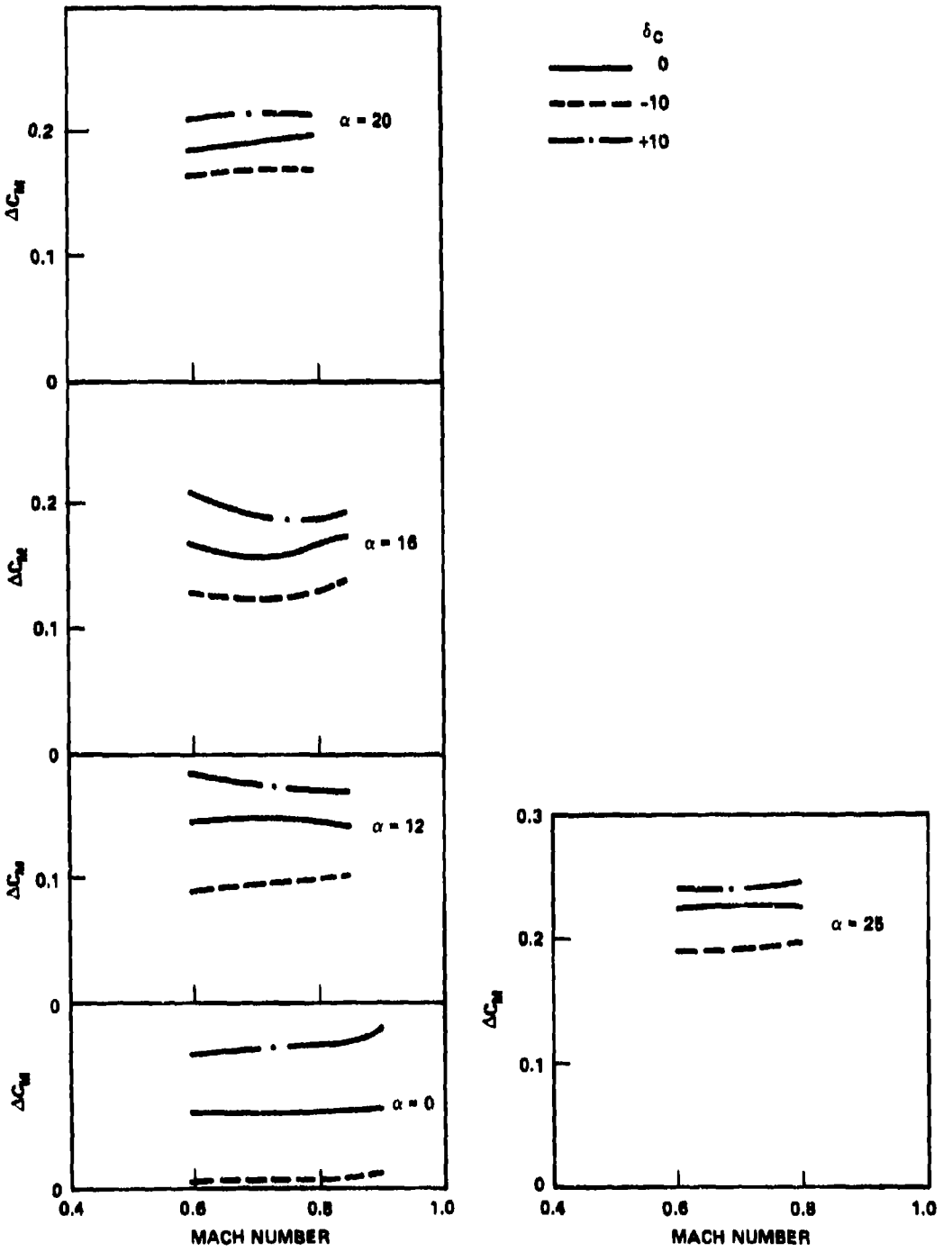

Figure 33b - Position P_3 on 25-Degree Wing

Figure 33 (Continued)

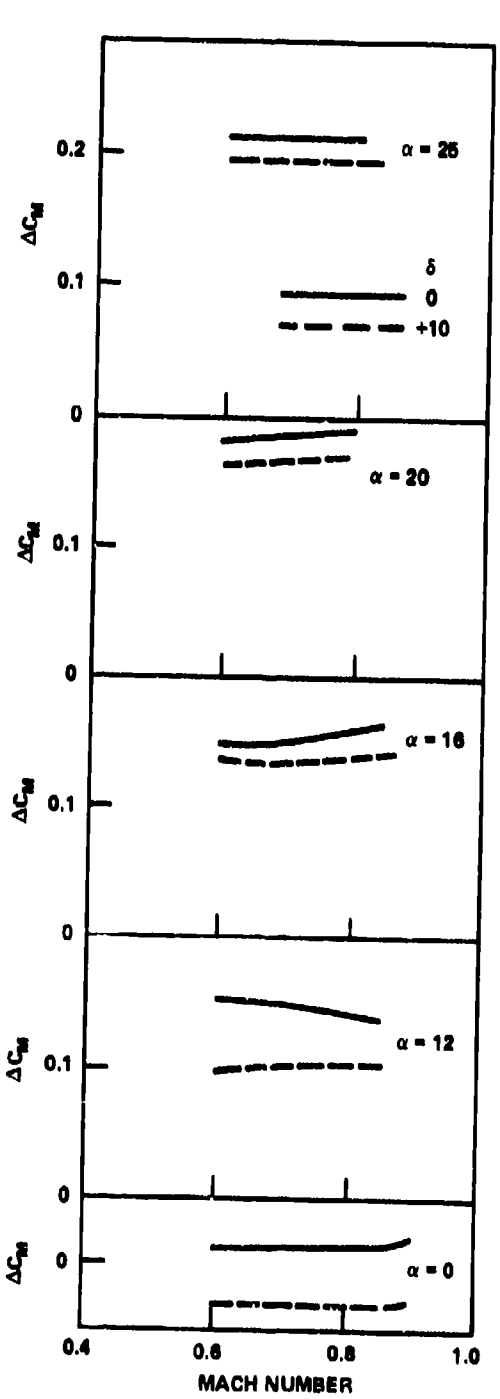

Figure 33c - Position P_1 on 25-Degree Wing

deflection. As angle of attack is increased, there is a reduction in incremental moment for the positive deflection when compared with the corresponding negative deflection. This is particularly true for the 25-degree wing model.

At the far canard location P_1, on the 25-degree wing model, there is a sizable reduction in the magnitude of incremental moment when the angle of attack is increased. A comparison of the increment at 0 degrees $\Delta C_M \sim 0.1$ and 12-degrees angle of attack $\Delta C_M \sim 0.02$ indicates a probable canard stall. Beyond 12-degrees angle of attack ΔC_M due to positive deflection is larger.

It is interesting to note the difference in behavior between the 25-degree and 50-degree wing models with increasing Mach number. The 25-degree wing model shows only small changes in ΔC_M with increasing Mach number. The 50-degree wing model, however, exhibits a rise in ΔC_M with Mach number at low angles of attack and a decrease in ΔC_M with Mach number at high angles of attack. Thus it appears that the canard on the 25-degree wing is relatively insensitive to Mach number, whereas the 50-degree wing model exhibits significant changes. These changes, however, are due to the canard on the 50-degree wing having a more favorable effect on delaying outer wing panel separation, thus moving the overall vehicle center of pressure further aft.

As proof of these statements data for the incremental center of pressure shift with Mach number are presented in Figure 34. The incremental center of pressure is defined as $\Delta C_D = C_P - C_{P_{M=0.6}}$, where $C_P = CM/C_L$. Data are presented at constant angle of attack for both 25- and 50-degree sweep models. As shown, deflection of the canard has only minimal effect on the incremental C_P shift for the 25-degree sweep model. The 50-dagree model exhibits significant changes in ΔC_P between positive and negative canard deflections and these changes increase with increasing angle of attack. As shown, positive deflection causes an increase in aft center of pressure travel and this increase is greater than the basic wing-body. Since it is unlikely that the canard stall angle would be less for the 50-degree wing than for the 25-degree wing, the difference between the two

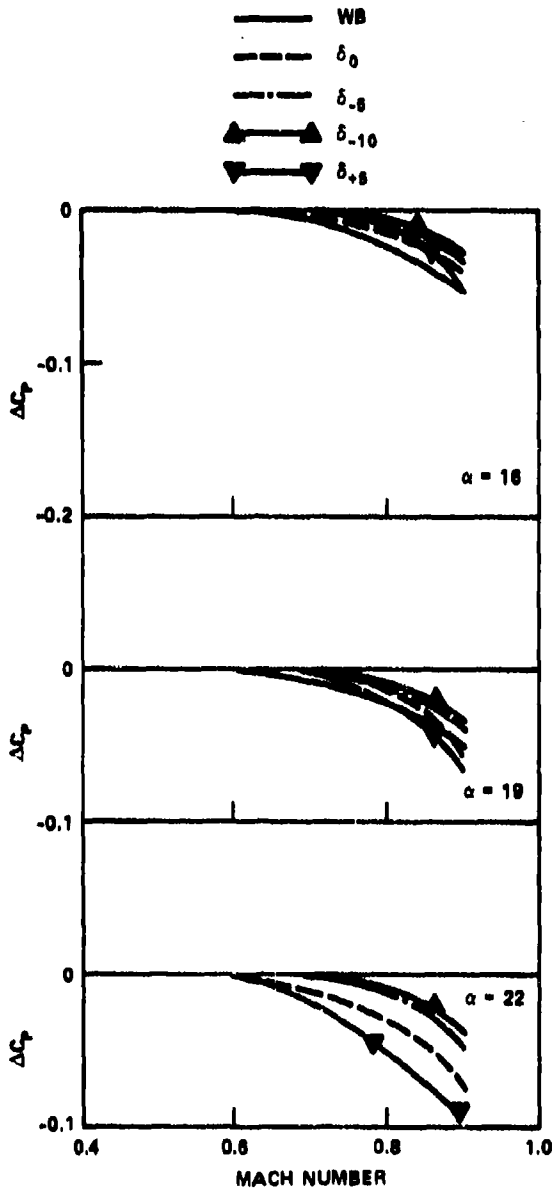

Figure 34a - Deflection for 50-Degree Wing

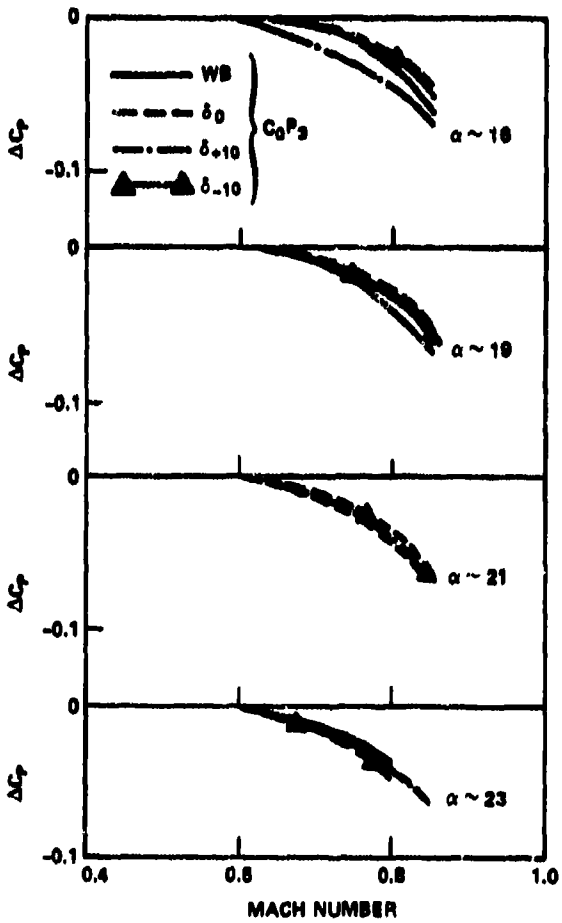

Figure 34b - Deflection for 25-Degree Wing

Figure 34 - Effect of Canard Deflection on Center of Pressure

center of pressure movements must be due to the main wing shape. In order to have an aft C_p shift, the canard on the 50-degree wing must be delaying stall over the outboard panel of the 50-degree wing, thus moving the overall wing center of pressure aft.

The remainder of the incremental moment data due to canard deflection are presented in Figure 35. These data are for the three canards C_1, C_2, and C_3 located at positions P_3 and P_6. The deflection angles are 0 and -5 degrees for these two positions. The deflection angles are 0, -5, and -10 degrees for the C_0 canard located at position P_6. Data for the C_0 canard at position P_3 have already been presented in Figure 33. In general, canard deflection does not change the trend of incremental moment with Mach number for any of the canards. Differences do occur with angle of attack for the various canard shapes. The low aspect ratio canards C_0 and C_1 exhibit a larger reduction in moment at high angles of attack than at low angles of attack.

This behavior is in keeping with the previous discussion in that the low aspect ratio canards have a greater influence on the wing center of pressure. This influence is diminished somewhat by negative deflections.

The higher aspect ratio canards C_2 and C_3 show only small changes in incremental moment with deflection. The incremental moment is reduced by negative deflection, but the trends with Mach number are approximately the same for either deflection angle.

The variation of canard control power $C_{M_{\delta_c}}$ with angle of attack is presented in Figure 36. Data are presented for Mach numbers of 0.6 and 0.8 for both 25- and 50-degree sweep models. The data were obtained from Figures 33 and 35, and are based primarily on $\delta_c = 0$ and -5 degrees. In general, canards C_0 and C_1 show very little difference with Mach number at positions P_3 and P_6. Increasing Mach number improved $C_{M_{\delta_c}}$ at position P_2 for canard C_1 on the 50-degree wing and position P_1 for the 25-degree wing with canard C_0. Canard control power, $C_{M_{\delta_c}}$ tended to increase with angle

Figure 35 - Incremental Pitching Moment Due to Canard Deflection

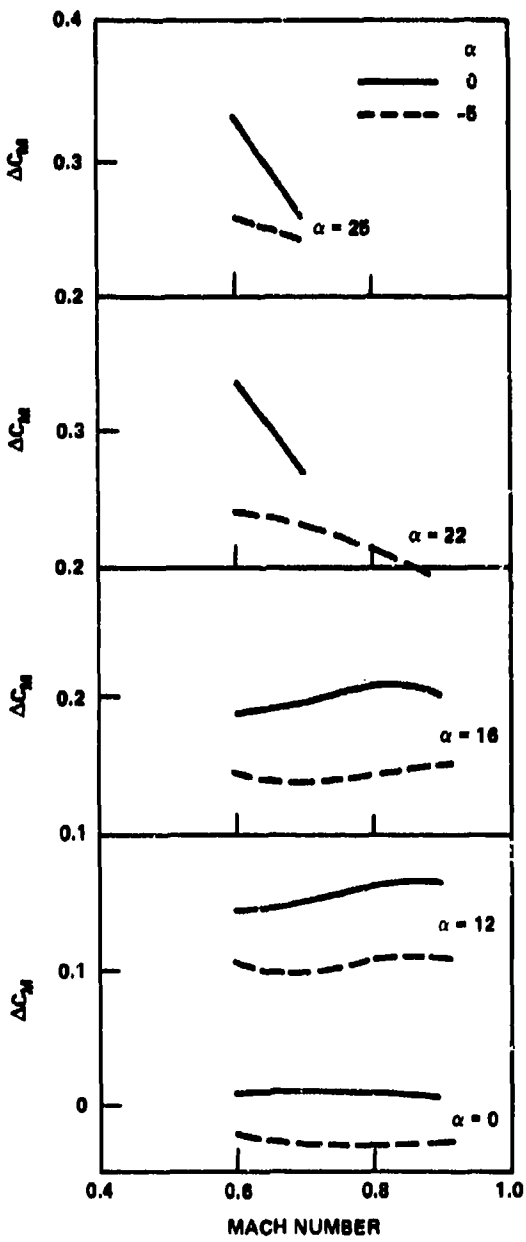

Figure 35a - Canard C_1 on 50-Degree Wing at Position P_2

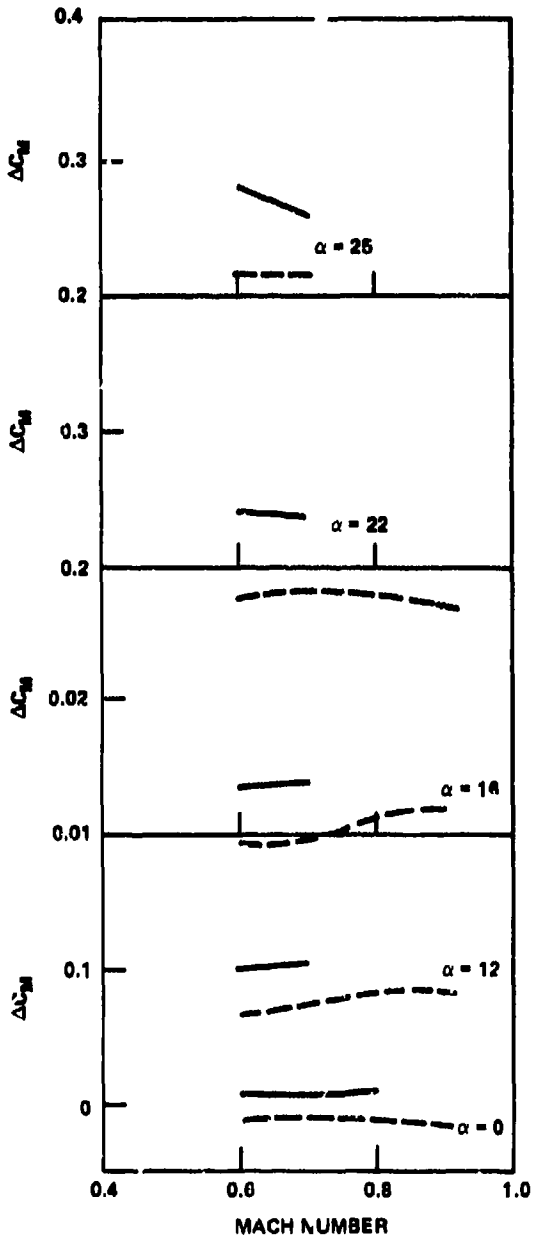

Figure 35b - Canard C_1 on 50-Degree Wing at Position P_3

Figure 35 (Continued)

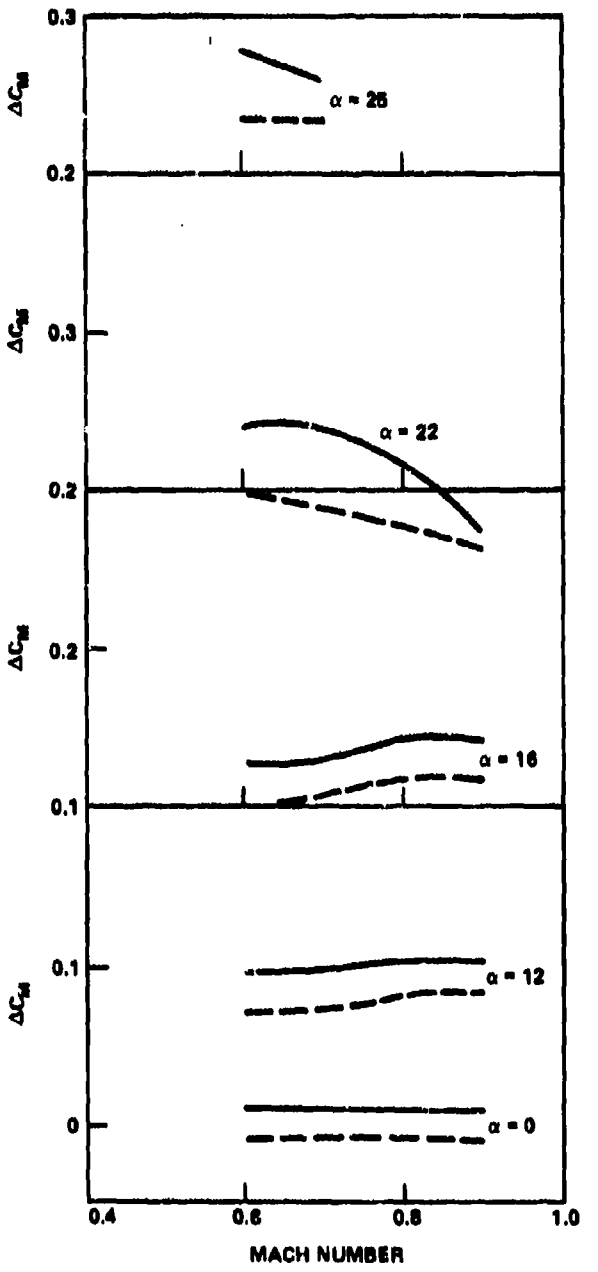

Figure 35c - Canard C_l on 50-Degree Wing at Position P_6

Figure 35 (Continued)

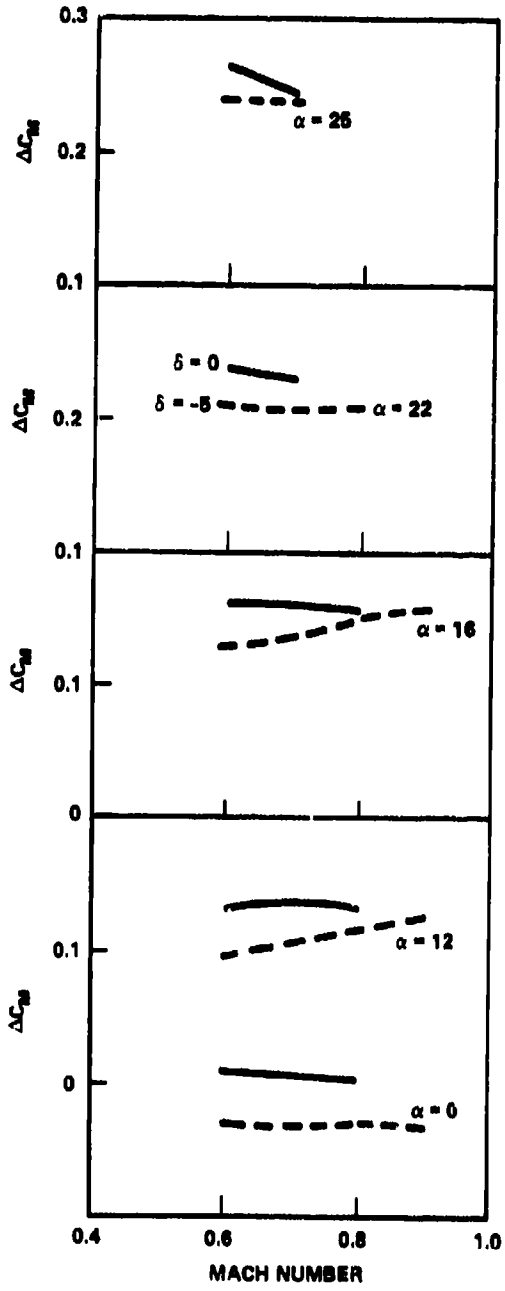

Figure 35d - Canard C_2 on 50-Degree Wing at Position P_3

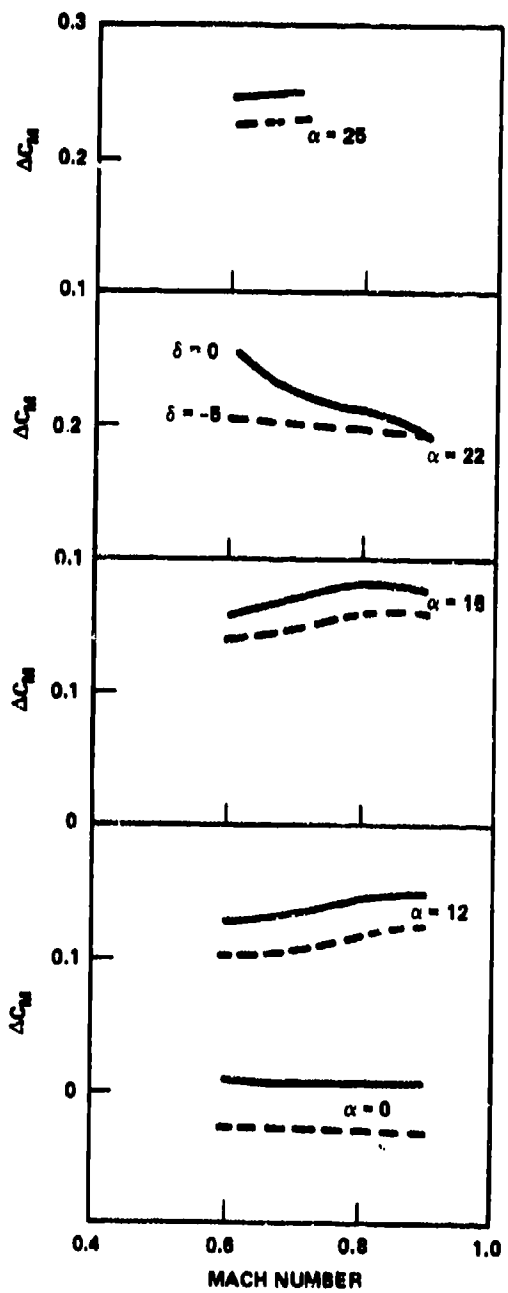

Figure 35e - Canard C_2 on 50-Degree Wing at Position P_6

Figure 35 (Continued)

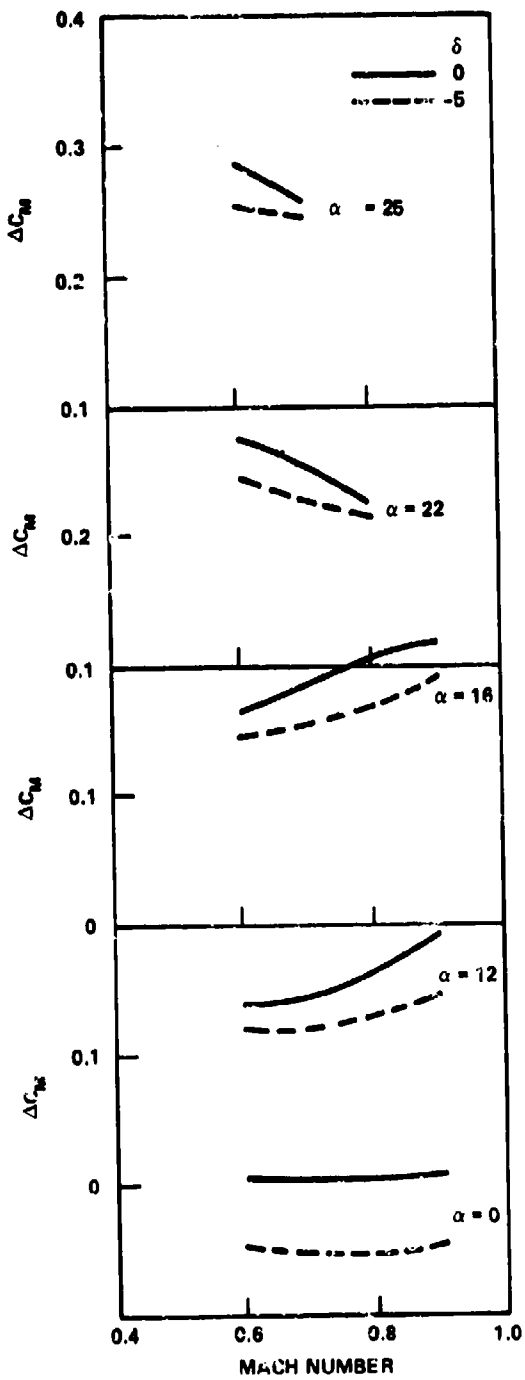

Figure 35f - Canard C_3 on 50-Degree Wing at Position P_3

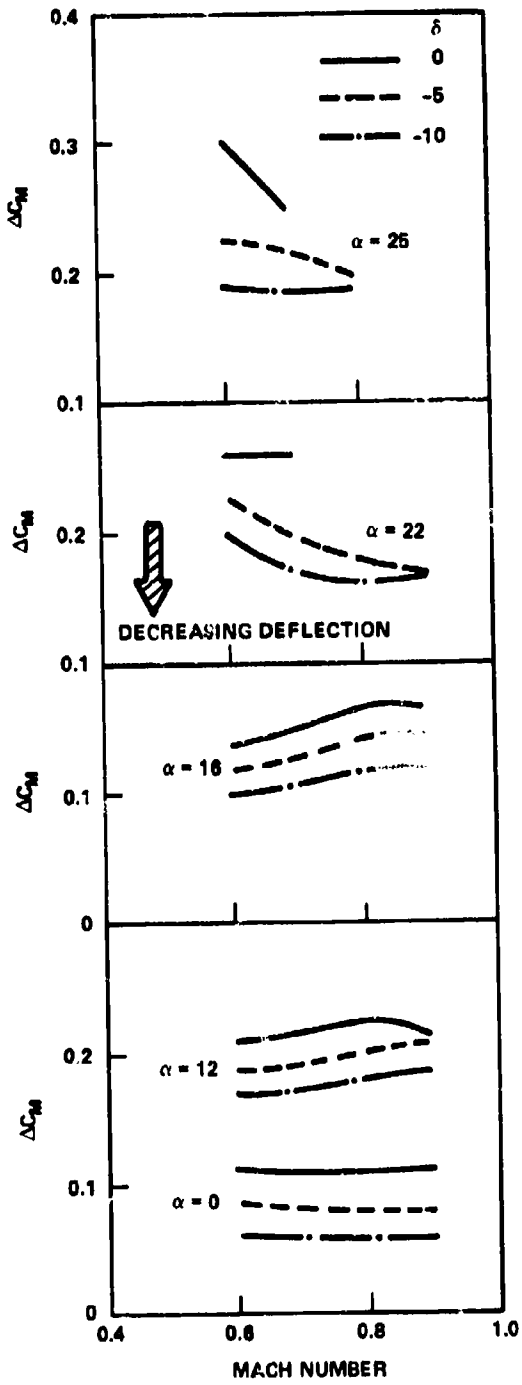

Figure 35g - Canard C_0 on 50-Degree Wing at Position P_6

Figure 36 - Canard Control Power versus Angle of Attack at Mach Numbers of 0.6 and 0.8

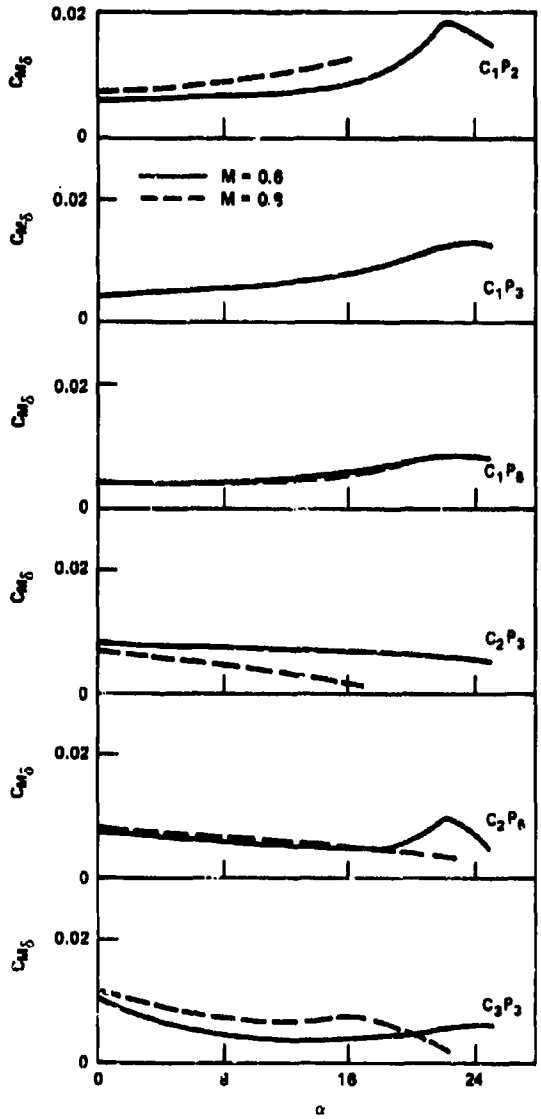

Figure 36a - Canards C_1, C_2, and C_3 on the 50-Degree Wing

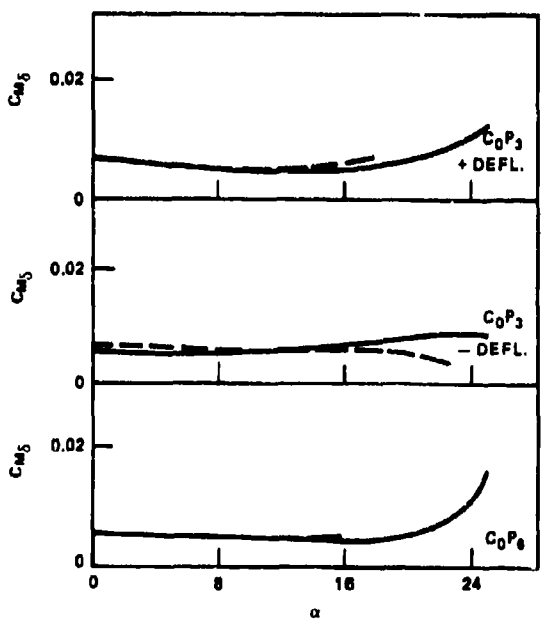

Figure 36b - Canard C_0 on the 50-Degree Wing

Figure 36 (Continued)

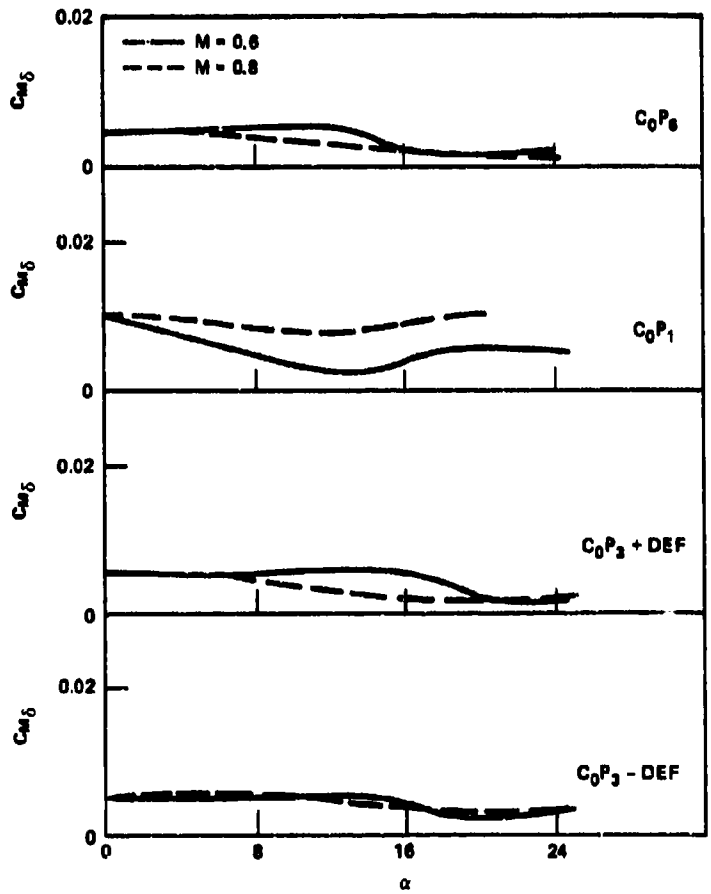

Figure 36c - Canard C_0 on the 25-Degree Wing

of attack for canards C_0 and C_1 on the 50-degree wing, however, $C_{M_{\delta_c}}$ decreased for the 25-degree wing. With increasing angle of attack, $C_{M_{\delta_c}}$ decreased for the high aspect ratio canards C_2 and C_3. Canard control power based on positive and negative deflections are presented in Figure 36c for canard C_0 on both models. There are no significant differences between the data for either positive or negative deflections until high angles of attack. At α = 25 degrees the positive deflection had a slightly higher $C_{M_{\delta_c}}$ for the 50-degree wing and a lower value for the 25-degree wing.

TRISURFACE CONFIGURATION

The basic pitching moment characteristics of the horizontal tail, canard, and trisurface configurations are presented in Figure 37 for both models at M = 0.6. The canard is deflected to -5 degrees on the 50-degree sweep model. As shown, the canard configuration exhibits no nosedown break, whereas the horizontal tail configuration breaks the stability at lift coefficient of 0.73 and 0.93 for the 25- and 50-degree models, respectively. Angles of attack for the nosedown break are 12 degrees for the 25-degree model and 19 degrees for the 50-degree model. Stable pitching moment breaks also occur, however, for the trisurface configurations at higher lift coefficients and higher angles of attack. In addition, the magnitude of the pitching moment change is not as severe for the trisurface configuration as those experienced by the horizontal tail configurations.

In both cases the increase in stability is delayed approximately 3-degrees angle of attack beyond the corresponding angle of attack of the horizontal tail.

The variation of the incremental pitching moments with Mach number for the three difference configurations is presented in Figure 38. Data are presented for both wing sweeps. The incremental moment data for the horizontal tail and the 25-degree wing model are relatively constant with Mach number, however, this is not the case for the 50-degree wing model. Between 0- and 8-degrees angle of attack, the variation with Mach number is

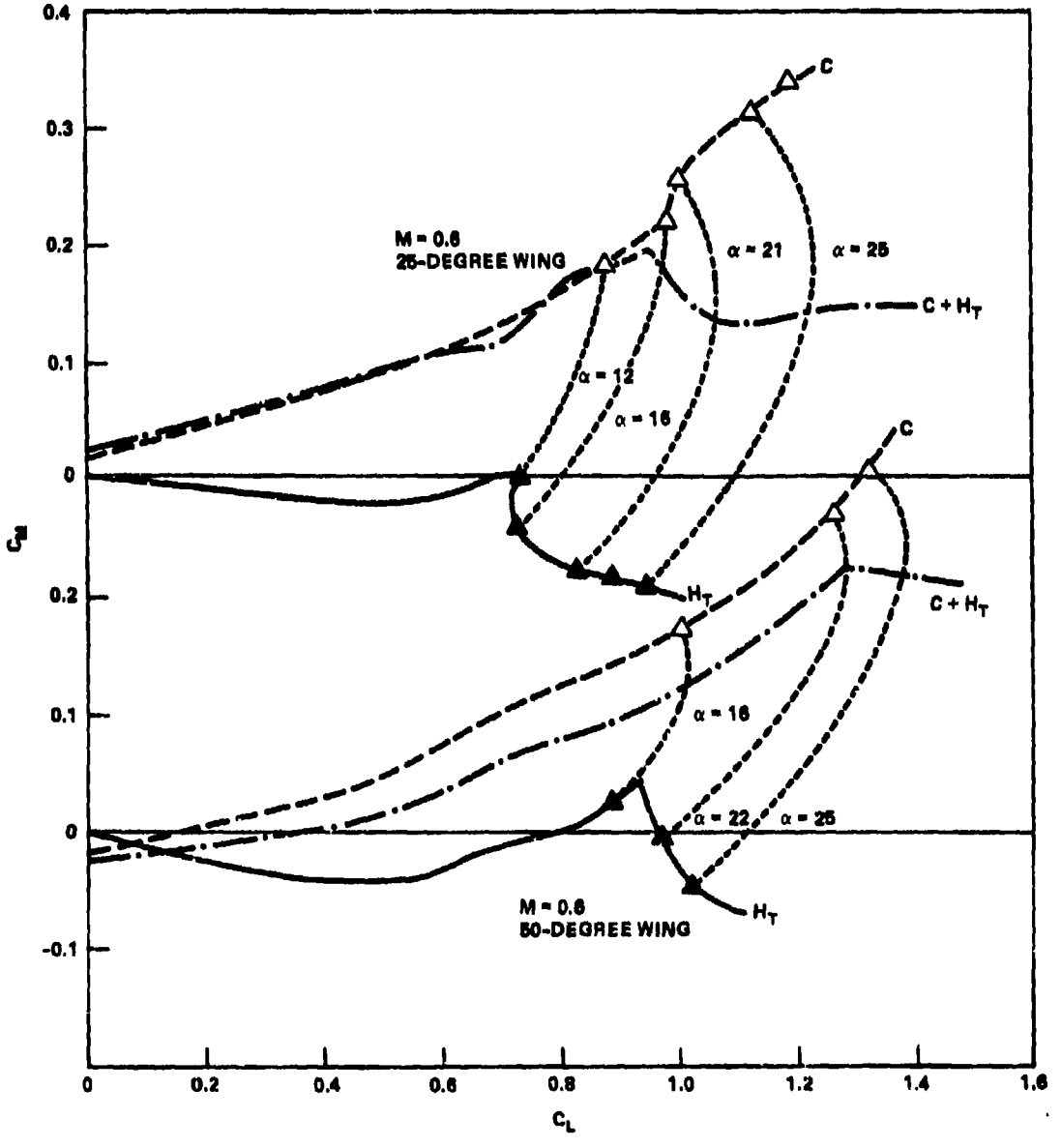

Figure 37 - Pitching Moment Characteristics of Tail, Canard, and Trisurface Configurations

Figure 38 - Incremental Moment Characteristics of Tail, Canard, and Trisurface Configurations

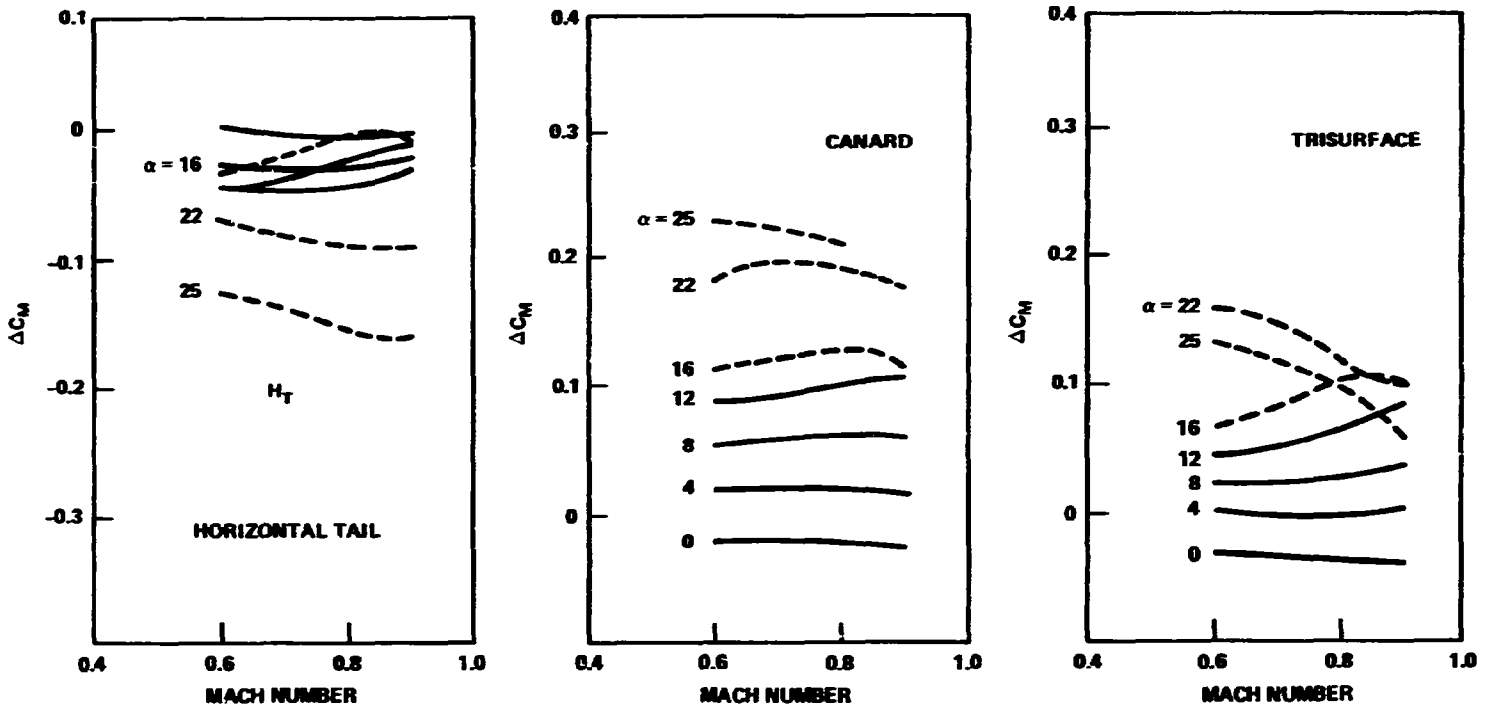

Figure 38a - Moment Characteristics for 50-Degree Wing

Figure 38 (Continued)

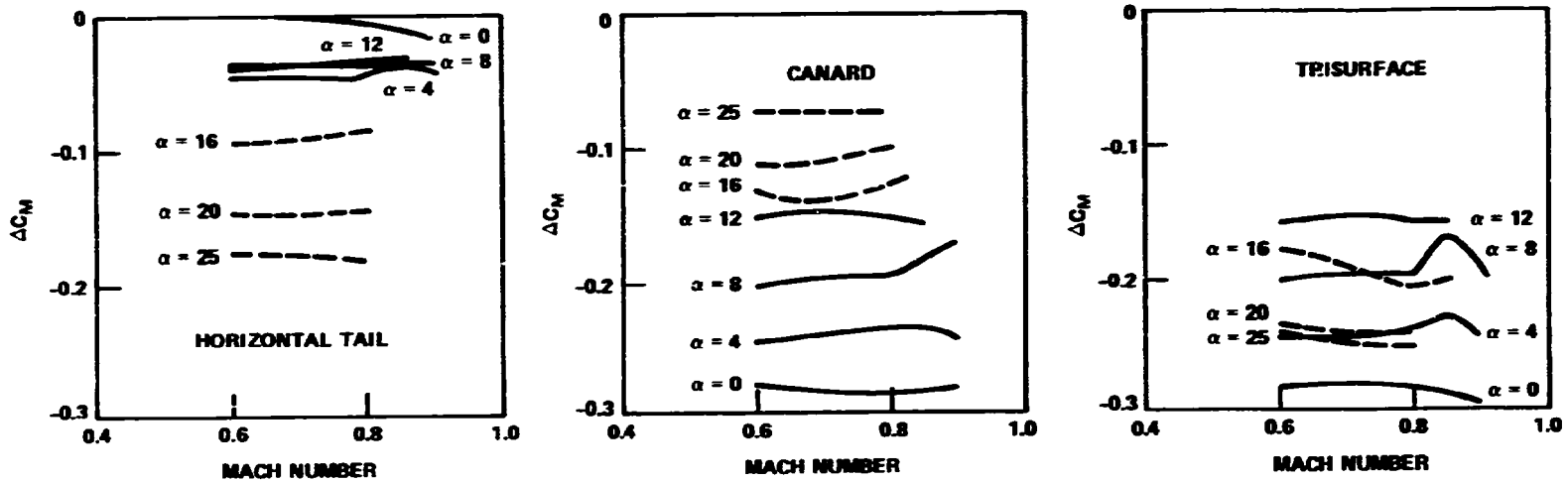

Figure 38b - Moment Characteristics for 25-Degree Wing

relatively constant. At 12 to 16 degrees the model begins to pitchup and the magnitude of this pitchup becomes more severe with increasing Mach number. Similarly, after the pitching moment break ($\alpha \sim 19$ degrees) the magnitude of the nosedown moment is increased with increasing Mach number.

The canard configurations show relatively constant incremental moment variation with Mach number.

The trisurface configuration behaves in a manner similar to the horizontal tail on the 50-degree wing model, i.e., increasing pitchup tendency between 12- and 16-degrees angle of attack with Mach number and increasing nosedown moments with Mach number after the nosedown break. The trisurface configuration on the 25-degree model behaved in a manner similar to the horizontal tail configuration.

To determine the amount of interference between canard-wing horizontal tail and the incremental changes due to the addition of the separate surfaces, Figure 39m is presented. Shown is a comparison of the measured increment due to the trisurface configuration and the sum of the increments of the horizontal tail and canard. Data are presented at Mach numbers of 0.6 to 0.8. As shown, the measured increments are consistently higher for the 25-degree wing than the sum of the increments indicating a reduction in the moment contribution due to the horizontal tail. This reduction is perhaps due to a change in wing downwash over the horizontal tail. This change is a result of the changed loading over the inboard portion of the wing due to the canard. The trend of the incremental moment with increasing angle of attack is the same for the measured and summed increments, and the nosedown break occurs at approximately the same angle of attack. After the break, the curves are approximately parallel indicating that superposition of individual components is possible.

Similar trends are noted for the 50-degree wing model, however, the differences between measured and summed increments are smaller at low angles of attack. The nosedown break is shifted to the higher angle of attack for the measured values rather than for the summed values, indicating changes of the characteristics of the horizontal tail due to the canard.

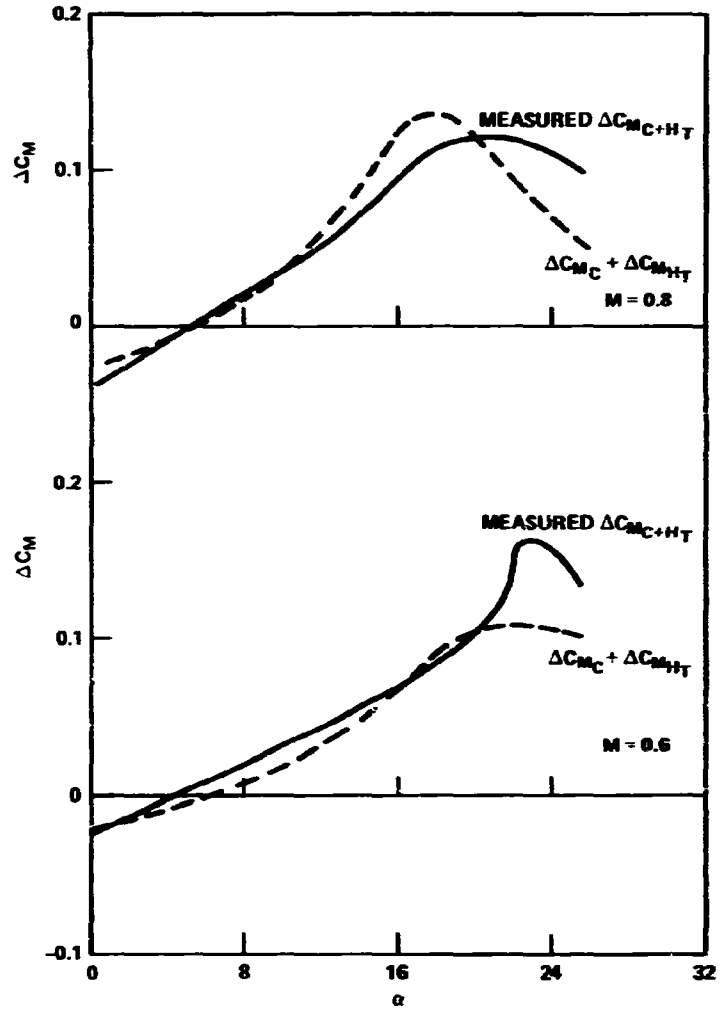

Figure 39a - Incremental Moments for 50-Degree Wing

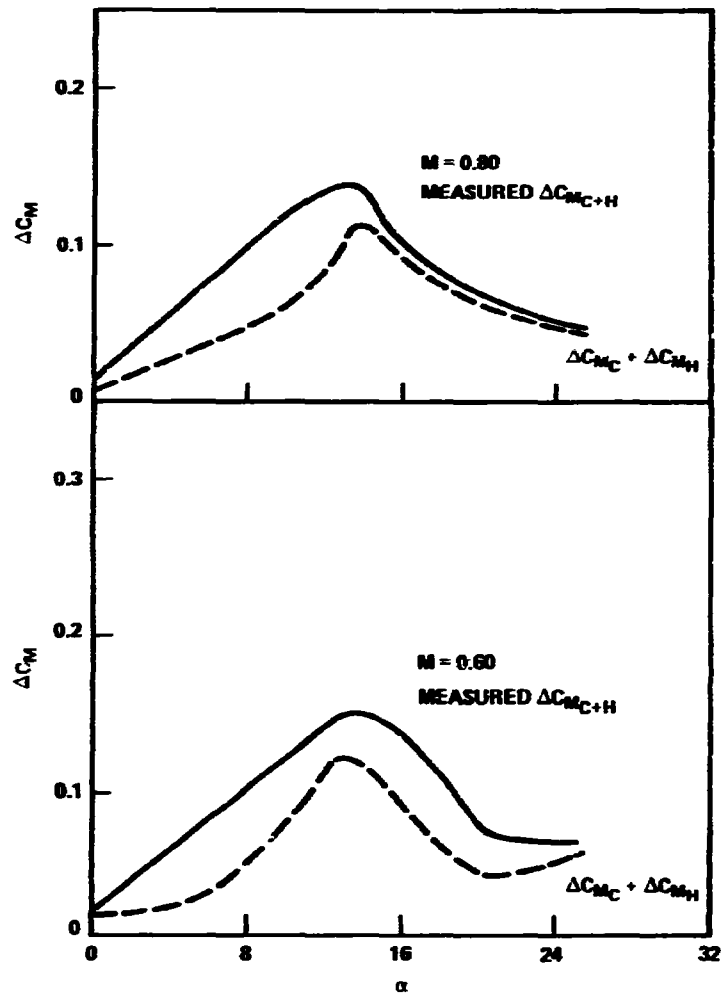

Figure 39b - Incremental Moments for 25-Degree Wing

Figure 39 - Comparison of Measured and Summed Incremental Moments of the Trisurface Configuration

The trend with increasing angle of attack is approximately the same for both measured and summed increments.

In the section on lift it was stated that the close-coupled canard is a poor trimming device. This is due primarily to two reasons; the first reason being the proximity to the wing necessary to obtain beneficial interference and the second reason being the large increment in drag due to positive canard deflections at low angles of attack. Figure 40 presents comparison data between the canard located at three longitudinal stations and the horizontal tail located at 1.5 wing chords aft of the wing center of gravity. The geometry of the canard and horizontal tail are the same, corresponding to canard C_0. The data are in the form of C_{M_δ} at lift coefficients of 0, 0.6, and 0.9. To take out the differences in longitudinal position, the data have been divided by the ratio of the corresponding longitudinal distance divided by the wing mean aerodynamic chord, $\ell c/\bar{c}$. At low lift coefficients the tail has the better ability to generate pitching moments and it is only at the higher lift coefficients that the canard, located at position P_3, has an advantage.

The canard at position P_3, however, only has a nondimensional moment arm $\ell c/\bar{c}$ of 1.0 versus the tail moment arm of 1.5 for position P_8, indicating that the horizontal tail is better or equal to the canard even at the high lift coefficient.

A further measure of the efficiency of the canard or horizontal tail as a trimming device is the ratio of moment generated to drag produced by surface deflection.

These data are shown in Figure 41. Here again, the horizontal tail has an advantage at lift coefficients of 0 and 0.6 until a Mach number of 0.9 is reached. It is only at the higher lift coefficients where the canards show a distinct advantage primarily due to the large lift loss resulting from tail deflection, which, in turn, causes a large increase in drag.

Negative deflections of the canard do not cause large drag increments, and C_{M_δ} is approximately the same as that for positive deflections. Thus, the penalty of using the canard for trim is small or can even be slightly

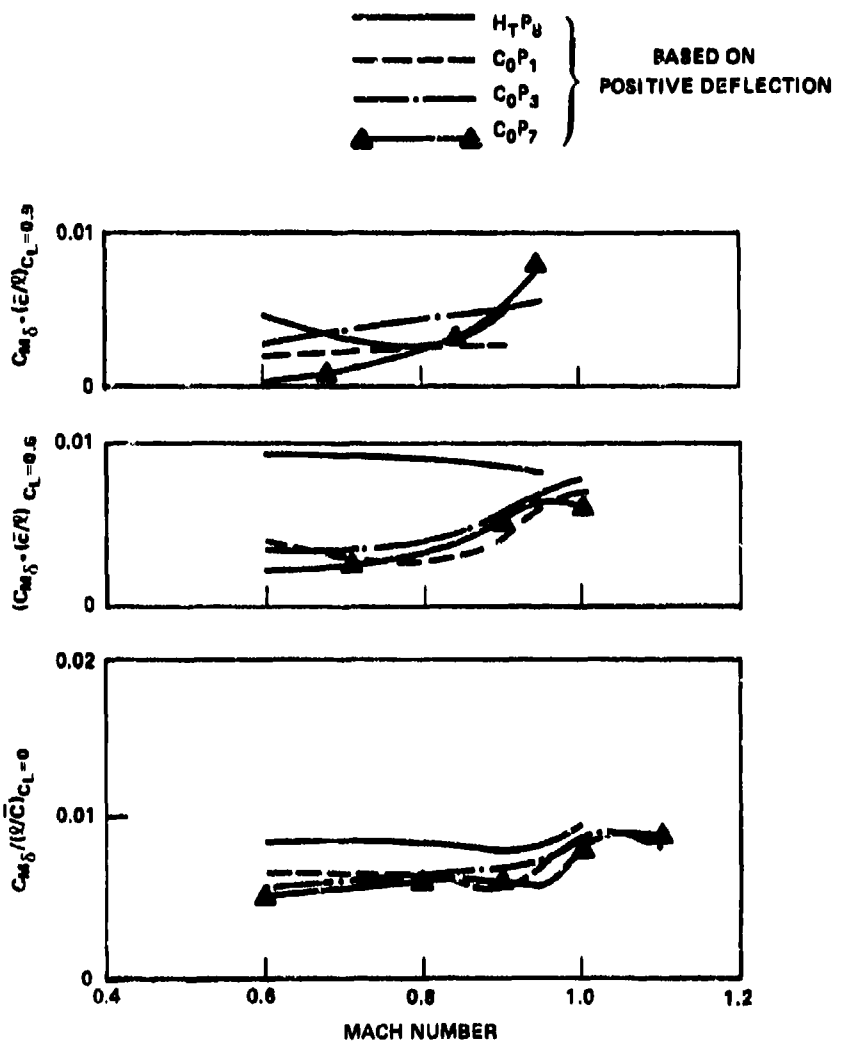

Figure 40 - Normalized Control Power

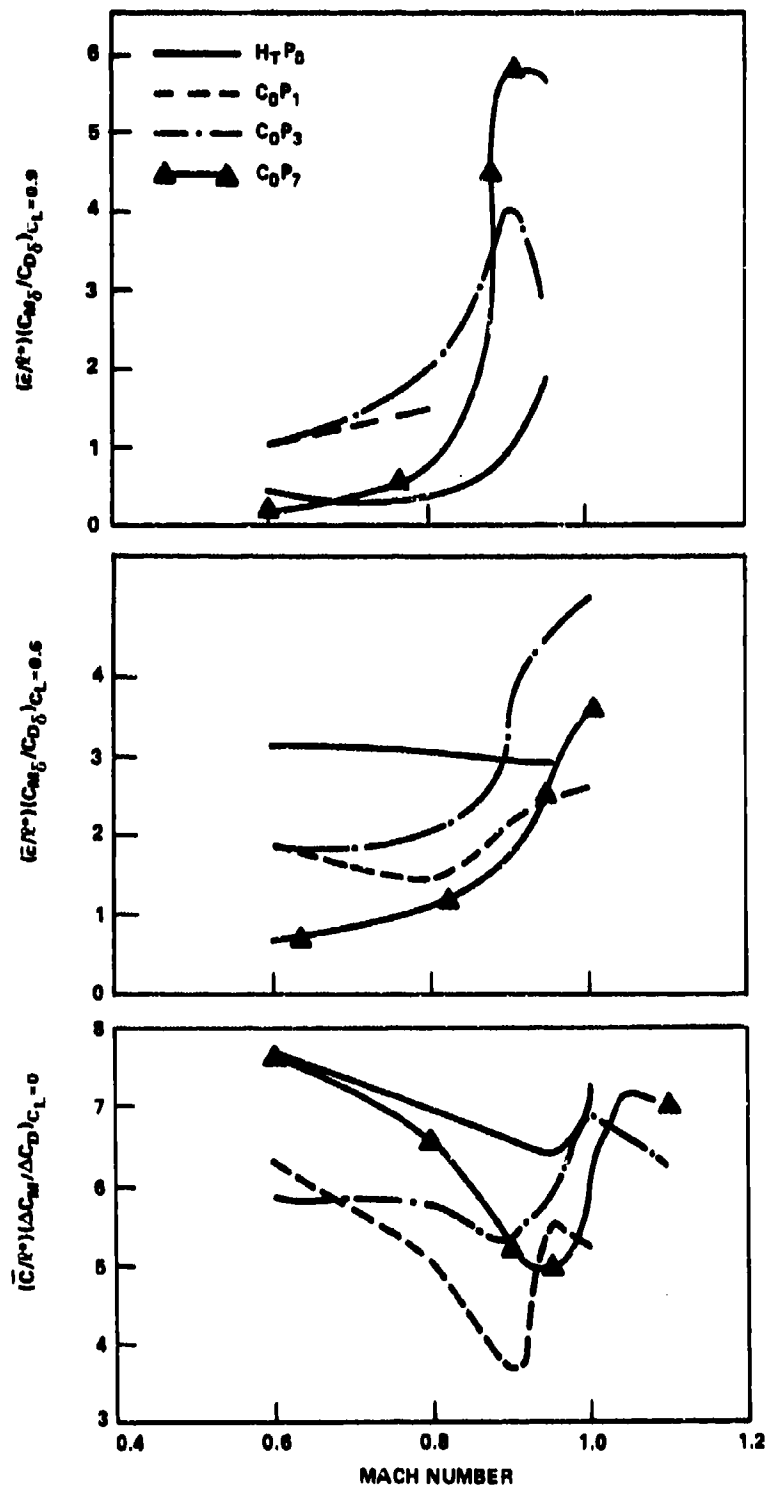

Figure 41 - Control Surface Efficiency

beneficial. The horizontal tail, however, when deflected positively, generates increased lift and, thus, performance is benefited by small positive deflections. Data on positive tail deflections are not available for the two models used in this volume, however, data are available on the F-4 aircraft which indicate significant drag reductions for positive tail deflection. These drag reductions are larger than those exhibited by negative canard deflections. Thus, it is felt that whether the aircraft is stable (positive canard deflections, negative tail deflections to trim) or unstable (negative canard, positive tail deflections) the horizontal tail is the more efficient trimming device at low-to-moderate lift coefficients. At high lift coefficients, where negative tail deflections cause large lift losses and the likelihood of horizontal tail stall is possible due to positive tail deflections, the canard can be used for trim purposes in conjunction with the horizontal tail.

The canard, in conjunction with the horizontal tail, improves the control power of the horizontal tail at moderate to high angles of attack as shown in Figure 42. Horizontal control power is presented for the horizontal tail on the 25-degree wing model both with and without the canard. As indicated in the figure, at low angles of attack, C_{M_δ} is slightly reduced when the canard is on the aircraft. With increasing angle of attack, the canard on configuration exhibits larger values of C_{M_δ} than the canard off data. This is primarily due to the delay of separation on the main wing due to the canard. These same data are presented as a function of angle of attack at Mach numbers of 0.6 and 0.8 in Figure 43.

DRAG

The primary effect of the canard on drag is to reduce wing separation thus improving the induced drag of the configuration. The improvement in drag is shown in Figure 44. Figure 44 presents the lift-to-drag ratio variation with Mach number for both 25- and 50-degree models evaluated both with and without canards. The data are presented at constant lift coefficients of 0.9 and 1.0 for the 25- and 50-degree wing models, respectively.

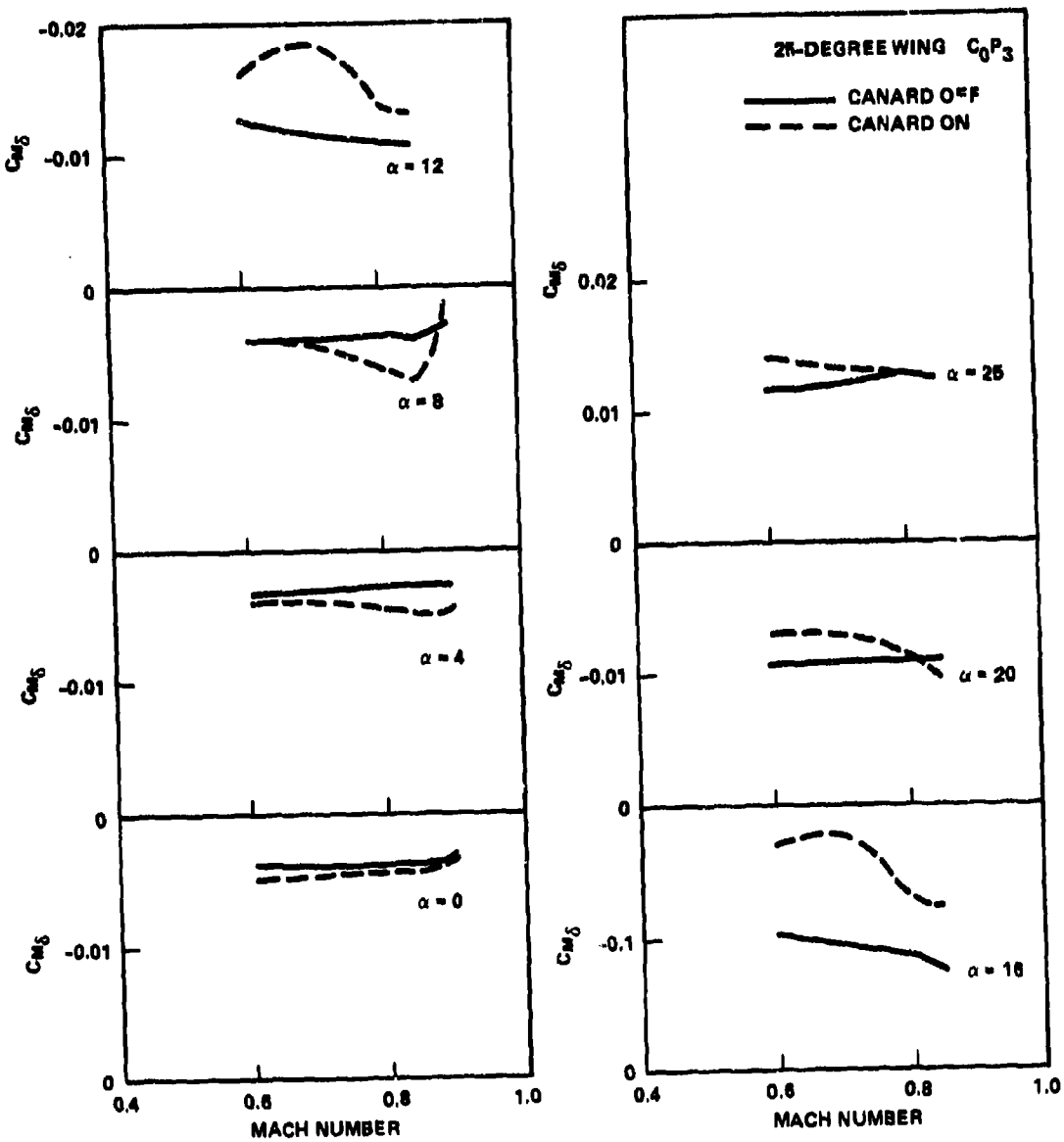

Figure 42 - Effect of Canard on Horizontal Tail Control Power at Constant Angle of Attack

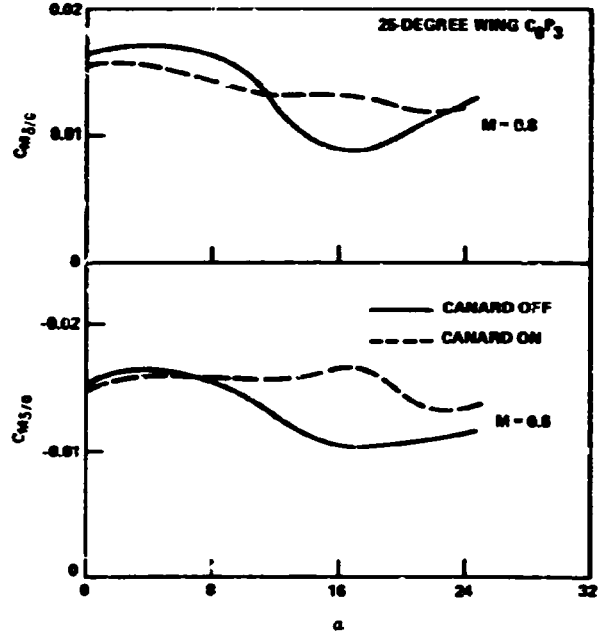

Figure 43 - Effect of Canard on Horizontal Tail Control Power at Constant Mach Number

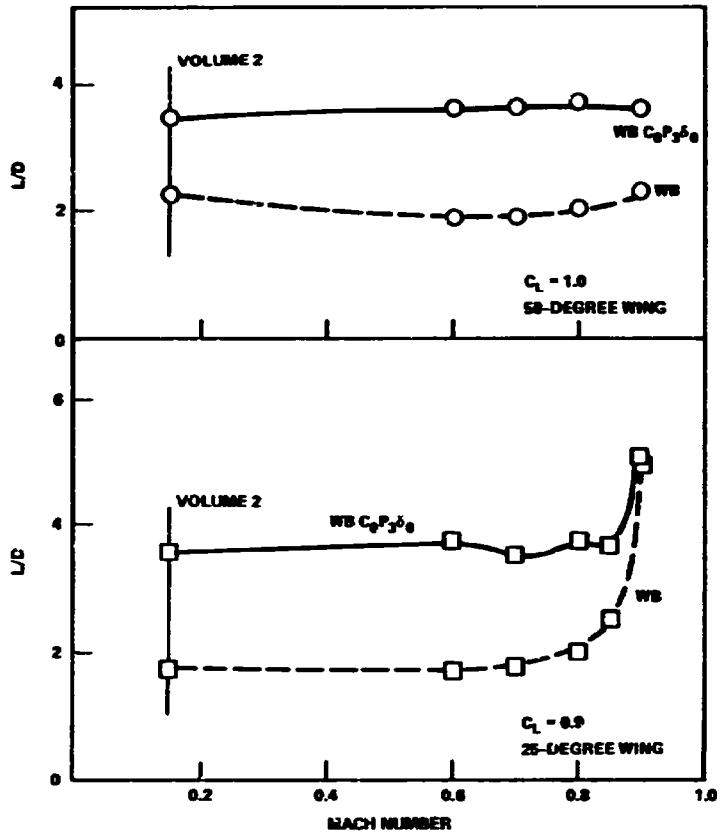

Figure 44 - Lift-to-Drag Ratio, at Constant Lift Coefficient

As shown, the lift-to-drag ratios (L/D) are relatively constant with Mach number up to the point where strong compressibility effects occur.

These compressibility effects occur at a Mach number of 0.7 for the 25-degree wing model and there is a steady increase in L/D for the basic 25-degree wing model beyond this point. This increase in L/D is primarily due to a reduction in the angle of attack to obtain $C_L = 0.9$. The variation of acquired angle of attack is shown in Figure 45.

As indicated in the figure, the required angle of attack for the basic 25-degree wing-body drops off fairly rapidly, whereas, the required angle of attack for the canard configurations is relatively constant up to a Mach number of 0.85.

The 50-degree model exhibits relatively constant L/D for both canard off and on configurations and the angle of attack required is almost constant for the canard. The required angle of attack for the canard off configuration is beginning to drop off at the higher Mach numbers and as was shown in Figure 6 at higher Mach numbers ($M \sim 1.0$). The difference between canard on angle of attack required and the wing-body angle of attack will be approximately the same in a similar manner to that of the 25-degree wing at $M = 0.9$.

The remainder of the discussion on drag will involve canard position, shape, and deflection and will be presented in the form of minimum drag coefficient C_{D_0}, induced drag factor k_1, and lift-to-drag ratio L/D.

POSITION

The effect of canard position on the zero lift drag is presented in Figure 46 for the 50-degree wing model at Mach numbers between 0.6 to 1.10. Three positions are represented P_1, P_3, and P_7 as well as the basic wing-body. As expected from Volume 2, the forward position has the largest drag value throughout the Mach number range. Positions P_3 (most aft) and P_7 (lowest) have approximately the same value up to $M = 1.0$ where position P_3 has the lowest value.

Figure 47 presents the wave drag of the configurations presented in Figure 46. This wave drag was determined by subtracting the drag value at

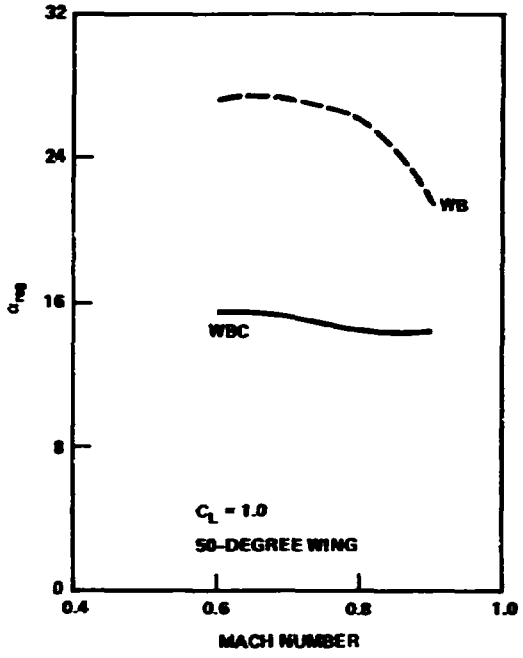

Figure 45a - Angle of Attack for 50-Degree Wing

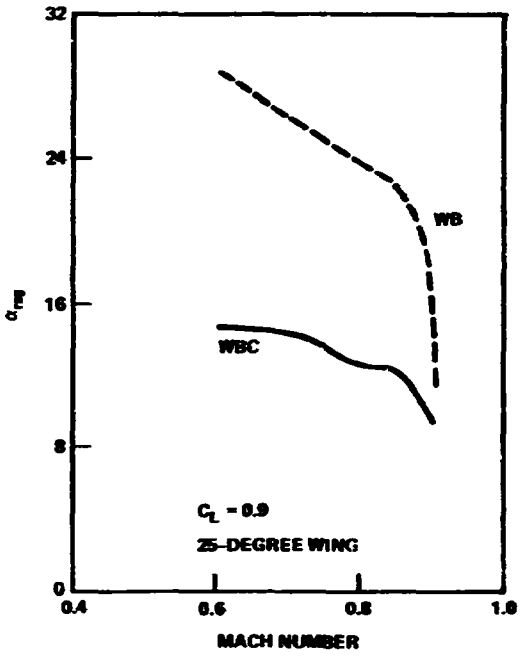

Figure 45b - Angle of Attack for 25-Degree Wing

Figure 45 - Required Angle of Attack

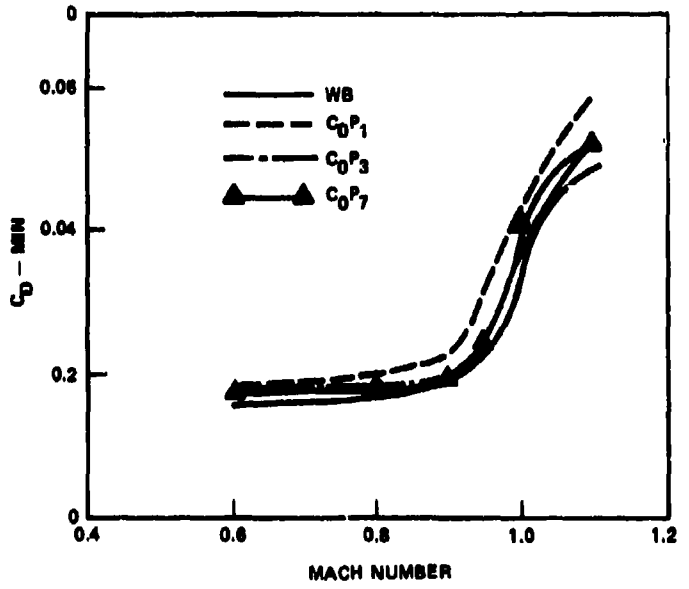

Figure 46 - Effect of Canard Position on Minimum Drag

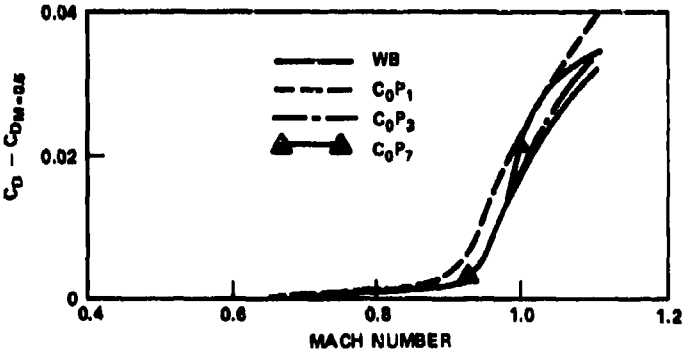

Figure 47 - Effect of Canard Position on Wave Drag

M = 0.6 from the values at the other Mach numbers. The canard at position P_3 has approximately the same wave drag as the basic wing-body, with position P_1 causing an earlier drag rise. These results were discussed somewhat in Volume 1, and are due to the good fairing of the canard at position P_3 into the overall aircraft area distribution, whereas position P_1 caused a distinct hump in the area distribution.

Canard longitudinal position did not have any appreciable effect on the minimum drag of the 25-degree wing model as shown in Figure 48. The canard does, however, delay the drag rise Mach number to a limited extent on the 25-degree sweep model as shown in Figure 49.

Figure 50 presents minimum drag as a function of canard longitudinal position at constant Mach number for both 25- and 50-degree wings. Canards C_0 and C_1 are used for the 50-degree wing and C_0 for the 25-degree wing. As at subsonic speeds drag is minimized at an $\ell c/\bar{c}$ of approximately 1.2 which is the location where the canard exposed trailing edge is slightly ahead of the wing leading edge.

The figure graphically illustrates the penalty which is paid at high transonic Mach numbers ($0.95 \leq M \leq 1.10$) for poor canard location, unless the area distribution is modified to account for the canard. This penalty is on the order of 50 to 80 counts of drag (0.0050 to 0.0080).

The effect of canard vertical location on minimum drag is presented in Figure 51. In general, canard vertical position has a minimal effect on $C_{D_{min}}$, however, lowering the canard increased minimum drag for canards C_0 and C_2 on the 50-degree wing model; the lower position had slightly less or equal minimum drag on the 25-degree wing model.

These trends with vertical position are the same as those observed at subsonic speeds and discussed in Volume 2.

The effect of canard longitudinal position on the induced drag factor k_1, at constant lift coefficient, is presented in Figure 52. Data are presented for lift coefficients of 0.5 and 1.0 at Mach numbers from 0.6 to 1.1. At the low lift coefficient the forward position P_1 has slightly less induced drag than the aft position P_3 at the low Mach numbers.

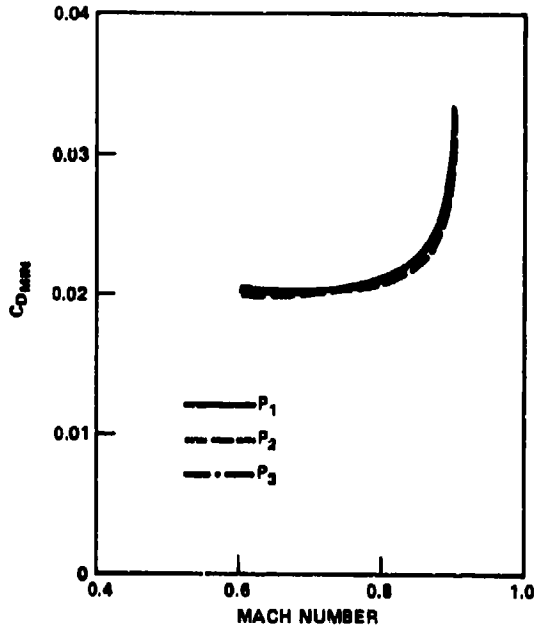

Figure 48 - Effect of Longitudinal Canard Position on Minimum Drag for the 25-Degree Wing

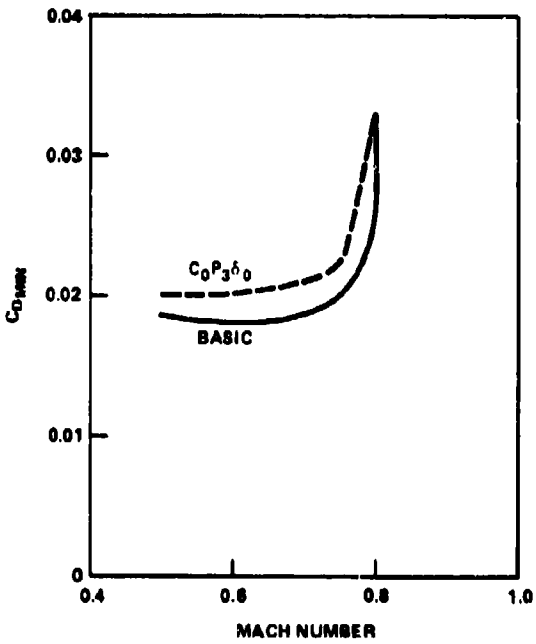

Figure 49 - Minimum Drag of the 25-Degree Wing with and without Canard

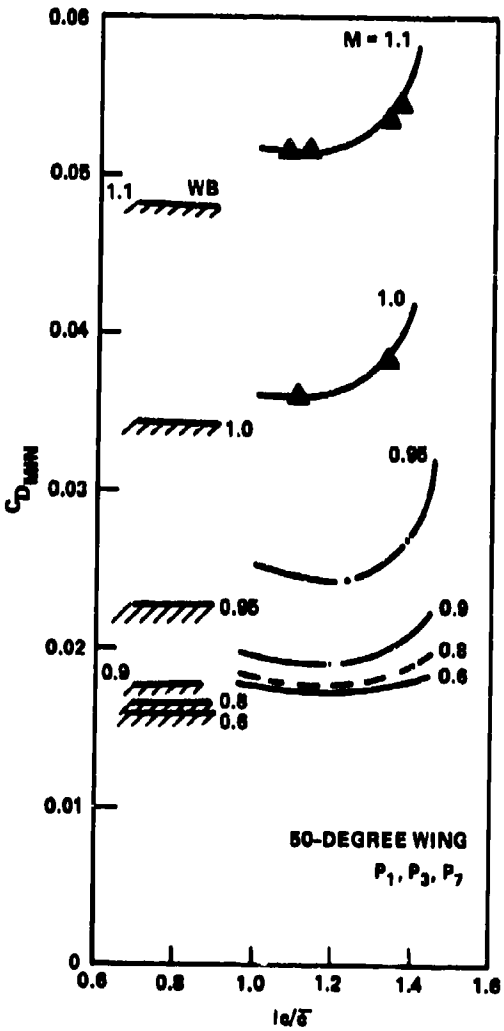

Figure 50a - Canard C_0 on 50-Degree Wing

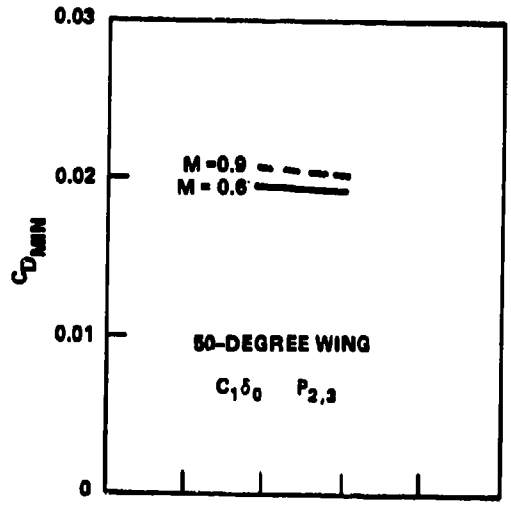

Figure 50b - Canard C_1 on 50-Degree Wing

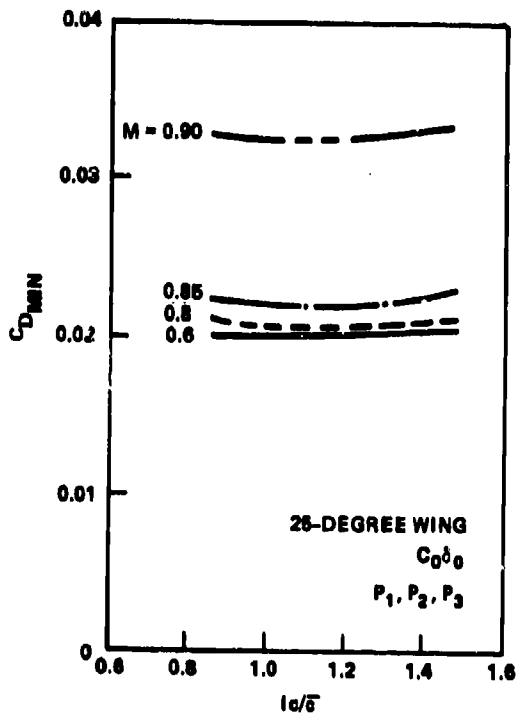

Figure 50c - Canard C_0 on 25-Degree Wing

Figure 50 - Effect of Canard Longitudinal Position on Minimum Drag at Constant Mach Number

Figure 51 - Effect of Canard Vertical Position on Minimum Drag

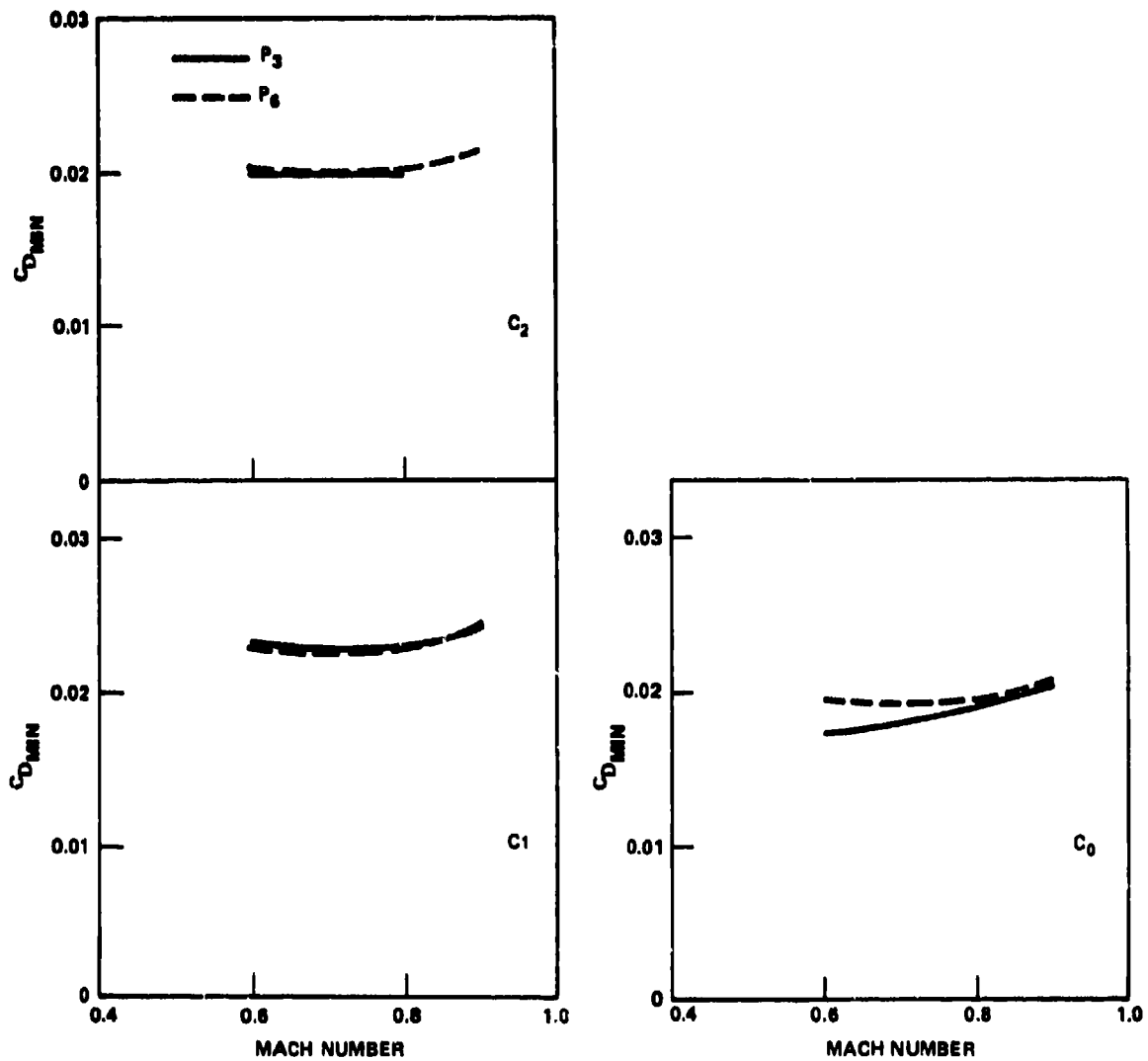

Figure 51a - Position of 50-Degree Wing

Figure 51 (Continued)

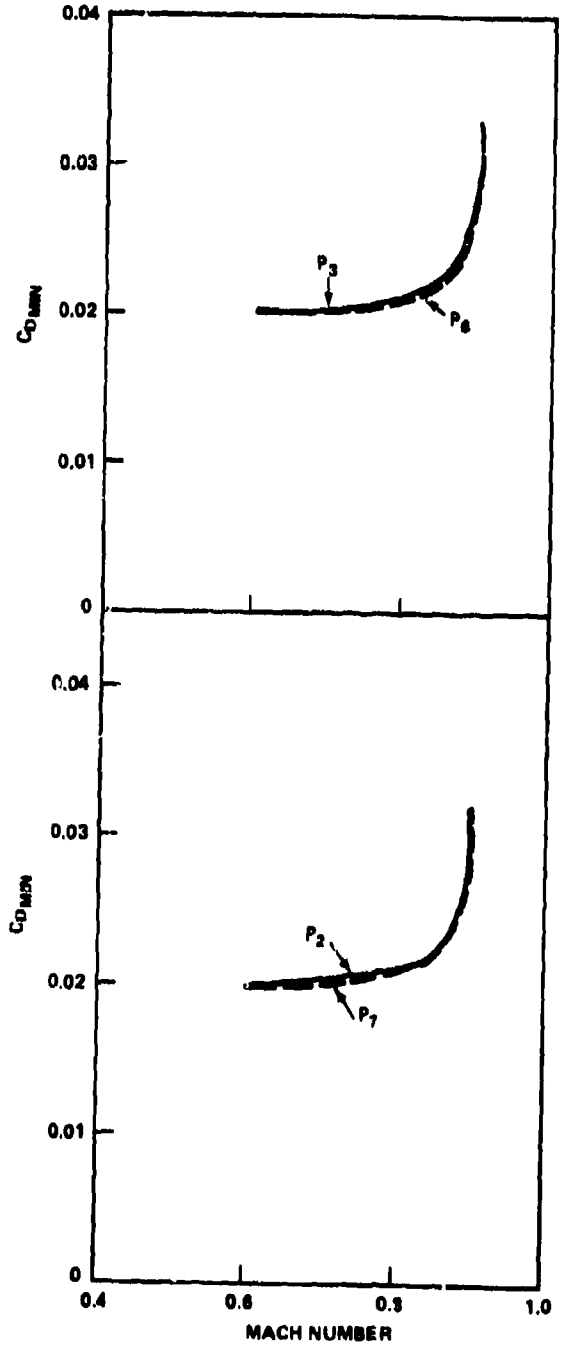

Figure 51b - Position of 25-Degree Wing

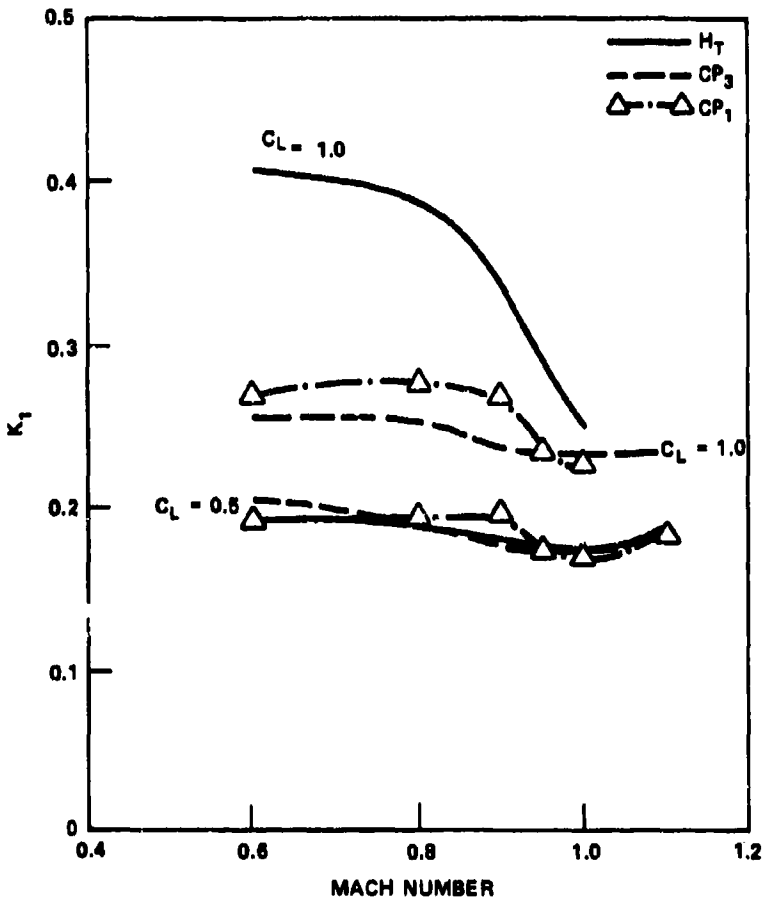

Figure 52 - Effect of Canard Position on Induced Drag

This trend was also evident in Volume 2, and is due, in part, to the unfavorable interference of the canard at position P_3 at low lift coefficients. In the Mach number range between 0.75 to 0.95 the aft position had lower induced drag. Beyond M = 0.95, there is little effect of canard position.

At the higher lift coefficient, C_L = 1.0, the aft position has lower induced drag up to M = 0.95 but beyond M = 0.95 position has little or no effect.

Induced drag factor at constant angle of attack for canards C_0 on both 50- and 25-degree models and canards C_1 on the 50-degree model is shown in Figure 53. The trends noted for Figure 52 also occur in Figure 53. At low angles of attack and Mach number, the canard in the forward position has less induced drag factor than the aft position; however, as angle of attack is increased, the aft position has the lowest induced drag factor. It is evident that at speeds near the sonic velocity, canard position has minimal effect on induced drag factor. The data in Figure 53 show that moving the C_1 canard forward to position P_2 generates lower induced drag factors than at position P_3. This phenomena was discussed in Volume 2, and is due to the fact that position P_2 for the 60-degree delta canard C_1 corresponds to position P_3 for canard C_0 in terms of canard-wing overlap position.

The effect of canard vertical position on induced drag factor is shown in Figure 54 for canards C_0, C_1, and C_2 at positions P_3 and P_6 for the 50-degree wing and canard C_0 at positions P_2, P_3, P_6, and P_7 for the 25-degree wing. Induced drag factor was, in general, increased by lowering the canard on the 50-degree wing. On the 25-degree wing the canard nearest to the plane of the wing P_7 exhibited the highest induced drag factor over most of the angle of attack range. When the canard was at the proper longitudinal station $\ell/\bar{c} \sim 1.0$, lowering the canard improved the induced drag at high angles of attack.

The variation of L/D with Mach number for the canards at various longitudinal stations is presented in Figure 55. Data are presented for maximum lift to drag ratio $(L/D)_{max}$ and L/D at lift coefficients of 1.0

Figure 53 - Effect of Canard Position on Induced Drag at Constant Angle of Attack

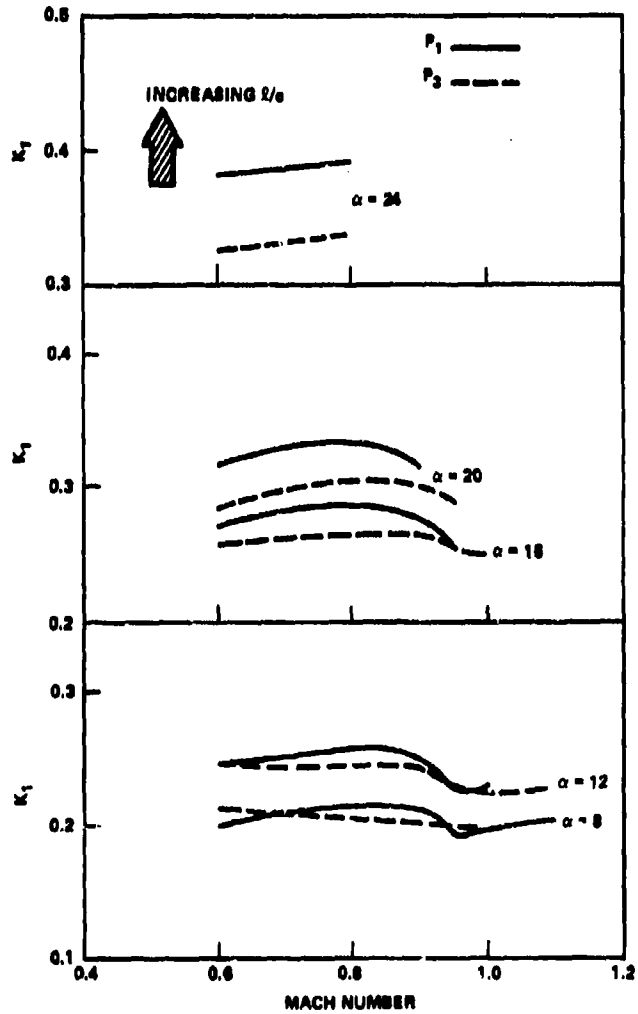

Figure 53a - Canard C_0 on 50-Degree Wing

Figure 53 (Continued)

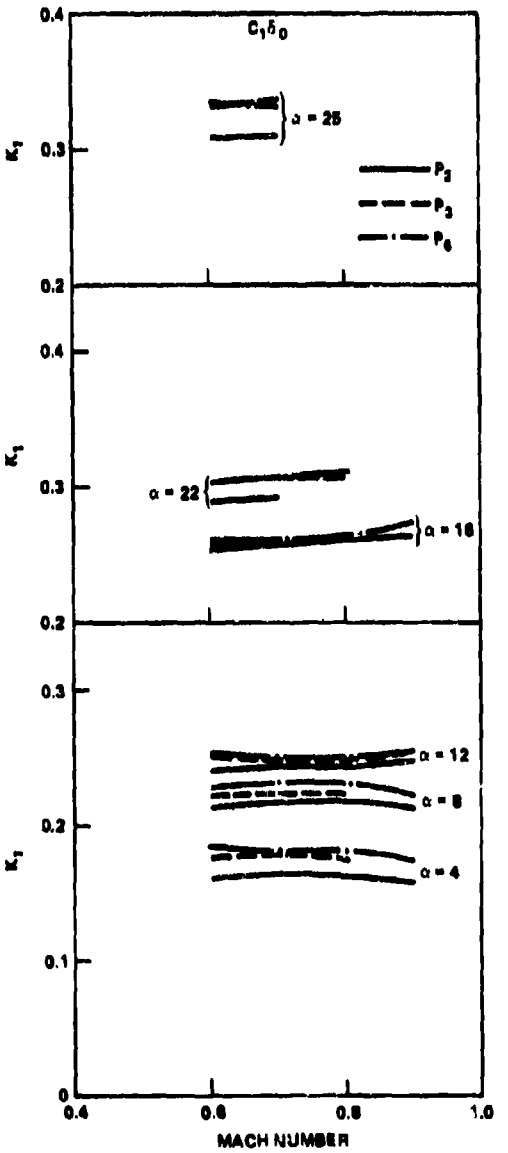

Figure 53b - Canard C_1 on 50-Degree Wing

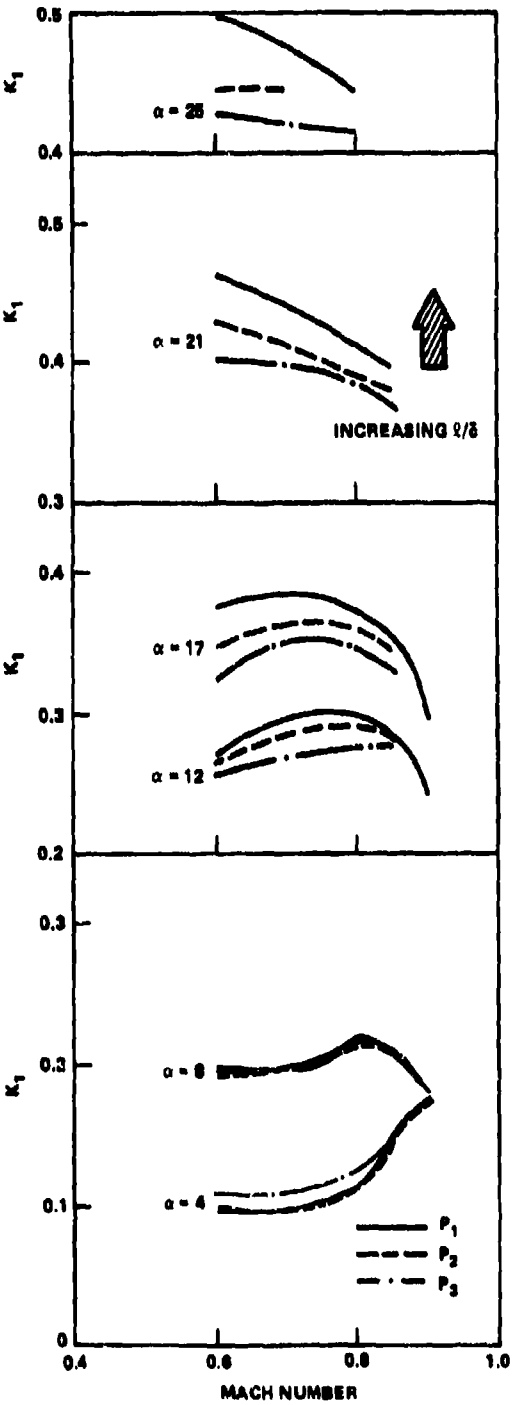

Figure 53c - Canard C_0 on 25-Degree Wing

Figure 54 - Effect of Vertical Position on Induced Drag Factor

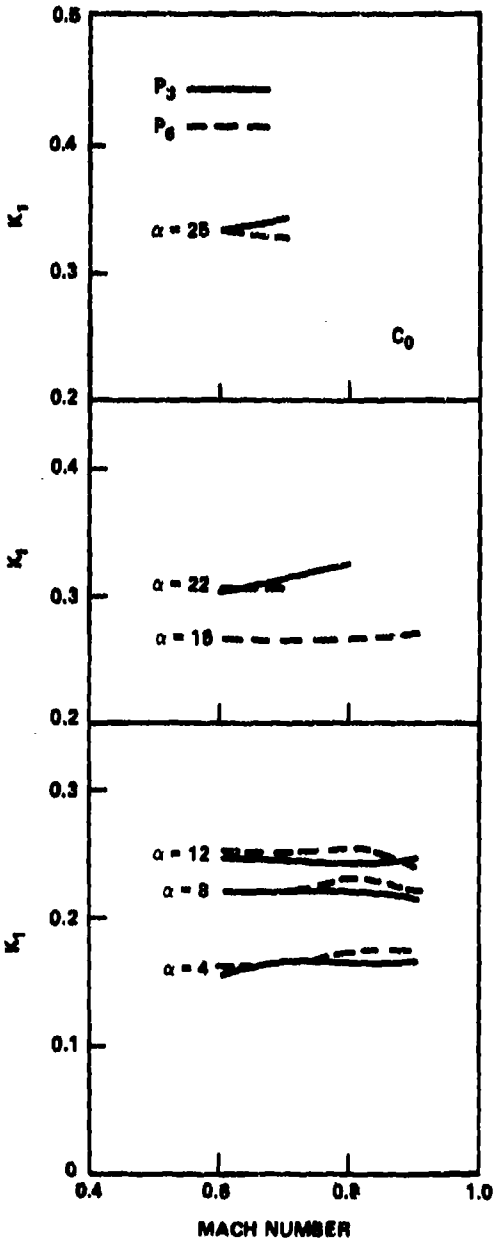

Figure 54a - Canard C_0 on 50-Degree Wing

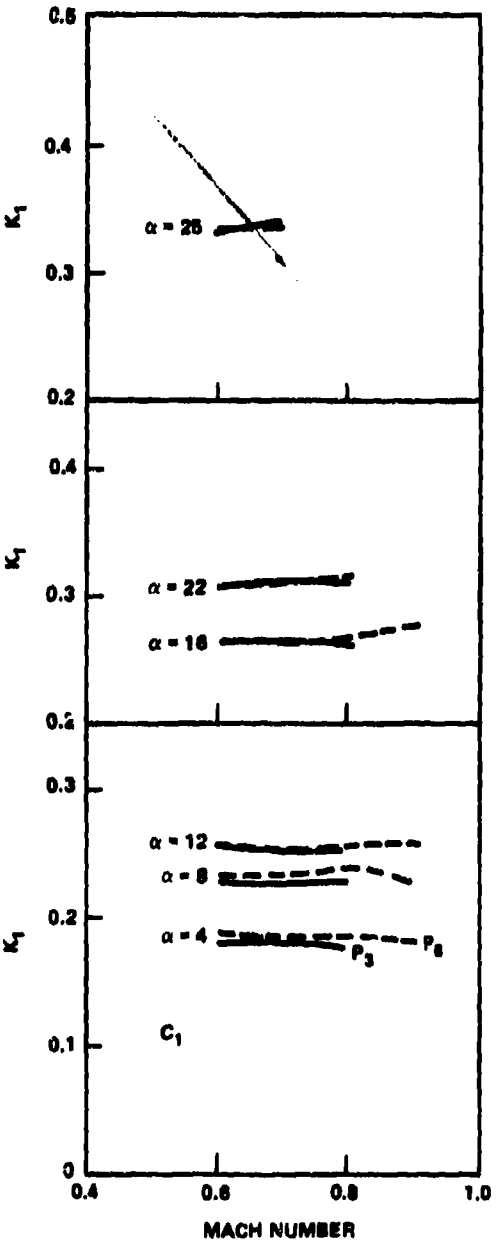

Figure 54b - Canard C_1 on 50-Degree Wing

Figure 54 (Continued)

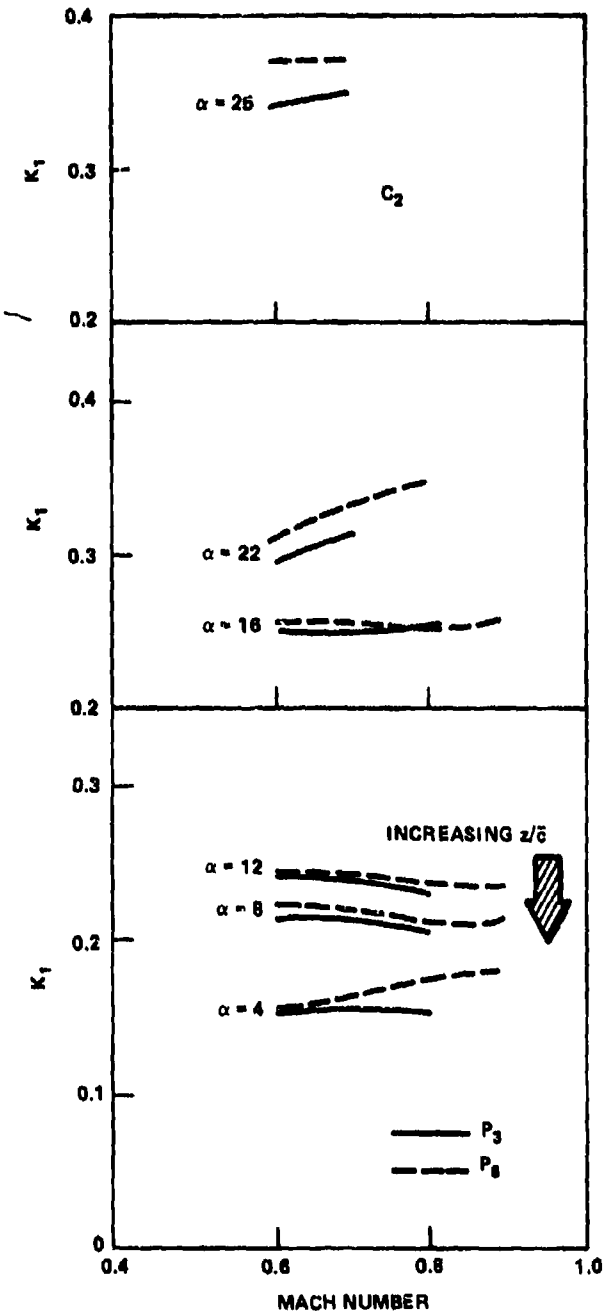

Figure 54c - Canard C_2 on 50-Degree Wing

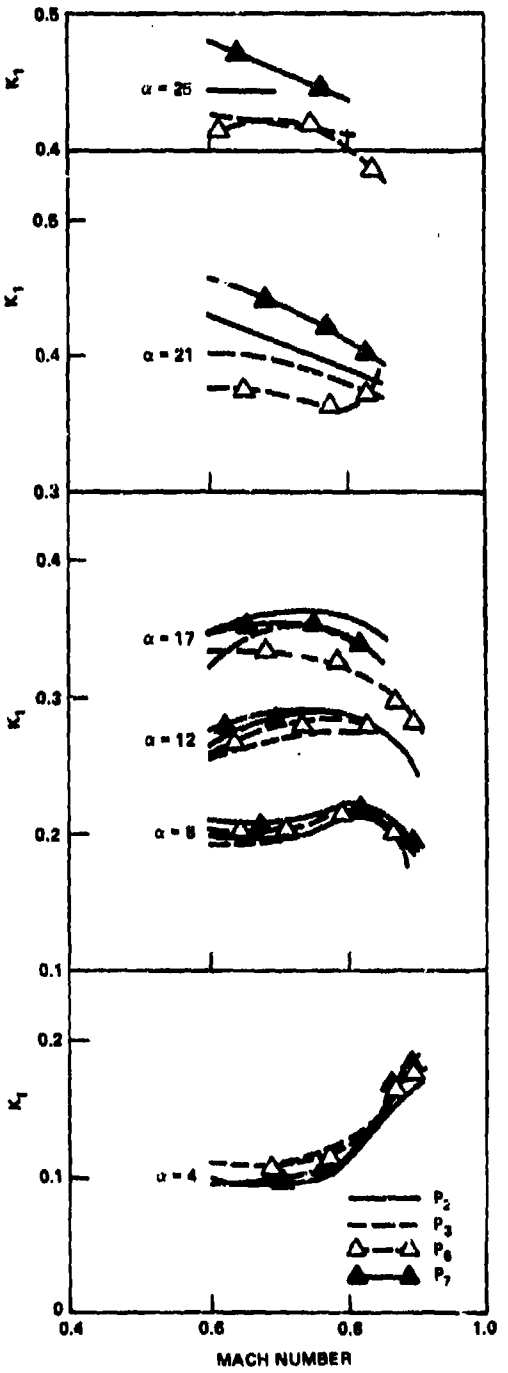

Figure 54d - Canard C_0 on 25-Degree Wing

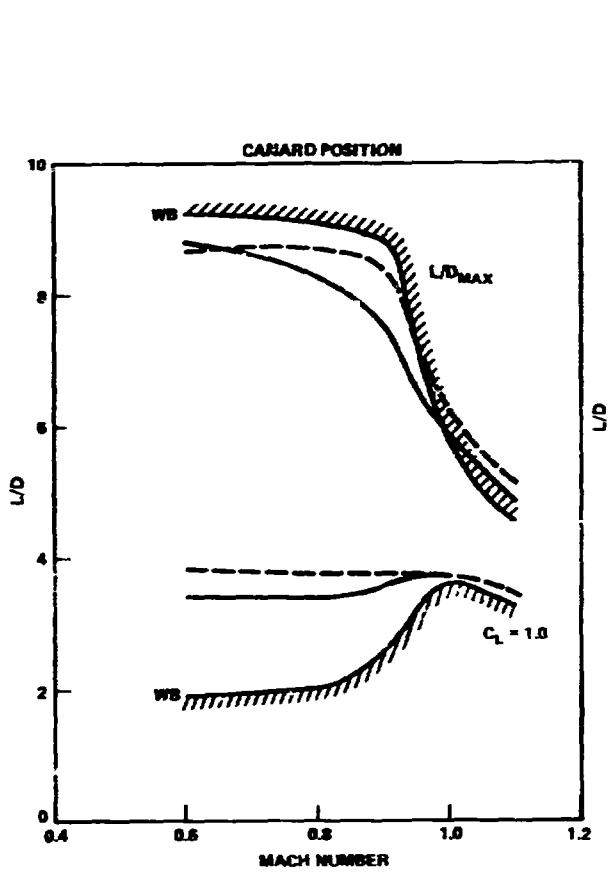

Figure 55a - Canard C_0 on 50-Degree Wing

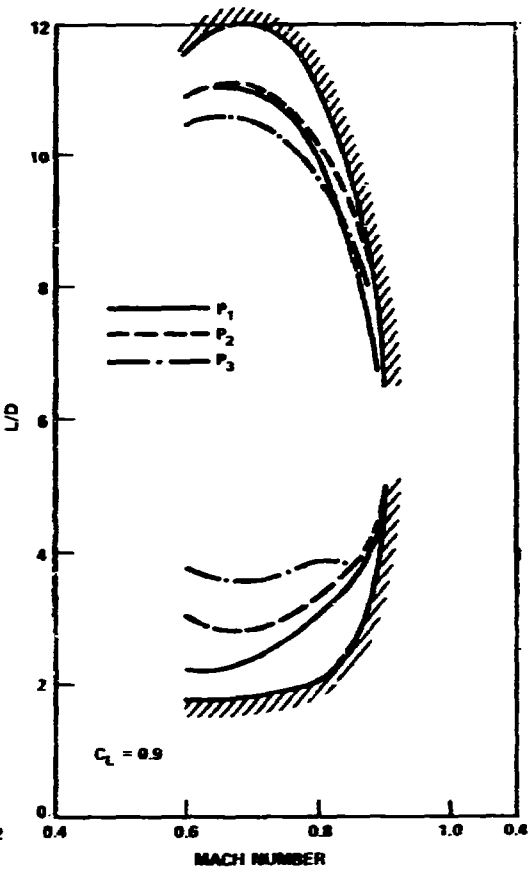

Figure 55b - Canard C_0 on 25-Degree Wing

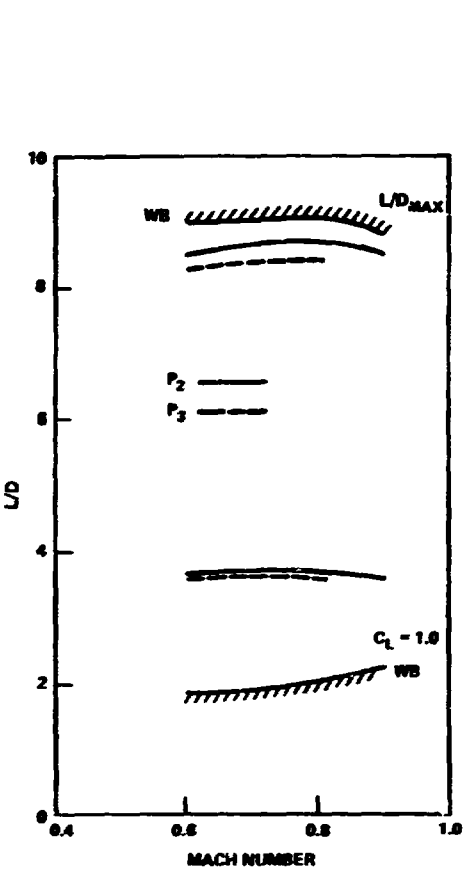

Figure 55c - Canard C_1 on 50-Degree Wing

Figure 55 - Effect of Longitudinal Position on Lift-to-Drag Ratio

and 0.9 for the 50- and 25-degree sweep models, respectively. Figure 55 presents data for the C_0 canard at positions P_1 and P_3 at Mach numbers from 0.6 to 1.1. Presented on the figure are the corresponding canard off values. The canard located at position P_3, most aft, had the highest L/D except at M = 0.6 where the most forward canard P_1 had a slightly higher value.

Both canard positions had lower values of $(L/D)_{max}$ than the basic wing-body at Mach numbers up to 0.95. At Mach numbers above 0.95 the maximum L/D for the canard at position P_3 exceeded the value of the basic wing-body, thus indicating that carrying the canard at transonic speeds does not penalize performance. The most forward canard had larger values of $(L/D)_{max}$ at Mach numbers greater than 1.0, however, the values were lower than those obtained at position P_3.

At the higher lift coefficient, L/D was approximately double that of the basic wing-body for the canard at position P_3 at low Mach numbers. As the Mach number increased, L/D remained relatively constant for the canard at position P_3. The basic wing-body, however, had a rapid increase in L/D due to the aforementioned decrease in required angle of attack in order to attain $C_L = 1.0$. This rapid increase in L/D brought the value of L/D to approximately the same value as that of the canard at position P_3. The L/D for the basic wing-body was slightly lower, however.

The forward canard position had lower values than the aft position and exhibited a rise in L/D between Mach numbers of 0.8 to 1.0 to bring the value up to that of the aft location.

It thus appears that at high transonic speeds ($M > 1.0$) and high lift coefficients, canard location has little effect on performance.

Similar characteristics are shown in Figure 55 for the 25-degree wing model. For $(L/D)_{max}$ the middle position P_2 had the highest value of L/D, with the aft position having the lowest value. At Mach numbers up to 0.87 the basic wing-body had larger values of $(L/D)_{max}$ than the canard configurations; above this Mach number the middle and aft locations P_2 and P_3 had equal or greater values of $(L/D)_{max}$.

At the higher lift coefficient, C_L = 0.9, the most aft position doubled the value of L/D of the basic wing-body. Lift-to-drag ratio falls off with forward canard movement. As with the 50-degree wing data, L/D is relatively constant for the most aft canard location. The data for the other canard locations and the basic wing-body exhibit a rapid increase in L/D between Mach numbers of 0.7 to 0.9. At the highest Mach number, M = 0.9, there is little discernable difference between L/D for any canard position or the basic wing-body.

Figure 55c presents data for the 50-degree canard C_1, at positions P_2 and P_3. Position P_2 was the optimum position at subsonic speeds and is also the optimum position at transonic speeds. As indicated in the figure, L/D is relatively constant with Mach number as was the case of the canard C_0, at position P_3 in Figure 55a.

The effect of canard vertical location on L/D is presented in Figure 56. Data are presented for canards C_0, C_1, and C_2 at positions P_3 and P_6 for the 50-degree model and canard C_0 at positions P_3, P_6, P_2, and P_7 for the 25-degree model. As at subsonic speeds, lowering the canard reduces both $(L/D)_{max}$ and L/D at high lift coefficients. The incremental loss in L/D is relatively constant with Mach number.

CANARD SHAPE

The variation of minimum drag with canard shape is presented in Figure 57. The low aspect ratio, high sweep canards C_0 and C_1 exhibited the lowest drag throughout the Mach number range presented.

Canards C_0, C_1, and C_2 all exhibit the same increase in drag with Mach number. Canard C_3 had the highest minimum drag and also exhibited an early drag rise. This early rise is expected and is due to the low sweep of the canard.

The induced drag factor for the various canard shapes is presented in Figure 58. As at subsonic speeds, induced drag is minimized by low sweep and high aspect ratio at low angles of attack and Mach number. With increasing angle of attack the reverse is true; induced drag is minimized by the higher sweep canards.

Figure 56 - Effect of Vertical Position on Lift-to-Drag Ratio

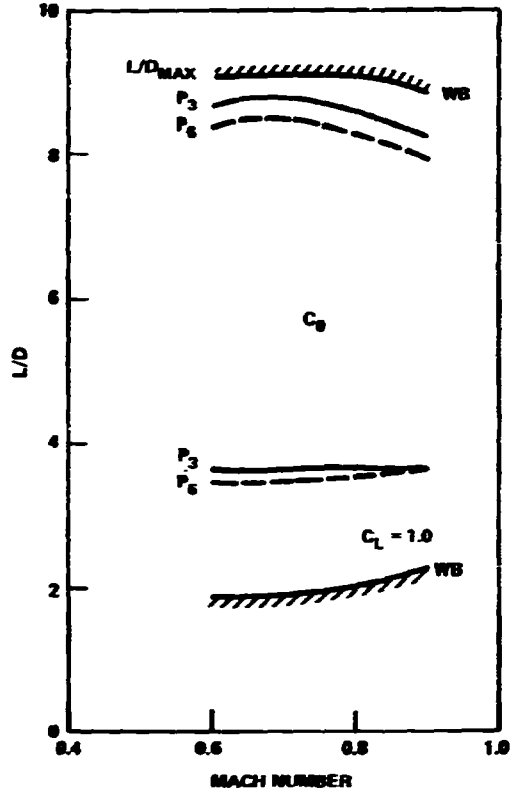

Figure 56a - Canard C_0 on 50-Degree Wing

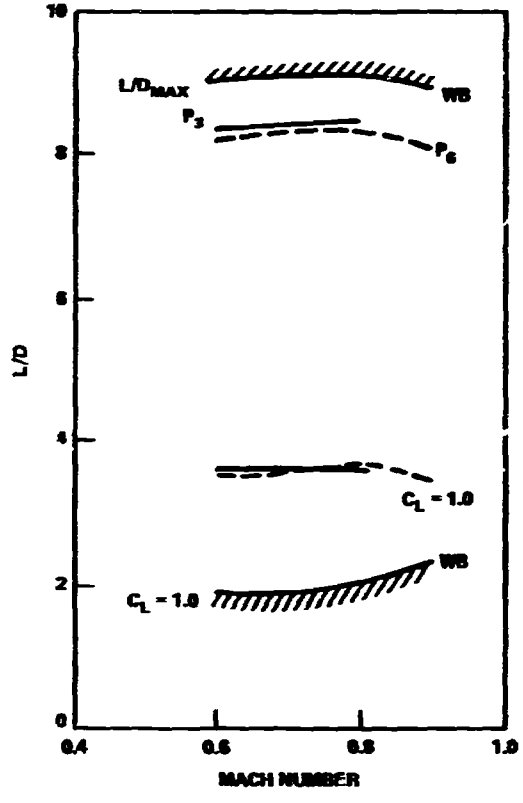

Figure 56b - Canard C_1 on 50-Degree Wing

Figure 56 (Continued)

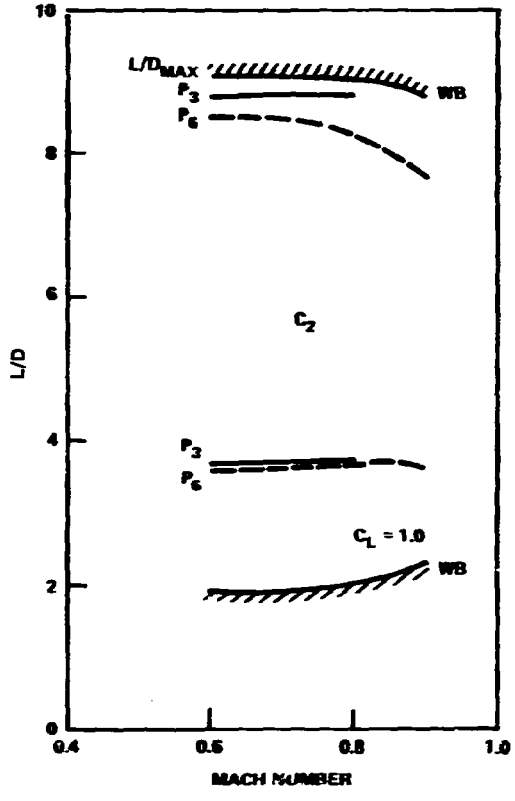

Figure 56c - Canard C_2 on 50-Degree Wing

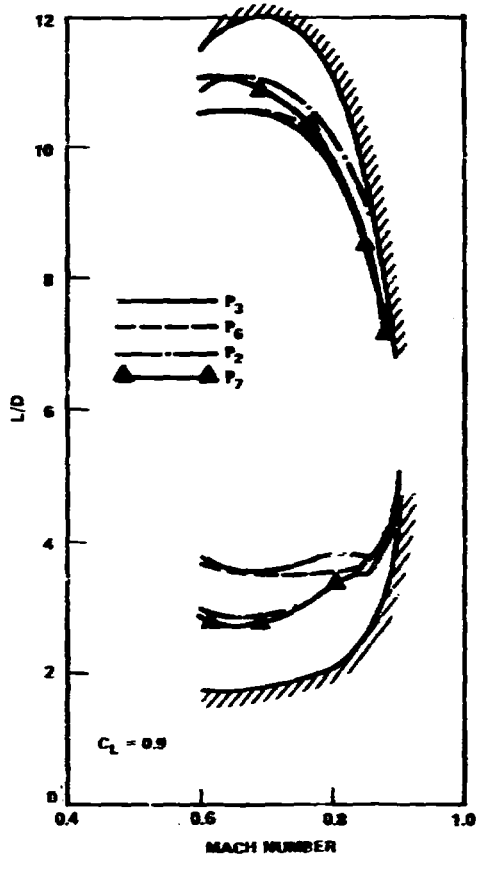

Figure 56d - Canard C_0 on 25-Degree Wing

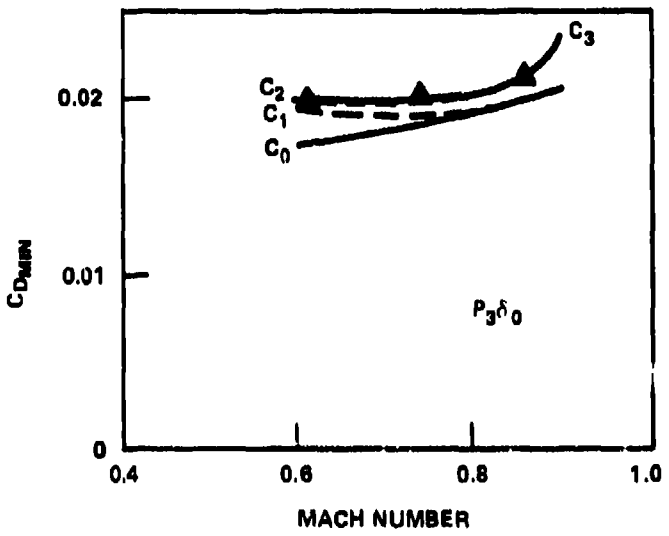

Figure 57 - Effect of Canard Shape on Minimum Drag

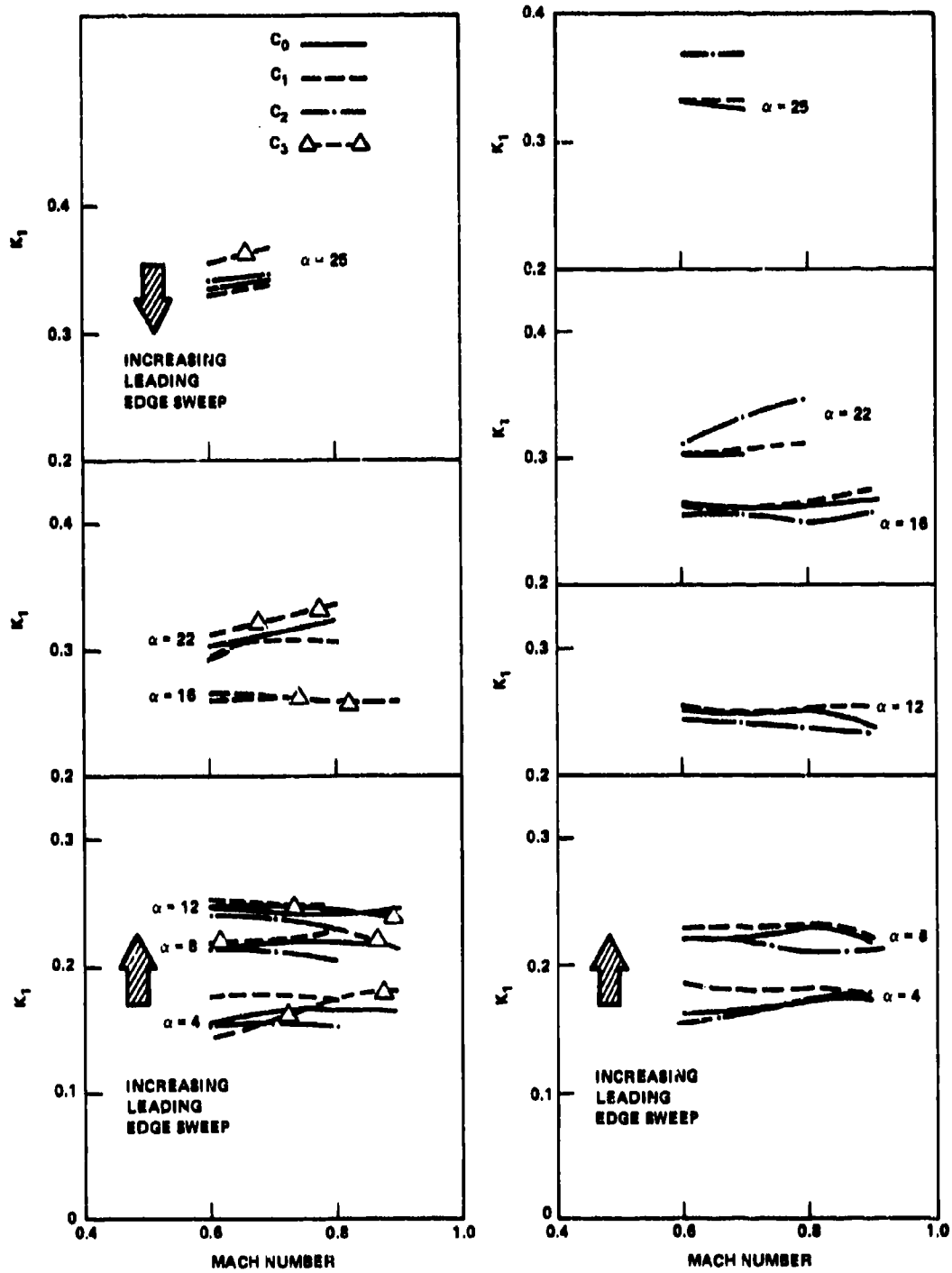

Figure 58a - Position P_3

Figure 58b - Position P_6

Figure 58 - Effect of Canard Shape on Induced Drag Factor

The variation of L/D for the various shapes is presented in Figure 59. Data are presented at positions P_3 and P_6. At both positions the 45-degree high aspect ratio canard had the highest value of $(L/D)_{max}$ up to a Mach number of 0.8, beyond this Mach number the high sweep canards had a higher value. The low sweep canard C_3, had a rapid drop off in $(L/D)_{max}$ with Mach number due to the aforementioned early drag rise. Behavior of $(L/D)_{max}$, at low transonic speeds was similar to that described in Volume 2 at subsonic speeds. Low sweep, high aspect ratio canards perform better. At the higher C_L, canard C_2 was slightly better than the other three canards, and canard C_3 was the poorest. There is, however, little difference between any of the shapes at the higher lift coefficient. This behavior is in keeping with that observed at subsonic speeds.

DEFLECTION

The parameter which has the greatest influence on drag of the close-coupled canard is deflection. A 10-degree deflection of the canard can increase the minimum drag of the aircraft by as much as 100 counts (0.01) thus causing a large reduction in the maximum L/D. In addition, deflection has a large influence on the induced drag factor. These changes will be discussed in the following section.

Minimum drag coefficient $C_{D_{min}}$, as a function of canard deflection, is presented in Figure 60.

The data are for the C_0 canard located at position P_3 on both 25- and 50-degree models.

The range of deflections is from -10 to +10 degrees. Figures 60a and 60b present data for the 50-degree wing. As indicated, the increment in minimum drag is relatively constant with Mach number. Minimum drag occurs at zero deflection as expected with small negative deflections causing only a slight drag increase. Figure 60c presents data for the 25-degree wing. Here, drag due to deflection is not constant but rather increases for positive deflections. This increase is shown in Figure 61 where the incremental drag is plotted against Mach number at constant deflection. A definite decrease in drag rise Mach number is observable for the positive

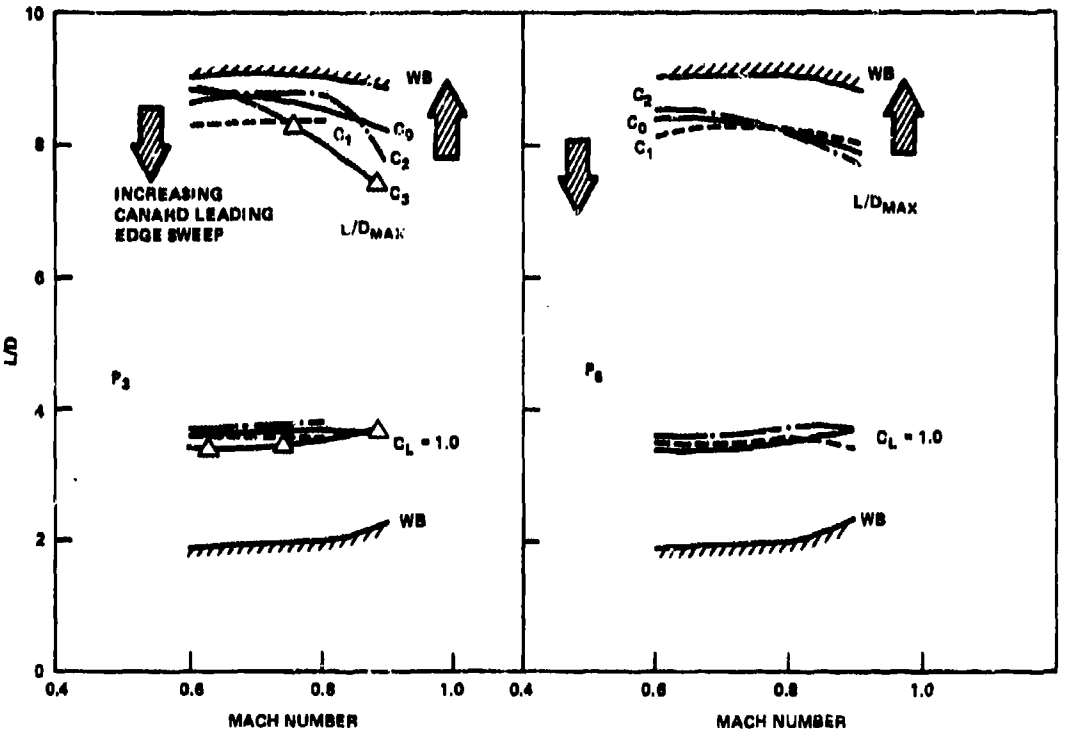

Figure 59a - Position P_3

Figure 59b - Position P_6

Figure 59 - Effect of Canard Shape on Lift-to-Drag Ratio

Figure 60 - Minimum Drag as a Function of Canard Deflection

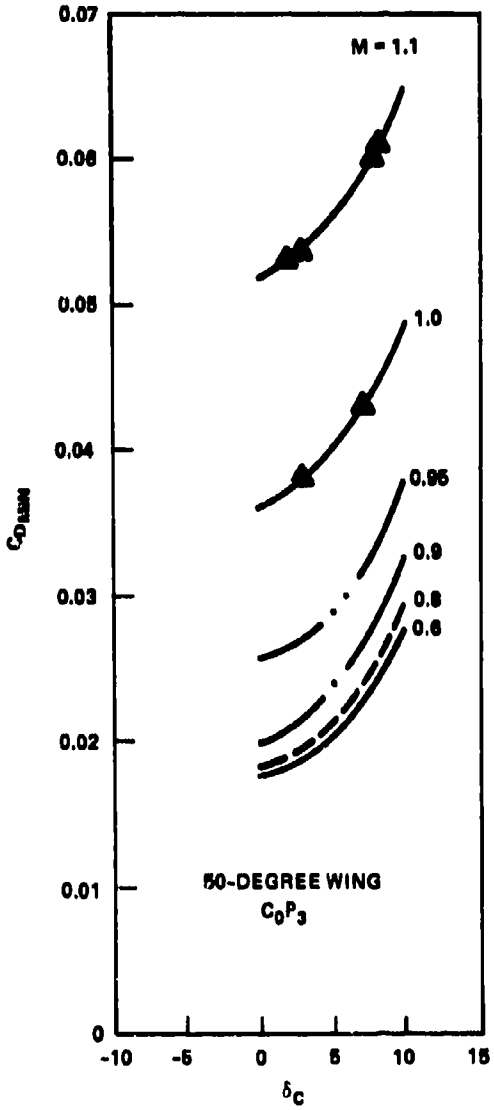

Figure 60a - Positive Deflection on 50-Degree Wing

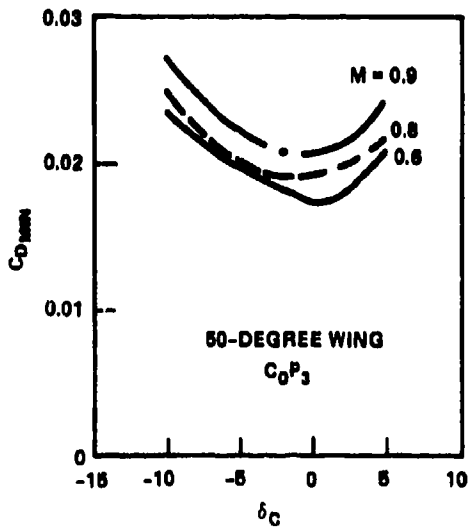

Figure 60b - Positive and Negative Deflections on 50-Degree Wing

Figure 60 (Continued)

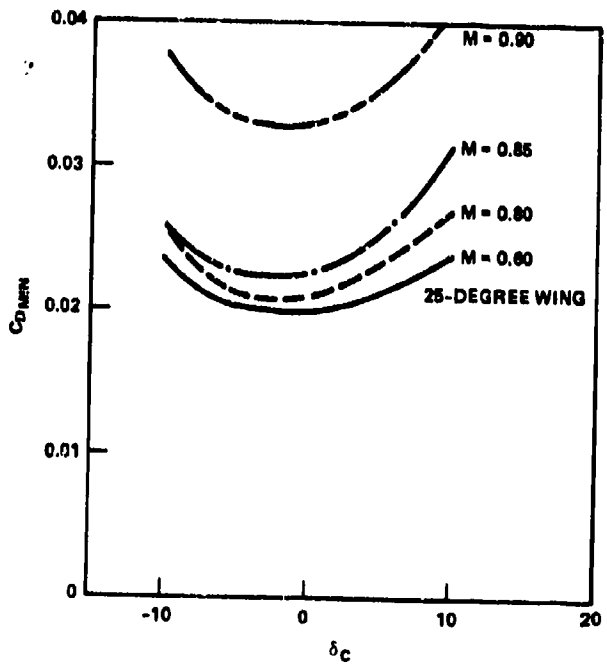

Figure 60c - Positive and Negative Deflections on 25-Degree Wing

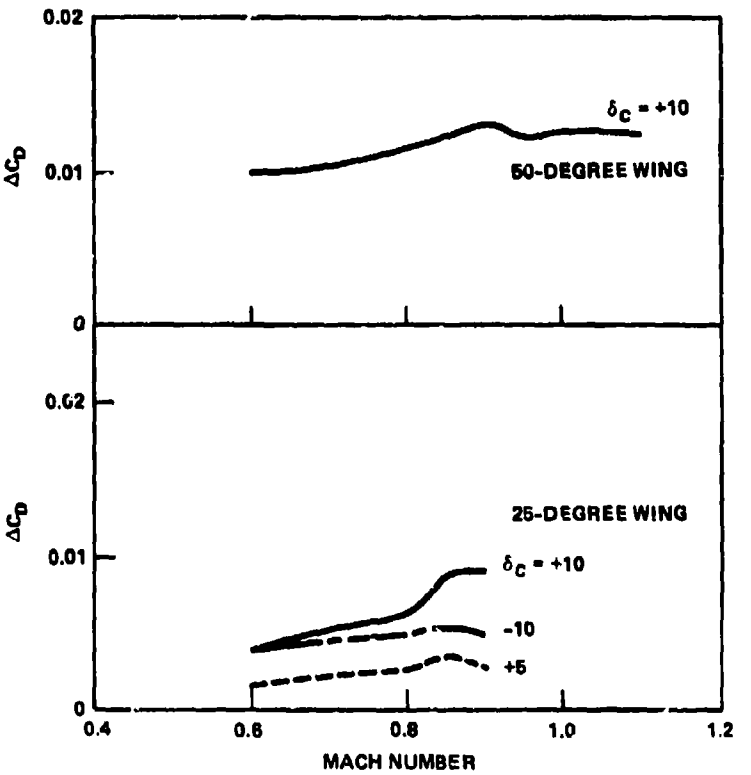

Figure 61 - Incremental Drag Due to Canard Deflection

10-degree canard deflection. A slight drag rise is also evident for the positive 10-degree deflection on the 50-degree wing, however, it is only about half the magnitude of the rise on the 25-degree wing and not as abrupt.

The second major effect of canard deflection is to modify the induced drag factor of the overall configuration. Negative canard deflections reduce the induced drag factor k_1 while positive deflections increase k_1. This variation in induced drag factor is presented in Figure 62. The data are for both positive and negative deflections and the canard is C_0 located at position P_3 for both wing sweeps.

The effect of deflection on the higher sweep wing is relatively constant with Mach number and decreases with increasing angle of attack. The 25-degree wing shows a larger variation with Mach number primarily due to the lower critical Mach number. There is also little decrease in the magnitude of induced drag factor change with angle of attack. From the data presented, it is clear that negative canard deflections can improve the overall configuration efficiency.

The majority of the remaining data on induced drag variation due to deflection are concerned with negative deflections and are presented in Figure 63. Data are presented for the four canard shapes at position P_3 and canards C_0, C_1, and C_2 at position P_6. The canard C_1 is also presented at position P_2. In general, deflection angle was limited to -5 degrees.

Data for the 25-degree wing are for canard C_0 at position P_6 and position P_1 for -10 and +10 degrees, respectively. The variation of induced drag factor with deflection is similar to that discussed previously, with one exception. This exception is the data for canard C_1 located at position P_2. This configuration had a reversal in induced drag factor at angles of attack of 20 degrees or larger. The deflected canard had larger values of k_1 than the undeflected. In Volume 2 it was shown that there was a lower gap ratio boundary in which lift was lost. The data from Figure 19 for this configuration indicate that there is perhaps an upper boundary also where the favorable effects of the canard begin to diminish. The behavior is analogous to a slat in which, if the gap is too large,

Figure 62 - Effect of Deflection on Induced Drag Factor

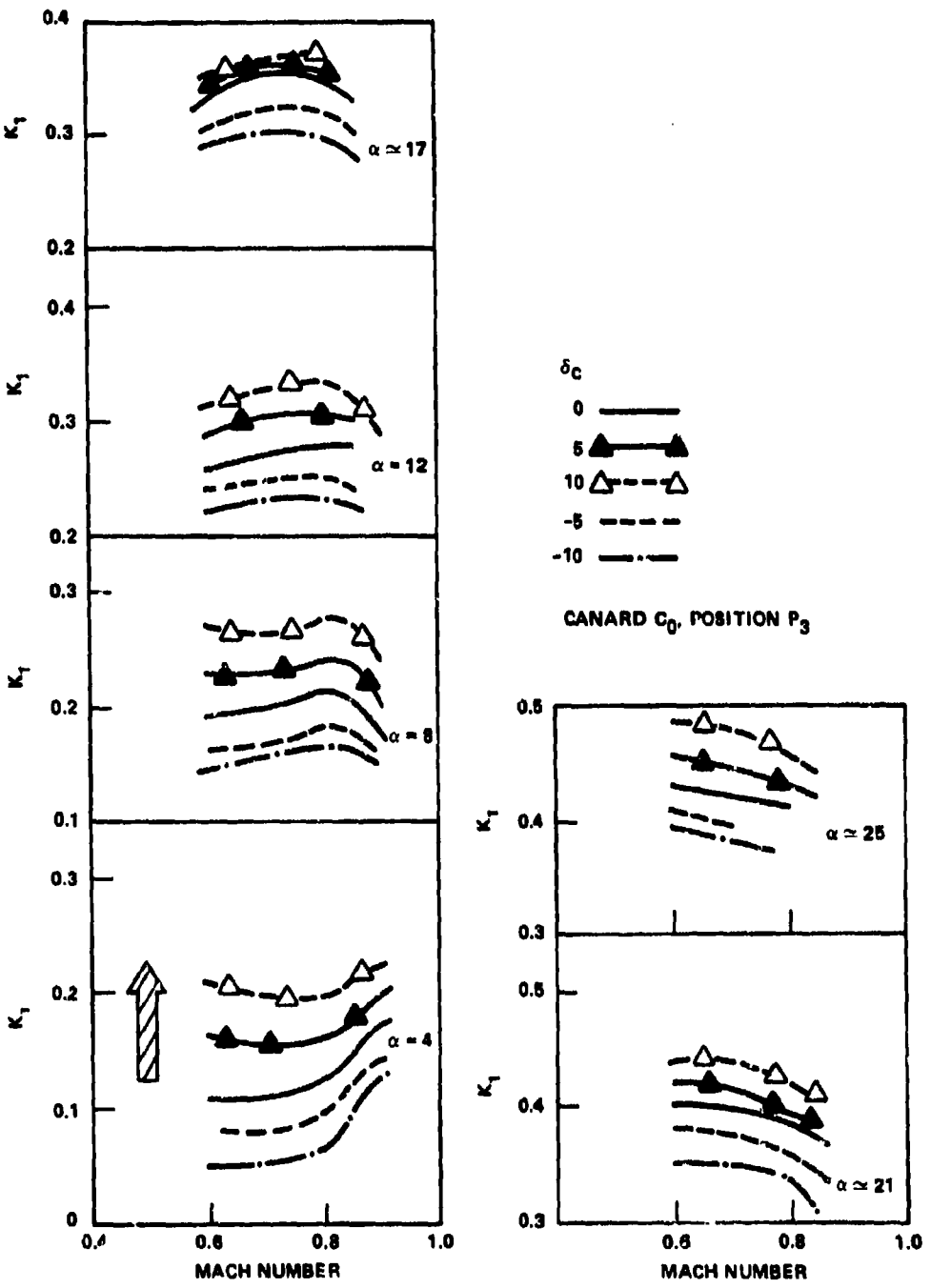

Figure 62a - Deflection on 50-Degree Wing

Figure 62 (Continued)

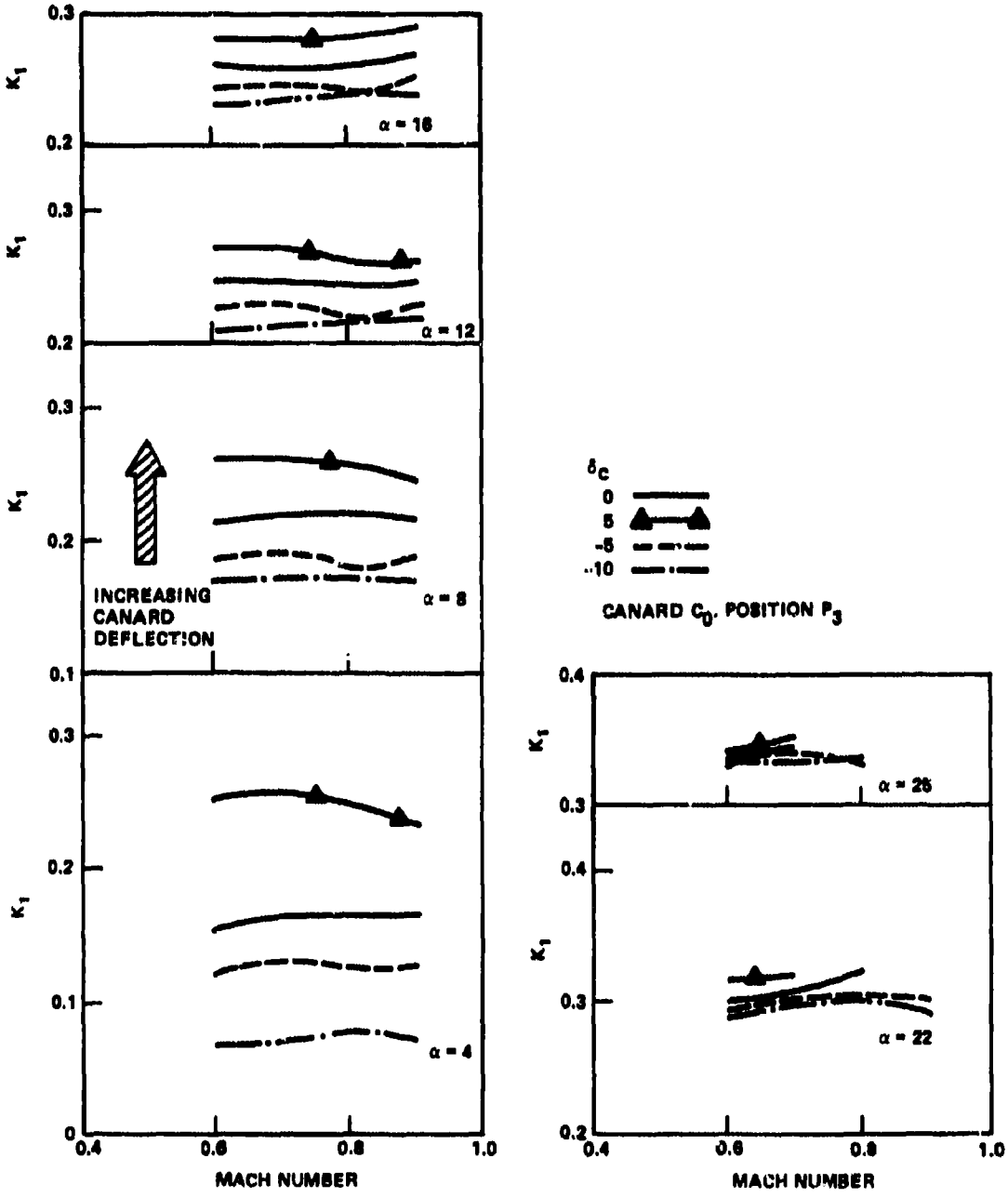

Figure 62b - Deflection on 25-Degree Wing

Figure 63 - Effect of Canard Deflection on
Induced Drag Factor

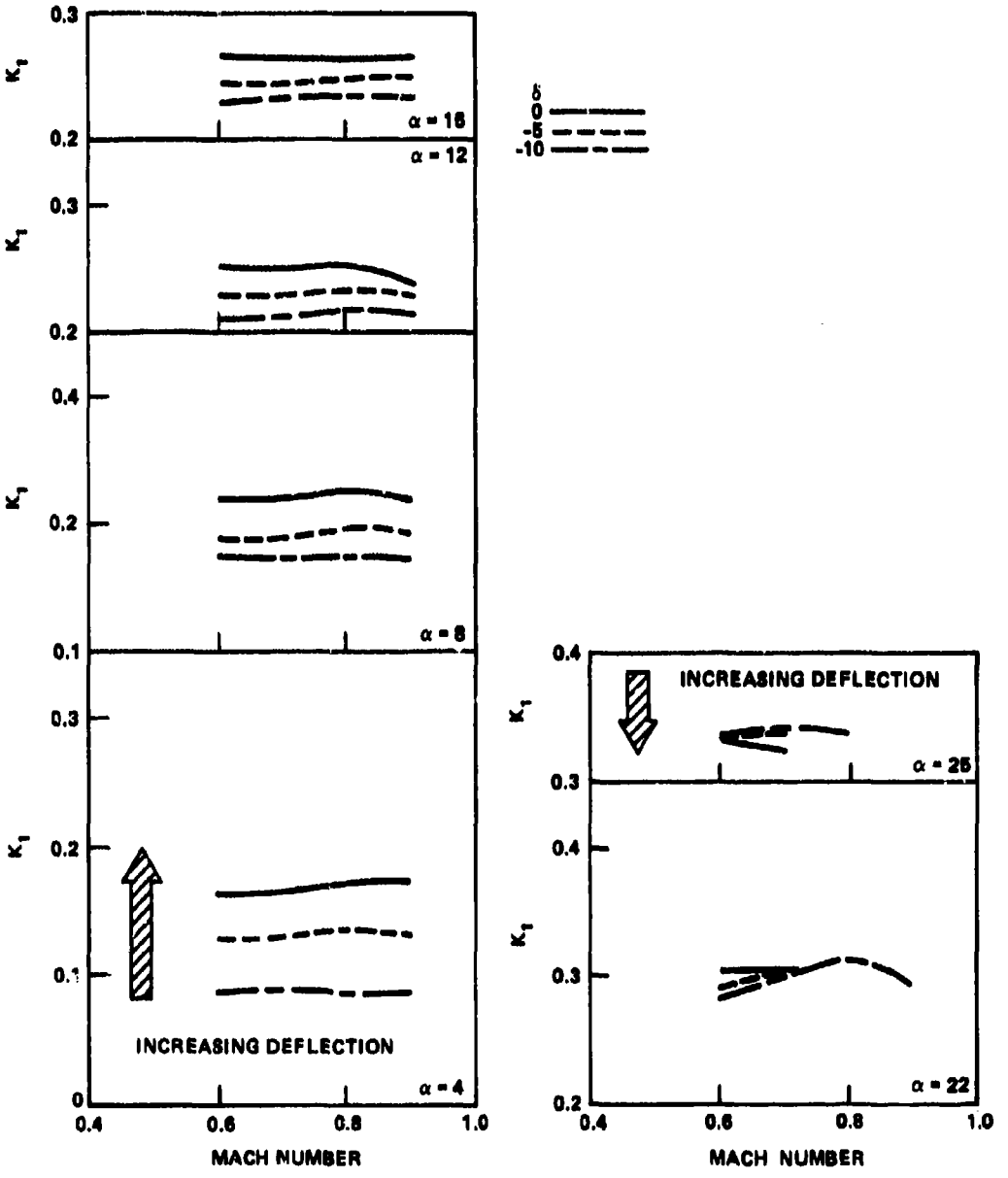

Figure 63a - Deflection for C_0 P_6 on 50-Degree Wing

Figure 63 (Continued)

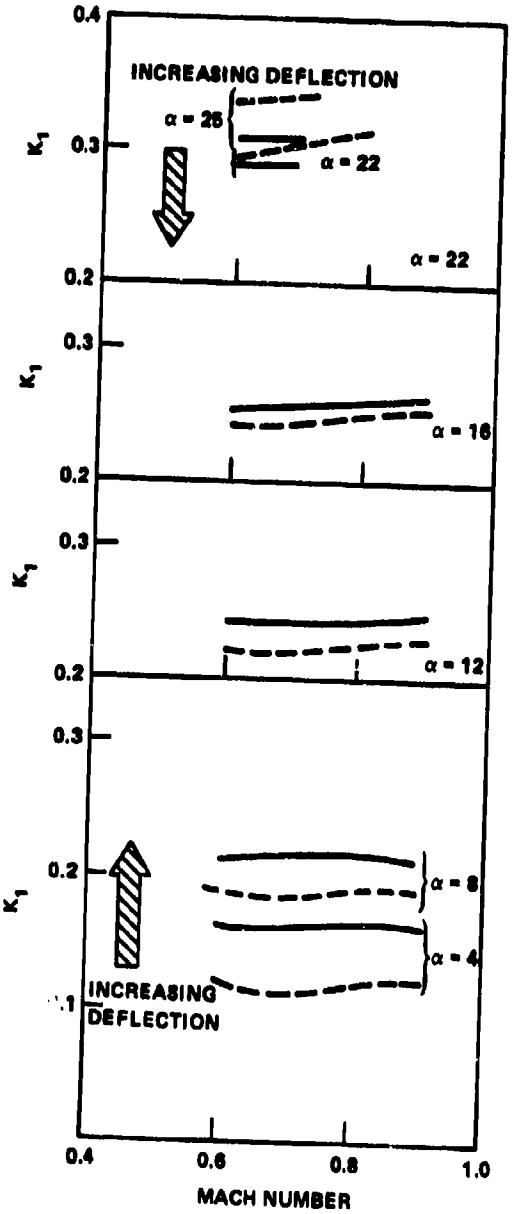

Figure 63b - Deflection for $C_1 P_2$ on 50-Degree Wing

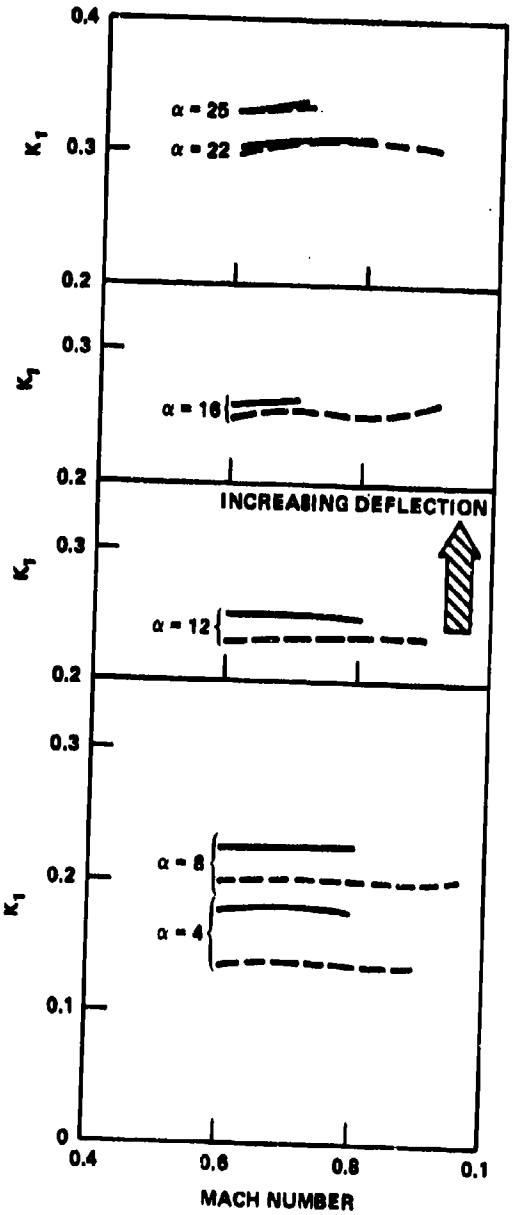

Figure 63c - Deflection for $C_1 P_3$ on 50-Degree Wing

Figure 63 (Continued)

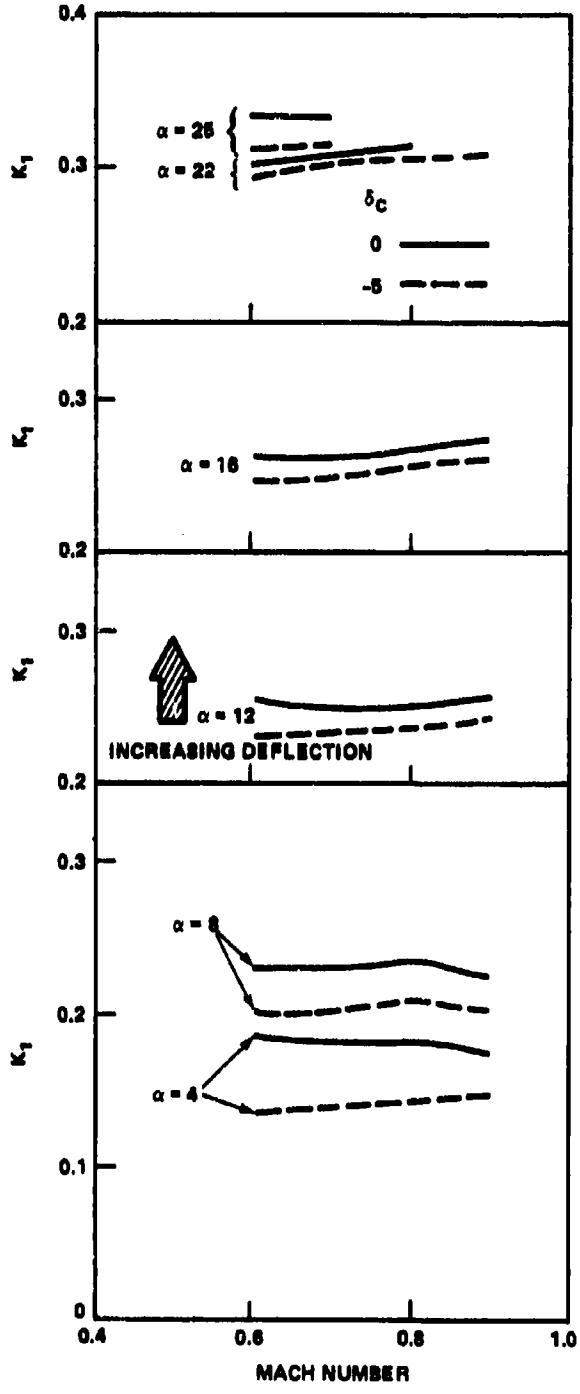

Figure 63d - Deflection for C_1 P_6 on 50-Degree Wing

Figure 63 (Continued)

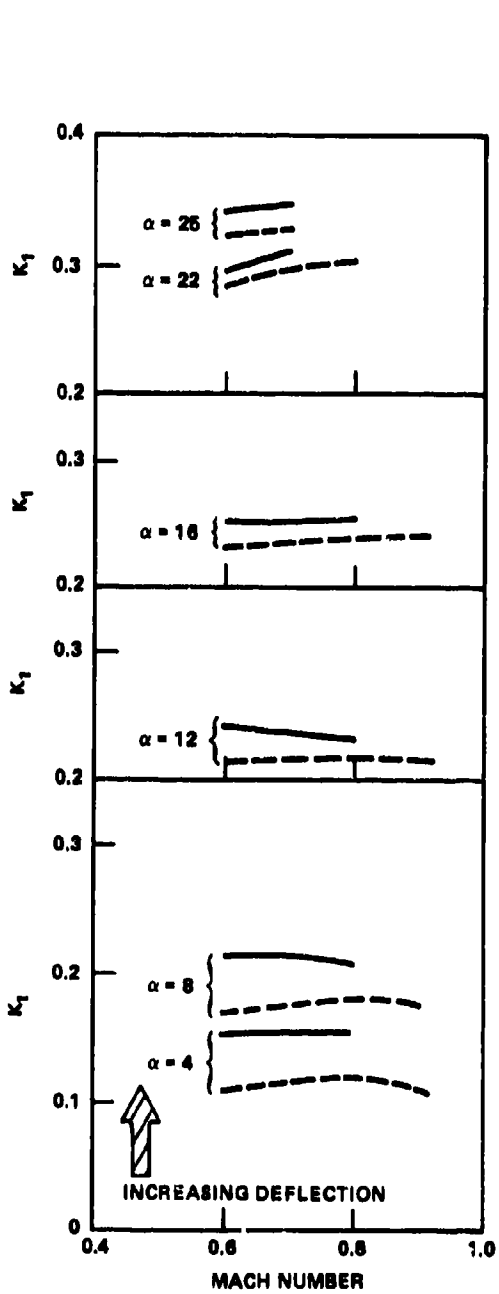

Figure 63e - Deflection for C_2 P_3 on 50-Degree Wing

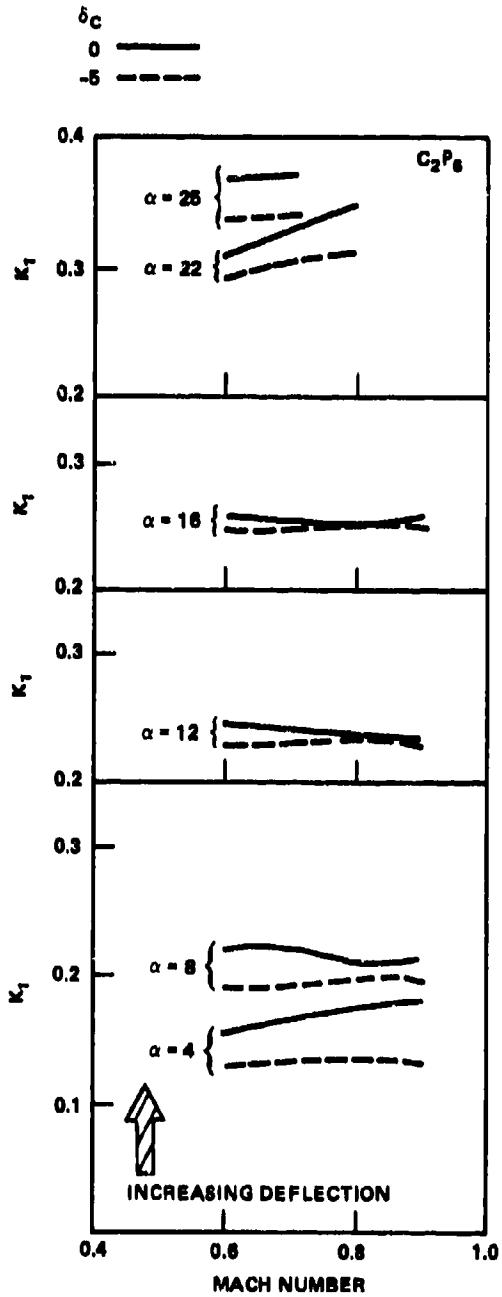

Figure 63f - Deflection for C_2 P_6 on 50-Degree Wing

Figure 63 (Continued)

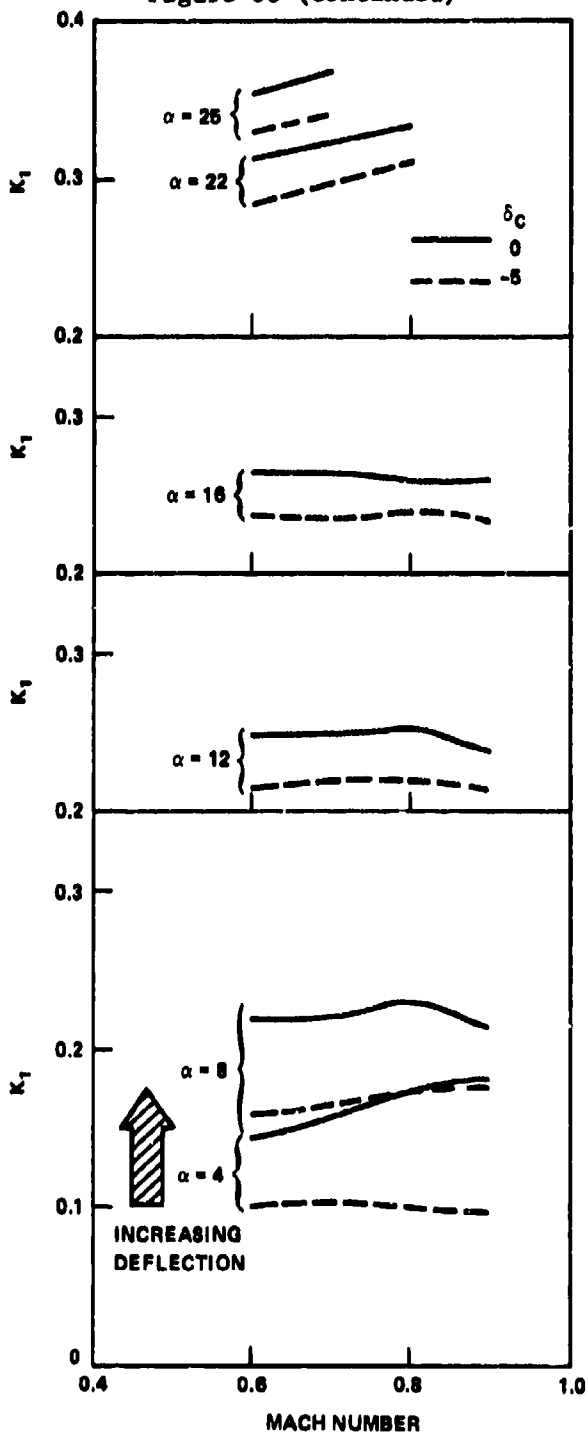

Figure 63g - Deflection for C_3 P_3 on 50-Degree Wing

Figure 63 (Continued)

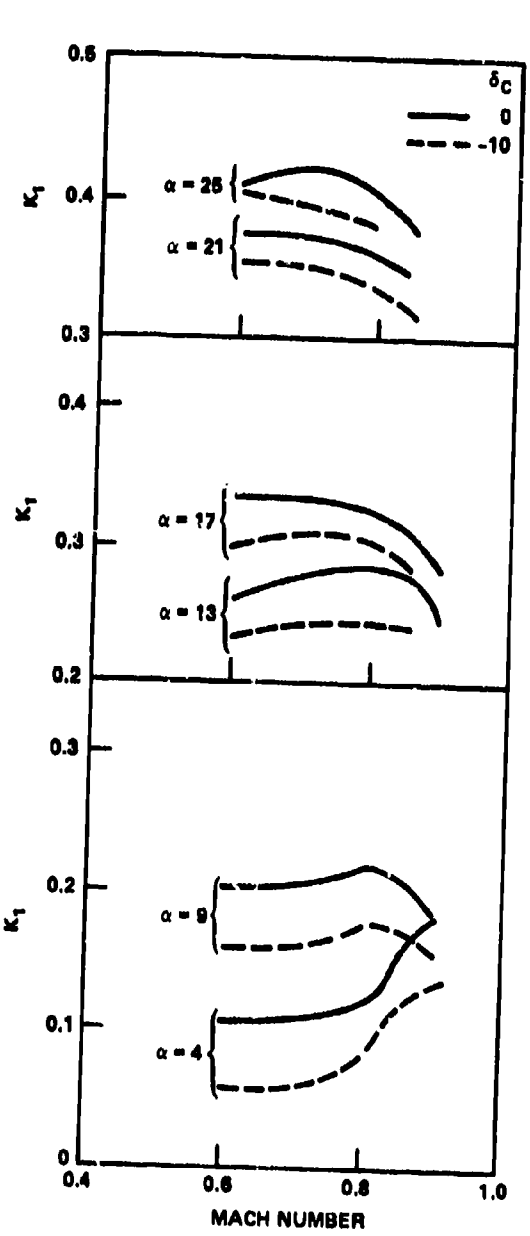

Figure 63h - Deflection for C_0 P_6 on 25-Degree Wing

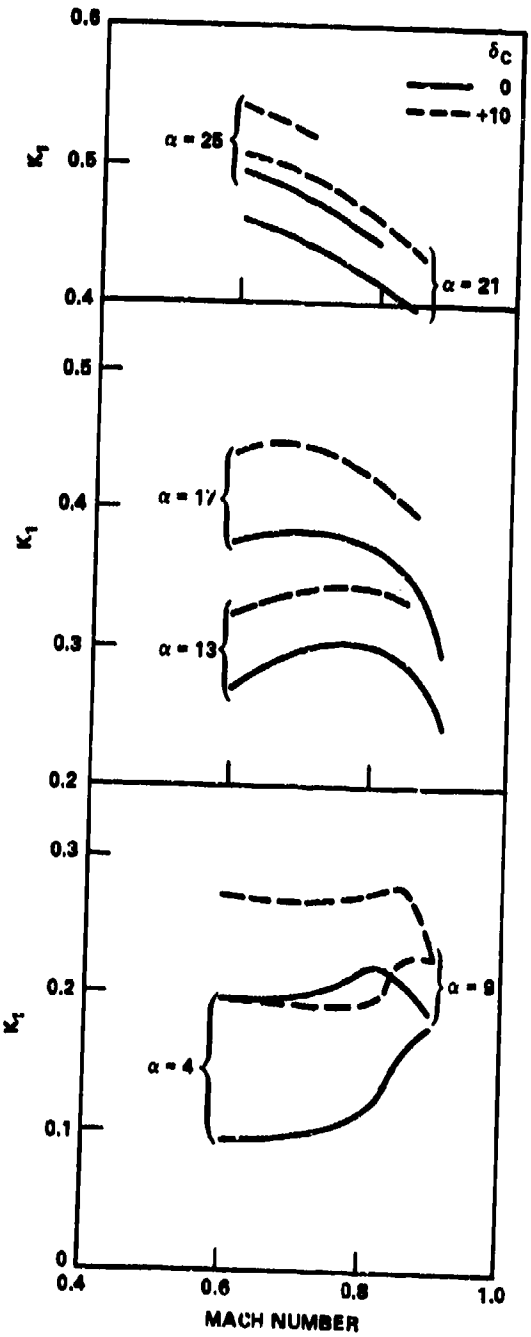

Figure 63i - Deflection for C_0 P_1 on 25-Degree Wing

the slat effectiveness is reduced. At present, data are not sufficient to determine the actual magnitude of the distance of this critical gap height.

The final segment of this discussion on drag due to canard deflection is on the L/D variation.

The effect of a positive 10-degree deflection on the maximum L/D for the 50-degree wing is presented in Figure 64. Deflecting the canard caused a reduction in $(L/D)_{max}$ of approximately 30 percent when compared to the nondeflected canard. The magnitude of this loss is relatively constant until the drag rise, when it is reduced significantly due to the large increase of drag on the overall configuration. Thus, the additional drag due to the deflection is a smaller percentage of the total minimum drag. Similar trends occur for the 25-degree sweep model as indicated in Figure 65. Figure 65 includes data for both positive and negative canard deflections for both models. With increasing Mach number, the penalty in L/D for positive deflections is significantly reduced, this is due, however, to the large increase in drag due to compressibility.

Negative deflections increase $(L/D)_{max}$ for both wing sweeps. The increase in $(L/D)_{max}$ occurred at both negative deflections on the 25-degree wing but only at -5-degrees deflection on the 50-degree wing. At the higher lift coefficients, canard deflection does not significantly change L/D.

The remaining data on the variation of L/D due to deflection is presented in Figure 66. Data are presented for canards C_1, C_2, and C_3 at position P_3 for the 50-degree model and canards C_0, C_1, and C_2 at position P_6.

Canard C_0 was evaluated at positions P_3 and P_6 for the 25-degree wing model. As in the previous discussion, light negative deflections, $\delta_c \sim -5$ degrees, increased $(L/D)_{max}$ over the $(L/D)_{max}$ of the undeflected configuration. At the higher lift coefficient, deflection made little difference in L/D for the 50-degree wing. A negative 10-degree deflection at position P_6 for the 25-degree wing model, however, reduced L/D at $C_L = 0.9$ by 0.5. This reduction also occurred at position P_3 for the 25-degree wing as presented in Figure 65.

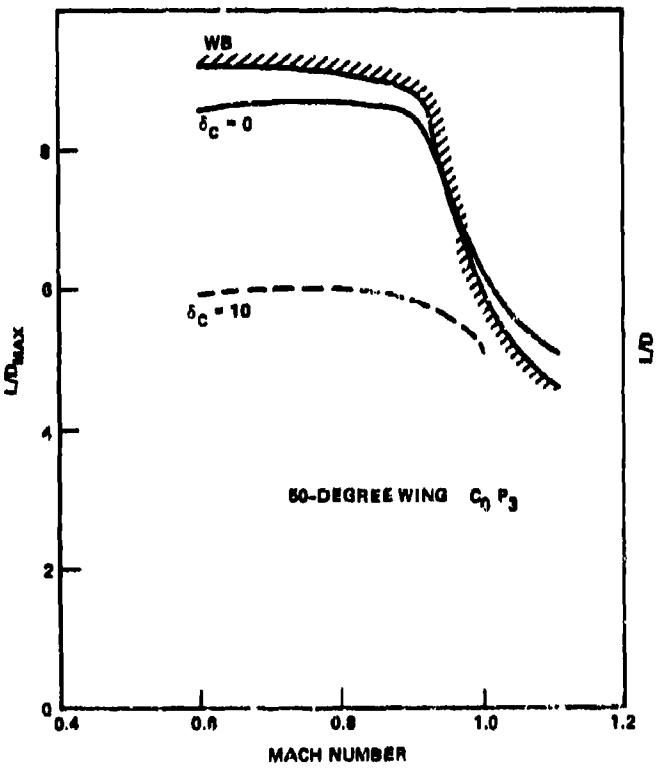

Figure 64a - Positive Canard Deflection

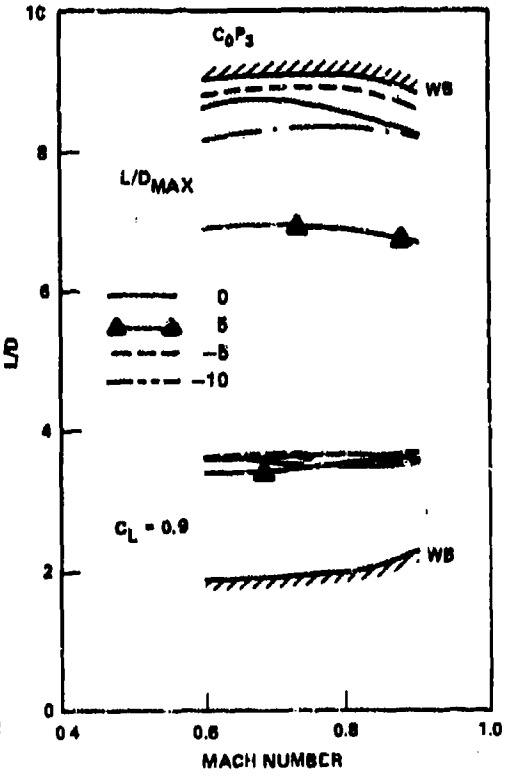

Figure 64b - Positive and Negative Deflections

Figure 64 - Effect of Canard Deflection on Lift-to-Drag Ratio for the 50-Degree Wing

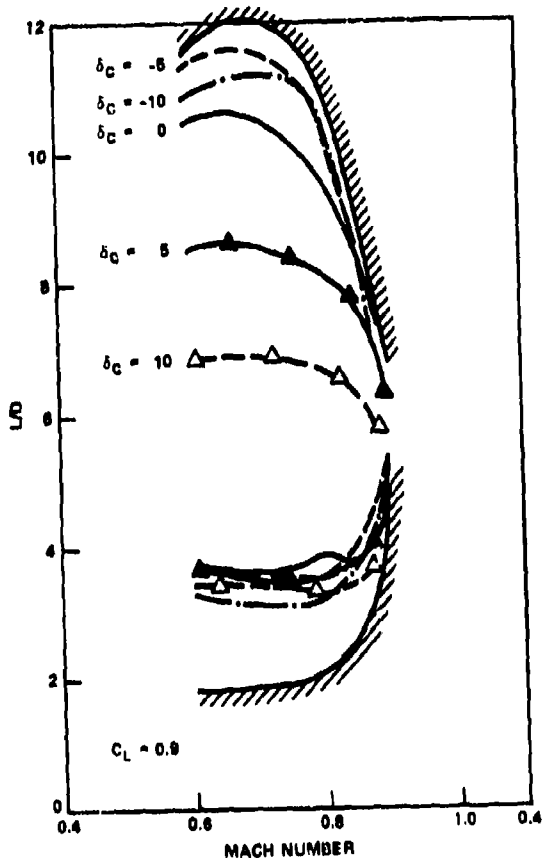

Figure 65 - Effect of Canard Deflection on Lift-to-Drag Ratio for the 25-Degree Wing

Figure 66 - Effect of Canard Deflection on Lift-to-Drag Ratio

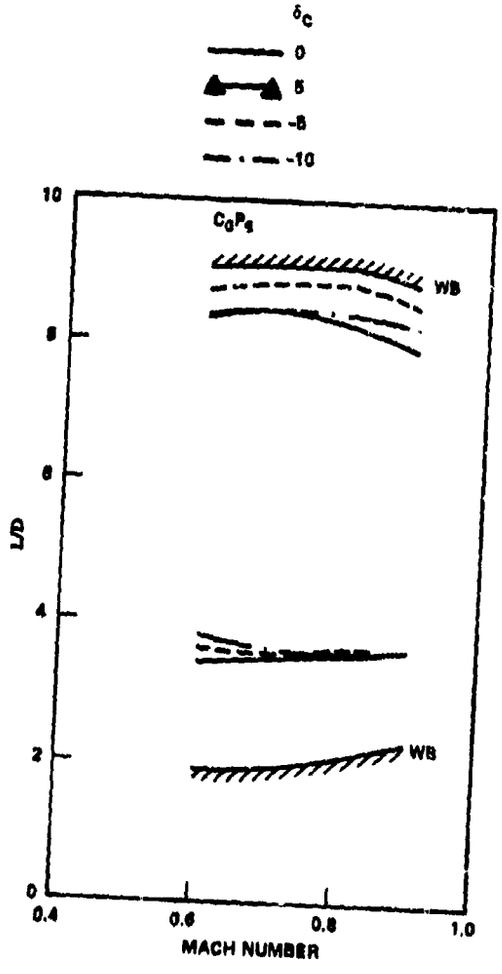

Figure 66a - Canard C_0 on 50-Degree Wing

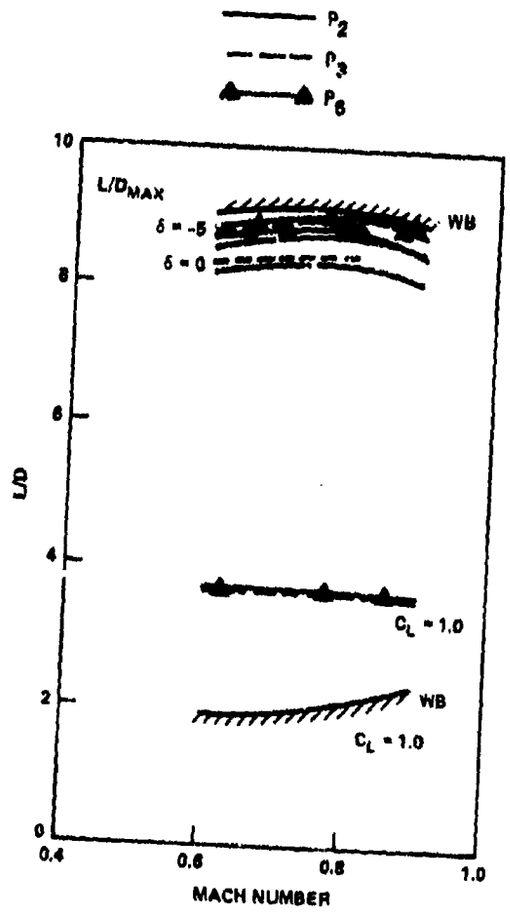

Figure 66b - Canard C_1 on 50-Degree Wing

Figure 66 (Continued)

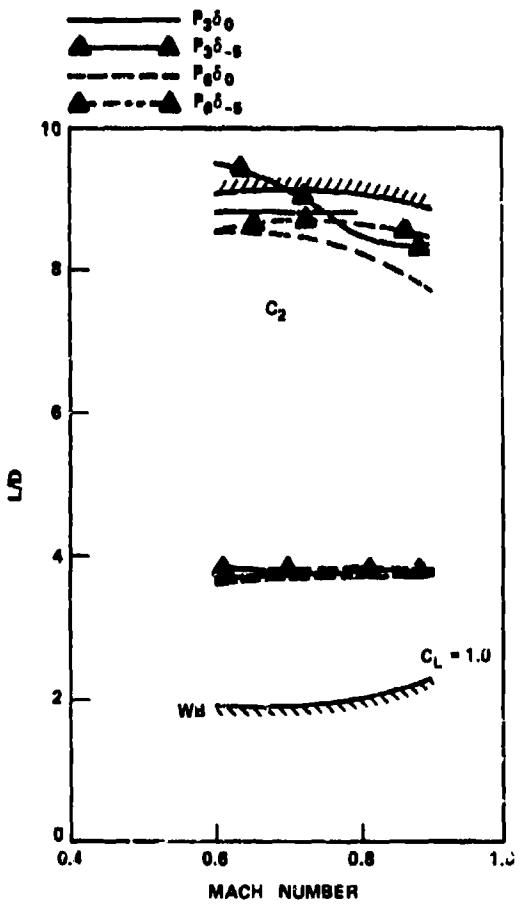

Figure 66c - Canard C_2 on 50-Degree Wing

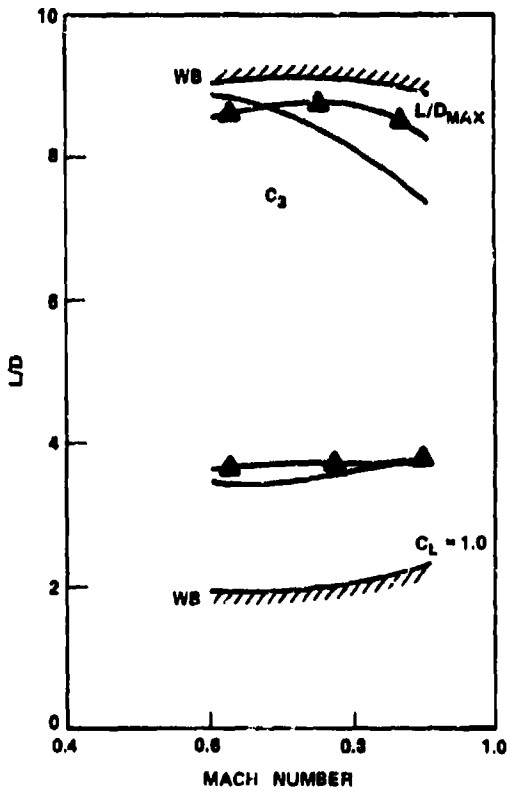

Figure 66d - Canard C_3 P_3 on 50-Degree Wing

Figure 66 (Continued)

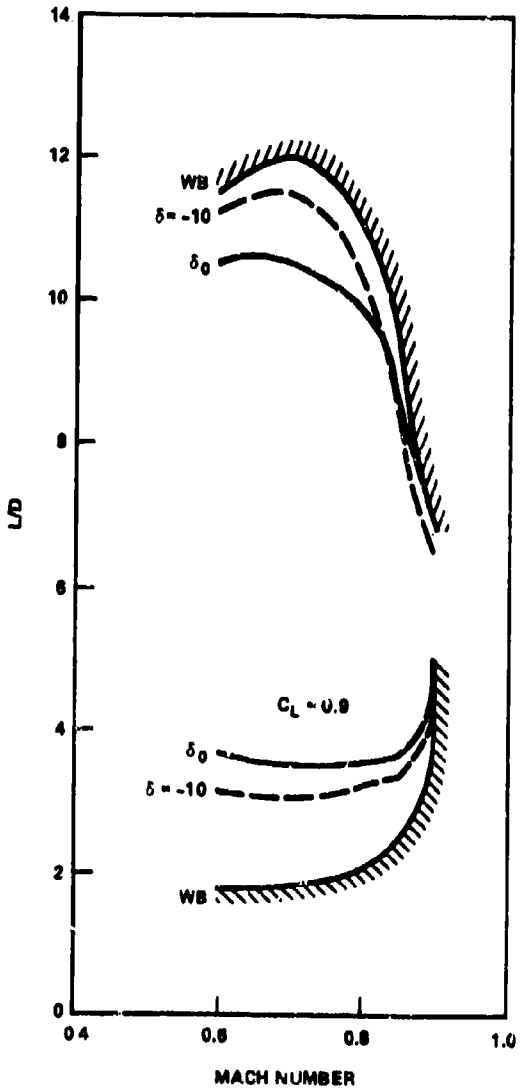

Figure 66e - Canard C_0 P_6 on 25-Degree Wing

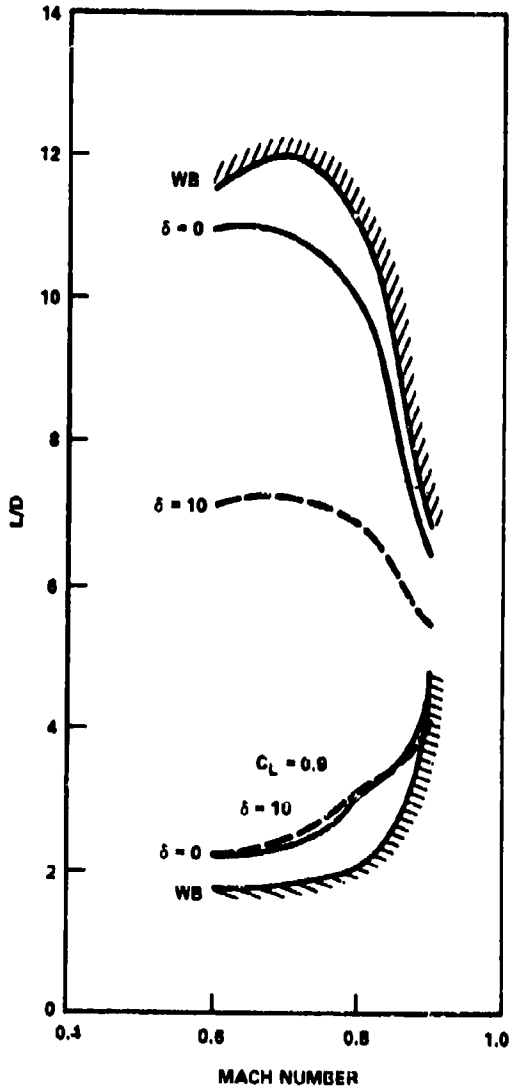

Figure 66f - Canard C_0 P_1 on 25-Degree Wing

TRISURFACE CONFIGURATIONS

The carrying of a canard on a normal aircraft configuration consisting of wing-body-tail incurs a drag penalty. This penalty is primarily due to friction drag or $C_{D_{min}}$. This penalty is shown in Figure 67. The configurations presented in Figure 67 are that of the basic wing-body, wing-body-tail, wing-body-canard, and trisurface configurations. Data are presented for various canard and horizontal tail deflections for both wing configurations.

As with the canard alone, adding the canard to the wing-body-tail configuration causes a small drag increment which is relatively constant. This increment is slightly smaller than that due to the canard alone, thereby indicating that the canard is reducing the drag of the horizontal tail.

This increase in minimum drag due to the addition of the canard is offset by the lower values of induced drag factor of the trisurface configuration which is presented in Figure 68. This reduction is most significant at the higher angles of attack, where the trisurface configuration had consistently lower values of k_1 than the canard alone at angles of attack of 16 degrees or better.

The penalty in minimum drag caused by the additional surface results in a reduction in maximum L/D as shown in Figure 69. The data in Figure 69 are untrimmed and, as will be discussed in Volume 4 of this report when the configuration is trimmed, the penalty in $(L/D)_{max}$ due to carrying the canard can be reduced almost completely. At the higher lift coefficient there is no penalty for carrying the canard and the trisurface aircraft has approximately the same value as the canard alone.

The data in Figure 69 are at 0-degree tail deflection. In order to trim at higher lift coefficients negative tail deflections are required for a stable configuration. Lift-to-drag ratios for the wing-body-tail and trisurface configuration at tail deflection of -10 degrees are presented in Figure 70. As shown, adding the canard to the configuration increases L/D by approximately 50 percent for both wing sweeps.

Figure 67 - Comparison of Minimum Drag of Canard, Horizontal Tail, and Trisurface Configurations

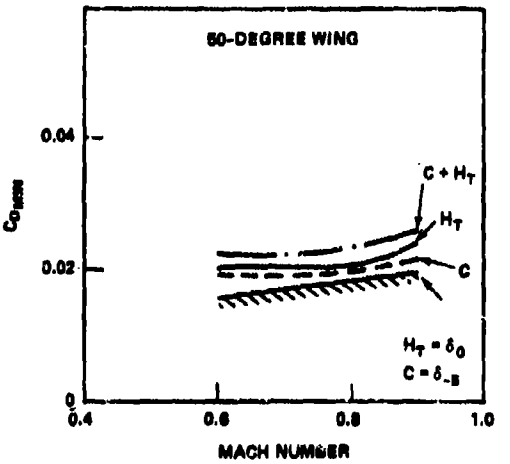

Figure 67a - $\delta_{H_T} = 0$, $\delta_c = -5$

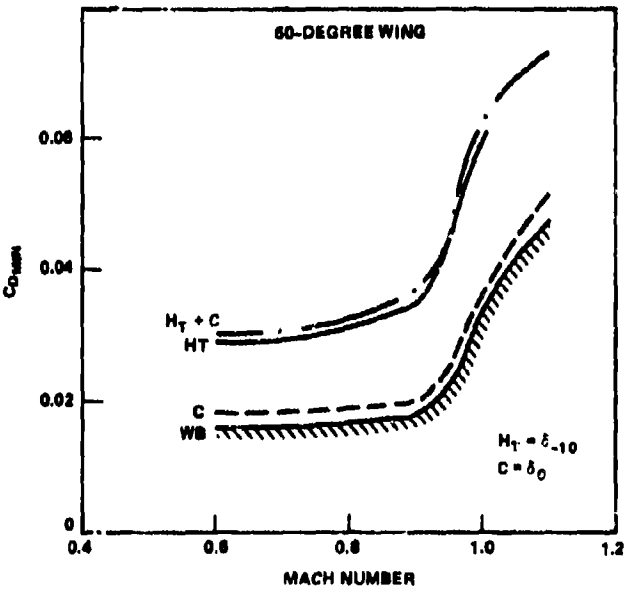

Figure 67b - $\delta_{H_T} = -10$, $\delta_c = 0$

Figure 67 (Continued)

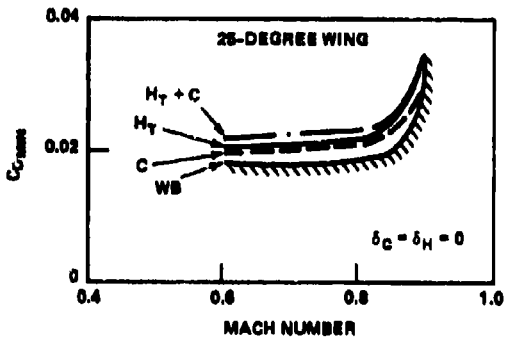

Figure 67c - $\delta_{H_T} = 0$, $\delta_c = 0$

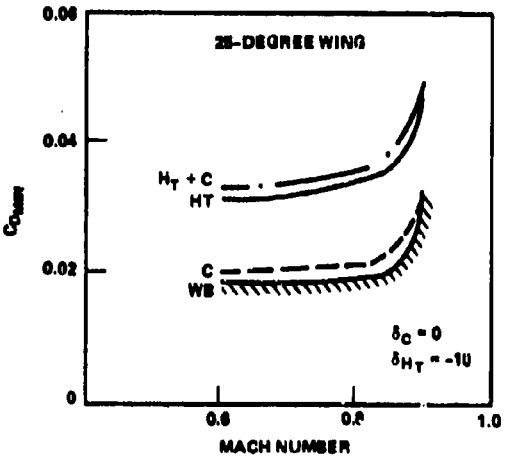

Figure 67d - $\delta_{H_T} = -10$, $\delta_c = 0$

Figure 68 - Induced Drag Factor for Canard, Horizontal Tail, and Trisurface Configurations

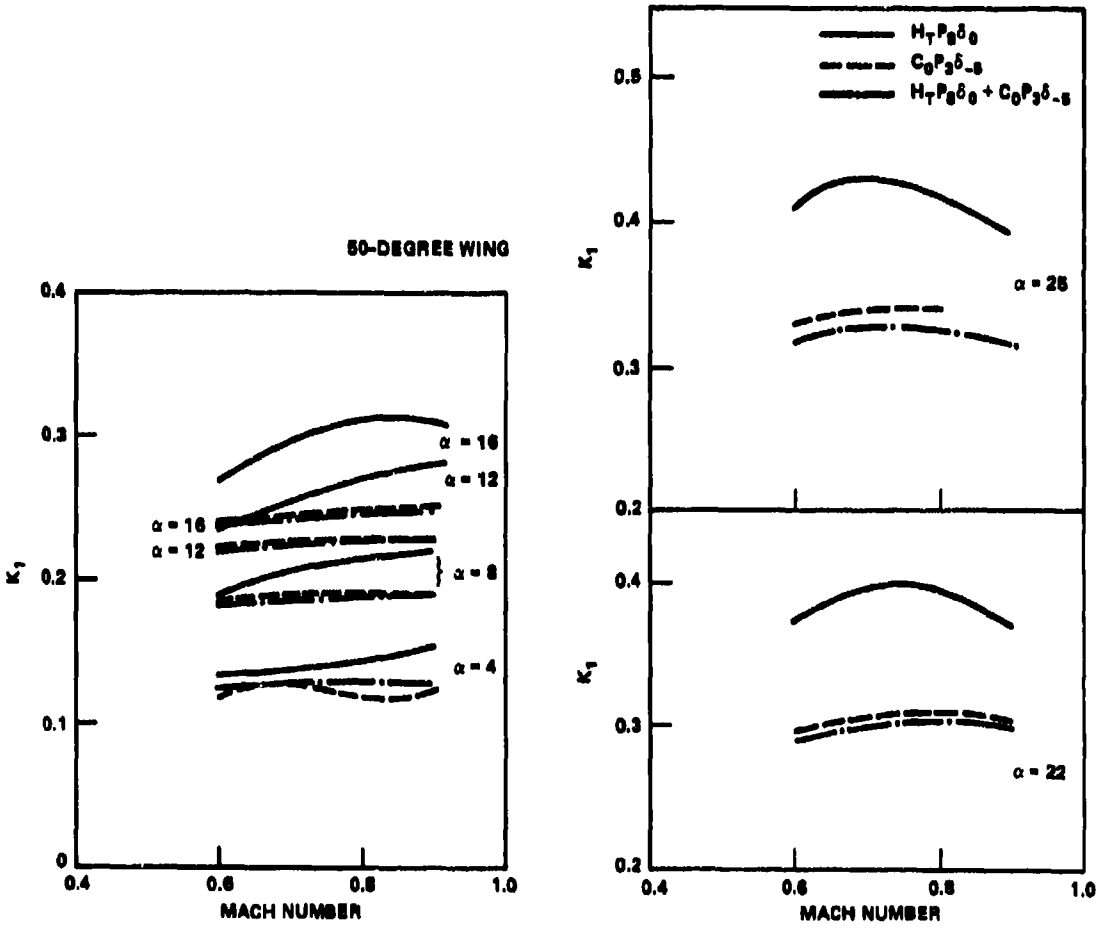

Figure 68a - Induced Drag for 50-Degree Wing

Figure 68 (Continued)

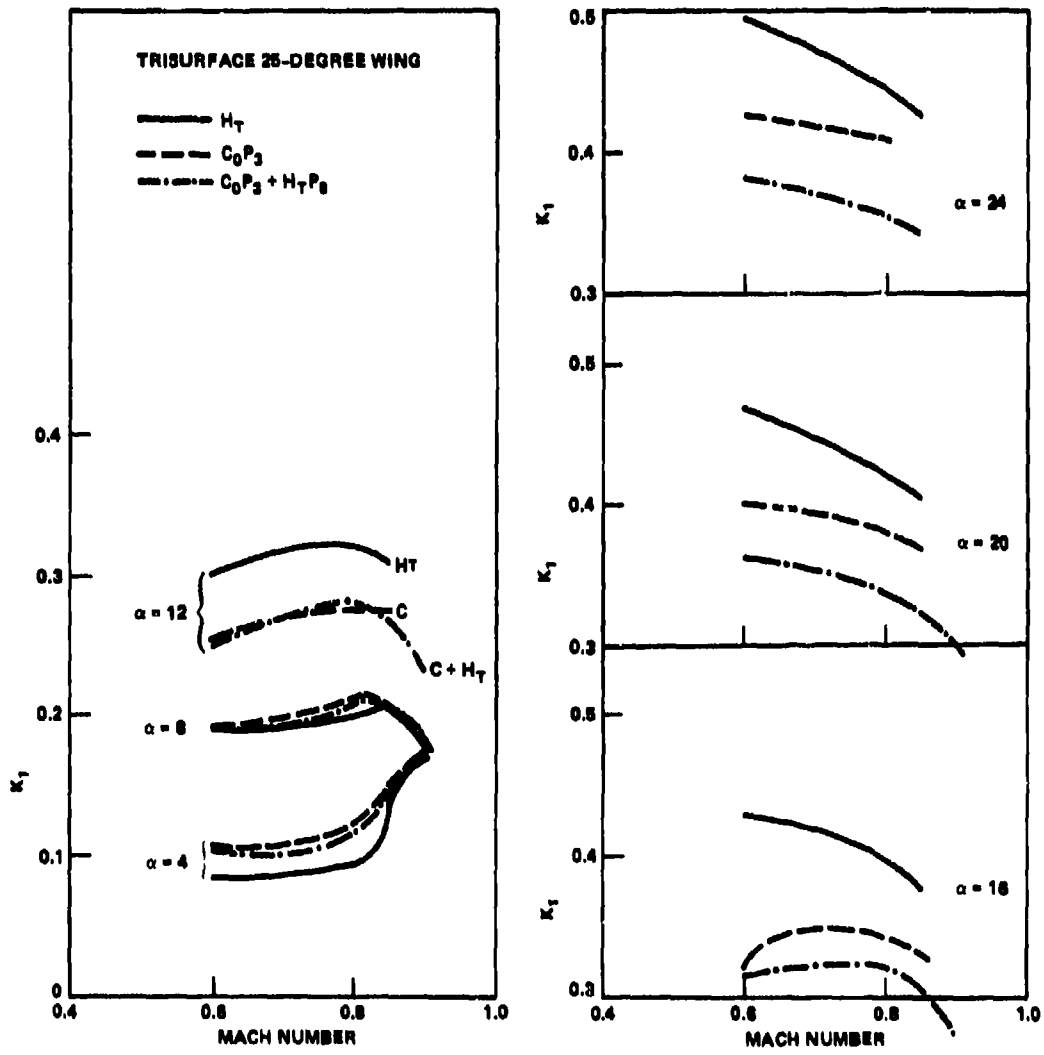

Figure 68b - Induced Drag for 25-Degree Wing

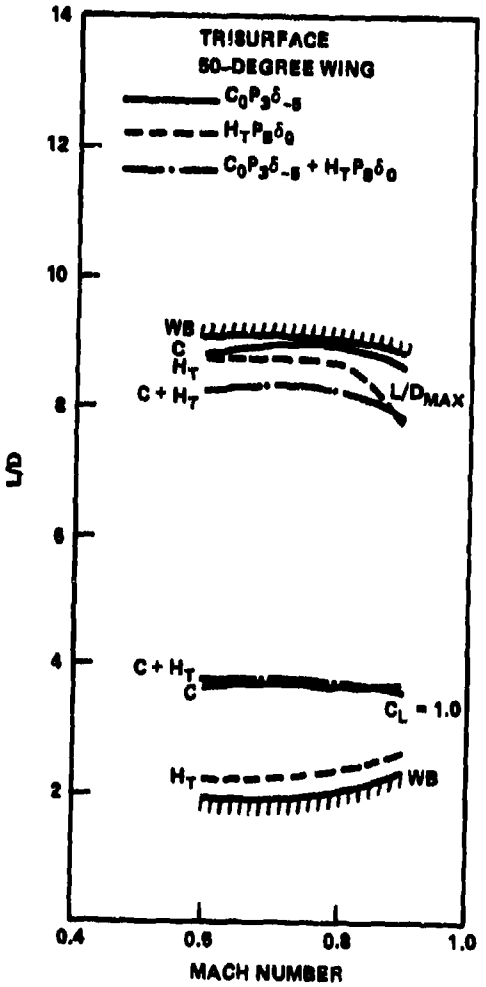

Figure 69a - Lift-to-Drag Ratios for 50-Degree Wing

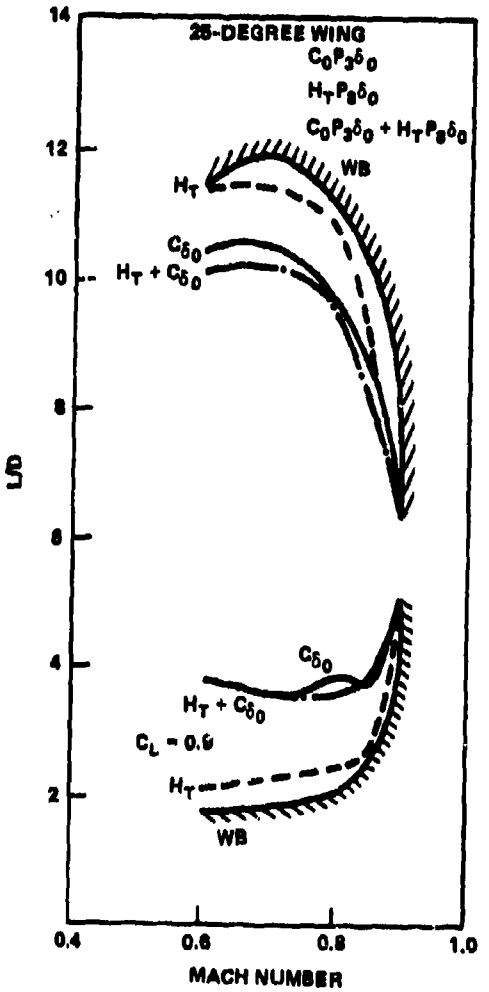

Figure 69b - Lift-to-Drag Ratios for 25-Degree Wing

Figure 69 - Lift-to-Drag Ratios for Canard, Horizontal Tail, and Trisurface Configurations

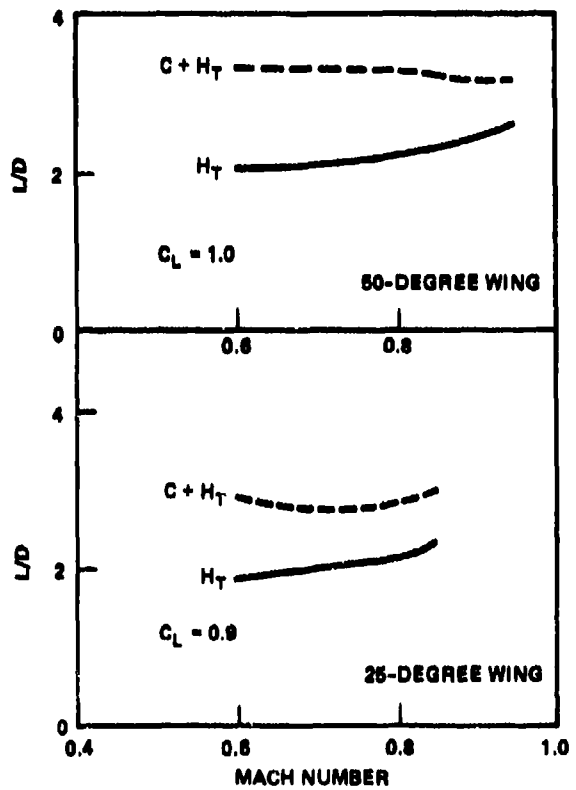

Figure 70 - Lift-to-Drag Ratios at C_L = 1.0 and 0.9 for 50- and 25-Degree Wings, Horizontal Tail, and Trisurface Configurations with Horizontal Tail Deflected -10 Degrees

BUFFET

The close-coupled canard has a favorable effect on buffet onset lift coefficient and intensity. Both 50- and 25-degree sweep models were fitted with wing root bending moment gages, and root mean square (RMS) values of wing bending moment were taken.

A discussion of and means of obtaining these data are given by Ottensoser.[4] He indicates that the canard had little favorable effect on the 25-degree wing primarily due to the early onset of buffet (B.O.) caused by the low wing sweep. The present discussion will, therefore, be limited to the 50-degree sweep model.

Several methods are available for obtaining the buffet onset lift coefficient. These methods include RMS data, axial force data, and lift data. With an actual aircraft, RMS data can be taken in small increments at constant load factor, one "g" in most cases, and buffet onset can be reasonably determined. In the wind tunnel, however, in order to obtain one "g" condition, i.e., constant normal force with varying angle of attack, it is necessary but not practical to vary the dynamic pressure. Thus, RMS data for a tunnel model does not give a true indication of when buffet onset actually occurs, but rather an indication of the dynamic contribution of a varying normal force. In addition, for a wind tunnel model, the tunnel turbulance and compressor acoustics can excite the model.

The axial force characteristics often used for buffet onset determination include the zero values of the first and second derivatives of axial force with lift coefficient $\partial C_A/\partial C_L$ and $\partial^2 C_A/\partial C_L^2$. An additional means of buffet onset determination is the deviation of the actual lift curve from the ideal or low angle lift curve slope. It is this method, in conjunction with tha axial force methods, which has been used to determine buffet onset lift coefficient in this report.

Buffet onset lift coefficient is taken to be that value which deviates 5 percent from the predicted low angle of attack value. The lift curve slope for prediction was taken between 0- and 5-degrees angle of attack.

An example of this technique is presented in Figure 71 for both basic wing-body and canard-wing-body. Shown in the figure are the axial force variations for both configurations and the values of $\partial C_A/\partial C_L = 0$ and

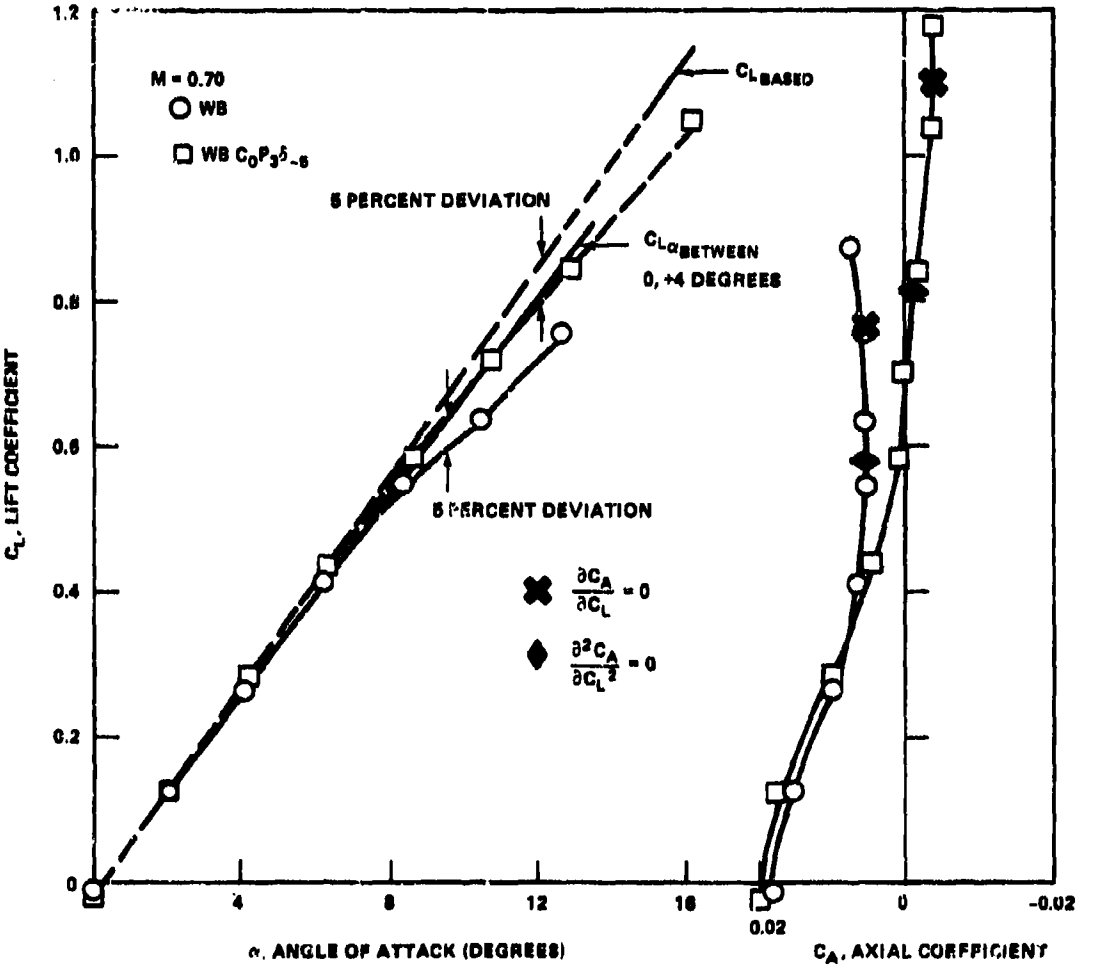

Figure 71 - Comparison of Lift Curve Deviation and Axial Force Techniques for Buffet Onset Determination

$\partial^2 C_A/\partial C_L^2 = 0$ for each. As indicated, the lift curve deviation method gives values of buffet onset lift coefficient approximately the same as those at the second derivative zero values and lower values than the first derivation values. The incremental difference between each method, however, is approximately the same ($0.2 < \Delta C_{L_{B.O.}} \leq 0.3$). Thus, while the exact buffet onset lift coefficient may not be known, it is felt that the observed trends are valid.

The effect of canard position on buffet onset lift coefficient and angle of attack is shown in Figure 72. Data are presented for canards C_0 and C_2 at positions P_3 and P_6 and for canard C_1 at positions P_2, P_3, and P_6. The deflection angle is -5 degrees for all canard shapes. As indicated in Figure 72, buffet onset lift coefficient and angle of attack are larger for the canard configurations than for the basic wing-body. The magnitude of this increase rapidly diminishes with Mach number, however. In general, the high-aft position P_3 gave better results than the low position P_6.

The increase in buffet onset lift coefficient varied from a ΔC_L of 0.40 at M = 0.6 to 0.10 at M = 0.9. It should be noted that these data are based primarily on the 5-percent lift curve deviation.

The axial force criteria give larger improvements for the canard on data as shown in Figure 73. Figure 73 presents the variation of $\partial C_A/\partial C_L$ with lift coefficient for Mach numbers 0.6, 0.7, 0.8, and 0.9. Canard on and off data are both shown. As indicated, the range of $\partial C_A/\partial C_L = 0.0$ is between C_L's 0.73 and 0.44 for the basic wing-body versus a range of 1.16 to 0.84 for the canard configuration.

This range is shown in Figure 74. The axial force criteria predicts a larger, more constant increment in buffet onset lift coefficient than the lift deviation method; this increment is on the order of 0.4. It thus appears that the data in Figure 73 are somewhat conservative in determining the buffet onset C_L particularly at the higher Mach numbers.

The effect of canard shape on buffet onset is presented in Figure 75. Data are presented for the four shapes at position P_3. At low Mach numbers the higher sweep canards generated the highest buffet onset lift

Figure 72 - Effect of Canard Position on Buffet Onset Lift Coefficient and Angle of Attack

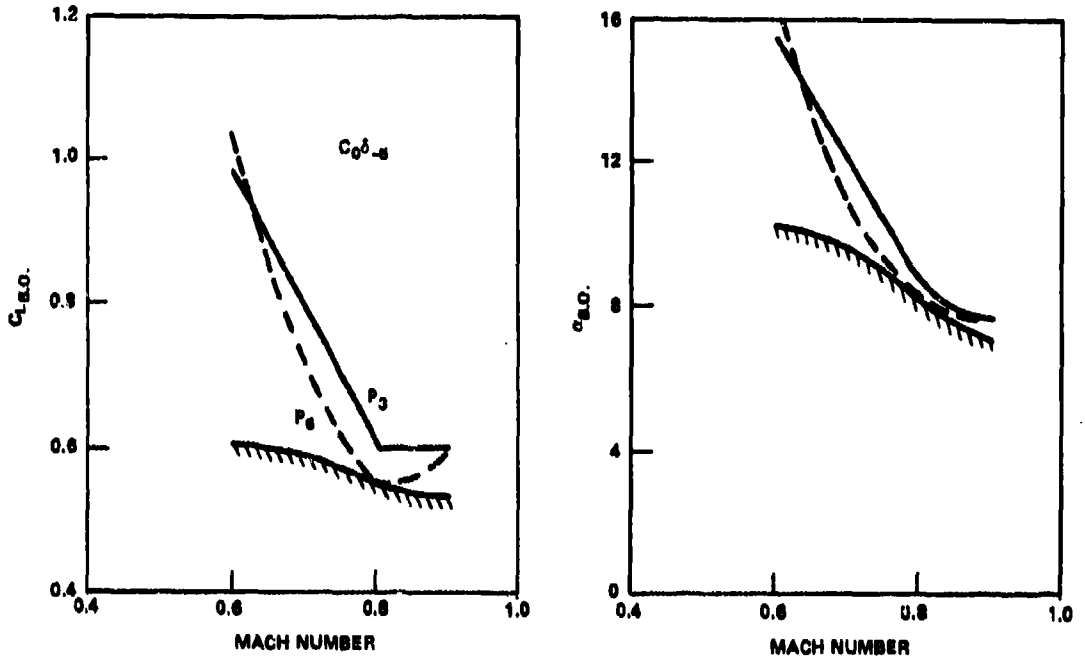

Figure 72a - Position for Canard C_0

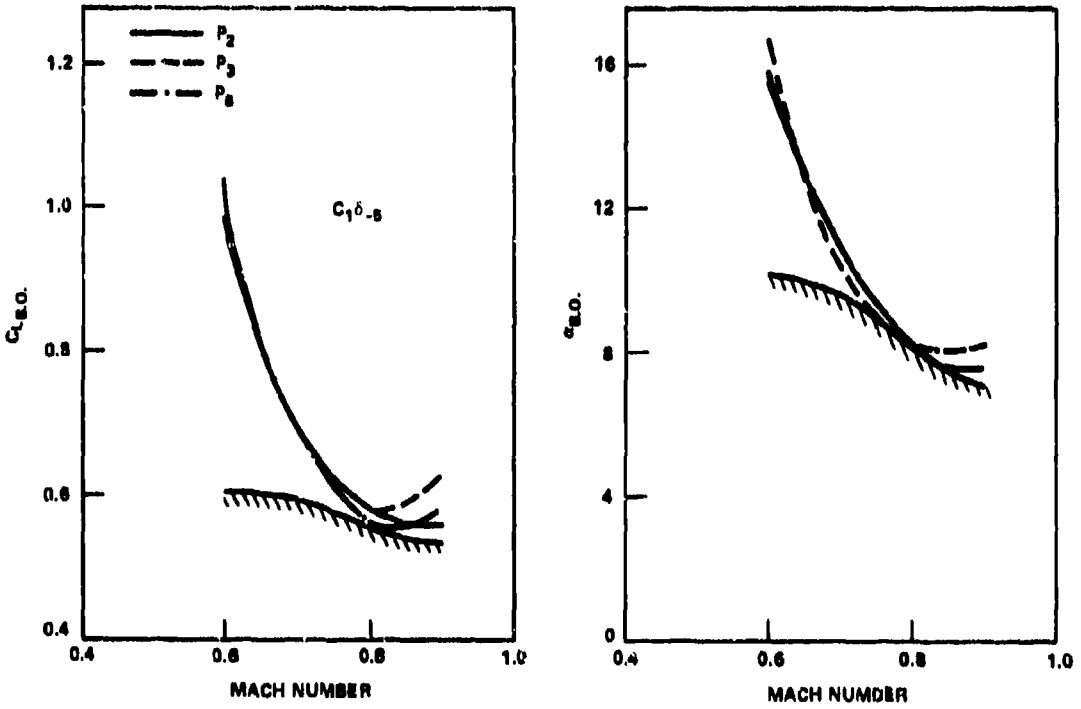

Figure 72b - Position for Canard C_1

Figure 72 (Continued)

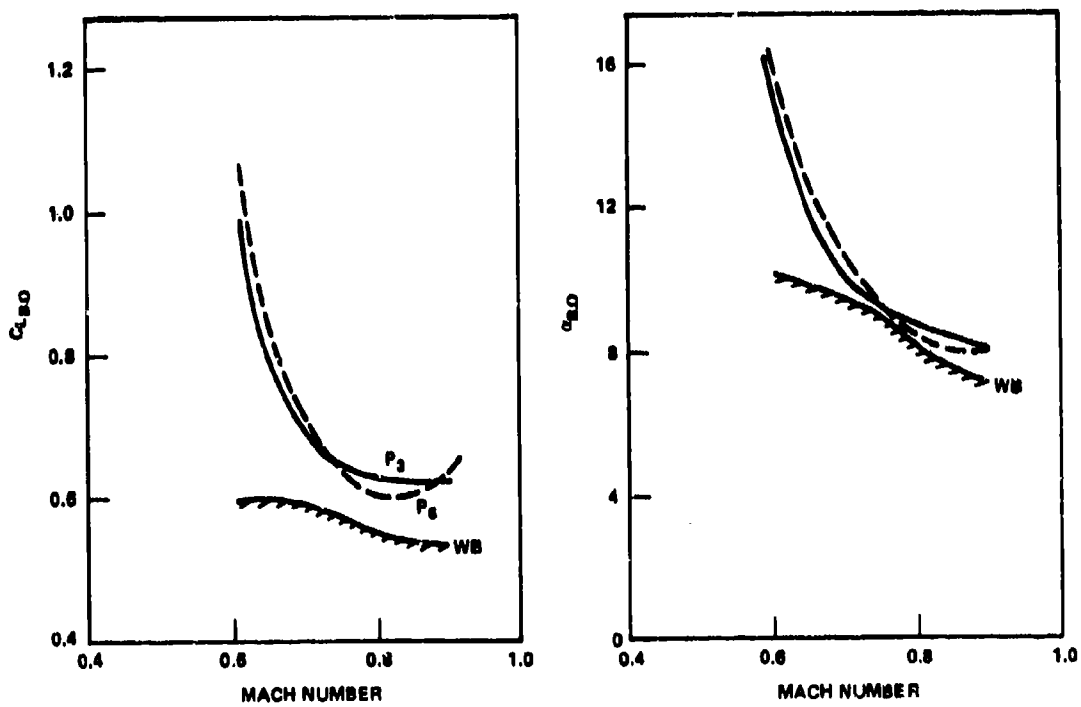

Figure 72c - Position for Canard C_2

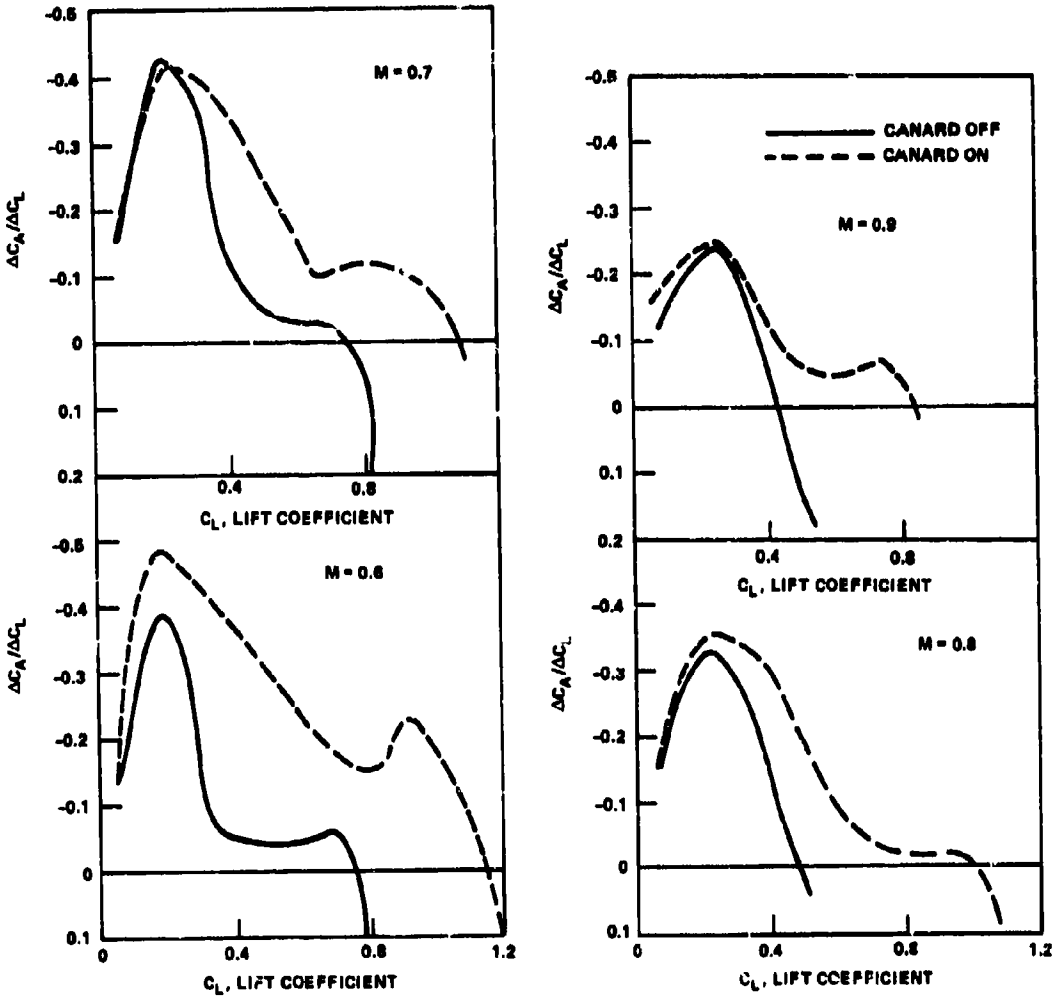

Figure 73 - Variations of Axial Force Slope with Lift Coefficient

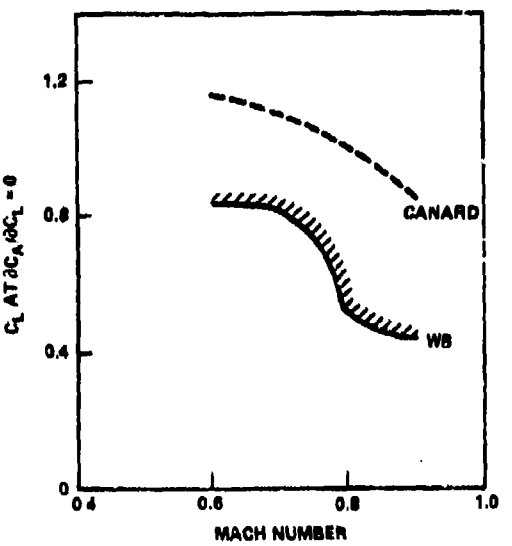

Figure 74 - Comparison of Buffet Onset Lift Coefficient Based on Axial Force Criteria for Canard and Wing-Body

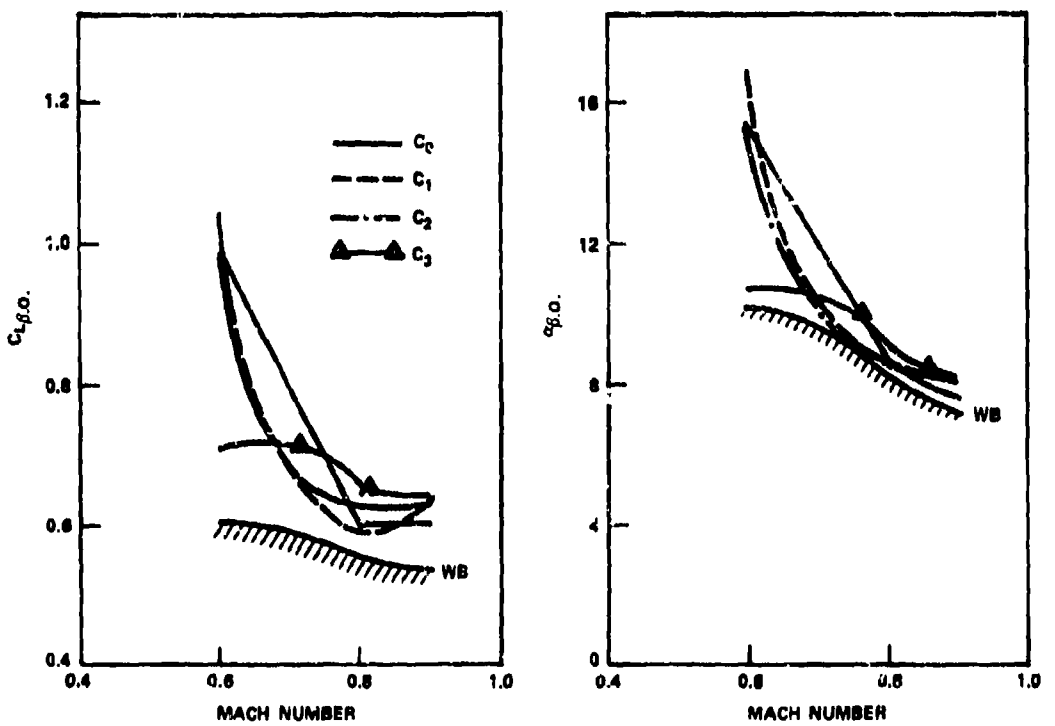

Figure 75 - Effect of Canard Shape on Buffet Onset Lift Coefficient and Angle of Attack

coefficient. As Mach number is increased, the lowest sweep canard C_3 performed best. This is due to the fact that canard C_3 has the highest values of C_{L_α} at low angles of attack ($\alpha < 12$ degrees), thus higher overall configuration lift coefficients are possible. Angle of attack for buffet onset is not significantly different for any of the canards at high Mach numbers. In an overall sense, canard C_2 performed best.

Canard deflection is presented in Figure 76. The negative canard deflection configuration had lower values of buffet onset lift coefficient over most of the Mach number range based on the lift curve deviation method presented. Based on the axial force criteria this was not the case. Positive canard deflections exhibited very little negative change in axial force with increasing lift coefficient, whereas negative deflections exhibit reductions in axial force. This difference in axial force behavior may be due to flow separation of the canard when positively deflected. Thus the canard itself may be buffeting at an early lift coefficient, whereas the canard is still preventing separation of the main wing.

The last data on buffet onset to be presented are shown in Figure 77. Comparison data on the horizontal tail and canard are presented. As shown, the presence of the horizontal tail has little effect on buffet onset lift coefficient whereas the canard has a significant effect. Thus the increase in buffet onset lift coefficient is not due merely to the additional area of the canard or horizontal tail, but rather due to the favorable interference between canard and wing.

BUFFET INTENSITY

It was mentioned earlier that it is often difficult to estimate buffet onset from RMS data in the wind tunnel. The RMS data does, however, give an excellent representation of the buffet intensity. Since the model in the wind tunnel is not at constant load factor, or in nonturbulent air, incremental buffet intensity will be presented. This incremental intensity was obtained by subtracting the RMS value at zero lift coefficient and dividing by half the total value of the lift force on the model, lift = $qSw\ C_{L/2}$.

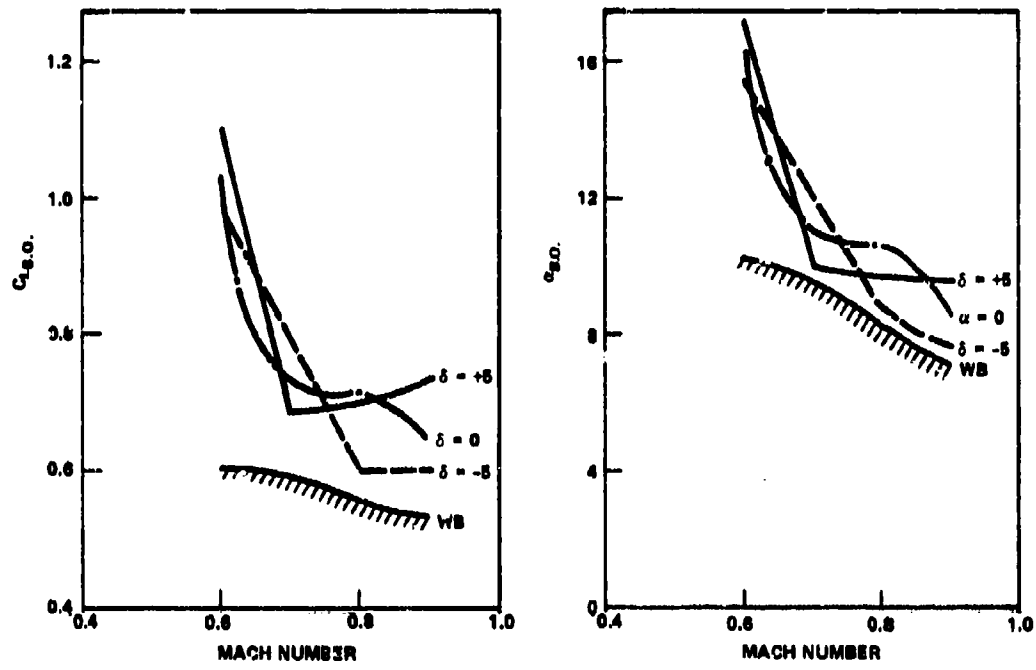

Figure 76 - Effect of Canard Deflection on Buffet Onset Lift Coefficient and Angle of Attack

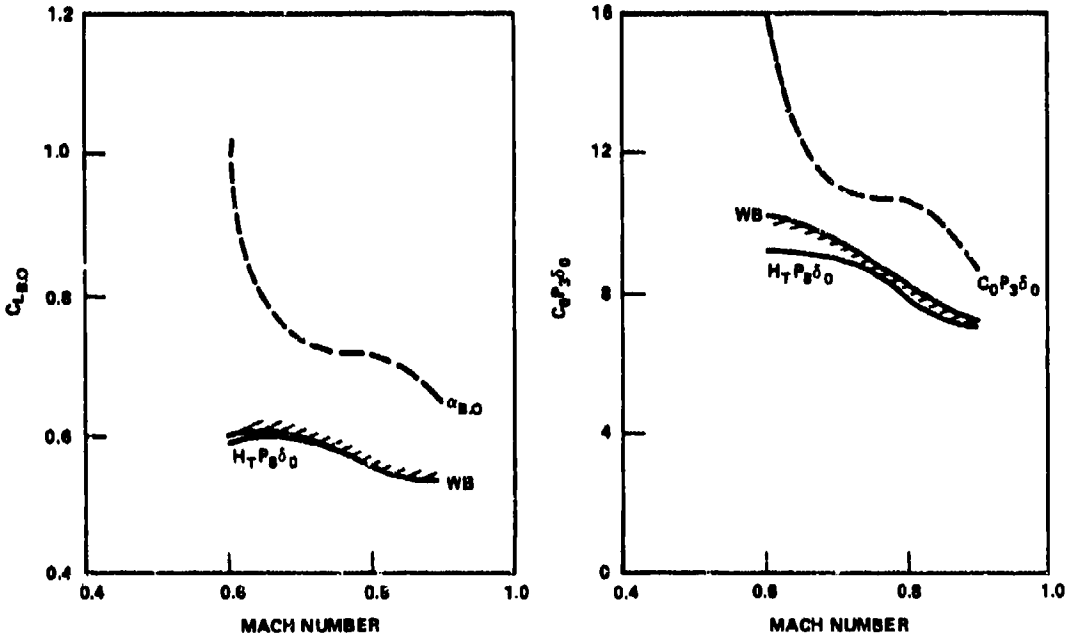

Figure 77 - Comparison of Buffet Onset Lift Coefficient and Angle of Attack for Horizontal Tail, Canard, and Basic Wing-Body

It was found that the data from the four Mach numbers evaluated for each configuration when plotted as incremental RMS, collapsed into a single line, albeit with a deal of scatter. Examples of this form of plot are shown in Figure 78 for the basic wing-body and the wing-body-canard.

The following discussion is based on the mean value curve of the various configurations.

The plots from which the mean lines were obtained are given in Appendix B. Actual RMS bending moment values are given in Reference 4.

A comparison of the buffet intensity between the canard, wing-body and horizontal tail is given in Figure 79. Data are plotted both as functions of C_L and angle of attack. As shown, buffet intensity is reduced for the canard configuration when compared with either basic wing-body or wing-body-horizontal tail. This is true, whether plotted versus angle of attack or lift coefficient. Thus the canard configured aircraft can pull higher load factors for equal buffet intensity.

Canard position had only a minimal effect on buffet intensity (as shown in Figure 80) for canard C_0. Strong influences are shown for the high aspect ratio canard C_2, where lowering the canard had a beneficial effect. Similarly, moving the canard aft improved the buffet intensity for the 60-degree canard C_1.

Figure 81 presents the effect of canard shape. The 45-degree canard C_0 had the lowest level of buffet intensity over most of the C_L range evaluated; however, intensity increased rapidly in the C_L range between 1.0 and 1.3. Beyond a lift coefficient of 1.15 the low sweep canard had the lowest level. Data, however, are not available for this canard beyond a C_L of 1.28.

Positive deflection of the canard appears to have a beneficial effect on buffet intensity as shown in Figure 82. Data are, however, insufficient to verify this effect in further detail.

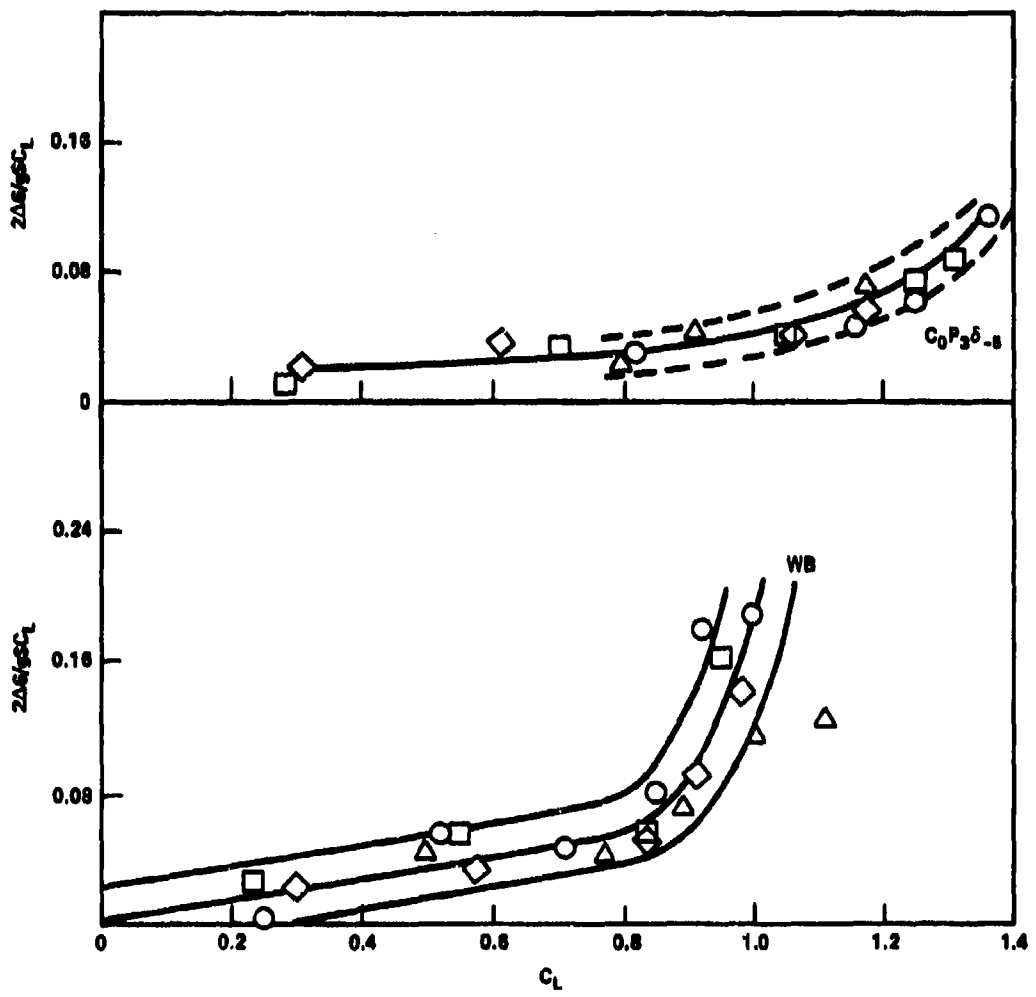

Figure 78 - Incremental Buffet Intensity for Basic Wing-Body and Wing-Body Canard

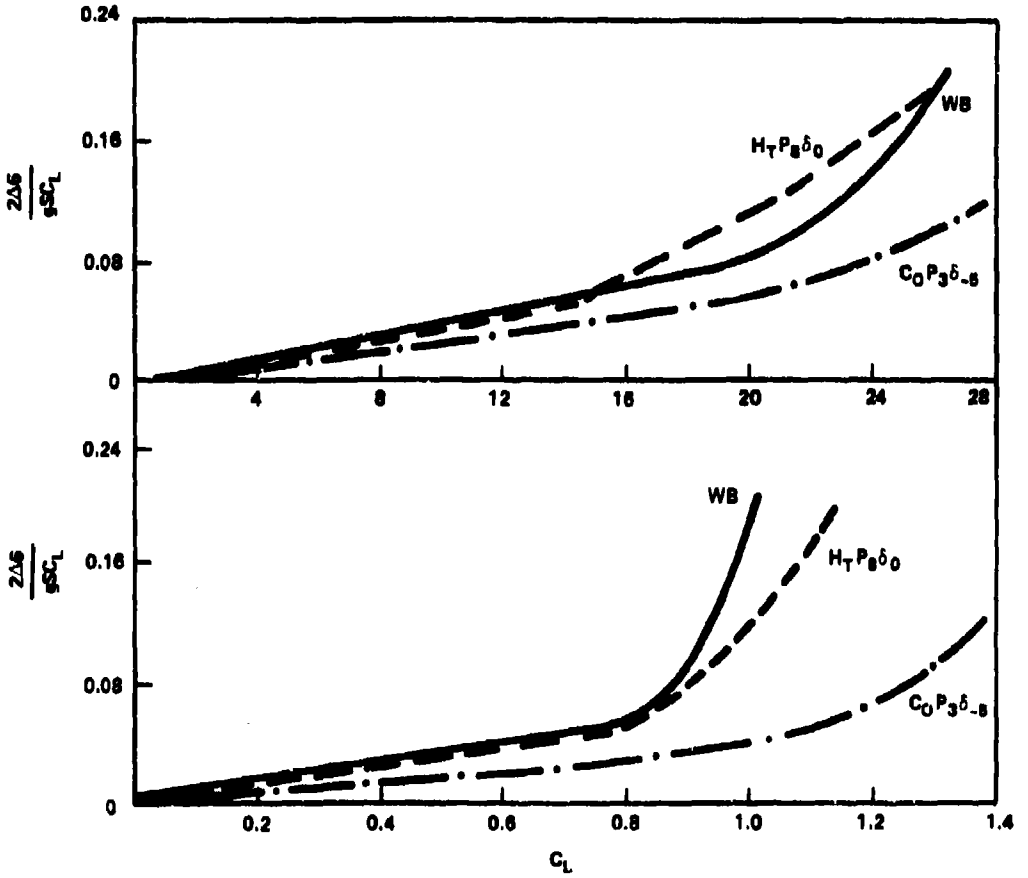

Figure 79 - Comparison of Incremental Buffet Intensity for Horizontal Tail, Canard, and Wing-Body as Functions of Lift Coefficient and Angle of Attack

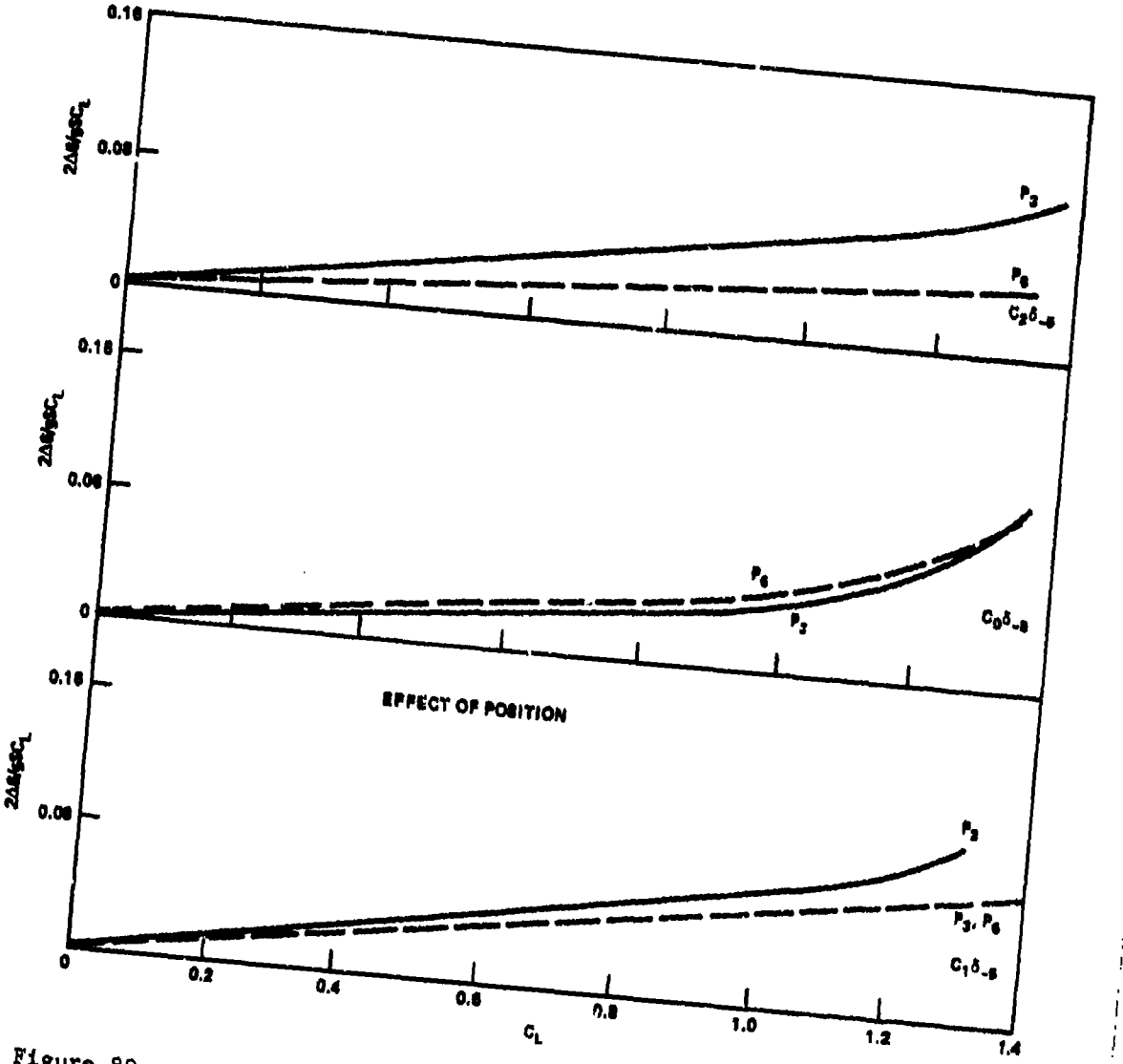

Figure 80 - Effect of Canard Position on Incremental Buffet Intenaity

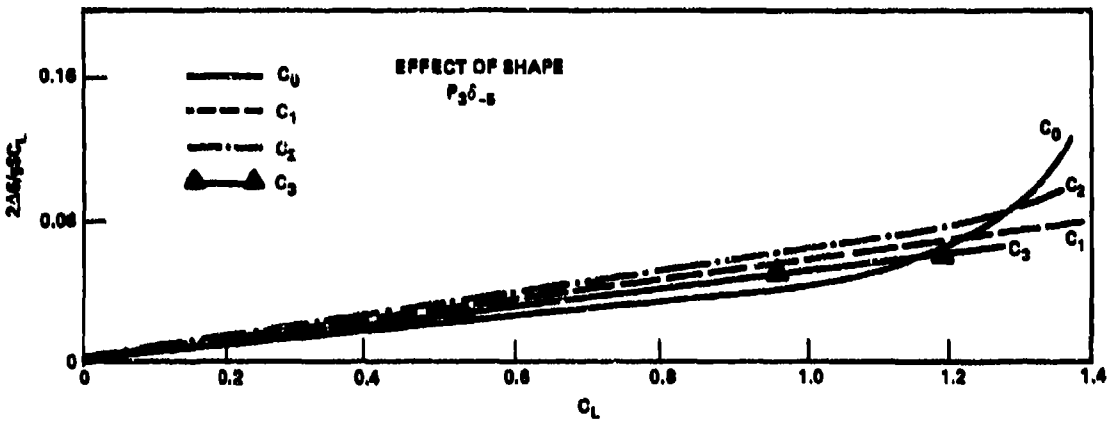

Figure 81 - Effect of Canard Shape on Incremental Buffet Intensity

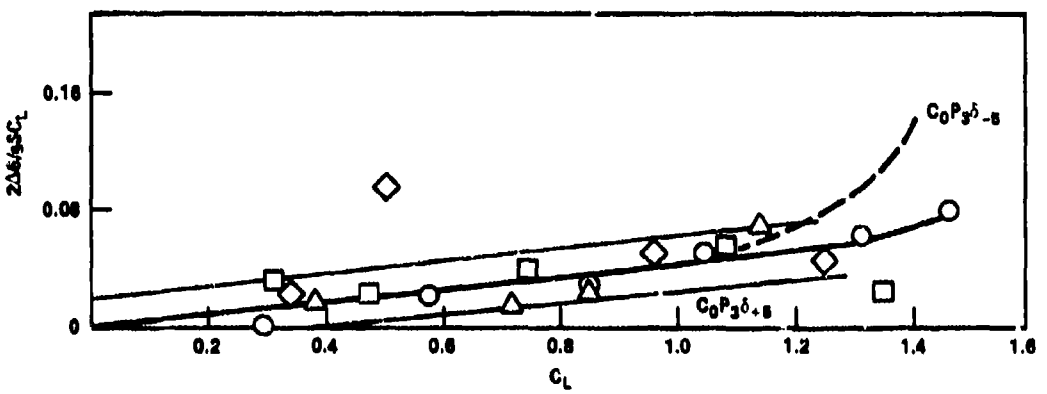

Figure 82 - Effect of Canard Deflection on Incremental Buffet Intensity

SUPERSONIC SPEEDS

The previous discussion in this volume was based on three wind tunnel entries in the DTNSRDC 7- × 10-foot Transonic Wind Tunnel. The data to be discussed in this section were obtained in the DTNSRDC 18-inch Blowdown Supersonic Tunnel. Data were taken at Mach numbers of 0.67, 1.88, and 2.48. The model used was a geometrically similar half model of the 50-degree model. Both canard and horizontal tail were evaluated separately and in conjunction with each other. Canard and horizontal tail shapes were the 45-degree truncated delta canard, C_0. No variation of position was attempted and the canard was located at position P_3. Horizontal tail was located at position P_9.

The raw data, from which the previous analysis at transonic speeds was obtained, has been published.[1-3] The supersonic data, however, have not been published; therefore, both incremental and complete configuration data will be presented in this section.

Lift, drag, and pitching moment of the basic wing-body, wing-canard, and wing-tail are presented in Figure 83 at Mach numbers of 1.88 and 2.48. In contrast to the data at subsonic and transonic speeds the canard has less lift than the horizontal tail. The horizontal tail generates more than double the incremental lift at M = 1.88 and no incremental lift is evident for the canard at M = 2.48. Examination of the pitching moment shown in Figure 83c indicates, however, that the canard is lifting due to the forward shift in neutral point. It thus appears that the shock wave interference between canard and wing causes a significant lift loss on the main wing. Similarly, this loss in lift causes an increase in drag as reflected in the lift-to-drag ratio data presented in Figure 83b. The horizontal tail is clearly superior in performance at both Mach numbers.

The only significant incremental data which can be obtained from Figure 83 are those of incremental moment which are presented in Figure 84. As shown, incremental moment slope is relatively linear at both Mach numbers.

Stability characteristics in the form of center of pressure, C_M/C_N, neutral point $\partial C_M/\partial C_N$ and pitching moment slope C_{M_α} are presented in Figure 85. As shown, the center of pressure shift for the canard is approximately

Figure 83 - Longitudinal Characteristics of the Canard, Horizontal Tail, and Wing-Body at M = 1.88 and 2.48

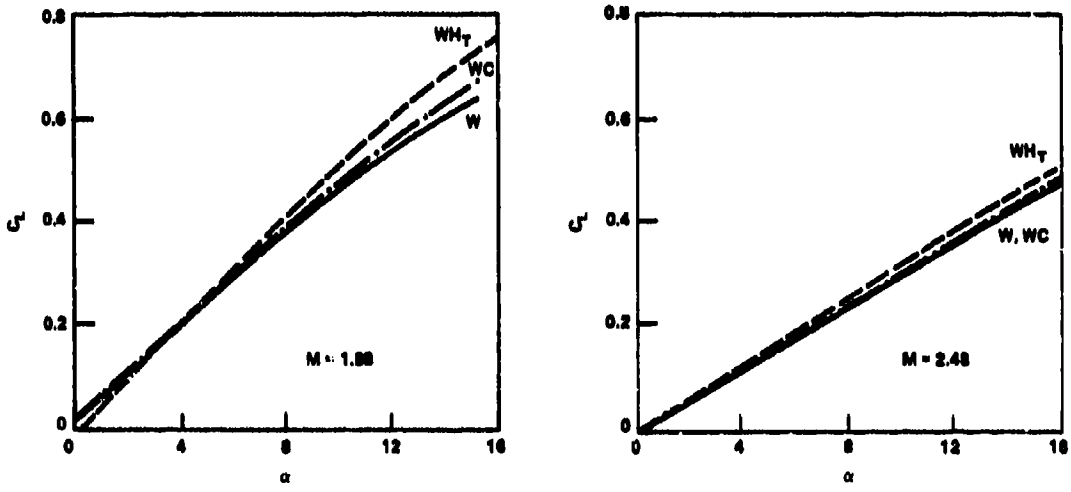

Figure 83a - Lift

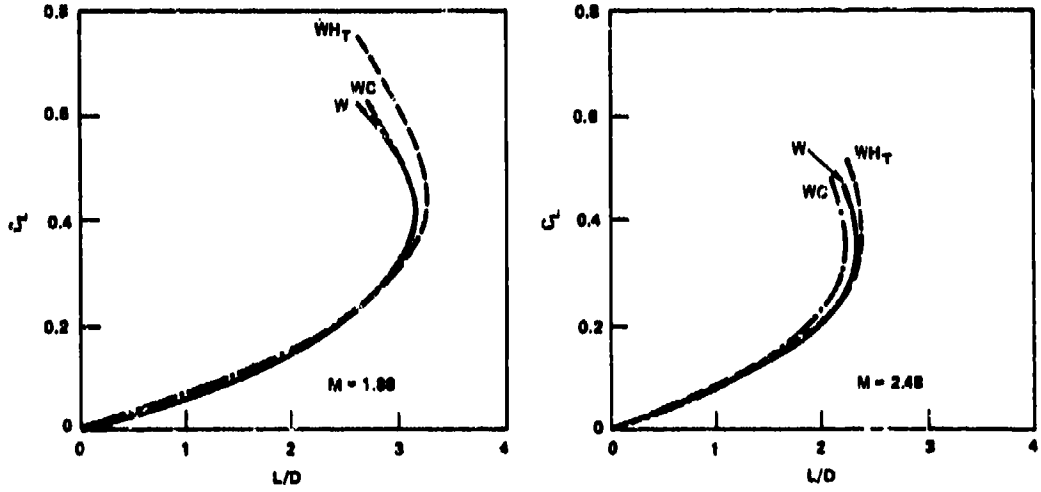

Figure 83b - Lift-to-Drag Ratio

Figure 83 (Continued)

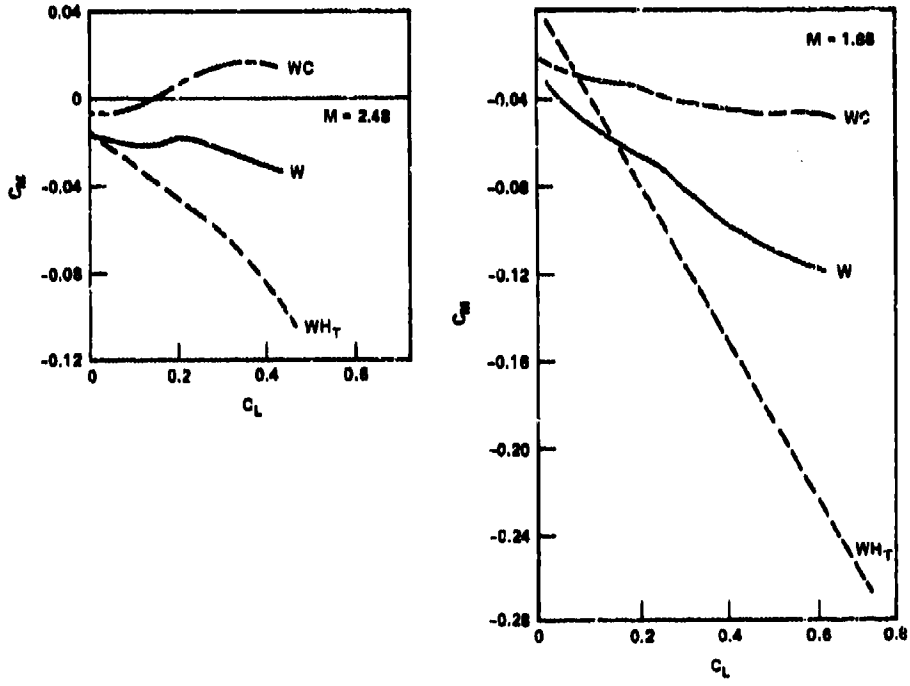

Figure 83c - Pitching Moment

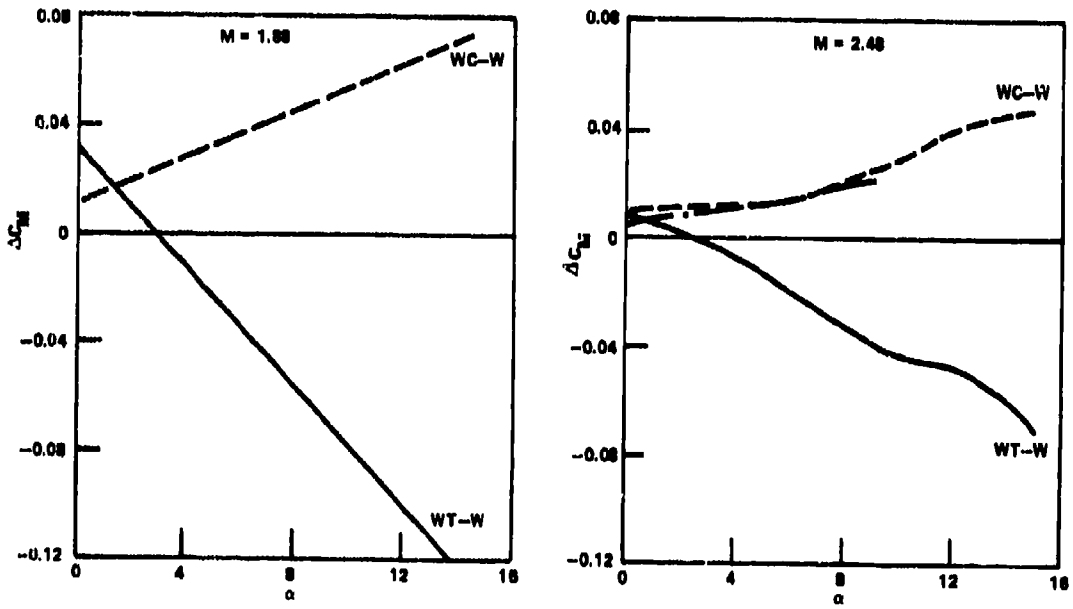

Figure 84 - Incremental Pitching Moment of Canard and Horizontal Tail

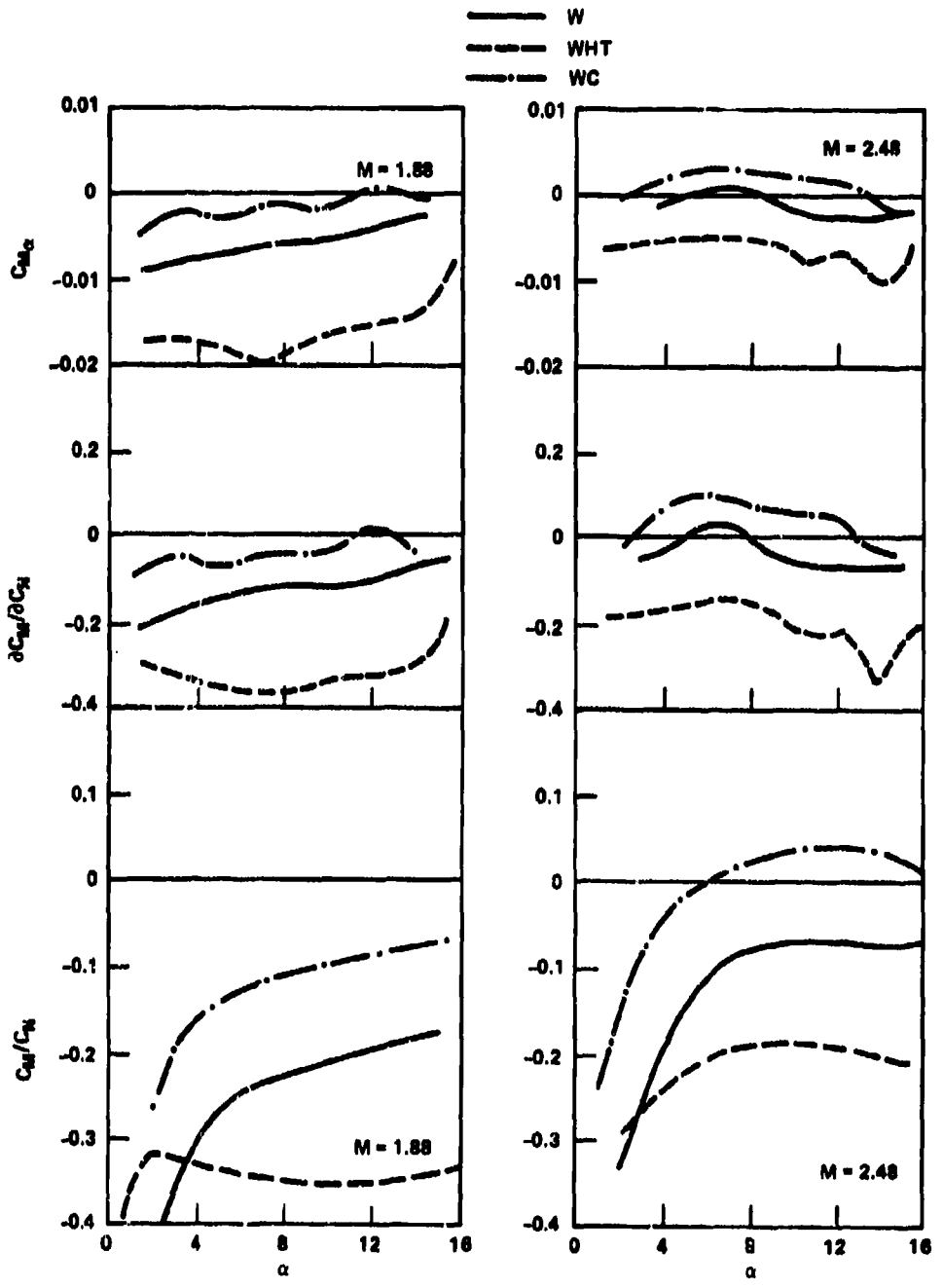

Figure 85 - Stability Characteristics of Canard Horizontal Tail and Wing-Body at Mach Numbers of 1.88 and 2.48

the same at both Mach numbers and is parallel to the basic wing-body. Similarly, the neutral point shift due to the canard is approximately constant with Mach number. This is not the case for the horizontal tail as indicated in Figure 85. Figure 86 presents the incremental change in neutral point for both canard and tail. The canard is relatively constant. The contribution of the horizontal tail, however, is reduced with increasing Mach number. The data in Figure 86 have been normalized with respect to moment arm and are presented in Figure 87. At the low Mach number the horizontal tail is the more efficient stability modifying device. This is also true at the high Mach number but to a lesser extent.

The majority of the data taken from the supersonic wind tunnel program were based on the trisurface configuration and the basic characteristics of this configuration are presented in Figure 88. Data are presented for Mach numbers of 0.67, 1.88, and 2.48.

The lift data at all three Mach numbers are similar to data discussed previously. At the low Mach number the canard has a significant effect by increasing lift, however, at the supersonic Mach numbers very little incremental lift is being generated. Similarly, lift-to-drag ratio is increased by the presence of the canard at lift coefficients greater than 0.45 at the low Mach number but little change is noted at the higher Mach numbers.

Incremental lift and moment are presented in Figure 89. As shown, both incremental moment and lift decrease with increasing Mach number. Pitching moment does not decrease at the same rate as incremental lift thereby indicating the canard is causing a lift loss on the main wing.

The model used in obtaining these data was a half-model. By using the rolling moment gage of the balance it is possible to obtain the lateral center of pressure C_ℓ/C_N of the configuration. This variation is presented in Figure 90.

At the low Mach number (M=0.67) the lateral C_p is further out for the canard off configuration up to a normal force coefficient of 0.6. Beyond this value of normal force coefficient the canard on configuration has the largest value. In general, as the stall on a swept wing progresses the lateral center of pressure moves toward the wing root and the wing becomes less efficient. It can be seen, however, that the canard delays this

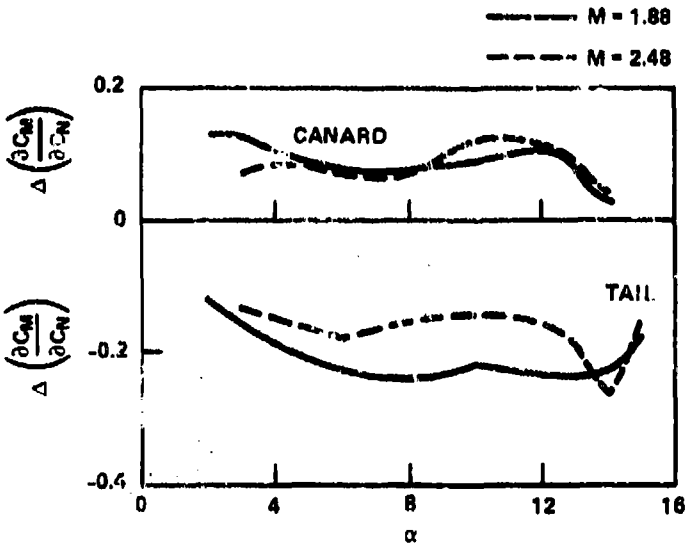

Figure 86 - Incremental Neutral Point Change Due to Canard and Horizontal Tail

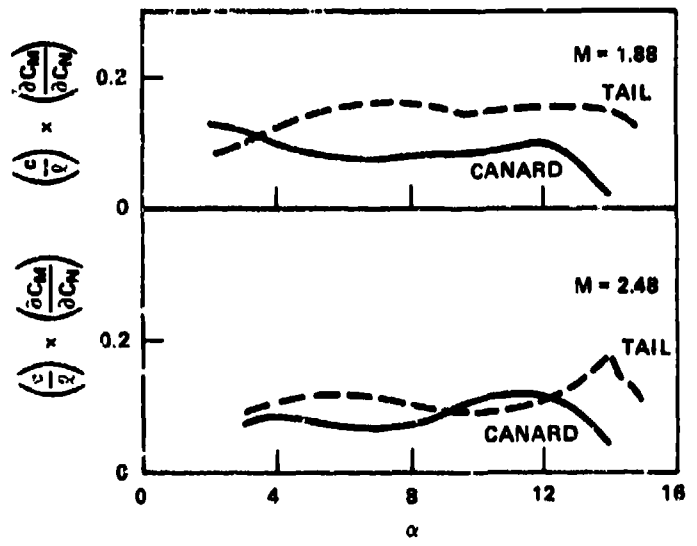

Figure 87 - Normalized Absolute Incremental Neutral Point Change

Figure 88 - Longitudinal Characteristics of Horizontal Tail and Trisurface Configurations

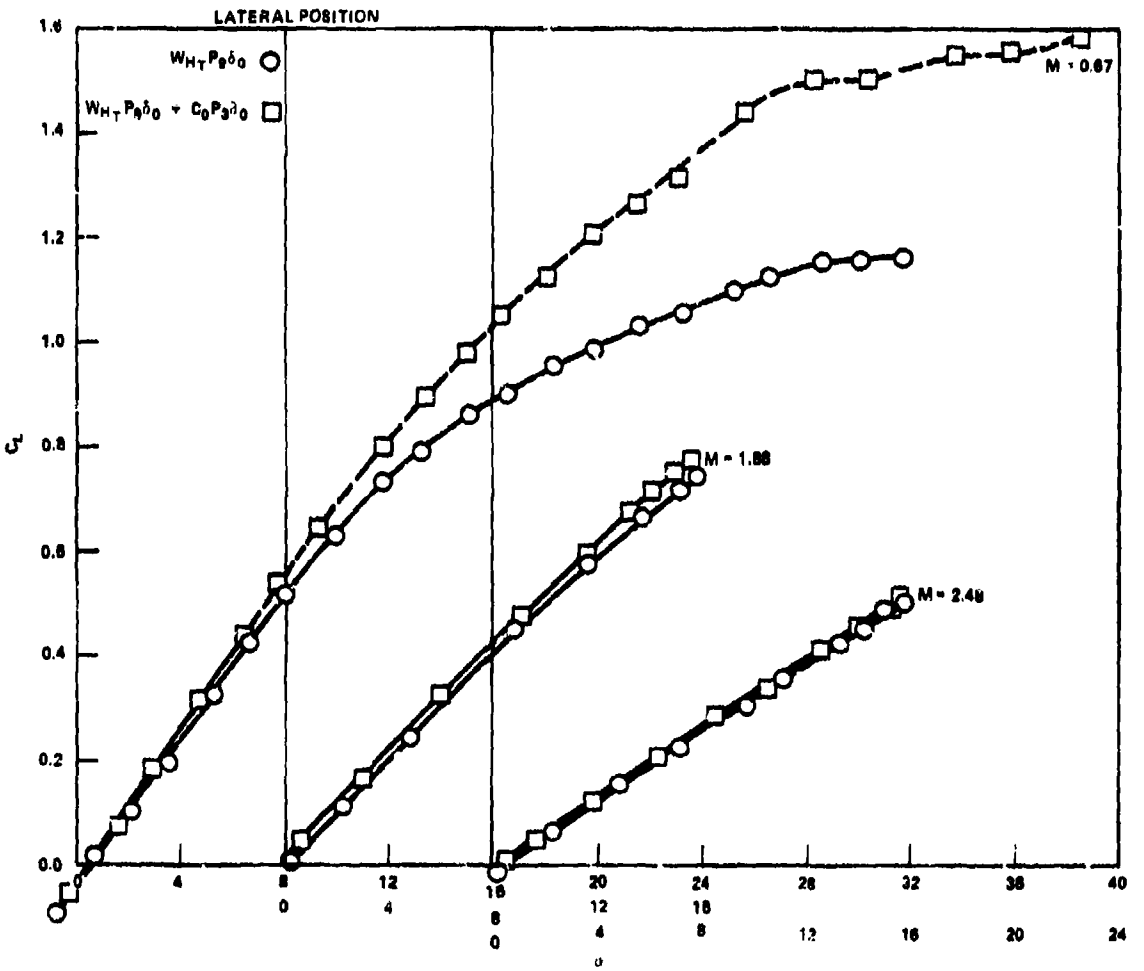

Figure 88a - Lift

Figure 88 (Continued)

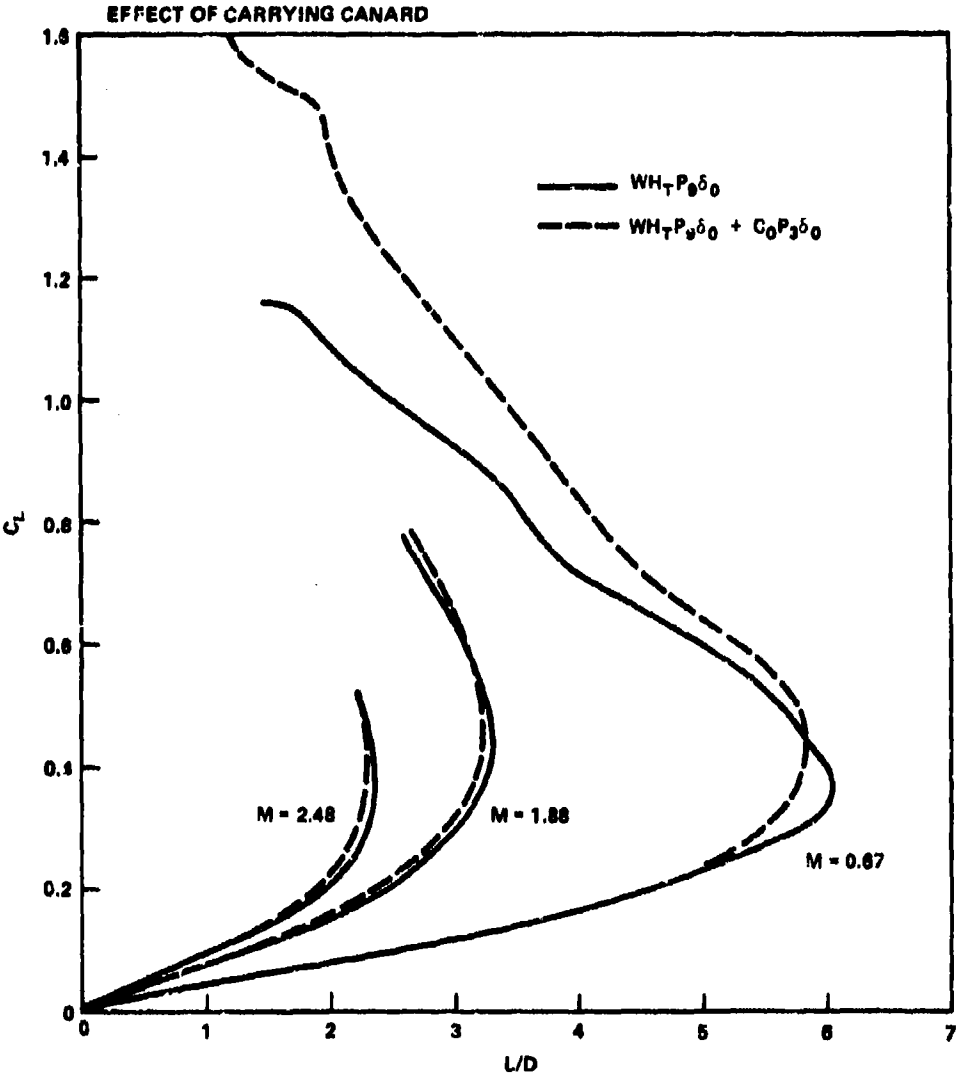

Figure 88b - Lift-to-Drag Ratio

Figure 88 (Continued)

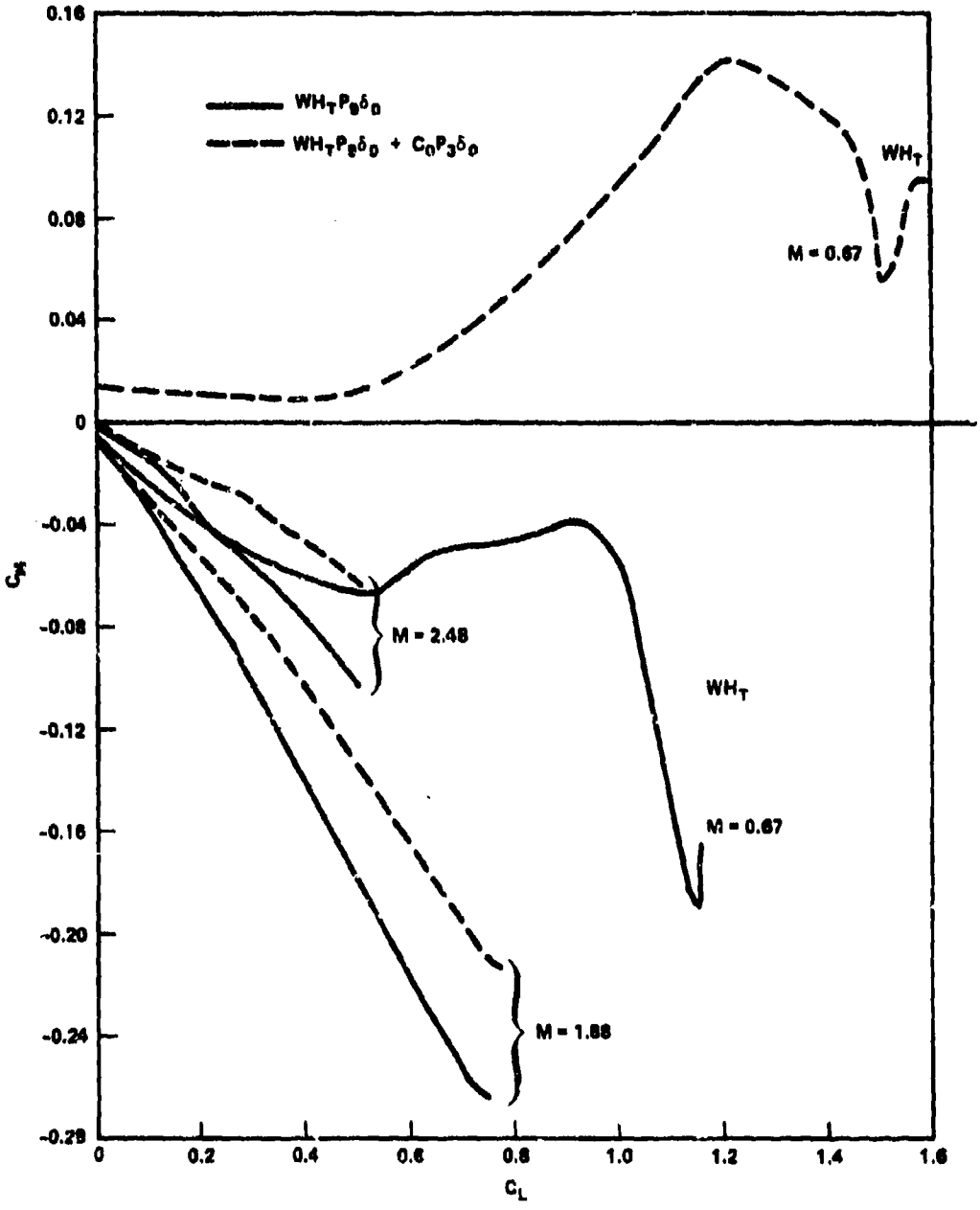

Figure 88c - Pitching Moment

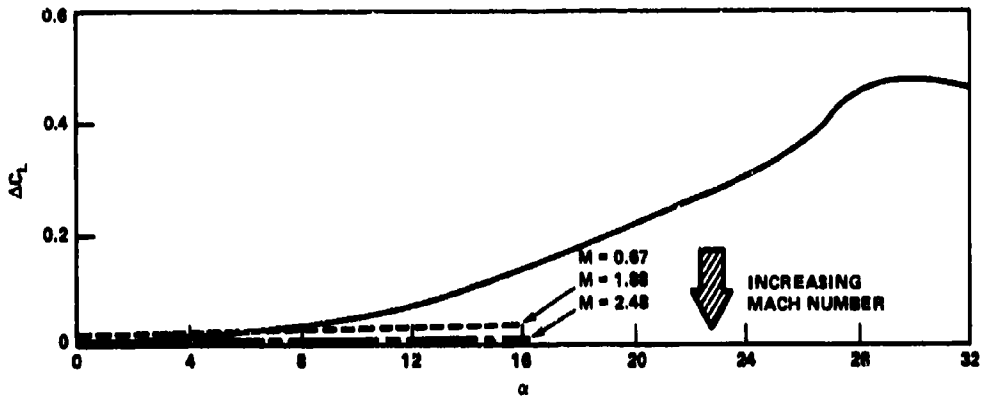

Figure 89a - Incremental Lift

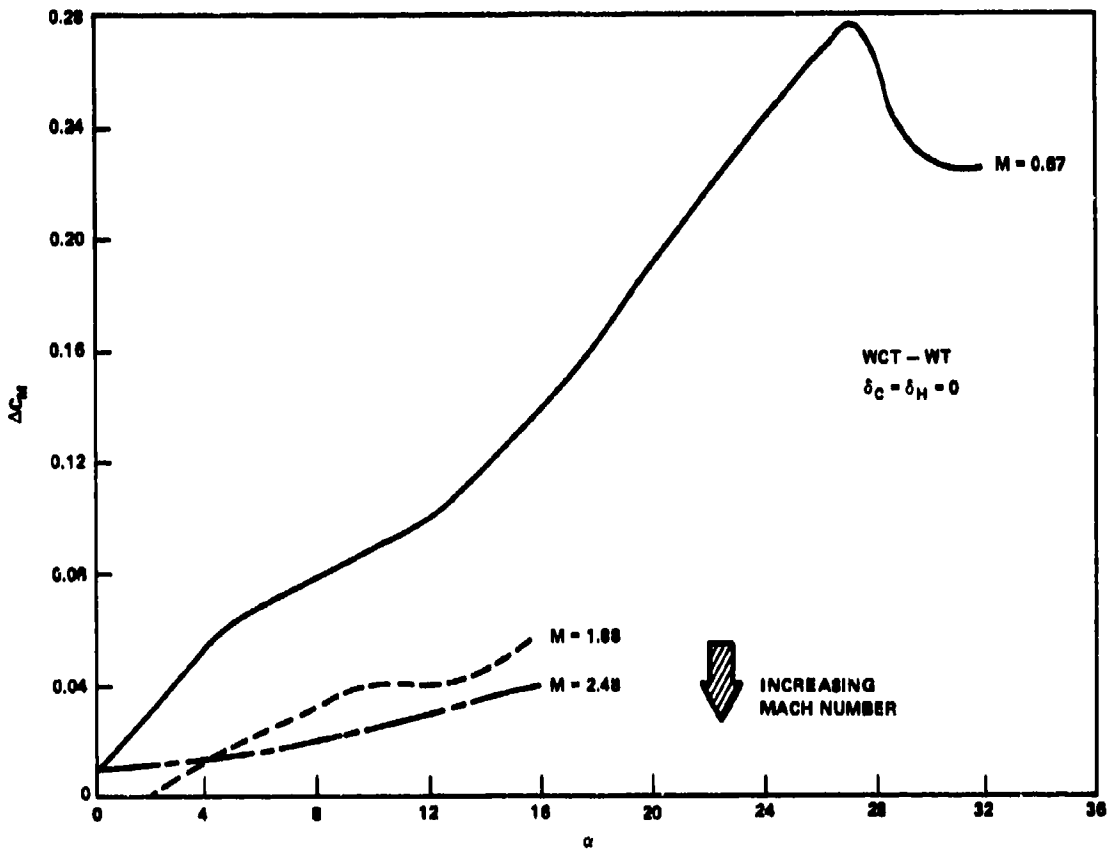

Figure 89b - Incremental Pitching Moment

Figure 89 - Incremental Lift and Pitching Moment Due to Canard

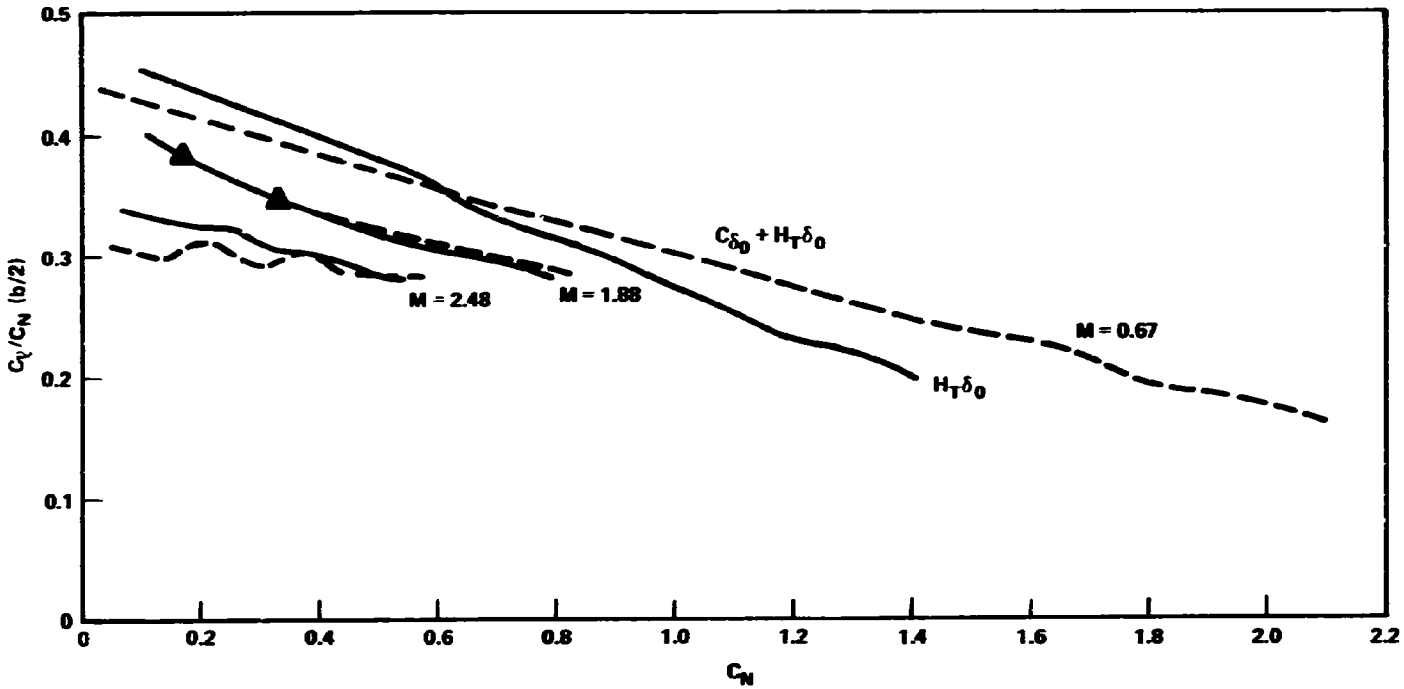

Figure 90 - Lateral Center of Pressure for Horizontal Tail and Trisurface Configurations

inward movement of the center of pressure to higher normal force values. As Mach number is increased, little canard effect is noted on lateral center of pressure and at the highest Mach numbers the effect is detrimental. The canard on data also indicates an oscillatory change in lateral center of pressure with increasing C_N. The exact cause of this oscillatory change is unknown but may be due to the changing position of the canard trailing edge shockwave on the main wing.

The stability characteristics of the wing-body-tail and trisurface configurations are presented in Figure 91. As expected, installation of the canard moves the center of pressure forward at all Mach numbers as shown in Figure 91. Similarly the canard causes a forward movement of the aircraft neutral point as presented in Figure 91b. Examination of the variation of neutral point and pitching moment slope indicates the surprising result that there are regions of angle of attack where the trisurface configuration is more stable than the canard off configuration. This is shown most clearly at the low Mach number between 27- and 31-degrees angle of attack and at lower angles of attack with increasing Mach number. This increase in stability is due not only to delay of flow separation over the outer wing panels but also to a modification of the downwash over the tail thereby delaying the horizontal tail stall angle.

The effect of canard deflection at supersonic speeds is presented in Figure 92. As at transonic and subsonic speed, deflection has little effect on the lift characteristics.

Zero lift drag is increased by both positive and negative deflections as shown in Figure 92b, however, with increasing angle of attack drag, due to negative deflections, is negligible.

Negative deflection caused a lower incremental change in moment than did the corresponding positive deflection at M = 1.88. At M = 2.48 the incremental change is approximately the same for either positive or negative deflection.

Canard deflection has only a minimal effect on the stability characteristics of the configuration as shown in Figure 93. Negative deflection tended to make the stability more oscillatory in nature than did the positive deflection.

Figure 91 - Stability Characteristics of Horizontal Tail and Trisurface Configurations

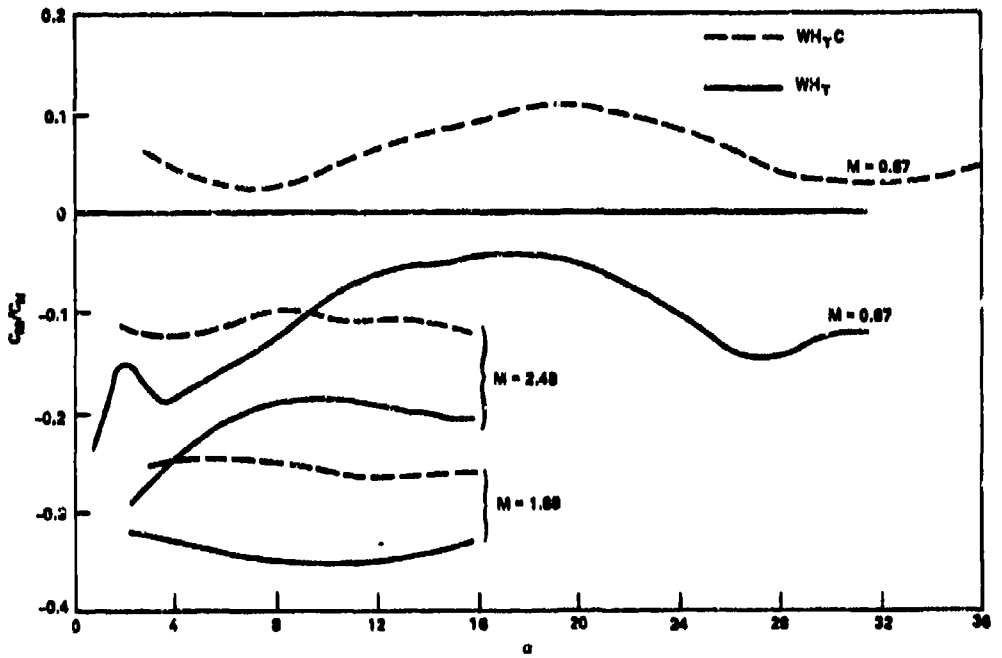

Figure 91a - Center of Pressure

Figure 91 (Continued)

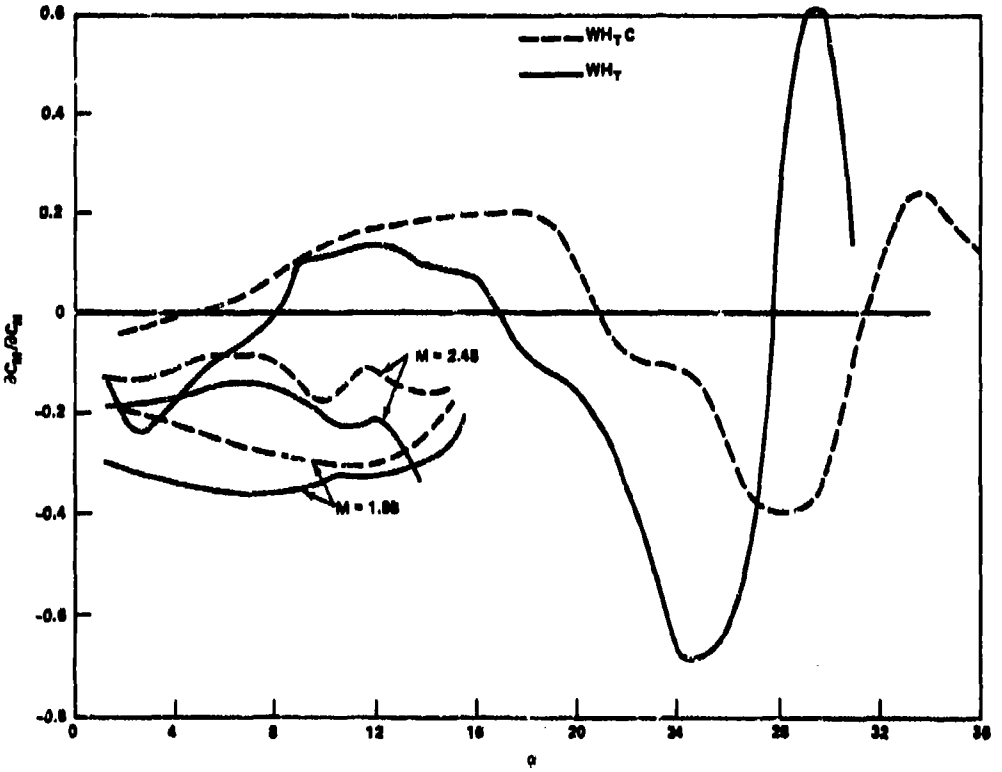

Figure 91b - Neutral Point

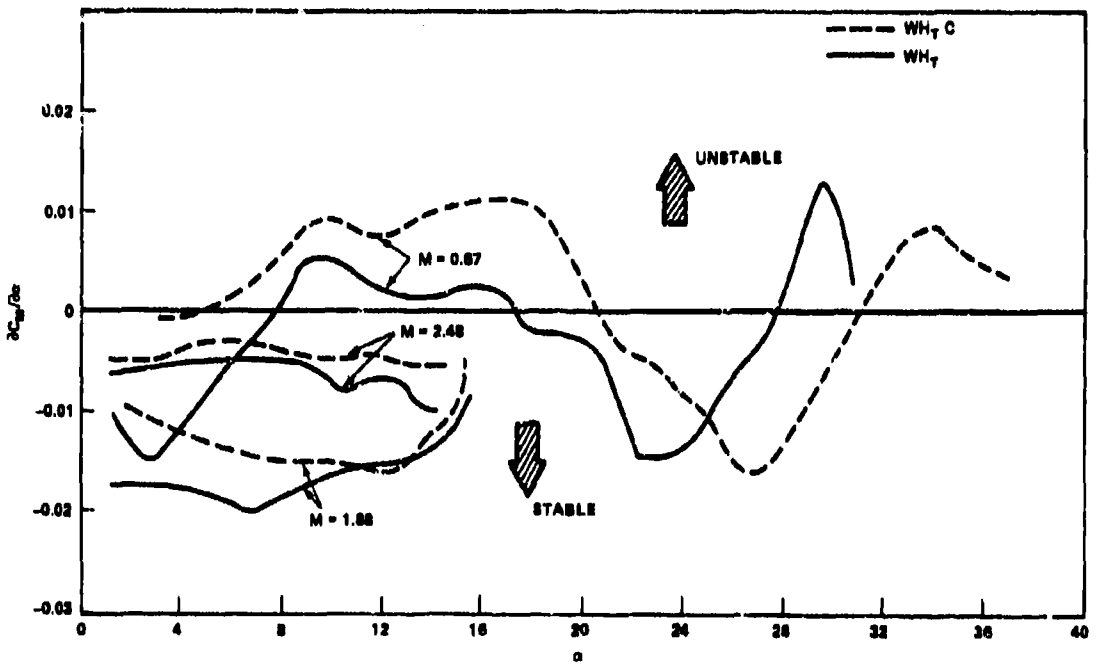

Figure 91c - Pitching Moment Slope

Figure 92 - Effect of Canard Deflection on the Longitudinal Characteristics

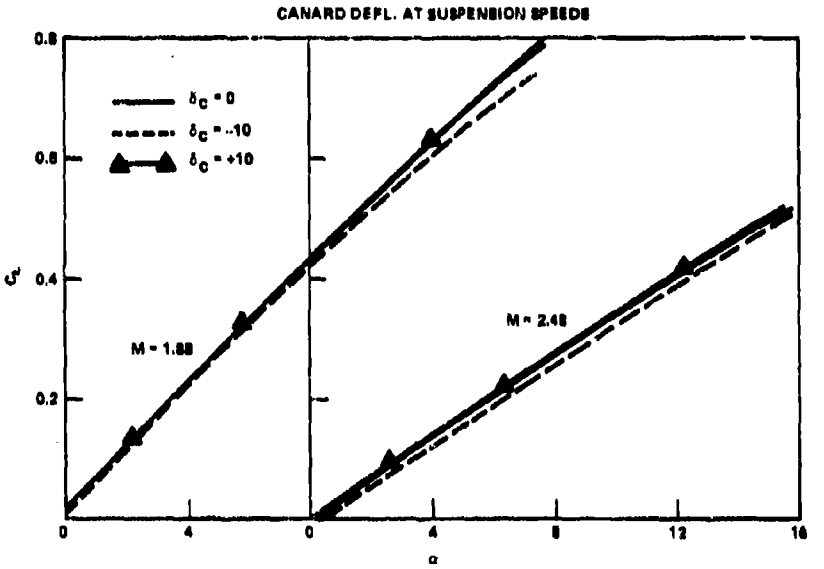

Figure 92a - Lift

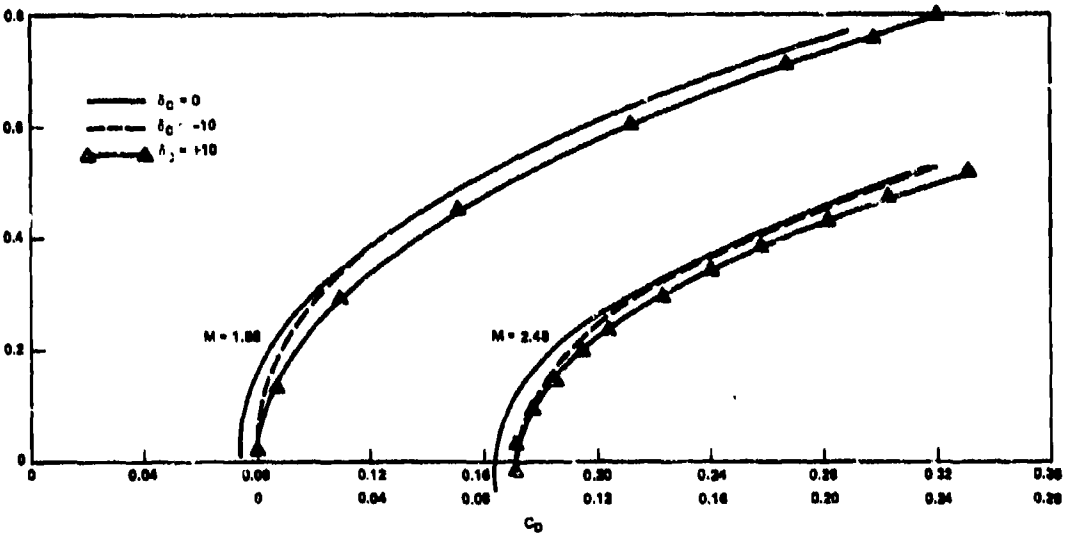

Figure 92b - Drag

Figure 92 (Continued)

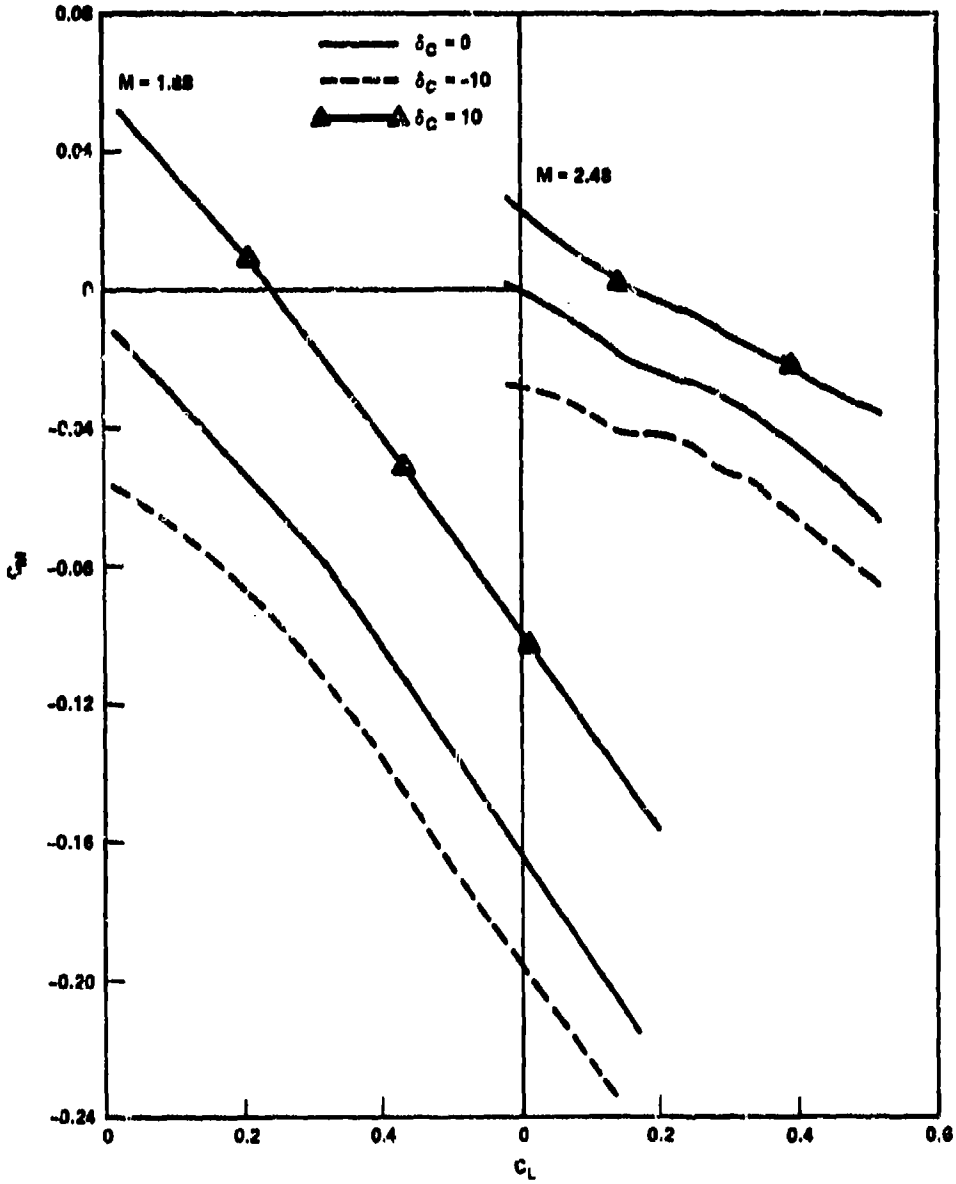

Figure 92c - Pitching Moment

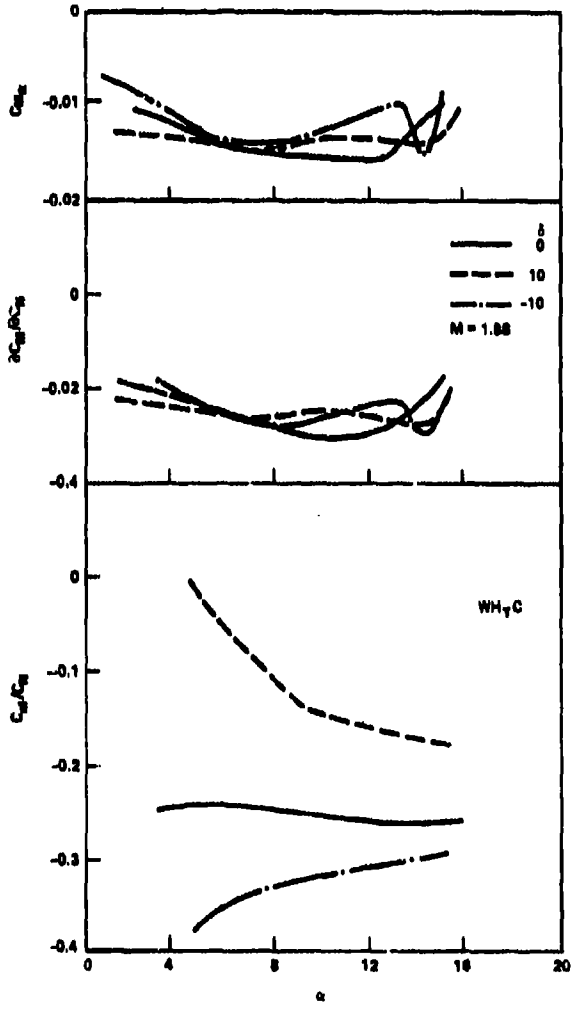

Figure 93a - M = 1.88

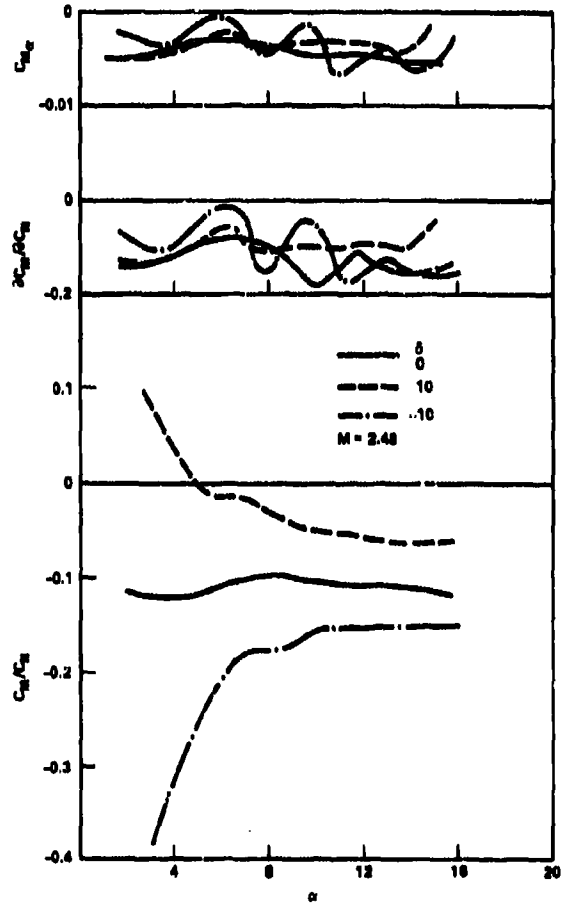

Figure 93b - M = 2.48

Figure 93 - Effect of Canard Deflection on Stability Characteristics

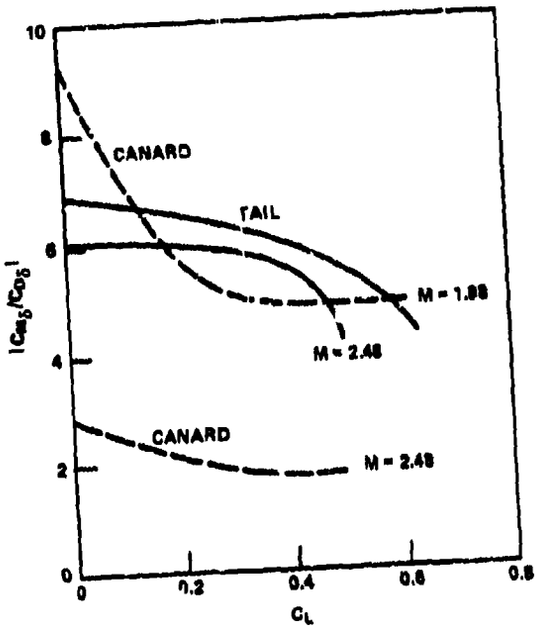

Figure 94 - Trim Efficiency

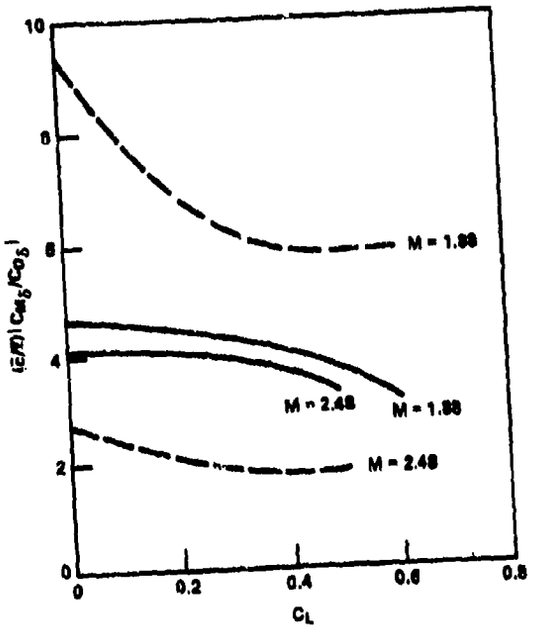

Figure 95 - Normalized Trim Efficiency

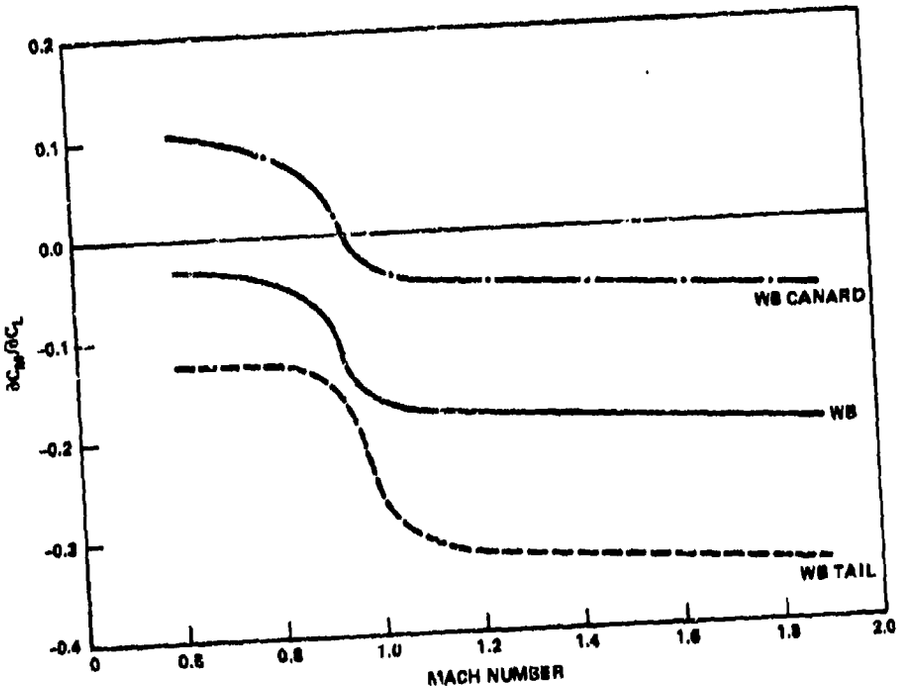

Figure 96 - Neutral Point Variation for Canard, Horizontal Tail, and Wing-Body at Mach Numbers from 0.6 to 1.88

A comparison of the trimming efficiency of the canard and horizontal tail is presented in Figure 94. Data are for positive canard deflection and negative tail deflection; the deflection angle is 10 degrees for both tail and canard. The efficiency is equal to incremental moment divided by drag due to deflection $C_{M_\delta}/C_{D_\delta}$. Over most of the lift coefficient range the horizontal tail is the superior trimming device. This is particularly true at M = 2.48.

Normalized trim efficiency is presented in Figure 95. At M = 1.88 the canard is superior to the horizontal tail, however, at M = 2.48 the canard is inferior. The canard exhibits a large decrease in surface efficiency with Mach number, due perhaps to canard-wing shock interaction. The horizontal tail has only a minimal decrease in surface efficiency with Mach number.

The final data to be presented are from the transonic section of this volume and also include supersonic data and are shown in Figure 96. Figure 96 presents the variation of neutral point $(\partial C_M/\partial C_L)$ evaluated at a lift coefficient of 0.0 with Mach number. The configurations represented are the basic wing-body, wing-body-tail and wing-body-canard. As shown, the rate of neutral point shift with Mach number is approximately the same for both wing-body and wing-body-canard.

The horizontal tail configuration, however, becomes slightly more stable ($\Delta h \sim 0.04\bar{c}$) between subsonic and supersonic speeds.

SUMMARY

The preceeding volumes of this report have enumerated certain improvements on the lift, drag, and pitching moment due to the presence of a close-coupled canard on the basic aircraft characteristics at subsonic speeds. These improvements also occur at transonic speeds albeit somewhat modified. In general, the effectiveness of the canard in increasing lift and decreasing drag is reasonably independent of Mach number at Mach numbers below that Mach number where strong compressibility effects occur. When strong compressibility effects are present, the magnitude of the aerodynamic improvements diminishes with increasing Mach number. When true

supersonic speeds are reached M > 2.0 the effect of the close-coupled canard on the aerodynamics is negligible and, in fact, may be unfavorable.

The effect of such canard variables as position, shape, and deflection on lift, drag, pitching moment, and buffet at transonic and supersonic Mach numbers is given below.

LIFT

1. Increasing Mach numbers had little effect on the canard configurations, but increased the lift at constant angle of attack for the canard off configurations. The Mach number at which this occurred was a function of the wing sweep angle.

2. The canard position which optimized lift at subsonic speeds also was the best position at transonic speeds. Position does not, however, have a strong influence when strong compressibility effects are present.

3. High sweep canards maximize lift.

4. Lift changes due to canard deflection are relatively constant with Mach number.

5. Shock wave interaction between close-coupled canard and wing caused lift losses to the wing at supersonic speeds.

PITCHING MOMENT

1. The rate of neutral point aftward shift with Mach number is approximately the same for either canard on or off.

2. Incremental moment due to the canard decreased with increasing Mach number at high angles of attack. This behavior was particularly severe for forward mounted canards.

3. When the canard was located close to the wing ($Z_t/c \sim 0$), the pitching moment effectiveness was severely reduced with increasing Mach number.

4. For canards located further forward or lower than the optimum position, the rate of neutral point shift with Mach number was greater than the basic wing-body.

5. The canard position which exhibited the greatest incremental lift exhibited the greatest incremental moment change regardless of canard volume coefficient.

6. Low sweep canards exhibited greater incremental moments than high sweep canards.

7. Deflection does not effect incremental moment variation with Mach numbers.

8. Adding a canard to a configuration consisting of wing-body-horizontal tail increases the angle of attack at which pitch down occurs and increases horizontal tail control power.

9. The horizontal tail is a more efficient trimming device at low-to-moderate angles of attack when compared with a close-coupled canard. At high angles of attack the canard is more efficient. This is true for both stable and unstable configurations.

DRAG

1. Canard configurations exhibit relatively constant lift-to-drag ratios at high lift coefficients. Canard off configurations had a rise in lift-to-drag ratio with increasing Mach numbers.

2. Forward and downward movement of the canard causes an increase in minimum drag coefficient and induced drag.

3. Canard position has only a minimal effect on induced drag at Mach numbers greater than 0.95.

4. At low Mach numbers, low sweep, high aspect ratio canards maximize lift-to-drag ratio, with increasing Mach number, high sweep, low aspect ratio canards perform best.

5. Positive canard deflections cause a decrease in the drag rise Mach number and increases in both minimum drag and induced drag.

6. Small negative deflections increase the maximum lift-to-drag ratio. Negative deflections have little effect on lift-to-drag ratio at high lift coefficients.

7. The trisurfaced configuration had lower values of induced drag than either canard alone or horizontal tail configurations at angles of attack greater than 16 degrees.

8. At supersonic speeds, the penalty for carrying the canard is small.

9. Both positive and negative deflections increase minimum drag at supersonic speeds. Drag due to negative deflections reduces with increasing angle of attack.

BUFFET

The close-coupled canard delayed buffet onset and buffet intensity on the high sweep research model (λ = 50 degrees).

ACKNOWLEDGMENTS

The author wishes to thank John R. Krouse and Jonah Ottensoser for their help in obtaining and evaluating the data presented in this report. Additional acknowledgment is given to James H. Nichols and Dr. Roger J. Furey for their guidance and support.

APPENDIX A
MODEL GEOMETRY

The data presented in this report are based on two research models. The models consist of steel wings and a steel central core. Fuselages are wooden fairings surrounding the central core. The canards and horizontal tail are wood and fiberglass fairings built up around a steel spar. Attachment of the canards and horizontal tail is provided by steel plates flush with the fuselage. Seven canard and three horizontal tail mounting positions are provided. Each canard can be rotated through a deflection range from -10 to +25 degrees in 5-degree increments. Horizontal tail deflection range is from -25 to +10 degrees. Rotation point for both canards and horizontal tail is 40 percent of the exposed surface root chord. Moment reference point for both research models is 0.27 $\bar{c}$.

Detailed dimensions of the wings are given in Table 1. Table 2 presents dimensions of the four canards. Figure 97 shows the common fuselage shape for both models. Wing planform geometries are given in Figure 98. Canard geometry is given in Figure 99. Canard locations are presented in Figure 100. A photograph of the various model components is shown in Figure 101.

TABLE 1 - GEOMETRIC CHARACTERISTICS OF THE WINGS

	W1 (Λ = 50 Degrees)	W2 (Λ = 25 Degrees)
Airfoil Section (NACA)	*	64A008
Projected Area, square inches	304	295
Span, inches	35.50	42.00
Chord, inches		
Root (centerline)	15.38	12.20
Tip	1.90	1.90
Mean Aerodynamic Chord, inches		
Length	10.30	8.30
Spanwise Location from Body Centerline	6.70	7.90
Aspect Ratio	4.15	6.00
Taper Ratio	0.12	0.16
Sweepback Angle, degrees		
Leading Edge	50.0	25.0
Quarter Chord	45.5	20.0
Trailing Edge	23.5	-1.5
Incidence Angle, degrees	0	0
Dihedral Angle, degrees	0	0
Twist Angle, degrees	0	0

*64A008 Airfoil swept 25 degrees around 0.27 $\bar{c}$ chord line.

TABLE 2 - GEOMETRIC CHARACTERISTICS OF THE CANARDS

	C_0	C_1	C_2	C_3
Airfoil Section (NACA)	64A008	64A006	64A008	64A008
Exposed Area, square inches	39.8	39.8	47.2	49.3
Projected Area, square inches	76.0	89.5	76.0	76.0
Exposed Semi-Span, inches	5.74	4.79	7.60	7.60
Total Span, inches	16.28	14.38	20.00	20.00
Chord, inches				
Root (centerline)	8.73	12.45	6.70	6.12
Root (exposed)	6.33	8.30	5.31	5.00
Tip	0.59	0	0.90	1.48
Aspect Ratio	3.50	2.31	5.26	5.26
Taper Ratio	0.07	0	0.13	0.24
Sweepback Angle, degrees				
Leading Edge	45	60	45	25
Trailing Edge	0	0	22.8	0
Dihedral Angle, degrees	0	0	0	0

NOTE: VERTICAL TAIL WAS NOT TESTED WITH THE 25-DEGREE LEADING-EDGE SWEEP-WING (W2)

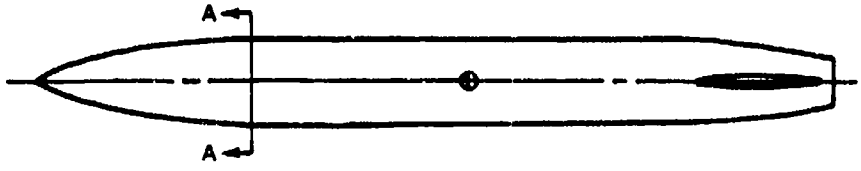

Figure 97a - Top View

SECTION A-A

ALL DIMENSIONS ARE IN INCHES (CENTIMETERS)

WIDTH = 4.75 (12.06); HEIGHT = 4.15 (10.54)
UPPER CORNER RADIUS = 1.00 (2.54)
LOWER CORNER RADIUS = 0.25 (0.64)

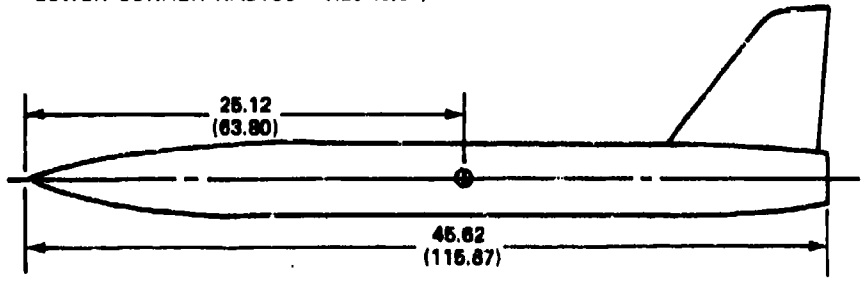

Figure 97b - Side View

Figure 97 - Research Aircraft Fuselage

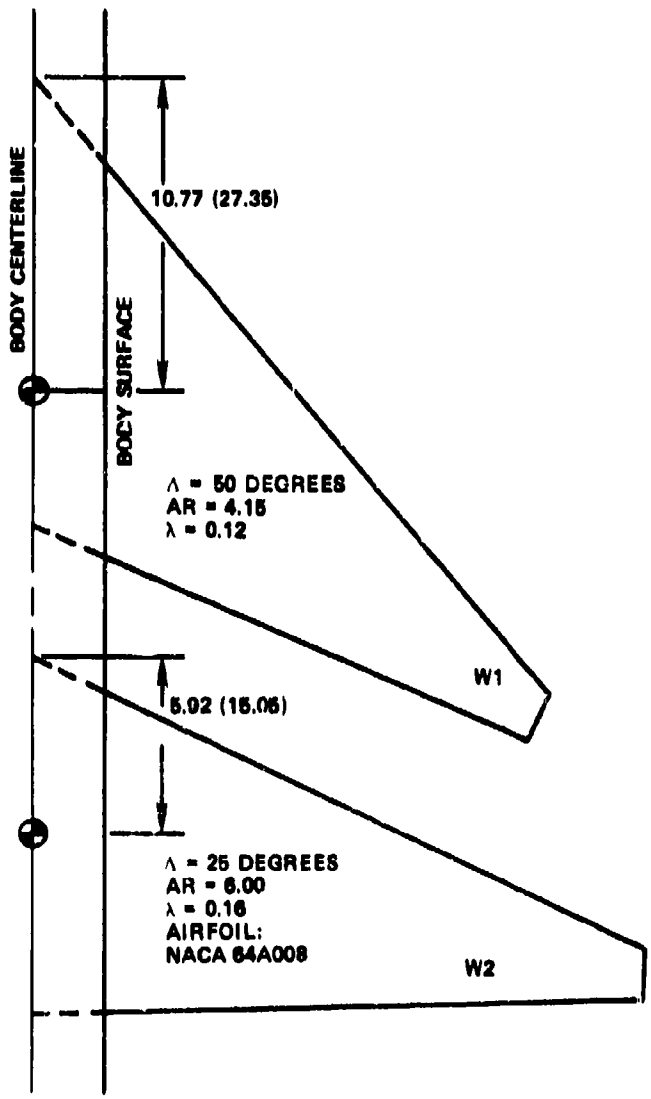

Figure 98 - Planform View of the Wings

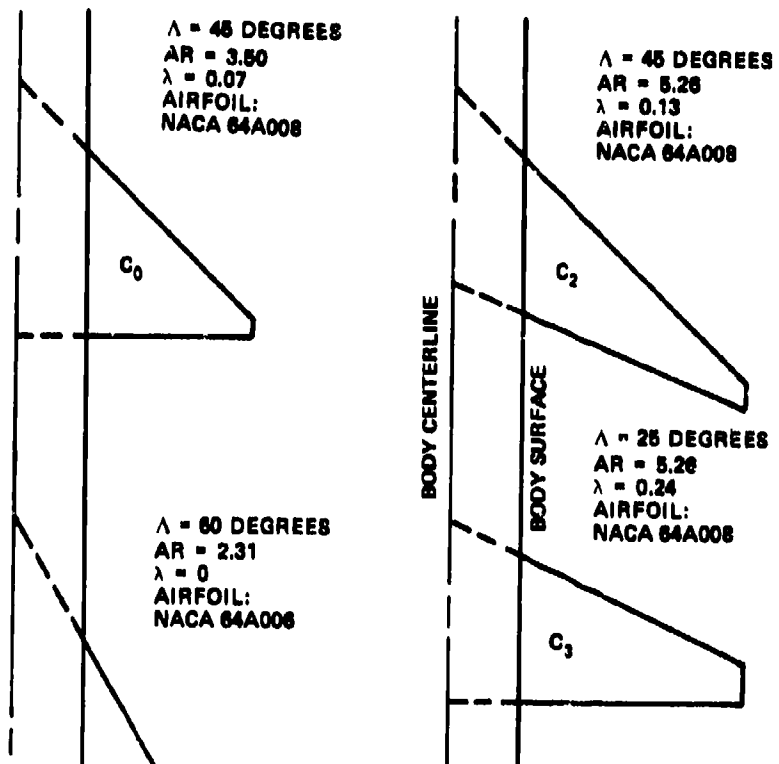

Figure 99 - Planform View of the Canards

NOTE: ALL DIMENSIONS ARE IN INCHES (CENTIMETERS)

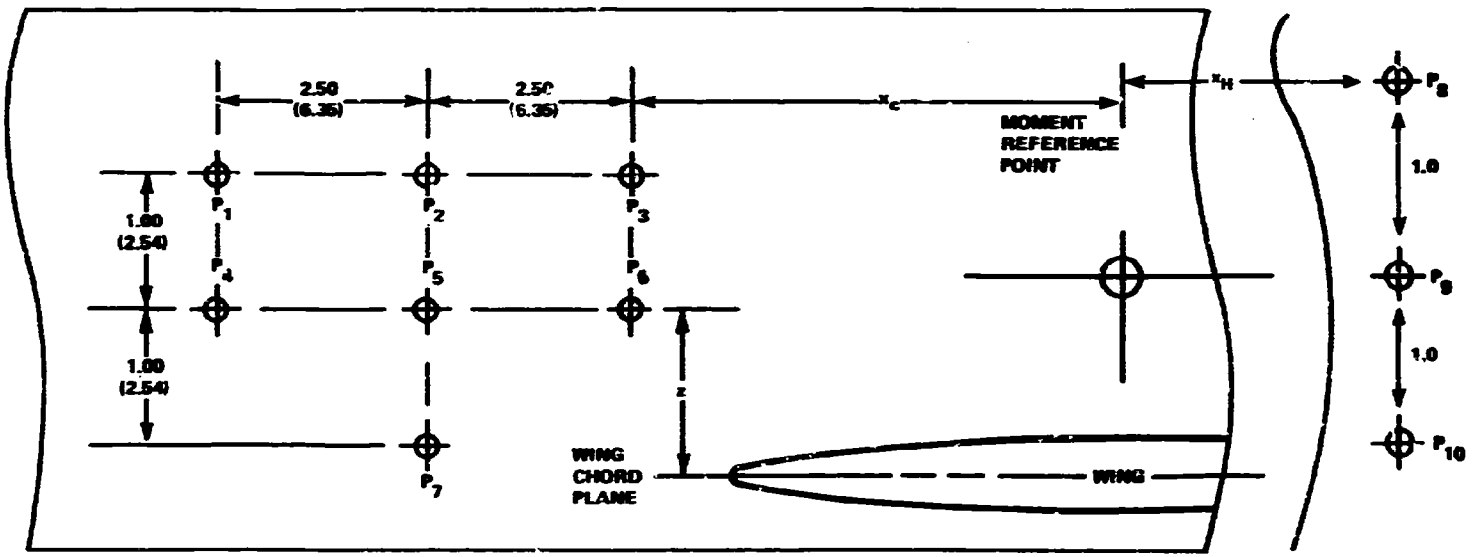

W1 (Λ = 50 DEGREES): x_c = 10.00 (25.40); z = 1.40 (3.56), x_H = 15.00 (38.10)

W2 (Λ = 25 DEGREES): x_c = 7.18 (18.24); z = 1.14 (2.90)

Figure 100 - Canard Pivot Locations

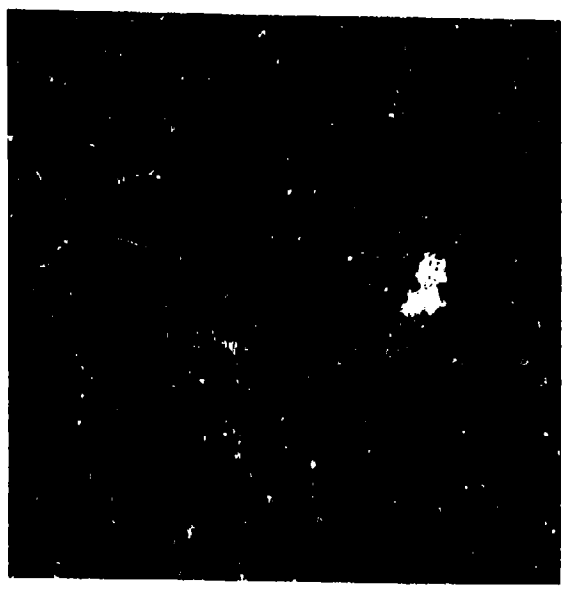

Figure 101 - Wind Tunnel Model Components

APPENDIX B
BUFFET INTENSITY

Presented in this appendix are the actual data used in obtaining the values of buffet intensity presented in the section on buffet.

The data as presented have the value of σ (root mean square bending moment, RMS at zero angle of attack) removed from each data point. All data are for the 50-degree sweep model. Data for the basic wing-body are presented in Figure 102. Data for the horizontal tail are presented in Figure 103. Canard C_0 is shown in Figure 104. Figures 105, 106, and 107 present data for Canards C_1, C_2, and C_3, respectively.

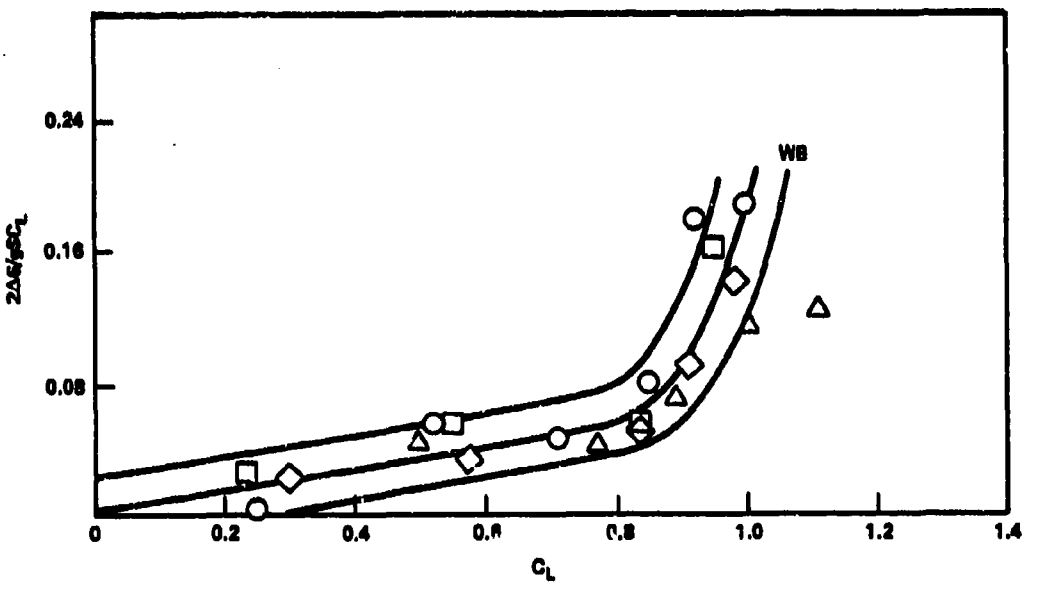

Figure 102 - Incremental Root Mean Square Data for the 50-Degree Wing-Body

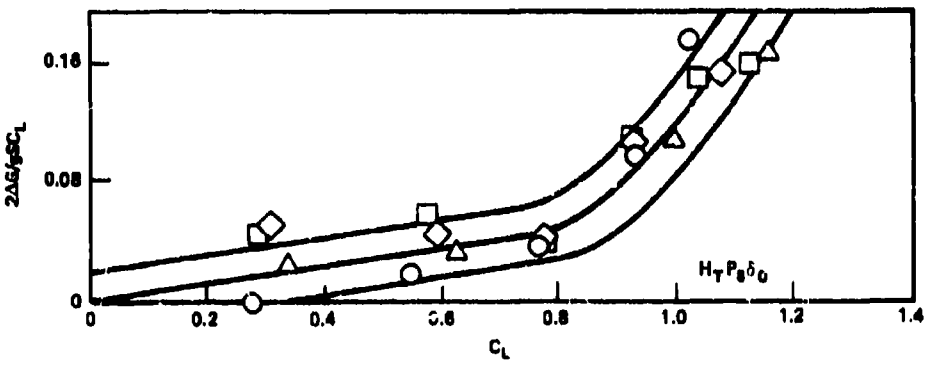

Figure 103 - Incremental Root Mean Square Data for the Horizontal Tail

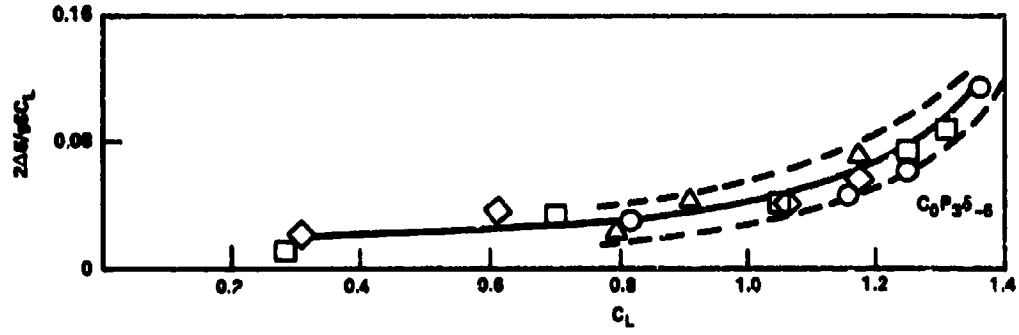

Figure 104a - Position P_3, -5-Degree Deflection

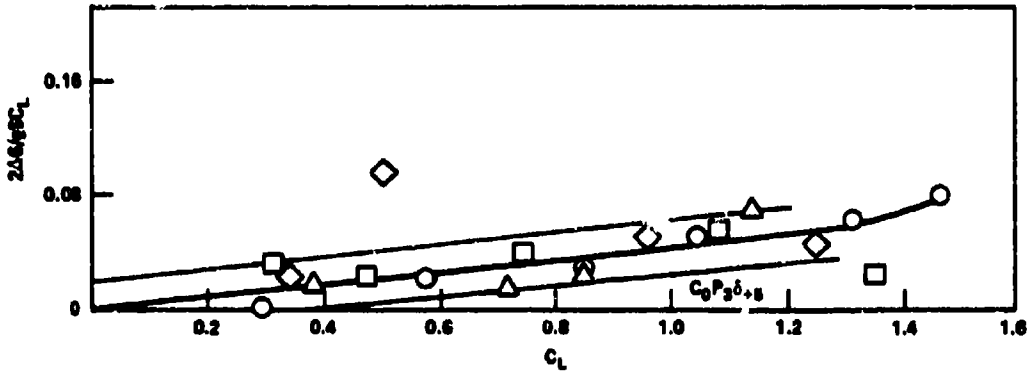

Figure 104b - Position P_3, 5-Degree Deflection

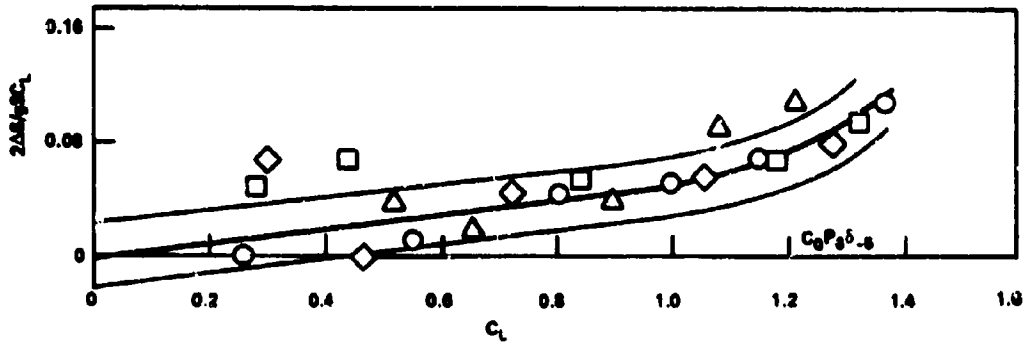

Figure 104c - Position P_6, -5-Degree Deflection

Figure 104 - Incremental Root Mean Square Data for Canard C_0

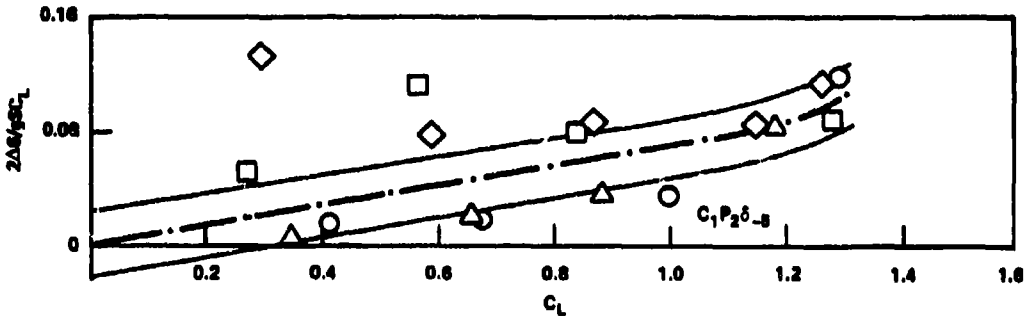

Figure 105a - Position P_2

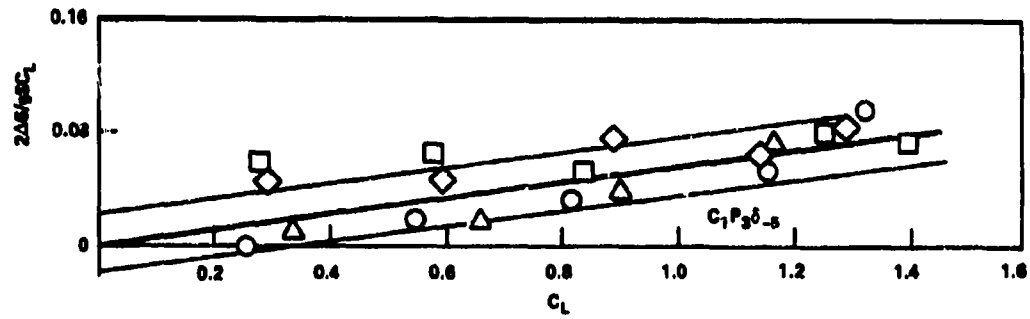

Figure 105b - Position P_3

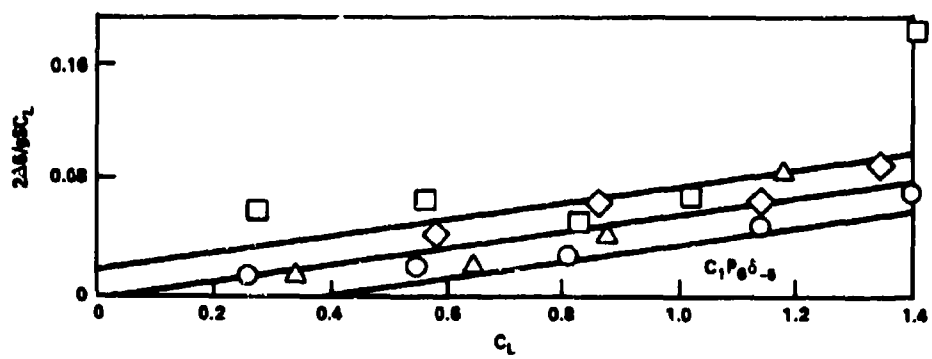

Figure 105c - Position P_6

Figure 105 - Incremental Root Mean Square Data for Canard C_1 at -5-Degree Deflection

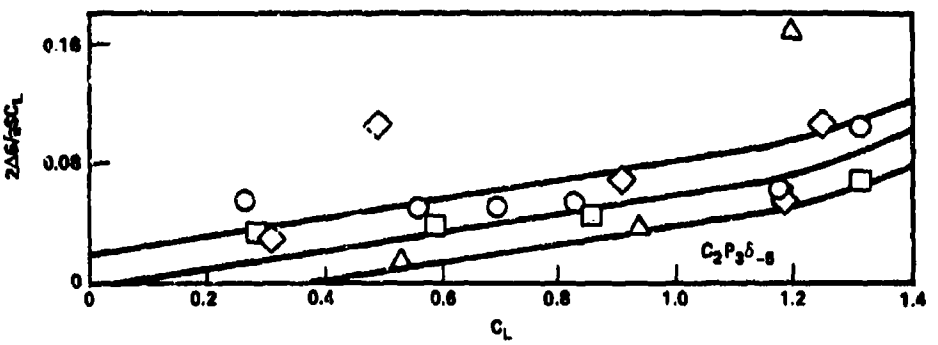

Figure 106a - Position P_3

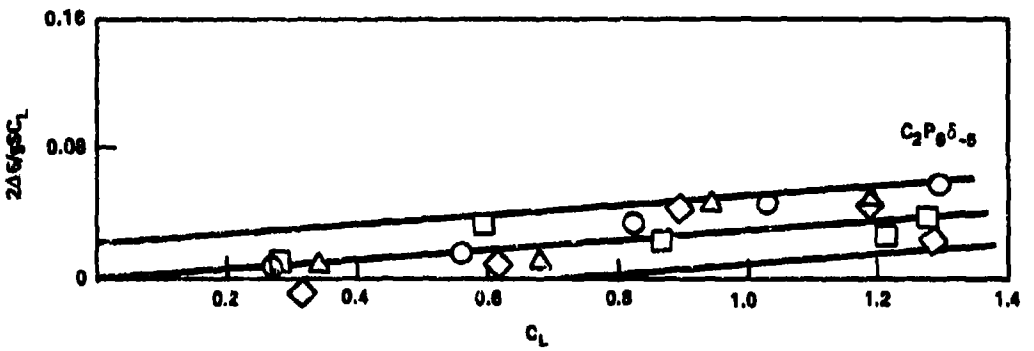

Figure 106b - Position P_6

Figure 106 - Incremental Root Mean Square Data for Canard C_2 at -5-Degree Deflection

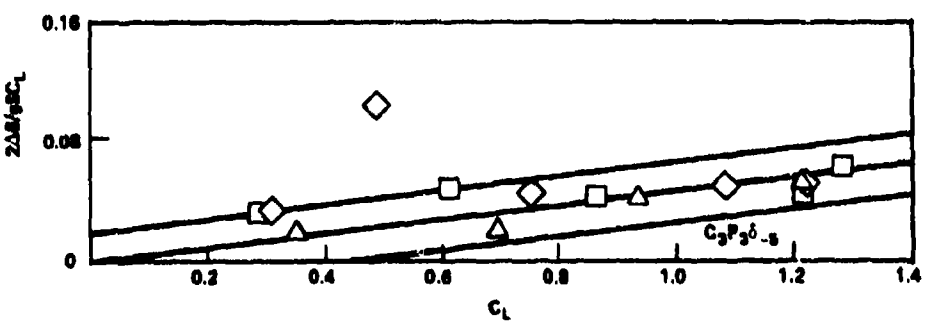

Figure 107 - Incremental Root Mean Square Data for Canard C_3 at Position P_3 and -5-Degree Deflection

REFERENCES

1. Lacey, D.W., "Transonic Characteristics of Close-Coupled Canard and Horizontal Tail Installed on a 50-Degree Sweep Research Aircraft Model," NSRDC ASED AL-81 (Aug 1972).

2. Ottensoser, J., "Test Data on the Transonic Aerodynamic Characteristics of Close-Coupled Canards with Varying Position and Deflection Relative to a 25° Swept Wing," NSRDC ASED AL-87 (Jan 1972).

3. Ottensoser, J., "Test Data on the Transonic Aerodynamic Characteristics of Close-Coupled Canards with Varying Planform Position and Deflection Relative to a 50° Swept Wing," NSRDC ASED AL-88 (May 1972).

4. Ottensoser, J., "Parametric Analysis of Close-Coupled Canard Transonic Aerodynamics for a Generalized Wing-Body Configuration," DTNSRDC ASED 399 (May 1977).

INITIAL DISTRIBUTION

Copies	
1	OUSD (R&E)/Mr. Makepeace
1	DARPA/COL. Krone
1	CHONR 704/R. Whitehead
1	NAVMAT 08T23
3	NADC 1 Terry Miller (V/STOL Project Office) 1 Bill Becker 1 Carman Mazza
1	NAVPGSCOL 1 Lou Schmidt
9	NAVAIRSYSCOM 1 AIR 03E 1 AIR 03PA 3 AIR 320 4 AIR 530
12	DTIC
2	AFFDL 1 CAPT Bill Sotomayer 1 R. Dyer
1	NASA, HQ/Scientific Tech Info Branch
1	NASA Ames/Preston Nelms
3	NASA Langley 1 Joe Chambers 1 Blair Gloss 1 Bill Henderson
1	Calif. Inst of Tech Grad Aero Labs
1	U. of Cincinnati/Lib
1	U. of Maryland/Lib

Copies	
1	MIT/Lib
1	N. Carolina State U./ Raleigh Lib
1	Stanford U./Lib
1	Virginia Polytech Inst/Lib
1	Boeing Aerospace Company/ H. Yoshihara
1	General Dynamics/Fort Worth/ C.E. Kuchar
1	Grumman Aerospace Corporation/ Nick Dannerhoffer
1	Lockheed-California/ Andy Byrnes
2	McDonnell Douglas Corp/ St. Louis 1 Jim Sinnett/MCAIR 1 Jim Hess/MCAIR
1	Northrop Corp Labs/ I. Waller
1	Rockwell International, Columbus/Lib
1	Rockwell International, Science Center
1	Vought Corporation/H. Diggers

CENTER DISTRIBUTION

Copies	Code	Name
10	5211.1	Reports Distribution
1	522.1	Library (C)
1	522.2	Library (A)
2	522.3	Aerodynamics Library

DTNSRDC ISSUES THREE TYPES OF REPORTS

1. DTNSRDC REPORTS, A FORMAL SERIES, CONTAIN INFORMATION OF PERMANENT TECHNICAL VALUE. THEY CARRY A CONSECUTIVE NUMERICAL IDENTIFICATION REGARDLESS OF THEIR CLASSIFICATION OR THE ORIGINATING DEPARTMENT.

2. DEPARTMENTAL REPORTS, A SEMIFORMAL SERIES, CONTAIN INFORMATION OF A PRELIMINARY, TEMPORARY, OR PROPRIETARY NATURE OR OF LIMITED INTEREST OR SIGNIFICANCE. THEY CARRY A DEPARTMENTAL ALPHANUMERICAL IDENTIFICATION.

3. TECHNICAL MEMORANDA, AN INFORMAL SERIES, CONTAIN TECHNICAL DOCUMENTATION OF LIMITED USE AND INTEREST. THEY ARE PRIMARILY WORKING PAPERS INTENDED FOR INTERNAL USE. THEY CARRY AN IDENTIFYING NUMBER WHICH INDICATES THEIR TYPE AND THE NUMERICAL CODE OF THE ORIGINATING DEPARTMENT. ANY DISTRIBUTION OUTSIDE DTNSRDC MUST BE APPROVED BY THE HEAD OF THE ORIGINATING DEPARTMENT ON A CASE-BY-CASE BASIS.